Characterising the phenotypic and functional role of monocyte-derived foam cells in atherosclerosis

by

Jenefa Begum

A thesis submitted to the University of Birmingham for the degree of

DOCTOR OF PHILOSOPHY

Institute of Cardiovascular sciences

College of Medical and Dental sciences

University of Birmingham

May 2024

UNIVERSITY OF
BIRMINGHAM

University of Birmingham Research Archive

e-theses repository

This unpublished thesis/dissertation is copyright of the author and/or third parties. The intellectual property rights of the author or third parties in respect of this work are as defined by The Copyright Designs and Patents Act 1988 or as modified by any successor legislation.

Any use made of information contained in this thesis/dissertation must be in accordance with that legislation and must be properly acknowledged. Further distribution or reproduction in any format is prohibited without the permission of the copyright holder.

Abstract

Atherosclerosis is a chronic inflammatory disease characterised by the accumulation lipid deposits within the arterial wall, leading to restricted blood flow and increased risk of cardiovascular events. Central to the development of atherosclerosis is the formation of foam cells which are derived from macrophages as a result of excessive accumulation of modified low-density lipoproteins (LDL). Upon oxLDL internalisation, macrophages transform into foam cells through the storage of lipid droplets that are primarily composed of cholesteryl esters which can be hydrolysed to generate free cholesterol. The balance between lipid uptake, storage, and degradation within foam cells is critical to maintain cholesterol homeostasis. Dysregulation in these processes contribute to foam cell persistence and plaque progression. Foam cells contribute significantly to the inflammatory microenvironment within plaque, causing perpetual local inflammation, recruitment of immune cells and plaque instability. The interplay between lipid metabolism and inflammatory signalling within foam cells exacerbates their retention and survival.

Understanding the inflammatory role of foam cells in atherosclerosis is crucial for identifying novel therapeutic targets aimed specifically at reducing foam cell-driven inflammation. However, till today identifying and characterising foam cells within atherosclerotic plaques remains a challenge due to significant overlap in markers with other immune cells. One of the aims of this study is to characterise foam cells both at a protein and genomic level via flow cytometry analysis, bulk RNA-sequencing and whole genome spatial transcriptomics to identify potential markers specific to foam cells themselves. Contradictory to the nature of a foam cell phenotype, our results

show that foam cells exhibit an anti-inflammatory and lipid metabolising profile genomic profile which coincides with existing data from recent transcriptomic studies.

Given that plaque is a heterogenous cellular environment, investigating the role of foam cells in isolation may not accurately represent their realistic function. Therefore, in this study I also examined the functional characteristics of foam cells in co-culture with endothelium in vitro. This approach allowed us to identify changes in lipid mediator secretion due to cell-cell crosstalk where I identified an enrichment in pro-inflammatory prostaglandin secretion in foam cell-endothelial cell co-cultures compared to foam cells alone.

In conclusion this study explores the characterisation of foam cells using multiple different avenues. I found that minimal differences were observed between macrophage and foam cell profiles and that monocyte-origin appear to have little to no effect on the genotype of foam cells. Additionally, I show that the foam cells potentially exhibit their pro-inflammatory functional phenotype through cellular crosstalk with endothelium via the secretion of pro-inflammatory lipid mediators.

Acknowledgements

First and foremost, I would like to say a huge thank you to Professor Ed Rainger, who as my primary supervisor have been an absolute joy to work with. I am so grateful to you for giving me this opportunity in the first place as well as giving me the independence to develop myself as a scientist. Your knowledge, patience and guidance throughout has been instrumental in getting me this far and I will definitely miss the sense of humour you always brought to our weekly meetings!

I also want to say a massive thank you to Dr Asif Iqbal. As my secondary supervisor you have been incredible throughout this journey and helped in more ways than I can express gratitude for. Thank you for always believing in me at times when I doubted myself and pushing me to get to where I am today. Your kindness and continuous motivation have truly helped during my PhD and I am forever grateful for all your help.

A special thank you to Dr Helen McGettrick, for being a great mentor and for always giving me opportunities to enhance my career portfolio. Not only have you been inspirational to work with professionally, but you've also convinced me to take my physical fitness seriously, thanks to your exercise group! I'd also like to extend my gratitude to Dr Myriam Chimen for being patient with all my experimental queries and Dr Ingrid Dimitru for always being so supportive of my work.

I would also like to acknowledge the British Heart foundation and the University of Birmingham for funding this research.

To every member of the Leukocyte trafficking group, past and present, thank you for making this journey filled with such great memories and I will forever cherish

your friendship and company as part of my PhD experience. First, I'd like to thank Danielle, for all the costa coffee catchups, evening deep lab chats and laughs that I will forever be grateful for. Adel thank you for bringing your unique sense of humour to the group and for your wise words of wisdom that I will always cherish. Areeba, although you've only joined the group fairly recently, I want to thank you for being such an incredible friend to me and I am forever grateful for the bond that we have. Thanks to Sophie for always putting up with my rants when things were going wrong in the lab and to Poppy for being a such an entertaining desk buddy. Thanks to Laleh and Juma for always providing me sweet treats so that I would never I go hungry in the office and Abbey for the inspirational chats. Jonny, thank you for all the GIFs and your friendship and Mustafa for your absolute kindness. Samantha, for all your help with my lab related queries as well as Dean for someone I could always go to for advice. I'd like to also thank Alyssa, Harry, Kathryn and Mussarat for the random entertaining lab chats and to all other members of LTG and friends that I've made at the university that have been a part of this journey. I also can not forget to express my thanks to every blood donor who donated blood for my project.

Most importantly I want to express my heartfelt gratitude to my family and friends and who have supported me all the way – without them I simply would not have gotten through this PhD. Thank you to my good friends (Rahana, Aqsa and Saba) for the post work catchups and for being such a positive influence throughout this journey. A huge thank you to my father for his continuous encouragement, support and for always being so proud of me, my brothers for all the lifts after late nights in the lab and my sister in-law for her endless support and kindness. Thank you to my adorable nieces and nephews for being such a blessing in my life and being my constant source of

entertainment whilst writing my thesis. A special thank you to my sister, who has been my biggest supporter and the one person I could always go to for help, advice and comfort. I will forever be grateful for you. Lastly, my mother who has been my absolute rock. You have always been the one to encourage me during my PhD and supported me during the toughest of times. I can not repay you for all that you do for me. Above all, I would like to thank God Almighty for giving me the faith, strength, and good health to persevere throughout this PhD and for teaching me to never give up hope. Although this journey has been a tough one, I am lucky to have had an amazing experience and have the opportunity meet some of the most amazing people that have all contributed to something special in my life.

Table of Contents

Chapter 1. Introduction 1

1.1. Inflammation 1
1.1.1. An overview of inflammation 1
1.1.2. Inflammatory resolution 2
1.1.3. Leukocyte recruitment and trans-endothelial migration 3
1.1.4. The vascular endothelium 8

1.2. Monocytes 12
1.2.1. Monocyte origin and development 12
1.2.2. Monocyte subsets and their characterisation 13
1.2.3. Monocyte subsets and their function during steady state 15
1.2.4. Monocyte subsets and their function during inflammation 16

1.3. Macrophages 19
1.3.1. Macrophage origin and developments 19
1.3.2. Macrophages and their role during homeostasis 20
1.3.3. Macrophages and their role during inflammation 21
1.3.4. Macrophage polarisation 23

1.4. Atherosclerosis 25
1.4.1. Pathogenesis of atherosclerosis 25
1.4.2. The role of endothelial activation during atherogenesis 31
1.4.3. Monocytes in atherosclerosis 33
1.4.4. Macrophages in atherosclerosis 35

1.5. Foam cells 38
1.5.1. Foam cell formation 38
1.5.2. Cholesterol metabolism 40
1.5.3. The cellular identity and phenotypic characteristics of foam cells 45

1.6. Polyunsaturated fatty acids (PUFAs) and their role in inflammation 47
1.6.1. Omega-6 and omega-3 PUFAs 47
1.6.2. Specialised pro-resolving mediators (SPMs) 50

1.7. Project aim 53

Chapter 2. Materials and Methods 55

2.1. Ethical approval 55

2.2. Isolation of peripheral blood mononuclear (PBMCs) cells and neutrophils from whole blood 55

2.3. Monocyte isolation 56
2.3.1. $CD14^+$ mixed monocyte isolation 56
2.3.2. $CD14^+$ $CD16^-$ monocyte isolation 57
2.3.3. $CD14^+CD16^+$ monocyte isolation 57

2.4. Monocyte cell culture and differentiation into macrophages and foam cells 58

2.4.1. Culture of monocyte-derived macrophages 58
2.4.2. Polarisation of macrophages 59
2.4.3. Culture and treatment of monocyte-derived foam cells 59
2.4.4. Reconstitution and storage of Eicosapentaenoic acid 60
2.4.5. Oil red O staining 60
2.4.6. Analysis of uptake of oxLDL (dil-oxLDL) 61
2.4.7. Macrophage dissociation 61

2.5. Flow cytometry staining and analysis 62
2.5.1. Extracellular antibody cell surface staining 62
2.5.2. Intracellular CD68 antibody staining 62
2.5.3. Flow cytometry staining procedure for macrophage characterisation 63
2.5.4. Flow cytometry analysis 63

2.6. Detection of protein in culture supernatants 67
2.6.1. Enzyme-linked immunoassay (ELISA) 67
2.6.2. Cytokine array 67

2.7. In *vitro* static transmigration assay 68
2.7.1. Expansion and cryopreservation of endothelial cell 68
2.7.2. Endothelial cell culture 68
2.7.3. Preparation of macrophage and foam culture supernatants of endothelial cells stimulation 69
2.7.4. Endothelial cell stimulation 69
2.7.5. Static transmigration assay 70
2.7.6. Dissociation of endothelial cells for staining 70

2.8. Co-culture assays 72
2.8.1. Monocyte culture and differentiation in transwell inserts 72
2.8.2. Seeding endothelial cells on transwell insets to establish co-cultures 72
2.8.3. Sample collection of lipidomic analysis 72
2.8.4. Immunofluorescence staining of transwell filters 73

2.9. Lipidomics 73

2.10. Real-time quantitative polymerase chain reaction (RT-qPCR) 74
2.10.1. RNA extraction 74
2.10.2. cDNA conversion 75
2.10.3. Quantitative RT-qPCR 76

2.11. Bulk RNA-sequencing 76
2.11.1. Preparation of sequencing libraries 76
2.11.2. RNA sequencing analysis 77
2.11.3. Analysis of differentially expressed genes 77

2.12. Spatial transcriptomics 78
2.12.1. GeoMX Whole Transcriptome Atlas (WTA) assay 78
2.12.2. GeoMX RNA data quality control (QC) 79
2.12.3. GeoMX DSP data analysis 80

2.13. Statistical analysis 80

Chapter 3. In Vitro characterisation of human monocyte-derived macrophages 81

3.1. Introduction 81

3.2. Results 83

3.2.1. Isolation and purification of monocyte subsets 83

3.2.2. Monocyte-derived macrophage differentiation in autologous serum vs MCSF 86

3.2.3. Target selection for macrophage flow cytometry panel design 90

3.2.4. Fluorophore selection for selected targets in flow panel 92

3.2.5. Indirect labelling of stabilin-1 antibody with fluorescently labelled antibody 92

3.2.6. Single antibody stain analysis 98

3.2.7. The effects of macrophage detachment methods on surface protein expression 101

3.2.8. Time course for macrophage polarisation to macrophage subtypes 103

3.3. Discussion 110

3.3.1. Optimisation of MDM culture 110

3.3.2. The design and validation of a flow cytometry panel for macrophages 112

3.3.3. Characterisation of macrophage phenotypes 114

Chapter 4. Human monocyte-derived foam cell formation and characterisation 118

4.1. Introduction 118

4.2. $CD14^+CD16^-$ (classical) monocytes assimilate oxLDL more readily than $CD14^+CD16^+$ (non-classical) monocytes 120

4.3. Monocytes have an increased pro-inflammatory cytokine profile compared to macrophages and foam cells 122

4.4. Bulk RNA sequencing (RNA-seq) analysis of monocytes, macrophages and foam cells derived from $CD14^+CD16^-$ (classical) and $CD14^+CD16^+$ (non-classical) monocyte subsets 125

4.4.1. Bulk RNAseq experimental design and data transformation 125

4.4.2. Differential gene expression between $CD14^+CD16^-$ and $CD14^+CD16^+$ monocyte subsets 129

4.4.3. Monocyte subsets cluster distinctly to ofam cells and macrophages 135

4.4.4. Monocytes display a pro-inflammatory transcriptomic signature compared to macrophages and foam cells 137

4.4.5. Foam cells and macrophages generated from classical and non-classical monocytes show very similar transcriptomic expression profiles 140

4.5. Foam cells are enriched for genes regulating cholesterol transport 148

4.6. Characterisation of monocyte-derived foam cells via flow cytometry analysis . 150

4.6.1. Generation of foam cells derived from various forms of modified LDL 150

4.6.2. Characterisation of foam cell subtypes via flow cytometry 153

4.6.3. Foam cells generated from polarised macrophages demonstrate minimal differences in their phenotypic and secretory profile 156

4.7. Discussion 163
4.7.1. Monocytes display a pro-inflammatory signature that is gradually lost upon differentiation 163
4.7.2. Foam cells display an anti-inflammatory and lipid metabolising profile 166
4.7.3. Characterisation of foam cell subtypes and their effect on macrophage polarisation states 169
4.7.4. The impact of modified LDL on the polarisation state of macrophages 171

Chapter 5. Spatial transcriptomic profiling of human coronary arterial plaque tissue 175

5.1. Introduction 175

5.2. Experimental design and rational for spatial transcriptomic profiling 177

5.3. The rationale for spatial transcriptomic data analysis 180

5.4. Spatial CD68 gene expression in coronary artery tissue 183

5.5. Spatial CD11c (ITGAX) gene expression in coronary artery tissue 187

5.6. Spatial gene expression analysis specifically in plaque ROIs within human coronary artery tissue 192

5.7. Discussion 197

Chapter 6. Investigating the inflammatory phenotype of foam cells in vitro 202

6.1. Introduction 202

6.2. Foam cells activate endothelium minimally in monoculture 204

6.3. Rationale for investigating the secretory profile of foam cell and endothelial (EC) co-cultures 209
6.3.1. Experimental design for co-culture assays 209
6.3.2. Lipidomics analysis of foam cell-EC co-culture supernatants 212

6.4. Effects of EPA on oxLDL uptake and foam cell formation 216

6.5. Discussion 220
6.5.1. Foam cells in mono-culture vs co-culture 220
6.5.2. The therapeutic potential f EPA in the treatment of atherosclerosis 224

Chapter 7. Concluding remarks 228

References 230

List of figures

Figure 1-1: The role of shear stress on vascular endothelium 11
Figure 1-2: Leukocyte recruitment and transmigration in atherosclerosis. 30
Figure 1-3: Cholesterol metabolism in macrophage-derived foam cells. 44
Figure 2-1: Analysis of adhered and transmigrated neutrophils in static migration assays......71
Figure 3-1 Purification of $CD14^{+}CD16^{-}$ and $CD14^{+}CD16^{+}$ monocyte subsets 85
Figure 3-2 Macrophage differentiation in autologous serum vs MCSF.....88
Figure 3-3 Size and circularity index of day 6 macrophages differentiated with autologous serum vs MCSF 89
Figure 3-4 Emission spectra of fluorochrome for 11-colour macrophage flow cytometry panel 94
Figure 3-5 Gating strategy for macrophage flow cytometry panel 96
Figure 3-6 Gating strategy to confirm binding of primary unconjugated Stabilin-1 antibody to Alexa-fluor 700 fluorescently labelled secondary antibody......97
Figure 3-7 Median fluorescence intensity of macrophages stained individually with anti-CD86, anti-CD204, anti-CD206, anti-CD86 or in combination with all antibodies in the panel.....99
Figure 3-8 Median fluorescence intensity of macrophages stained individually with anti-CD11c, anti-CD36, anti-CD80, anti-Stabilin-1, anti-MerTK, anti-HLA-DR or in combination with all antibodies in the panel 100
Figure 3-9 Frequency and median fluorescence intensity of CD86 and CD206 surface markers following detachment from plastic using various dissociation methods.....102
Figure 3-10 TNF-α secretion from macrophages polarised towards an M1 and M2 phenotype 105
Figure 3-11 Flow cytometry analysis of macrophages for anti-CD206 and anti-CD80 antibodies on M0, M1 and M2 macrophage phenotypes. 106
Figure 3-12 Flow cytometry analysis of M1-like macrophage markers on M0, M1 and M2 macrophage phenotypes. 107
Figure 3-13 Flow cytometry analysis of anti-CD68, anti-CD11c and anti-MerTK macrophage markers on M0, M1 and M2 macrophage phenotypes......108
Figure 3-14 Flow cytometry analysis of scavenger receptors on M0, M1 and M2 macrophage phenotypes. 109

Figure 4-1: DiI-OxLDL uptake in $CD14^{+}CD16^{-}$ vs $CD14^{+}CD16^{+}$ monocyte-derived macrophages. 121
Figure 4-2: TNF secretion from untreated and oxLDL treated monocyte subsets upon differentiation....123
Figure 4-3: Upregulation of pro-inflammatory cytokines in culture supernatants from monocytes compared to macrophages and foam cells....124
Figure 4-4: Schematic diagram of monocyte, macrophage and foam cell mRNA sample collection for bulk-RNAseq. 127
Figure 4-5: Total read counts and distribution of transformed bulk-RNAseq data for monocytes, macrophages and foam cells. 128
Figure 4-6: Classical, $CD14^{+}CD16^{-}$ (C) and Non-classical $CD14^{+}CD16^{+}$ (NC) monocytes cluster distinctly 130
Figure 4-7: Differentially expressed gene (DEGs) between classical and non-classical monocyte subsets 131
Figure 4-8: K means clustering of top 1000 genes in $CD14^{+}CD16^{-}$ and $CD14^{+}CD16^{+}$ monocytes subsets 134
Figure 4-9: Foam cells and macrophages cluster together, distinctly from monocytes 136
Figure 4-10: Top 50 variably expressed genes of monocytes, macrophages and foam cells.....138
Figure 4-11: K means clustering of top 1000 genes in of monocytes, macrophages and foam cells. 139
Figure 4-12: Foam cells and macrophages do not cluster distinctly based on cell type or cell origin. 142
Figure 4-13: Top 50 variably expressed genes of foam cells and macrophages derived from $CD14^{+}CD16^{-}$ and $CD14^{+}CD16^{+}$ monocytes subsets 143
Figure 4-14: Differentially expressed gene (DEGs) between foam cells and macrophages derived from monocyte subsets....144
Figure 4-15 **Enrichment analysis of differentially expressed genes based on** 147
Figure 4-16: An increase in lipid metabolism genes in human monocyte-derived monocytes macrophages and foam cells 149
Figure 4-17: Cytokine profile of foam cells generated from ox-LDL, ac-LDL and ma-LDL.....152
Figure 4-18: Flow cytometry analysis on foam cell phenotypes 155

Figure 4-19: Experimental design for macrophage polarisation and treatment with modified forms of LDL 158
Figure 4-20: TNF secretion profile of foam cells derived from polarised macrophages. 159
Figure 4-21: Flow cytometry analysis of anti-CD68, anti-CD11c and anti-MerTK macrophage markers on foam cells derived from polarised macrophages. 160
Figure 4-22: Flow cytometry analysis of anti-CD80, anti-CD86, anti-MHC II and anti-CD206 macrophage markers on foam cells derived from polarised macrophages. 161
Figure 4-23: Flow cytometry analysis of anti-CD36, anti-CD204, and anti-Stabilin-1 macrophage markers on foam cells derived from polarised macrophages. 162
Figure 5-1: Schematic diagram of digital spatial profiling (DSP) assay workflow using nanostring GeoMX DSP. 178
Figure 5-2: Microscopy images of fluorescently labelled human coronary artery tissue sections with selected ROIs for GeoMX digital spatial profiling (DSP). 179
Figure 5-3: Unsupervised hierarchical clustering of genes according to localisation in coronary artery tissue sections 181
Figure 5-4: Box plot of CD68 and ITGAX (CD11c) gene counts in CD45+CD4+ vs CD45+CD4- ROIs 182
Figure 5-5: The variation in CD68 gene expression in coronary artery tissue based on disease severity and tissue localisation 185
Figure 5-6: Gene expression in coronary artery tissue in CD68high vs CD68low ROIs 186
Figure 5-7: The variation in ITGAX (CD11c) gene expression in coronary artery tissue based on disease severity and tissue localisation 189
Figure 5-8: Gene expression in coronary artery tissue in CD11chigh vs CD11clow ROIs 190
Figure 5-9: Gene expression within plaque ROIs of coronary artery tissue that are of varying disease severity 194
Figure 5-10: Gene expression within plaque of coronary artery tissue within ROIs that are CD68high and CD68low 195
Figure 6-1: Endothelial activation using macrophages and foam cell mono-culture supernatants 206
Figure 6-2: Flow cytometry staining and analysis of endothelium pre- and post-enzymatic detachment 207

Figure 6-3 Expression of endothelial activation markers following treatment with macrophage and foam cell mono-culture supernatants.....208
Figure 6-4 Co-culture of endothelium with macrophages and foam cells 211
Figure 6-5: Biosynthesis of lipid mediators by macrophage and foam cells co-cultured with endothelium 214
Figure 6-6: Biosynthesis of lipid mediators by macrophage and foam cells co-cultured with endothelium 215
Figure 6-7: Effects of EPA on oxLDL uptake for foam cell formation 218
Figure 6-8: Effects of EPA on genes associated with cholesterol transport.....219

List of tables

Table 1-1: PRRs and their respective PAMPs/DAMPs 7
Table 2-1 Flow cytometry antibody panel 65
Table 2-2 Isotype controls for flow cytometry panel 66
Table 3-1 List of targets for flow cytometry panel and functional relevance 91
Table 3-2 Relative fluorochrome brightness and predicted target abundance 95
Table 4-1: Top 30 downregulated genes in non-classical monocytes compared to classical monocytes 132
Table 4-2: Top 30 upregulated genes in non-classical monocytes compared to classical monocytes 133
Table 4-3: Top 30 down-regulated genes in $CD14^{+}CD16^{+}$ monocyte-derived foam cells compared to $CD14^{+}CD16^{+}$ monocyte derived macrophages 145
Table 4-4: Top 8 up-regulated genes in $CD14^{+}CD16^{+}$ monocyte-derived foam cells compared to $CD14^{+}CD16^{+}$ monocyte derived macrophages 146
Table 4-5: Top 4 down-regulated genes in $CD14^{+}CD16^{-}$ monocyte-derived foam cells compared to $CD14^{+}CD16^{-}$ monocyte derived macrophages 146
Table 5-1: Pathways that are downregulated in $CD68^{high}$ ROIs 191
Table 5-2: Pathways that are downregulated in $CD11c^{low}$ ROIs 191
Table 5-3: Pathways that are downregulated in plaque ROIs of moderate disease severity 196

Statement of impact during COVID-19

The COVID 19 pandemic had a huge impact on my PhD studies and caused a lot of disruption to both my research and my personal life. My PhD start date (April 2020) coincided with the first lockdown which made it impossible for me to make a start in the lab. As lockdown restrictions were eased and lab access was regained (June 2020), the University student services were unable to provide me with an ID card for access on site for a further 4 months which further restricted my access to the lab and data output for the first year of my PhD.

My project was reliant heavily on human blood donors which I was unable to have access to most of the first year of my PhD due to COVID 19 social distancing guidelines. My project also had a large focus on carrying out human embryonic stem cell (HESC) work. However, due to COVID 19 restrictions our collaborators were unable to facilitate training for me in their lab in order to carry out this work, thus we were unable carry this work forward as part of my project. During the pandemic there were also manufacturing issues with reagents such as eicosapentaenoic acid (EPA) where suppliers were reporting low purity of the compound causing adverse effects on my research.

On a personal level, COVID 19 had a huge impact on my mental health as my father was diagnosed with a terminal illness around the start of my PhD and the initial lockdown. Dealing with both restricted access to labs and personal issues at home made it mentally challenging. Fortunately, I was able to apply for a 6 month extension from the University of Birmingham to assist in completing my experiments for my thesis.

Regardless of all the hurdles during my PhD I am grateful to have made it through the PhD programme and to have gained all the invaluable skills throughout the process.

Abbreviations

ABCA1	ATP-binding cassette transporter A1
ABCG1	ATP-binding cassette transporter G1
ACAT1	Acyl CoA acetyl transferase 1
AcLDL	Acetylated LDL
ACS	Acute coronary syndrome
ARA	Arachidonic acid
BSA	Bovine serum albumin
CANTOS	Canakinumab Anti-inflammatory Thrombosis Outcome Study
CCL	C-C chemokine ligand
CCR	C-C chemokine receptor
CE	Cholesteryl esters
COX	Cyclooxygenase
CYP450	Cytochrome P450
DAMP	Damage-associated molecular patterns
DC	Dendritic cell
DHA	Docosahexaenoic acid
EC	Endothelium cell
eNOS	Endothelial nitric oxide synthase
EPA	Eicosapentaenoic acid
ER	Endoplasmic reticulum
GPCR	G-protein coupled receptor
HLD	High density lipoprotein
ICAM-1	Intercellular adhesion molecule 1
IFNγ	Interferon-γ
IL	Interleukin
IL-1β	Interleukin-1 beta
JAM	Junctional adhesion molecule
KLF	Kruppel-like factor
LAL	Lysosomal acid lipase
LC-MS/MS	Liquid chromatography tandem mass spectrometry
LDL	Low-density lipoprotein
LDLR	Low-density lipoprotein receptor

LFA-1	Lymphocyte function-associated antigen 1
LOX	Lipid oxygenase
LPS	Lipopolyscaccharide
LT	Leukotrienes
LX	Lipoxin
Ma-LDL	Malondialdehyde LDL
Mac-1	Macrophage-1 antigen
MAPK	Mitogen-activated protein kinase
MCP-1	Monocyte chemoattractant protein-1
MCSF	Macrophage-colony-stimulating factor
MDM	Monocyte-derived macrophages
MerTK	Mer tyrosine kinase
MFI	Median fluorescence intensity
MHC II	Major histocompatibility complex II
MMP	Matrix metalloproteases
nCEH	Neutral cholesteryl ester hydrolase
NF-κB	Nuclear factor kappa B
NK	Natural Killer
NLR	nucleotide oligomerisation domain-like receptors
NO	Nitric oxide
NOD	Nucleotide oligomerisation domain
Nrf2	Nuclear factor erythroid 2-related factor 2
OxLDL	Oxidised LDL
PAMP	Pattern-associated molecular patterns
PECAM-1	Platelet endothelial cell adhesion molecule-1
PBMC	Peripheral blood mononuclear cell
PG	Prostaglandins
PLIN2	Perilipin-2
PPARα	Proliferator-activated receptor α
PPARγ	Proliferator-activated receptor γ
PRR	Pattern-recognition receptors
PSGL-1	P-selectin glycoprotein ligand 1
PTCR1	Protectin-conjugates in tissue regeneration 1

PUFA	Polyunsaturated fatty acids
REDUCE-IT	Reduction of Cardiovascular Events with EPA Intervention Trial
ROI	Region of interest
ROS	Reactive oxygen species
Rv	Resolvin
SPM	Specialised pro-resolving mediators
TAM	Tyro3/Axl/Mer
TGF-β	Transforming growth factor beta
Th	T-helper
TLR	Toll-like receptor
TNF	tumour necrosis factor
TX	Thromboxanes
VCAM-1	Vascular cell adhesion protein 1
VLA-4	Very late antigen 4
VLDL	Very low-density lipoproteins
VSMC	Vascular smooth muscle cells
VWF	Von Willebrand factor

Chapter 1. INTRODUCTION

1.1. Inflammation

1.1.1. An overview of inflammation

Inflammation is a complex protective defence mechanism employed by our immune system in response noxious stimuli such as pathogens, cellular stress responses and tissue injury (Medzhitov, 2008). This triggers a cascade of chemical and signalling events that promote the recruitment of specialised immune cells, with the aim of restoring tissue homeostasis. Physiological changes to the microcirculation play an active role in facilitating an inflammatory response via endothelial activation and increased vascular permeability, allowing extravasation of plasma proteins and leukocyte trafficking from blood vessels to sites of tissue damage (Chen et al., 2018). These modifications are accompanied by the production of inflammatory mediators that are released from tissue resident cells which alter the local tissue environment. Whilst an acute inflammatory response typically lasts for several days or weeks, dysregulated or excessive inflammation can lead to persistent immune cell activation and recruitment that drives the pathogenesis of a spectrum of chronic inflammatory diseases including atherosclerosis, rheumatoid arthritis and type 2 diabetes (Medzhitov, 2008, Nathan and Ding, 2010).

The nature of the initial stimulus dictates the course of the inflammatory process. This can be in the form of exogenous microbial structures and oxygenated lipoproteins recognised as pattern-associated molecular patterns (PAMPs) or endogenous signals

released upon cellular damage known as damage-associated molecular patterns (DAMPs) (Chen et al., 2018, Libby, 2007). Such structures are recognised by pattern-recognition receptors (PRRs) such as toll-like receptors (TLRs) expressed on the surface of innate immune cells including tissue resident macrophages as well intracellular nucleotide oligomerisation domain (NOD)– like receptors (NLRs) (Amarante-Mendes et al., 2018) (Table 1). PRR stimulation results in downstream signalling and inflammasome activation (through NLR oligomerisation) promoting the release of a combination of cytokines, chemokines and eicosanoids that mediate vascular changes and leukocyte recruitment to the local tissue in attempt to clear inflammatory stimuli (Mogensen, 2009, Harder et al., 2009). In the case of chronic inflammatory diseases, the initial inflammatory stimulus is often unidentifiable and is thought to be manifested in response to tissue malfunction and prolonged cellular stress due to ongoing inflammation. Hence why events that lead to chronic inflammation are partially understood (Medzhitov, 2010, Furman et al., 2019).

1.1.2. Inflammatory resolution

It is critical that an acute inflammatory response is actively terminated once the inflammatory stimulus is cleared via a process known as resolution. This entails a distinct set of anti-inflammatory mechanisms that begin the tissue restoration phase – a process driven primarily by tissue resident macrophages (Nathan and Ding, 2010, Maskrey et al., 2011). Clearance of apoptotic cells by macrophages promotes them to undergo a phenotypic switch from a pro-inflammatory to an anti-inflammatory state allowing them to release key cytokines, interleukin 10 (IL-10) and transforming growth factor beta (TGF-β) as well as matrix metalloproteases (MMPs) that suppress inflammation and mediate tissue remodelling (Watanabe et al., 2019, Fadok et al.,

1998, Michlewska et al., 2009). The biosynthesis of lipid mediators also plays a crucial role in regulating the resolution phase in which the classical pro-inflammatory eicosanoids, prostaglandins and leukotrienes are switched to generate pro-resolving lipoxins, resolvins and protectins that are enzymatically derived from essential fatty acids. These pro-resolving eicosanoids actively inhibit further neutrophil infiltration and promote macrophage phagocytosis (Serhan et al., 2008, Schwab et al., 2007).

Collectively, the shift in the production of pro-inflammatory cytokines, chemokines and lipid mediators favours a pre-resolving local environment in the tissue with the aim of restoring homeostatic conditions. However, dysregulated inflammatory resolution can be detrimental and is considered a major driver of chronic inflammatory diseases (Nathan and Ding, 2010). Failure to subside an acute inflammatory response can lead to perpetual tissue damage leading to systemic effects in all tissues and organs along with impaired normal immune tolerance and function (Furman et al., 2019).

1.1.3. Leukocyte recruitment and trans-endothelial migration

Leukocyte trafficking from peripheral blood to tissue marks a fundamental step during inflammation. This occurs following haemodynamic changes and expression of pro-inflammatory cytokines that enable specific leukocyte and endothelial cell interactions to occur via a network of adhesion molecules and chemotactic agents. Experimental approaches, including in vitro flow based assays and intravital microscopy have elucidated the well-defined stages of the leukocyte trafficking cascade; capture and rolling of leukocytes to endothelium, followed by firm adhesion, intraluminal crawling and trans-endothelium migration (Ley et al., 2007, Nourshargh and Alon, 2014).

The initial capture and rolling phenomenon of leukocytes on the vascular endothelium is mediated by the engagement of calcium-dependent selectins (P, E and L selectin) (Wright and Cooper, 2014, Hayashi et al., 2000, Luscinskas et al., 1994, Noble et al., 1996). Whilst L-selectin is expressed constituently on all leukocytes, P selectin is rapidly expressed on endothelium within minutes of an inflammatory trigger and is released from endothelial cell secretary granules known as Weibel-Palade bodies (Dole et al., 2005). Activated platelets also release P-selectin from a-granules, mediating platelet adhesion to monocytes by stimulating tissue factor expression on their surface – a process which initiates the coagulation cascade and contributes to thrombosis (Larsen et al., 1989, Celi et al., 1994, Ivanov et al., 2019). Endothelial expression of E-selectin is followed shortly (within hours of an inflammatory response) which is transcriptionally regulated with its expression induced by pro-inflammatory cytokines, tumour necrosis factor α (TNF-α) and interleukin-1 beta (IL-1β) released by tissue resident macrophages (Ghersa et al., 1994, Sheikh et al., 2003, Ott et al., 2007). Collectively these selectins interact with heavily glycosylated ligands with the major ligand being P-selectin glycoprotein ligand 1 (PSGL-1) expressed on leukocytes as well as CD44 and E-selectin ligand 1 which are specific to E-selectin (Zarbock et al., 2011, McEver and Cummings, 1997, Hidalgo et al., 2007). These low affinity, reversible bonds, coupled with low shear stress, facilitate slow rolling of leukocytes along activated endothelium (Mehta-D'souza et al., 2017).

Firm adhesion is facilitated primarily by activated leukocyte integrins that interact with their cognate ligand (cellular adhesion molecules) on the endothelial surface (Ley et al., 2007). Structurally integrins are composed of an α and a β subunit where they exist in low abundance and in a low affinity state under resting conditions.

G-protein coupled receptor (GPCR) signalling by chemokines and lipid chemoattractants released from activated endothelium are imperative for integrin function enabling them to adopt a high affinity, active conformation that mediates leukocyte arrest instantaneously (Mitroulis et al., 2015, Rainger et al., 1997, Alon and Shulman, 2011).

Leukocyte integrins are subdivided into β_1 and β_2 families, whereby very late antigen 4 (VLA-4) ($\alpha_4\beta_1$; CD49d/CD29), lymphocyte function-associated antigen 1 (LFA-1) ($\alpha_L\beta_2$; CD11a/CD11b) and macrophage-1 antigen (Mac-1) ($\alpha_M\beta_2$; CD11b/CD18) are the most studied in leukocyte recruitment (Mitroulis et al., 2015). Specificity of these integrin interactions varies on different leukocyte populations. VLA-4 is expressed on almost all leukocyte populations. In addition to its role in adhesion it also contributes to leukocyte tethering and rolling through its binding on vascular cell adhesion protein 1 (VCAM-1) on endothelium (Alon et al., 1995). On the other hand, β_2 integrins such as LFA-1 and Mac-1 are strictly associated with adhesion and trans-endothelial migration via its interaction with intercellular adhesion molecule 1 (ICAM-1) and ICAM-2 (Ostermann et al., 2002, Sumagin et al., 2010). Whilst LFA-1 expression is restricted mainly to lymphocytes, Mac-1 is expressed abundantly on myeloid cells, particularly on monocytes (Fagerholm et al., 2019, Wolf et al., 2018). It is important to acknowledge that these integrins do not act strictly in isolation but crosstalk between them facilitates adhesion of leukocytes to endothelium. The clustering of VLA-4 on monocytes in response to VCAM-1 engagement activates LFA-1 and Mac-1-induced adhesion to endothelium and blocking LFA-1 can inhibit VLA-4 interactions with VCAM-1 (May et al., 2000, Gronholm et al., 2016). It has been

proposed that this crosstalk is mediated by changes in the phosphorylation states of β_1 and β_2 subunits (Uotila et al., 2014).

Firmly adhered leukocytes subsequently leave the circulation by transmigrating across the endothelial barrier and into inflamed tissue. This process does not occur randomly as leukocytes appear to crawl along the endothelium, seeking transmigration exit sites known as 'hotspots' that are facilitated by heterogenous expression of ICAM-1 on the endothelial surface (Gronloh et al., 2022). The redistribution of junctional molecules including platelet endothelial cell adhesion molecule-1 (PECAM-1), CD99, the junctional adhesion molecule family (JAM) and their interaction with integrins (LFA-1 and Mac-1) crucially support the final stage of the leukocyte trafficking step (Bradfield et al., 2007, Sumagin et al., 2010, Ley et al., 2007). Given that each step in the leukocyte trafficking cascade is regulated to such a high degree, defects in any stage of the pathway can lead to dysregulated, pathogenic recruitment of immune cells as seen in chronic inflammatory disease such as atherosclerosis.

Table 1-1: PRRs and their respective PAMPs/DAMPs

Subtype	PRR	PAMP/ DAMP	References
TLRs	TLR1	Tri-acylated lipopeptide	(Takeuchi et al., 2002)
	TLR2	Di- and tri-acylated lipopeptides; Uric acid crystals	(Kang et al., 2009, Liu-Bryan et al., 2005)
	TLR3	Viral double stranded RNA	(Alexopoulou et al., 2001)
	TLR4	Lipopolysaccharide (LPS)	(Park et al., 2009)
	TLR5	Flagellin	(Forstneric et al., 2016)
	TLR6	Di-acylated lipopeptides	(Takeuchi et al., 2001)
	TLR7	Viral single stranded sRNA	(Lund et al., 2004)
	TLR8	Viral single stranded sRNA	(Jurk et al., 2002)
	TLR9	Un-methylated CpG DNA	(Takeshita et al., 2001)
NLRs	NLRP3	ATP; double stranded RNA	(Zha et al., 2016, Franchi et al., 2014)
	NOD1	Bacterial peptidoglycans	(Girardin et al., 2003)
	NOD2	Bacterial peptidoglycans	(Lauro et al., 2017)
RLRs	RIG-I	Viral double stranded sRNA	(Saito and Gale, 2008)
	LGP2	Viral double stranded sRNA	(Li et al., 2009)
	MDA5	Viral double stranded sRNA	(Feng et al., 2012)
C-type Lectins	MGL	GAlNac	(Pirro et al., 2019)
	Dectin-1	β-glucans	(Brown et al., 2003)
Scavenger receptors (SR)	SR-B1	Lipoproteins (HDL)	(Shen et al., 2018)
	CD36	Oxidised LDL	(Nicholson et al., 1995)
	SR-A1	Unmethylated CpG DNA; Proteoglycans	(Taban et al., 2022)

Toll-like receptors (TLR); Nod-like receptors, (NLR); NLR family pyrin domain containing 3 (NLRP3); Retinoic acid-inducible gene-I-like receptors (RLR)

1.1.4. The vascular endothelium

The blood vascular endothelium cells (EC) is central in the execution and regulation of an inflammatory response. As the primary gatekeeper of tissue, it is responsible for controlling vascular tone, permeability and leukocyte transmigration which is only permitted upon its activation in response to inflammatory stimuli (Pober and Sessa, 2007, Theofilis et al., 2021). The principal regulators of these processes are driven by endogenous nitric oxide (NO) (generated by endothelial NO synthase; eNOS) and prostacyclin produced by EC which promote vasodilation via smooth muscle relaxation and attenuated platelet activation under resting conditions (Archer et al., 1994, Araujo et al., 2011, Mitchell et al., 2008). The expression of flow-regulated transcription factors, kruppel-like factor-2 (KLF2) and nuclear factor erythroid 2-related factor 2 (Nrf2) are crucial in producing such vasoactive mediators which ultimately regulate EC inflammatory responses (SenBanerjee et al., 2004, Zakkar et al., 2009). Importantly, the ability to sequester endothelial-leukocyte interactions has been demonstrated using NO inhibitors, whereby NO production correlated with reduced transcriptional expression of adhesion molecules, VCAM-1 and E-selectin as well as membrane associated chemokines such as monocyte chemoattractant protein-1 (MCP-1/CCL2) by inhibiting nuclear factor kappa B (NF-κB) activation (Kubles et al., 1991, Caterina et al., 1995, Zeiher et al., 1995).

Additionally, haemodynamic forces can regulate endothelial activation and function at a mechanical level. Such shear stress-induced forces are mechano-transduced into biochemical signals that alter EC morphology and gene expression levels that influence the activity of leukocyte trafficking (Moazzam et al., 1997, Wragg et al., 2014). Laminar shear settings are associated with reduced vascular permeability

and expression of leukocyte adhesion molecules on the endothelial surface (Traub and Berk, 1998, Theofilis et al., 2021). Contrastingly, oscillatory shear stress forces (caused by disturbed flow), typically observed in arterial bifurcations are widely associated with reduced NO bioavailability, increased production of reactive oxygen species (ROS) and upregulated adhesion molecule expression, all of which are characteristic of endothelial dysfunction and predispose to increased plaque vulnerability (Chappell et al., 1998, Theofilis et al., 2021). Such signalling pathways are initiated by a combination of endothelial mechano-sensors of shear stress, including CD31 (PECAM-1) and Piezo1 which work in combination to remodel EC junctions (Fujiwara, 2006, Chuntharpursat-Bon et al., 2023).

Specifically, Piezo1 is a newly discovered ion channel expressed on ECs which plays a distinct role in inflammation depending on the nature of blood flow (Harraz et al., 2022, Liu et al., 2022a). Under shear stress conditions, Piezo1 activation leads to a controlled influx of calcium ions that promotes NO production and vascular vasodilation (Santana Nunez et al., 2023). Endothelial specific deletion of Piezo1 demonstrated impaired NO production, vascular function and hypertension in murine models highlighting the importance of Piezo1 in regulating vascular homeostasis under laminar flow (Wang et al., 2016, Iring et al., 2019). In contrast, in areas of disturbed flow, elevated and irregular expression of Piezo1 has recently been identified specifically at sites of plaque tissue and on ECs in *Apoe*$^{-/-}$ mice. Activation of Piezo1 in such models was associated with endothelial inflammation including increased expression of surface adhesion molecules (Lan et al., 2024). Thus, vascular shear stress has a profound effect on endothelial surface and junctional proteins, influencing their expression, distribution, and functional integrity. Dysfunctional endothelium due

to chronic inflammation will be discussed in more detail later in the thesis in the context of inflammatory cardiovascular disease (Figure 1-1).

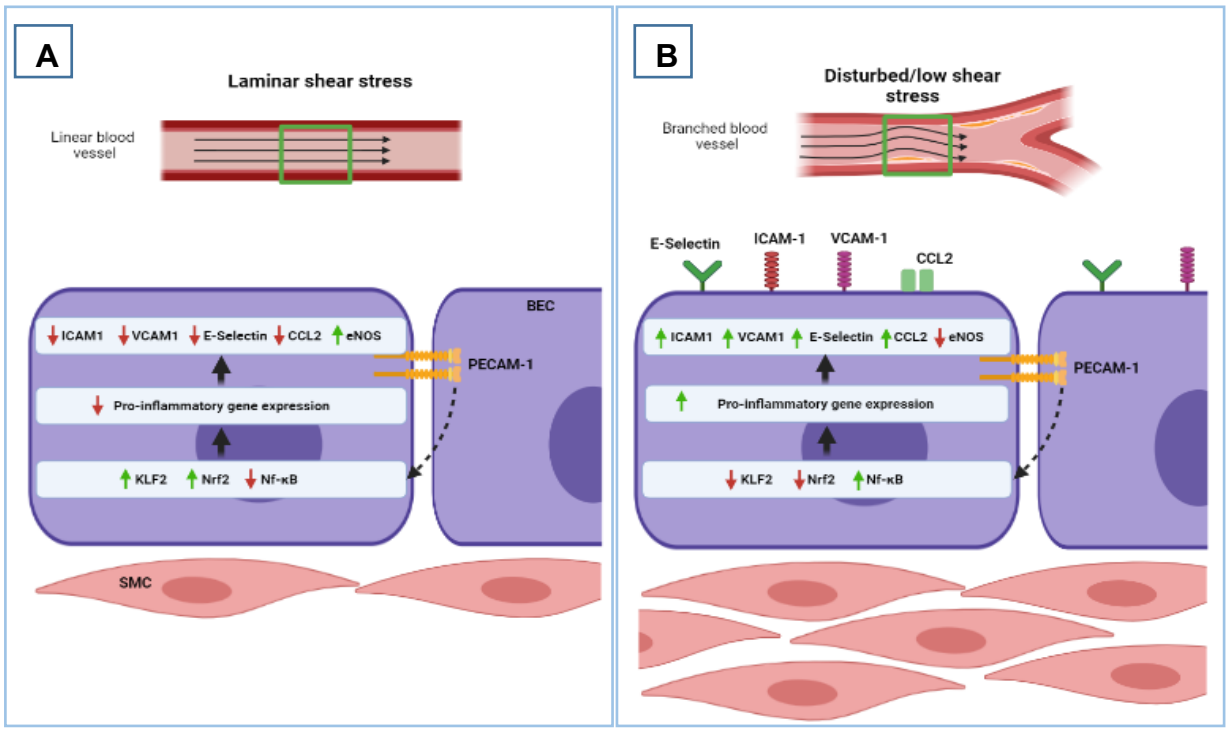


Figure 1-1: The role of shear stress on vascular endothelium

(A) Laminar shear stress is associated with reduced expression of adhesion molecules on the surface of vascular endothelium and secretion of chemoattractants such as CCL2. This is coupled with increased signalling via KLF2 and Nrf2 which promote vascular dilation and inhibit platelet coagulation which is considered athero-protective. **(B)** Oscillatory shear stress on the other hand observed in arterial bifurcations causes upregulation of adhesion molecules on the surface endothelium surface as well as increased NF-κb signalling which is responsible for inducing expression of pro-inflammatory genes during inflammatory disease (Diagram self-illustrated using Biorender)

1.2. Monocytes

1.2.1. Monocyte origin and development

Since the early introduction of the term ‘monocytes’ by Artur Pappenheim (in 1910) and Ilya Metchnikoff’s theory of phagocytosis (in 1892), subsequent years of research and investigation has allowed us to appreciate monocytes today as essential members of the mononuclear phagocyte system that are amongst the first cells to be recruited in an inflammatory response (Guilliams et al., 2018, Yona and Gordon, 2015, Iqbal et al., 2016). With a diameter measuring up to 20μm, monocytes are the largest of the leukocytes and constitute up to 5-10% of the circulating leukocyte population (Teh et al., 2019).

Monocytes are generated from primary lymphoid organs including the fetal liver during embryogenesis followed by the bone marrow during adult haematopoiesis where they are derived from the monocyte DC precursor and released into circulation upon the last cellular division (Naito et al., 1990, Fogg et al., 2006). During inflammatory conditions, secondary lymphoid organs such as the spleen can also behave as a peripheral monocyte reservoir and induce rapid monocyte recruitment as observed in atherosclerosis, with evidence indicating the expansion of splenic monocyte populations (Swirski et al., 2007, Leuschner et al., 2012, Robbins et al., 2012). Cytokines such as macrophage-colony-stimulating factor (MCSF) are imperative for their survival demonstrated by reduced circulating viable monocytes in MCSF-deficient mice and in vitro cell culture preparations (Becker et al., 1987, Dai et al., 2002, Kelley et al., 1999).

Monocytes have the unique ability to function as both effector and precursor cells for macrophages and dendritic cells, where they not only contribute to protective immunity but also act as major players in several disease pathologies (Kratofil et al., 2017, Teh et al., 2019). For many years it was believed that the sole purpose of circulating monocytes was to act as an intermediary for replenishing tissue resident macrophage pools (Furth and Cohn, 1968, Furth et al., 1972). However, technological advances have identified embryonic precursors for most (but not all) tissue resident macrophage populations that by-passed the monocytic stage and self-renewed in adulthood independently of peripheral blood monocytes. (Yona et al., 2013, Ginhoux et al., 2010, Guilliams et al., 2013).

1.2.2. Monocyte subsets and their characterisation

Early flow cytometry studies identified subpopulations of human monocytes according to their differential expression of CD14 (a PRR) and CD16 (a FCγ III receptor) proteins (Passlick et al., 1989). They have been broadly categorised into two main subsets defined as classical, $CD14^{+}CD16^{-}$ and non-classical, $CD14^{+}CD16^{+}$ monocytes, whereby the classical account for majority of the monocyte population (80-90%) (Ziegler-Heitbrock et al., 2010, Kapellos et al., 2019). The remaining (10-20%) non-classical subset can be further divided to give an intermediate subpopulation which express higher levels of CD14 than the non-classical and exist at low frequencies during homeostasis (Zawada et al., 2011, Grage-Griebenow et al., 2001, Gren et al., 2015, Wong et al., 2011, Merah-Mourah et al., 2020). Precise dissection of these two classes via flow cytometry gating strategies is challenging due to the

gradual changes in CD14 expression and so they are often collectively defined as $CD16^+$ (non-classical) cells (Ziegler-Heitbrock et al., 2010, Thomas et al., 2017). Although, 6-sulfo LacNAC (Slan) has been recently identified as a novel antigen restricted to the non-classical monocytes only which arguably enables distinction between the two subsets (Hofer et al., 2019).

Monocyte subsets can be further defined by gene expression profiles and additional surface markers including CX_3CR1 and HLA-DR (major histocompatibility complex II; MHC II) that are elevated on the non-classical monocytes with CCR5 being predominantly expressed by the intermediate subset (Wong et al., 2011, Ancuta et al., 2003, Geissmann et al., 2003, Ziegler-Heitbrock et al., 1993). On the other hand, markers such as CCR2, CD11b and CD36 are more abundantly expressed on the classical monocytes (Wong et al., 2011, Thomas et al., 2017, Gren et al., 2015, Roussel et al., 2017, Kapellos et al., 2019). Generally, the classification of monocytes subsets is applicable to other species as well as humans (Ziegler-Heitbrock, 2014). Notably, their murine counterparts are defined as $Ly6C^{high}CCR2^+CX_3CR1^{low}$ classical monocytes and $Ly6C^{low}CCR2^-CX_3CR1^{high}$ monocytes, equivalent to the non-classical population (Ziegler-Heitbrock et al., 2010, Guilliams et al., 2018). Proportionally, the classical:non-classical subsets exist at an equal ratio in mice (1:1) as opposed to in humans whereby the classical monocytes are more abundant (9:1) (Iqbal et al., 2016). Overall, the transcriptional profile between mice and human monocytes are broadly conserved, although some differences in gene expression exist. For example, peroxisome proliferator-activated receptor γ (PPARγ) expression is limited to murine monocytes only and absent on their human equivalents and opposing differences in phagocytic abilities and expression of phagocytic markers are evident across the two

species (Ingersoll et al., 2010, Gren et al., 2015). Hence, such differences should be taken into consideration when modelling human disease in mice.

1.2.3. Monocyte subsets and their function during steady state

Functionally, monocytes subsets exhibit incredible diversity which are dependent upon cellular localisation, environmental cues and the epigenetic landscape (Kapellos et al., 2019). However, it remains difficult to decipher the precise roles of each subset due to overlapping functions and conflicts in existing studies (Merah-Mourah et al., 2020).

Generally, monocytes in circulation are short lived with classical monocytes having the shortest lifespan of approximately 1 day whereas the non-classical are longer lived with a lifespan of around 7 days (Patel et al., 2017, Yona et al., 2013). This is supposedly a reflection of their function in steady state and inflammation whereby classical monocytes are more phagocytic and migratory in nature demonstrated by their increased expression in scavenger receptors (CD36 and CD163) and high levels of CCR2 which is required for monocyte mobilisation (Grage-Griebenow et al., 2000, Mukherjee et al., 2015, Tsou et al., 2007). In resting tissue, these monocytes are able differentiate into further mononuclear phagocytic cells. Interestingly it has been reported that Ly6C^{high} monocytes can constitutively migrate into resting tissue (mediated partially by L-selectin) without obligatory differentiation into macrophages where they can remain in a monocytic state for limited time during steady-state. The functional consequence of this is not entirely known, although they appear to demonstrate DC-like tissue surveillance properties with the ability to transport antigens to draining lymph nodes and increased expressed of MHC II (Jakubzick et al., 2013). Additionally, murine fate-mapping studies have revealed a developmental relationship

between monocyte subsets whereby classical monocyte ($Ly6C^{high}$) are able to sequentially convert into non-classical monocytes ($Ly6C^{low}$) via the intermediate subset under steady state and ultimately dictate the lifespan of its progeny (Yona et al., 2013, Yrlid et al., 2006).

Non-classical monocytes are notable for their role in continuously patrolling the luminal side of the vascular endothelium in a 'slow crawling' fashion with minimal transmigration during steady state (Auffray et al., 2007, Thomas et al., 2015b, Cros et al., 2010). This patrolling behaviour is dependent on both LFA-1 and CX_3CR1 as rapid dissociation of $Ly6C^{low}$ cells is observed with abrogation of either of these receptors in vitro (Carlin et al., 2013, Auffray et al., 2007). CX_3CR1 is expressed particularly highly on non-classical monocytes, and it is considered to provide a pro-survival signal via its interaction with CX_3CL1 (fractalkine), promoting their retention on the endothelium (Geissmann et al., 2003, Ancuta et al., 2003, White et al., 2014). Functionally, the patrolling mechanism appears to protect the endothelium from localised threat, as non-classical monocytes promote neutrophil recruitment and focal endothelial cell necrosis in response to TLR7-mediated danger signals (Carlin et al., 2013). Whilst intermediate monocytes are also express high levels of CX_3CR1, they appear to behave distinctly to the nonclassical subset as they do not actively patrol the endothelium (Cros et al., 2010).

1.2.4. Monocyte subsets and their function during inflammation

During inflammation monocytes are rapidly recruited from circulation to sites of tissue damage and infection via the leukocyte trafficking cascade, driven by conditioning of localised growth factors, pro-inflammatory chemokine, and cytokine signals (Shi and Pamer, 2011, Ley et al., 2007). Their recruitment aids in the clearance

of the initial inflammatory stimuli in order to restore tissue homeostasis. However, aberrant monocyte recruitment due to a dysregulated immune response can contribute to the pathogenesis of chronic inflammatory diseases including atherosclerosis and COVID-19 (Robbins and Swirski, 2010, Woollard and Geissmann, 2010, Vanderbeke et al., 2021).

Typically, classical monocytes are referred to as being 'pro-inflammatory' as they are the predominant subset recruited initially during infection (Serbina et al., 2008). Due to high expression of CCR2, they rapidly infiltrate tissue towards CCL2/MCP-1, where their main function has been highly attributed to phagocytosis (Mukherjee et al., 2015, Tsou et al., 2007). Non-classical monocytes are often classified as being anti-inflammatory by contributing more to wound healing processes. Yet, studies have shown in fact non-classical, $LY6C^{low}$ monocytes can be recruited even earlier than other monocyte subsets and contribute to the initial inflammatory response (Auffray et al., 2007). Although they account for a smaller proportion of the total monocyte population, activation of whole blood with LPS demonstrated that human non-classical monocytes were the main producers of pro-inflammatory cytokines TNFα and IL-1β, with minimal secretion of IL-10 compared to the classical subset (Mukherjee et al., 2015, Belge et al., 2002). Similar observations were seen following stimulation with other TLR ligands, showing increased production of IL-1, Il-12 and IL-6 by non-classical monocytes – all of which are upregulated during inflammation (Hofer et al., 2019).

Likewise, intermediates also demonstrate high phagocytic capacity as well as inflammatory function, with a greater ability to secrete pro-inflammatory cytokines in response to LPS compared to their classical counterparts. Their transcriptomic profile

is associated with an increased capacity for antigen presentation including high levels of HLA-DR, CD80 and CD86 and significantly higher expression of TLRs compared to the other two subsets (Passlick et al., 1989, Ziegler-Heitbrock et al., 1993, Mukherjee et al., 2015, Yang et al., 2014). Interestingly, several studies have reported an expansion of intermediate monocytes in chronic inflammatory diseases including rheumatoid arthritis, chronic kidney disease and atherosclerosis, whereby a greater proportion of intermediate monocyte was found to predict cardiovascular events in high-risk patients (Heine et al., 2012, Smiljanovic et al., 2018, SahBandar et al., 2020, Heine et al., 2008, Rogacev et al., 2012). The overlapping functional properties of intermediate monocytes suggests they are not a distinct endpoint of cellular differentiation but a transitional stage between classical and non-classical monocyte development.

Upon tissue infiltration monocytes have the capacity to differentiate primarily into macrophages (Shi and Pamer, 2011). The traditional dogma that classical monocytes differentiate into inflammatory macrophages and non-classical monocytes into anti-inflammatory macrophages is not entirely accurate. It appears that monocyte subsets can differentiate into macrophages that vary in their inflammatory degree based on monocyte subset, localisation and cellular signalling within the tissue microenvironment (Richards et al., 2013, Yang et al., 2014).

1.3. Macrophages

1.3.1. Macrophage origin and developments

Macrophages form an integral part of our immune system and were initially discovered by Metchnikoff in the early 19th century by their highly phagocytic phenotype (Epelman et al., 2014, Tauber, 2003). Since their discovery, evolutionary and ontological studies have revolutionised our understanding of macrophage biology based on their origins, development, and function both during homeostasis and inflammation. The traditional notion proposed by Van Furth suggesting that all tissue macrophages originate from circulating blood monocytes has been overturned due to recent technological advances utilising longitudinal fate-mapping models and transcriptional studies (Furth and Cohn, 1968, Furth et al., 1972, Yona et al., 2013, Lazarov et al., 2023). It is now apparent that most tissue resident macrophages are present in tissue before birth and are developed in the yolk sac during embryogenesis. These resident macrophages then go on to persist during adulthood and self-renew and proliferate independently of infiltrating monocytes (Ginhoux et al., 2010, Yona et al., 2013, Guilliams et al., 2013, Epelman et al., 2014). There are several exceptions to this paradigm showing intestinal resident macrophages requiring constant replenishment by LY6C^{hi} monocytes under steady state (Bain et al., 2013, Bain and Mowat, 2014).

Resident macrophages are located across almost all tissues and organs in the body, where they carry out tissue-specific functions based on distinct cues in their tissue microenvironments in order to maintain homeostasis (Mass et al., 2023, Lazarov et al., 2023). In response to inflammation and injury, peripheral blood monocytes are rapidly recruited to tissue and in the presence of surrounding cytokine signals, are able

to differentiate and acquire macrophage-like characteristics that behave distinctly to resident populations (Gordon and Taylor, 2005, Serbina and Pamer, 2006, Hoyer et al., 2019). Interestingly, upon loss of tissue resident macrophages, circulating monocytes are also able to replenish these populations under steady state and adopt a similar phenotype to resident tissue macrophages based on local gene expression and signals (Mosser and Edwards, 2008, Gordon and Taylor, 2005). However, it is informed that these repopulating monocytes fail to entirely recapitulate the transcriptomic profile of original resident macrophages highlighting the fact that both tissue-resident and monocyte derived macrophages are ultimately two distinct populations of dissimilar origin, development and function (Ginhoux et al., 2010, Lavin et al., 2014).

1.3.2. Macrophages and their role during homeostasis

As mentioned earlier, the fundamental attribute of macrophages is to phagocytose cellular debris and foreign material to perform tissue maintenance and surveillance (Park et al., 2022, Hirayama et al., 2017). Surface expression of scavenger receptors, TLRs and Tyro3/Axl/Mer (TAM) receptor tyrosine kinases allows binding of membrane components of pathogenic microorganisms, as well as apoptotic and necrotic cells, enabling macrophages to essentially ‘clean’ surrounding tissue (Li and Wu, 2021, Park et al., 2022). Clearance of apoptotic cells is essential to maintain immunological tolerance and eliminate pro-inflammatory stimuli (Zizzo et al., 2012). High levels of lipid phosphatidylserine found elevated on the surface of apoptotic cells are typically recognised by macrophages via the Mer tyrosine kinase (MerTK), a member of the TAM family involved in removal of early apoptotic cells. MerTK recognises phosphatidylserine through bridging molecule Gas6 resulting in the

suppression of pro-inflammatory signalling pathways (Burstyn-Cohen and Fresia, 2023, Healy et al., 2016, Zizzo et al., 2012). This homeostatic response enables macrophages to clear cellular debris without mounting an inflammatory immune response (Dransfield et al., 2015).

In addition to retaining their core phagocytic functions, macrophages are also capable of adapting to their place of tissue residence and contribute to complex processes such as angiogenesis, osteogenesis and neurogenesis (Park et al., 2022). Their integral role in preserving vascular integrity is demonstrated by impaired angiogenesis, cardiac function and vascular tone in murine models lacking MCSF – a key growth factor required for macrophage differentiation (Kubota et al., 2009, Lavine et al., 2014). Specifically in adventitial resident macrophages inhibition of MCSF resulted in increased arterial stiffness and collagen deposition correlating with increased susceptibility of atherosclerosis (Lim et al., 2018, van Popele et al., 2006). Similarly, the sentinel role of resident macrophages in bone is highlighted by catastrophic failure in bone repair models upon depletion of resident osteal macrophages (Alexander et al., 2011, Raggatt et al., 2014). Thus, one can appreciate the remarkable plasticity of macrophages based on their tissue microenvironment.

1.3.3. Macrophages and their role during inflammation

Based on their strategic localisation within tissue, resident macrophages pose as the first line of defence against invading pathogens, that are typically detected via TLRs (Varol et al., 2015, Mass et al., 2023, Gruber et al., 2018) . As opposed to the MerTK receptor, activation of TLR signalling triggers a cascade of signalling responses including activation of NF-κB and mitogen-activated protein kinase (MAPK) that drive

the production of pro-inflammatory cytokines such as TNF-α, IL-1β and interferon-γ (IFN-γ) required to propagate an inflammatory response (Lu et al., 2008, Swanson et al., 2020). Such responses activate core functional features of macrophages including phagocytosis, antigen presentation and secretion of immunomodulatory factors (cytokines and growth factors) with the aim of eradicating the initial stimuli (Mosser and Edwards, 2008, Park et al., 2022, Wynn et al., 2013).

As professional antigen presenting cells activated macrophages upregulate expression of MHC II and co-stimulatory molecules that stimulate CD4 T cell responses and B cell mediated antibody production (Fong et al., 2008, Arnold et al., 2015, Touil et al., 2023). It appears that this phenomenon is enhanced by the uptake of necrotic but not apoptotic cells (Barker et al., 2002). Subsequent secretion of inflammatory cytokines can promote recruitment of circulating monocytes into tissue giving rise to non-homeostatic differentiation into monocyte-derived macrophages (MDMs) (Park et al., 2022, Liu et al., 2019). In the cases of chronic disease resident macrophages fail to successfully resolve persistent inflammation causing rapid and aberrant recruitment of MDMs that can destroy resident macrophage niches required during steady state (Lavin et al., 2014, Okabe and Medzhitov, 2014). In addition to chemokine gradients (predominantly CCL2), circulating monocytes can also be trafficked into injured tissue via additional chemotactic agents, such as oxidised cholesterol which is responsible for the recruitment of monocytes into atherosclerotic plaques, giving rise to dysfunctional MDMs (Park et al., 2022, Moore and Tabas, 2011, Staprans et al., 2000). These newly recruited monocytes are subject to a hierarchy of various macrophage activation states that will be discussed in the next section.

1.3.4. Macrophage polarisation

Given the remarkable plasticity of macrophages, they can adopt and alter their phenotype based on environmental cues and signals from innate and adaptive immune responses, giving rise to macrophages of both pro- and anti-inflammatory in nature. Macrophages are traditionally classified into two major polarised states described as classical M1 and alternative M2 activated macrophages respectively (Mosser and Edwards, 2008, Stout et al., 2005, Martinez and Gordon, 2014).

Classical M1 macrophages are associated with a pro-inflammatory phenotype and are typically generated in during an immune response through activation of TLR agonists such as LPS causing the release inflammatory cytokines including TNF-α and IL-1β . The combination of both IFN-γ and TNF-α signalling is required to achieve M1 polarisation in vitro. In vivo, such signals are provided by TLR activation for TNF-α cytokine production. Both innate and adaptive immune cells are also required such as natural killer (NK) cells and T helper 1 (Th1) cells to drive maximal anti-bactericidal capacity. (Mosser and Edwards, 2008, Murray and Wynn, 2011, Borden et al., 2007). NK cells are an important transient source of IFN-γ which is then subsequently maintained by Th1 cells in order to sustain an M1 activated state (Dungan et al., 2014, Chen et al., 2023). On the other hand, alternative M2 macrophages are produced by resolving stimuli such as IL-4 or IL-13 that are typically known as Th2-related cytokines (Gordon and Martinez, 2010, Gause et al., 2013). This subset is classed as being anti-inflammatory, producing pro-resolving cytokines such as IL-10 and TGF-β. They are predominantly involved in tissue reparative and wound healing responses during inflammatory resolution (Mosser and Edwards, 2008).

Characterisation of both subsets are traditionally based on relative expression of multiple transcription factors, cell surface markers and cytokine profiles. Although, most often expression of many these markers is not restricted to one subset but distinction between the two populations is based on the varying degrees of their expression (Rostam et al., 2017). M1 macrophages are typically associated with high levels of co-stimulatory and antigen presentation markers including CD80, CD86 and MHC II (Jimenez-Uribe et al., 2019, Thiel et al., 2009, Ahmed and Ismail, 2020). Whilst CD80 expression typically being absent on M2 macrophages, CD86 and MHC II are both observed but to a lesser extent (Unuvar Purcu et al., 2022). M2 macrophages demonstrate enhanced phagocytic capacity and are presented with upregulated scavenger receptor expression such as CD36 and CD204 (Zizzo et al., 2012, Gordon and Martinez, 2010, Pennathur et al., 2015). They are also well defined by their expression of mannose receptor CD206 (Porcheray et al., 2005). Although it is important to note that expression of these markers appear to change over time based on macrophage circadian rhythm and different stimulation times which can greatly affect their levels both in vivo and in vitro (Cunningham et al., 2023, Collins et al., 2021, Unuvar Purcu et al., 2022).

Given the vast exposure of stimuli and environmental signals, it is apparent that macrophages can adopt multiple activation states that go beyond the traditional M1 and M2 classification which represent two extremes of a spectrum of activation responses (Mosser and Edwards, 2008, Munoz-Rojas et al., 2021). Transcriptomic analysis on human macrophages confirmed this phenomenon, where they identified specific transcription factors associated with at least nine different macrophage activation programmes (Xue et al., 2014). Subsequent studies have gone on to identify

additional macrophage subsets such as M4, M2a, M2b and M2c (Wang et al., 2019b, Gleissner et al., 2010, Li et al., 2022). However, overlap and lack of distinct markers for these subsets make is difficult to decipher precise populations. It is also evident that macrophages are not terminally polarised in a fixed state and are constantly evolving and altering activation states based on their microenvironment (Okabe and Medzhitov, 2014, Munoz-Rojas et al., 2021). Hence one can appreciate these studies are likely to have captured a single snapshot of macrophages in their continual switching of activation states.

Our understanding in macrophage biology during homeostasis and disease has enabled us to exploit macrophages as therapeutic targets for treatment (Chen et al., 2023). Whilst M1-like macrophages are important for driving effective immune responses against infection, their secretory factors can cause extensive tissue damage and expansion of Th17 cells that may serve as inflammatory perpetrators of chronic inflammatory diseases (Mosser and Edwards, 2008, El-Behi et al., 2011, Zambrano-Zaragoza et al., 2014). Whereas expansion of M2 macrophages can assist in cancer cell growth via immune suppression (Hao et al., 2012). Thus, regulating a balance between M1-mediated inflammation and M2-mediated resolution is critical to maintain homeostatic responses to inflammatory stimuli.

1.4. Atherosclerosis

1.4.1. Pathogenesis of atherosclerosis

Atherosclerosis is a chronic inflammatory, fibroproliferative disease of the arterial wall and remains the leading cause of cardiovascular disease (CVD)

associated mortality. It is not merely a cholesterol driven disease as assumed for much of the previous century but heavily driven by an intricate network of immune cells and inflammatory mediators (Wolf and Ley, 2019, Zhang et al., 1992, Weber and Noels, 2011, Soehnlein and Libby, 2021). Disease progression occurs over many years and is characterised by the formation of arterial plaque of great cellular and molecular complexity (Wolf and Ley, 2019). Prolonged build-up of atherosclerotic plaque can result in narrowing of the vessel lumen or complete thrombotic occlusion, which manifests major cardiovascular events such as acute coronary syndrome (ACS) (Moore and Tabas, 2011). Numerous studies have explored the relationship between inflammation and atherosclerosis and the first major clinical trial, known famously as the Canakinumab Anti-inflammatory Thrombosis Outcome Study (CANTOS) trial was amongst the first to consolidate the idea of targeting inflammation in human atherosclerosis. In the CANTOS trial, the use of canakinumab (an IL-1β monoclonal antibody) demonstrated a significant reduction in major adverse cardiovascular events, although levels of low-density lipoprotein (LDL) cholesterol levels only displayed modest reductions (Soehnlein and Libby, 2021).

The underlying pathophysiology of atherosclerosis is initiated by endothelial dysfunction, which as mentioned earlier on in the chapter in regulated by factors including haemodynamic forces, shears stress and key transcription factors (KLF2 and KLF4) that ultimately dictate the behaviour of endothelial cell structure and function (Cunningham and Gotlieb, 2005, Sweet et al., 2023). Plaque formation is particularly prone at sites of disturbed flow and areas of low shear stress since it is associated with reduced eNOS production, endothelial permeability, and vasodilation (Kong et al., 2017, Shirakura et al., 2023). Increased vascular permeability results in the

accumulation of LDLs that trigger persistent low-grade inflammation in the intima of the vessel wall (Geng et al., 2016, Zhang et al., 1992). Accumulated LDL are retained within the intima by the extracellular matrix, primarily via proteoglycan interactions where they become highly susceptible to biochemical modifications by ROS secreted by the inflammatory milieu (Williams and Tabas, 1995). This gives rise to oxidised LDL (oxLDL) which can promote injury and activation of quiescent endothelium, through expression of surface adhesion molecules and chemokine release that aberrantly recruit immune cells within the intima (Chen et al., 2002, Valente et al., 2014, Dimmeler et al., 1997). With monocytes being one of the first cells to be recruited, they can ingest oxLDL through scavenger receptors forming lipid-filled foam cells that form the critical early steps of arterial plaque formation (Herbin et al., 2016, Kopprasch et al., 2004). Unresolved inflammation can lead to successive recruitment of further adaptive immune cells, primarily being Th2 cells. The cumulative build up of lipids, cellular debris and necrotic cells triggers the formation of a necrotic core which is characteristic of vulnerable, unstable atherosclerotic plaques with increased susceptibly to rupture (Ross, 1995, Kolodgie et al., 2003).

Microscopic analysis of arteries from multiple age groups have advanced our understanding of atherosclerotic plaque progression and are broadly classified into 3 main categories being, the fatty streak, intermediate lesion and advanced lesion (Stary, 2000, Virmani et al., 2000, Bentzon et al., 2014). The formation of the early fatty streak marks the initial stages of plaque development defined by focal accumulations of lipid-filled monocyte derived foam cells (Ross, 1995). Such lesions are spread throughout the arterial tree, particularly at arterial bifurcations and branch points and can be observed within individuals as young as 10 years old (Frangos et al., 1999, Stary,

1989). Although, one does not assume these fatty streaks are atherosclerotic due to the potential for these lesions to regress in early stages (Hodis, 1995, Rahman and Fisher, 2018).

If left unresolved, these nascent fatty streaks can go on to develop fibroatheromas (intermediate lesions) consisting of layers of macrophages, foam cells, T cells and vascular smooth muscle cells (VSMC) that begin to form the necrotic core (Ross, 1995). Migration of VSMCs to the intima, promote the release of a matrix of collagen and elastin fibrils that form a fibrous cap varying in its thickness (Andreeva et al., 1997, Consuegra-Sanchez et al., 2024). Atheromas with a thin fibrous cap are typically identified by increased immune cell infiltration and loss of extracellular matrix making them increasingly prone to rupture resulting in potential cardiac death (Burke et al., 1997, Ross, 1995) (Figure 1-2). Both murine and human studies have shown that infiltrating immune cells can also invade the surrounding adventitia forming tertiary lymphoid structures that correlate with disease severity. These structures are composed predominantly of B and T cells that contribute to proatherogenic cytokine release and leukocyte recruitment into the intimal layer (Akhavanpoor et al., 2018, Houtkamp et al., 2001, Milutinovic et al., 2020).

Continual growth of such lesions leads to more advanced plaque formation and calcification causing restriction of the vessel lumen (Kramer et al., 2013). The enlarged necrotic core is concealed by dense layers of connective tissue which serves to increase plaque stability (Insull, 2009). Although, VSMCs can undergo a phenotypic switch and adopt macrophage like characteristics which is driven by transcription factor KLF4, leading to plaque remodelling and thinning of the fibrous cap over time (Zhang et al., 2022b, Soehnlein and Libby, 2021). Plaque remodelling is largely driven by

matrix metalloproteinases (MMPs) which are involved in the degradation of extracellular matrix proteins. Thus, higher MMPs levels, specifically MMP-7 and MMP-9 have been identified in regions of unstable plaque and have been associated with advanced cardiovascular disease (Volkov et al., 2018, Abbas et al., 2014). Increased activity of such MMPs may pose as potential biomarkers of plaque instability.

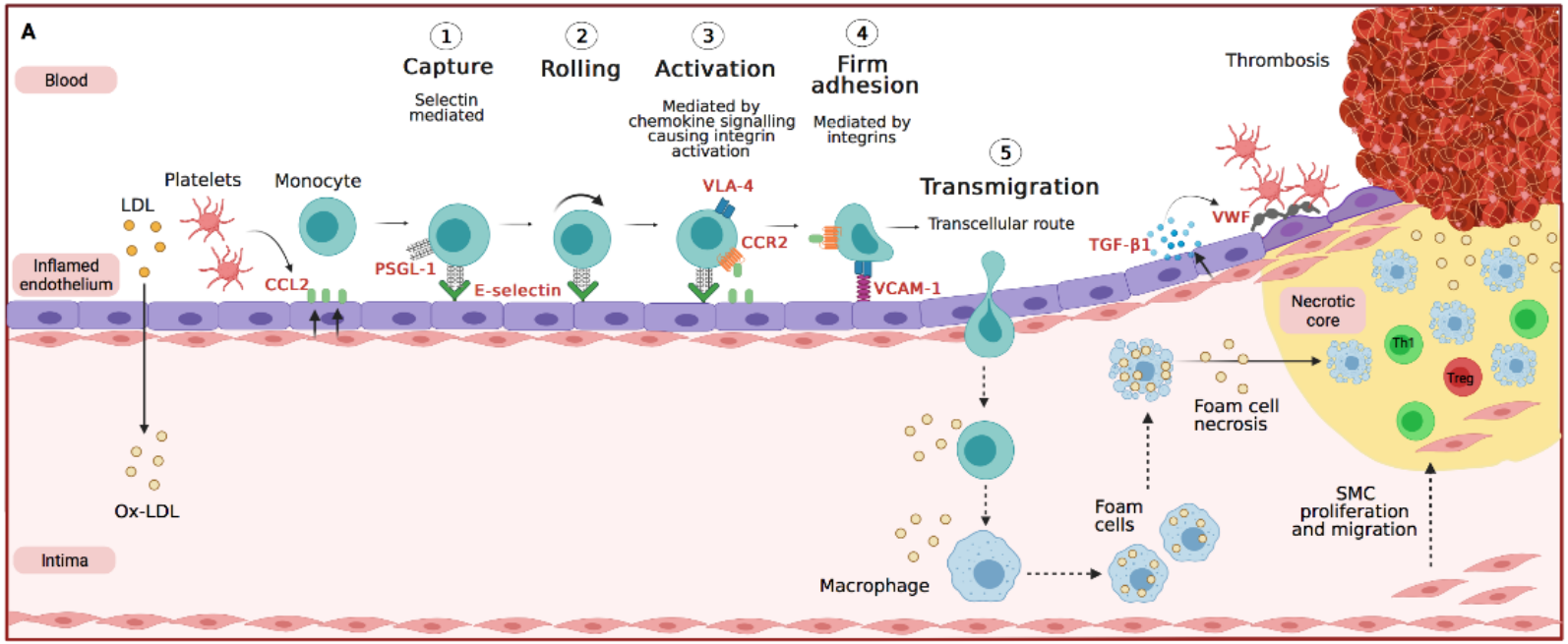


Figure 1-2: Leukocyte recruitment and transmigration in atherosclerosis.

Leukocytes are recruited into the intima via the classical adhesion cascade which contribute to plaque formation and thrombosis. Monocytes in circulation are recruited to the endothelium by chemotactic agents predominantly via CCL2 secretion by EC and platelets. Endothelial capture is mediated by E-selectin and its ligation to PSGL-1 on the surface of monocytes which promote rolling via low affinity interactions. CCR2-CCL2 chemokine signalling activates the VLA-4 integrin allowing firm adhesion of monocytes to occur via VCAM-1 ligation on endothelium. Subsequent transmigration into the intima via the transcellular route enables monocytes to differentiate into macrophages and ingest ox-LDL via scavenger receptors to generate lipid engorged foam cells. Accumulated ox-LDL eventually leads to foam cell necrosis which contribute to necrotic core formation, promoting plaque instability and rupture. Increased SMC proliferation and migration is also often observed in atherosclerosis which contributes to the necrotic core and promotes TGF-β1 release via crosstalk between neighbouring EC. This promotes increased platelet recruitment by upregulating von Willebrand factor (VWF) expression which is often observed in atherosclerosis and thrombosis (Adapted from Steinl and Kaufmann, 2015)

1.4.2. The role of endothelial activation during atherogenesis

The vascular endothelium forms the initial barrier for leukocyte transmigration into the intimal layer of the arterial wall. Numerous studies have utilised both *Apoe*$^{-/-}$ and *Ldlr*$^{-/-}$ mice models to investigate expression of adhesion molecules that regulate leukocyte recruitment and transmigration during atherogenesis (Zhang et al., 1992, Plump et al., 1992, Ishibashi et al., 1994). Selectins are crucial for the initial tethering of leukocytes to endothelium, and this has been demonstrated by Johnson et al, showing significantly smaller fatty streak formation in P-selectin and *Ldlr* double knockout mice (Johnson et al., 1997). This effect was further enhanced with E-selectin, P-selectin and *Ldlr* triple knockout mice where fatty streaks were five times smaller than single *Ldlr* knockout control mice (Dong et al., 1998). Subsequent firm adhesion of leukocytes is facilitated by integrins and their binding partners expressed on endothelium. The direct correlation in elevated VCAM-1 expression at sites of atherosclerotic lesions has been reported in several studies highlighting its supporting role in atherosclerosis (Masseau and Bowles, 2015, Fotis et al., 2012, Mu et al., 2015). For example, in *Apoe*$^{-/-}$ mice levels of VCAM-1 were found higher in lesion prone sites including arterial bifurcations (Nakashima et al., 1998). Furthermore, *Ldlr* and VCAM-1 double knockout mice presented with a greater degree of athero-resistance compared to *Ldlr*$^{-/-}$ alone (Cybulsky et al., 2001). Increased ICAM-1 levels have also been reported in *Apoe*$^{-/-}$ mice however, its role in atherogenesis appears to be inferior compared to VCAM-1 since deletion of VCAM-1 but not ICAM-1 significantly reduced nascent lesion formation (Cybulsky et al., 2001, Nakashima et al., 1998).

Homing of leukocytes to activated endothelium is further facilitated by secreted chemokines that are presented on the endothelial surface via glycosaminoglycans (Crola Da Silva et al., 2009). Recruitment of monocytes via the CCL2/CCL2 axis has received critical attention for its role in atherosclerosis (Zhang et al., 2022a). Importantly human aortic endothelial cells have shown to up-regulate expression of CCL2 following exposure to modified LDL leading to increased monocyte migration via CCR2 and both selective deletion and antibody blockade of CCL2 diminished lesion formation and macrophage accumulation in plaques in *Apoe*$^{-/-}$ mice (Schober et al., 2004, Boring et al., 1998, Cushing et al., 1990). Thus, dysfunctional and activated endothelium represents an initial hallmark of atherosclerotic disease development.

1.4.3. Monocytes in atherosclerosis

Monocytes are central in the development and progression of atherosclerosis and their recruitment into the arterial wall appears to be dependent on high levels of circulating LDL that are prone to oxidation (Østerud and Bjørklid, 2003). Increased monocyte production in the bone marrow has been reported in hypercholesterolemic animal models driven by growth factors MCSF and IL-3. Elevated circulating levels of monocytes are also found in patients with coronary artery disease (Wang et al., 2014). These monocytes are recruited to the earliest fatty lesions and are evident at all stages of plaque development (Østerud and Bjørklid, 2003). As mentioned earlier, initial homing and recruitment of monocytes is highly dependent on the CCL2/CCR2 axis, although the importance of additional chemokines including CCL5, CXCL1 and CX_3CL1 have also been implicated in the context of atherosclerosis (Tacke et al., 2007, Hilgendorf et al., 2015). Soehnlein et al demonstrated that in fact CXCL1 and CCR5 are predominantly involved in directly attracting monocytes to atherosclerotic lesions whilst CCL2 is more importantly involved in the mobilisation of monocytes in circulation (Soehnlein et al., 2013). Aside from the role of chemokines in recruitment, evidence for CX_3CL1 as a monocyte survival signal has been indicated, whereby absence of CX_3CL1 or its cognate receptor CX_3CR1 conferred with a significant reduction in levels of circulating monocytes and increased apoptosis of resident plaque macrophages that can be rescued by antiapoptotic factor Bcl2 expression (Landsman et al., 2009).

Following recruitment, monocytes are captured on endothelium primarily by P-selectin expressed both on activated on endothelium and platelets (Burger and Wagner, 2003). As well as direct recruitment of monocyte to endothelium, secondary

recruitment via platelet-EC interactions can also occur whereby activated platelets themselves can directly adhere to inflamed endothelium enabling monocytes to bind via PSGL-1 on their surface (Huo et al., 2003, Massberg et al., 2002). An additional scenario by which platelets interact with monocytes is via the formation of heterotypic monocyte-platelet aggregates formed in circulation prior to EC contact (Rinder et al., 1991). Formation of such aggregates are linked with athero-thrombotic diseases with increased prevalence observed in coronary artery disease (Furman et al., 1998). Subsequently, rolling monocytes interact with CCL2 expressed on endothelium leading to mainly VLA-4 integrin activation and stabilisation of adhesion on VCAM-1 (Alon et al., 1995). Prolonged blockade of VLA-4 demonstrated a significant reduction in leukocyte recruitment and neointimal growth, suggesting a critical role for its development of atherosclerotic lesions (Barringhaus et al., 2004). Upon transmigration into the intimal layer, monocytes can differentiate into macrophage and foam cells following assimilation of oxLDL.

Numerous studies have attempted to classify monocyte subsets in circulation during atherosclerosis. Murine models of hypercholesteremia are typically associated with elevated levels of Ly6C^{hi} monocytes which demonstrate an increased migratory phenotype and a greater propensity to infiltrate the arterial wall (Swirski et al., 2007). Yet, more recently, clinical human studies have reported a specific expansion of circulating intermediate monocytes in patients with unstable angina and in dialysis patients with increased cardiovascular disease risk (Justo-Junior et al., 2019, Heine et al., 2012). Similarly, patients with thin cap unstable atheroma, had the largest expansion of intermediate monocytes (Zhuang et al., 2017). A study looking at a cohort of healthy adults also identified a strong correlation between intermediate monocyte

counts and carotid intima-media thickness (a marker for atherosclerosis) suggesting levels of intermediate monocytes may act as a potential predictor of cardiovascular disease risk (SahBandar et al., 2020).

1.4.4. Macrophages in atherosclerosis

Macrophages are amongst the key players in the progression of atherosclerosis and acts as a major source of pro-inflammatory mediators in plaque (Moore et al., 2013). Within the intima, monocytes and macrophages begin scavenging accumulated oxLDL via scavenger receptors (considered as PRRs) on their surface. The rapid build-up of lipoproteins coupled with the dysfunctional clearance of stored cholesterol leads to the development of lipid-laden monocytes/macrophages that are classically described as foam cells (Ouimet et al., 2011, Flynn et al., 2019, Bobryhev et al., 2016).

Uptake of modified LDL via has significant functional and phenotypic consequences on macrophages causing changes in their inflammatory profile (Bobryhev et al., 2016). Typically, studies have demonstrated that incubation with modified LDL promote a pro-inflammatory phenotype in macrophages associated with increased TNF-α and IL-6 release and a phenotypic switch from an M2 to an M1-like nature (Al-Sharea et al., 2016, van Tits et al., 2011). This may be a result of enhanced TLR expression and activation in macrophages that is observed with oxLDL uptake. TLR4 in particular is highly associated with atherosclerotic plaques and its expression has shown to be necessary for oxLDL-induced macrophage differentiation into foam cells and atherosclerosis-associated inflammation (Howell et al., 2011, Higashimori et al., 2011). In addition, assimilation of cholesterol crystals by macrophages within atherosclerotic plaque can activate the NOD- LRR and pyrin domain-containing protein

(NLRP) 3 inflammasome leading to secretion of pro-inflammatory cytokine IL-1β (Duewell et al., 2010, Freigang et al., 2011). Interestingly it has been demonstrated that persistent activation of innate immune cells through PAMPs and DAMPs such as oxLDL can in fact lead to trained immunity in macrophages with enhanced cholesterol accumulation and expression of MMPs being observed in oxLDL-trained macrophages compared to controls. Hence, the concept of immunological memory is not just confined to adaptive immunity but also to the innate immune system (Bekkering et al., 2014, Zhong et al., 2020). Contrary to this, more recent studies have elucidated that lipid-laden macrophages (foam cells) adopt a contradictory anti-inflammatory transcriptional profile and 'deactivated' phenotype. Although, the functional relevance of this in the context of disease is not entirely clear and will be discussed further in following sections (Kim et al., 2018, Spann et al., 2012, Cochain et al., 2018).

The ratio of M1-like to M2-like activation states is largely dependent on the inflammatory environment within plaque (Wu et al., 2023). Histological examinations have revealed pro-inflammatory M1 macrophages are predominantly located within the shoulder regions of plaque that are more prone to rupture due to increased immune infiltration and higher lipid content. Whereas M2 anti-inflammatory macrophages are commonly found in more stable regions of plaque and near newly formed blood vessels (Stoger et al., 2012, Wang et al., 2019c). Whilst M2 macrophages are typically associated with inflammatory resolution and clearance of apoptotic cells, their increased expression of scavenger receptors makes them more susceptible to modified LDL uptake (van Tits et al., 2011, Bisgaard et al., 2016). This can lead to reduced KLF2 expression shifting M2 macrophages towards an M1-like proinflammatory phenotype (van Tits et al., 2011). As mentioned earlier, polarisation

of macrophages is a dynamic process as they are constantly changing their activation states based on surrounding signals. M2 macrophages also express higher levels of MMP-9 that is elevated in rupture-prone lesions due to its role in degrading extracellular matrix (Jager et al., 2016, Li et al., 2020b). Thus, the traditional dogma of M1 macrophages being pro-atherogenic and M2-macrophages being anti-atherogenic may not be so clearly defined and maybe dependent on the state and complexity of the disease environment.

Numerous studies have highlighted that regulating monocyte and macrophage emigration, proliferation and death is crucial in regressing atherosclerotic plaques. The number of macrophages in plaque correlates with disease progression as earlier lesions have a lower percentage of macrophages determined by the recruitment of monocytes in circulation. Particularly during the early stages of atherosclerosis, increased macrophage emigration is evident although this appears to diminish significantly with disease progression (Fisher, 2016). This process is driven by an intricate balance between guidance cues and chemokines that are modified upon cholesterol loading (Moore et al., 2013). For example, increased CCR7 expression is observed in macrophages within regressing plaques in conjunction with upregulated cell motility factors indicating a greater migratory capacity of these cells (Feig et al., 2011, Trogan et al., 2006). Whereas deficiency in mediators such as netrin-1 showed reduced plaque progression and macrophage egress in *Ldlr*$^{-/-}$ mice suggesting netrin-1 may play a role in macrophage retention in plaque (van Gils et al., 2012, Moore et al., 2013).

Whilst the majority of macrophages are typically replenished by circulating peripheral blood monocytes, more recently studies have demonstrated in fact lesional

macrophages in atherosclerosis are heavily derived from local proliferation of aortic macrophages (Murphy and Tall, 2014). Evidence for this was demonstrated in *Apoe*$^{-/-}$ mice joined by parabiosis, whereby chimerism of lesional macrophages were less than 5% and surprisingly 87% of BrdU labelling was incorporated in the host lesional macrophages, highlighting the idea that local proliferation is largely responsible for the accumulation of macrophages within plaque (Robbins et al., 2013).

Overall macrophages represent a central role in the development of atherogenesis through multiple mechanistic avenues as mentioned above. Thus, targeting these cells is highly attractive as therapeutic targets.

1.5. Foam cells

1.5.1. Foam cell formation

Foam cell formation is considered a hallmark of atherosclerotic disease and are a result unregulated internalisation and accumulation of modified lipids by macrophages. The presence of foam cells is detected at the very early stages of disease during the development of the initial fatty streak and the proportion of foam cells increases with continual progression of disease. In advanced lesions, excessive build-up of foam cells within plaque leads to necrosis and enlargement of the lipid core. Macrophages in plaque have shown to express structurally distinct scavenger receptors that were originally described for their ability to recognise and internalise various forms of modified LDL. OxLDL is considered the predominant modified form of LDL that drives atherogenesis and its uptake is mediated primarily via the CD36 scavenger receptor (Endemann et al., 1993, Tsukamoto et al., 2002). Numerous

studies in *Apoe*$^{-/-}$ mice lacking the CD36 receptor demonstrated significant reductions in atherosclerotic lesions (Febbraio et al., 2000, Moore et al., 2005). As a PRR, activation of CD36 triggers an innate immune response causing secretion of pro-inflammatory cytokines that promote further immune cell recruitment and oxidation of LDL (Stewart et al., 2010).

In addition to oxLDL, various other biochemically modified forms of LDL have been reported. OxLDL actually serves as an umbrella term encompassing a diverse range of oxidative alterations occurring within the LDL particle, such as the addition of a malondialdehyde group on to apolipoprotein B, forming malondialdehyde LDL (Ma-LDL). The process of acetylation can also occur during atherosclerosis forming acetylated LDL (acLDL) although its detection and significance is less frequent in vivo compared to oxLDL. It appears that macrophage scavenger receptors have varying degrees of affinity for different forms of modified LDL. For example, CD36 has been shown to have a lower affinity binding for acLDL compared to the classical oxLDL particles. Instead binding of acLDL is preferentially targeted to the CD204 scavenger receptor that is predominantly expressed on the surface of macrophages but also found on endothelial cells and VSMCs (Goldstein et al., 1979a, Lougheed et al., 1999). On the other hand, MaLDL which is a reactive aldehyde, is considered to be highly atherogenic and has increased affinity for the stabilin-1 scavenger receptor, although studies in *Ldlr*$^{-/-}$ mice with stabilin-1 deficiency demonstrated no alterations in plaque development (Nahon et al., 2019, Manta et al., 2022). This suggests that whilst stabilin-1 may play a role in lipid uptake, other mechanisms of lipid metabolism may compensate for its absence.

Although macrophages are considered the primary origin of foam cells, foam cells can also originate from alternate cells within the vessel wall (Aqel et al., 1985, Gown et al., 1986). The use of lineage-tracing studies, flow cytometry and single-cell RNA sequencing analyses have reported VSMCs as a major source of foam cell formation as they also express scavenger receptors on their surface similarly to macrophages, making them capable of ingesting modified LDL (Soehnlein and Libby, 2021, Owsiany et al., 2019, Durham et al., 2018). Additionally, these VSMCs can also undergo trans-differentiation, losing contractile markers and gain the expression of macrophage markers such as CD68 (Feil et al., 2014). Evidence for this has been presented in numerous studies showing that a large proportion of plaque macrophages are of VSMC origin (Allahverdian et al., 2014). Thus, therapeutic targeting of the phenotypic switch of VSMCs may prove to be a beneficial avenue to limit macrophage numbers in plaque.

1.5.2. Cholesterol metabolism

A pivotal stage of foam cell formation involves the handling and metabolism of cholesterol which includes uptake of cholesterol-carrying lipoproteins, cholesterol esterification and efflux (Javadifar et al., 2021, Ghosh et al., 2010). Within blood cholesterol typically exists in two forms being free cholesterol and as cholesteryl esters (CE) which are components of circulating lipoproteins, such as LDL (the major cholesterol-carrying lipoprotein), very low density lipoproteins (VLDL), and high density lipoproteins (HDL) (Gerl et al., 2018). Cholesterol processing is subject to rigorous regulation due to its importance in maintaining normal cellular function and homeostasis, including modulation of cellular membrane fluidity and serving as a primary substrate for bile acids and steroid hormones production (Brown and

Goldstein, 1986). However, persistent dysregulation of such pathways leads to excessive accumulation of cholesterol, that consequently lead to foam cell formation (Ghosh et al., 2010). Physiological uptake of LDL by macrophages is carried out by the LDL-receptor (LDLR) that is regulated by the content of cellular cholesterol. However modified LDL (such as oxLDL) is taken up by scavenger receptors as mentioned earlier in the chapter – a process that is unregulated leading to persistent and aberrant accumulation of cholesterol-carrying modified LDL observed typically during during foam cell formation (Javadifar et al., 2021).

Modified LDL is hydrolysed in the late endosome by lysosomal acid lipase (LAL) and these metabolised lipids are ligands for lipid-activated transcription factors, peroxisome proliferator-activated receptor α (PPARα) and PPARγ that induce expression ATP-binding cassette transporters A1 and G1 (ABCA1) and (ABCG1) that transport free cholesterol out of the cell (Hoeffner et al., 2023, Nagy et al., 1998, Westerterp and Tall, 2020). Cholesterol efflux is a critical event during cholesterol metabolism to unload excess cholesterol via cholesterol transporters (ABCA1 and ABCG1) (Westerterp and Tall, 2020). However, saturation of the efflux pathway results in accumulation of free cellular cholesterol that are re-esterified to form CEs by acyl CoA acetyl transferase 1 (ACAT1) - an enzyme found ubiquitously expressed in the endoplasmic reticulum (ER) (Rogers et al., 2015). CEs are stored in the form of lipid droplets and are hydrolysed by neutral cholesteryl ester hydrolase (nCEH) to generate free cholesterol required by the cell (Igarashi et al., 2010). The concerted balance of both enzymes (nCEH and ACAT1) is required to regulate cholesterol levels. An alternate mechanism for lipid droplet degradation is known as lipophagy – a selective form of autophagy that specifically targets lipid droplets for their catabolism. This

process involves engulfment of lipid droplets by autophagosomes causing release of free cholesterol for cellular efflux (Robichaud et al., 2022, Robichaud et al., 2021). However, overtime the build up of modified LDL surpasses the normal capacity of the cell to handle, leading to cellular stress and apoptosis (Figure 1-3).

Several strategies have been implicated in the regulation of CE accumulation including inhibition of ACAT1, which demonstrated up to a 90% reduction in aortic atherosclerosis in cholesterol fed rabbits as well a significant reduction in the aortic fatty streak region in hypercholesterolemic hamsters (Matsuo et al., 1995, Nicolosi et al., 1998). However contradicting studies have shown no changes in the development of atherosclerotic lesions along with the failure to inhibit foam cell formation in ACAT1 knockout *Apoe*$^{-/-}$ and *Ldlr*$^{-/-}$ mice models (Fazio et al., 2001, Fazio et al., 2005). In fact, a major consequence of ACAT1 inhibition is the accumulation of free cholesterol in the ER resulting in ER stress and toxicity (Ghosh et al., 2010). Similarly, targeting the suppression of nCEH showed a significant increase in CE accumulation and accelerated growth in atherosclerotic lesions in *Apoe*$^{-/-}$ and *Ldlr*$^{-/-}$ mice (Sekiya et al., 2009, Sekiya et al., 2014). Thus, future studies should focus on targeting such enzymes simultaneously in order to modulate cholesterol metabolism in macrophages.

Targeting cholesterol efflux pathways is an alternative strategy to promote the release of free cholesterol from the cell to extracellular acceptors such as HDL that transport cholesterol back to the liver for excretion (Javadifar et al., 2021, Ouimet et al., 2019). ABCA1 and ABCG1 are primarily involved in cholesterol efflux and deficiencies in these pathways have proven to increase the risk atherogenesis due to the accumulation of free cholesterol within the cell (Yvan-Charvet et al., 2007, Javadifar et al., 2021). Patients with mutations in the ABCA1 gene presented with

significantly low HDL levels as well an increased pro-inflammatory state within the arterial wall demonstrated by elevated pro-inflammatory gene expression and cytokine levels (Bochem et al., 2015). Interestingly it seems as though both transporters can compensate for the deficiency of one another since a marked increase in ABCG1 expression was observed in *Abca1*$^{-/-}$ macrophages (Yvan-Charvet et al., 2007). Expression of both ABCA1 and ABCG1 are regulated at both the transcriptional and translational levels by PPARs, and overexpression of both have shown to protect against atherosclerosis (Munch et al., 2012, Singaraja et al., 2002).

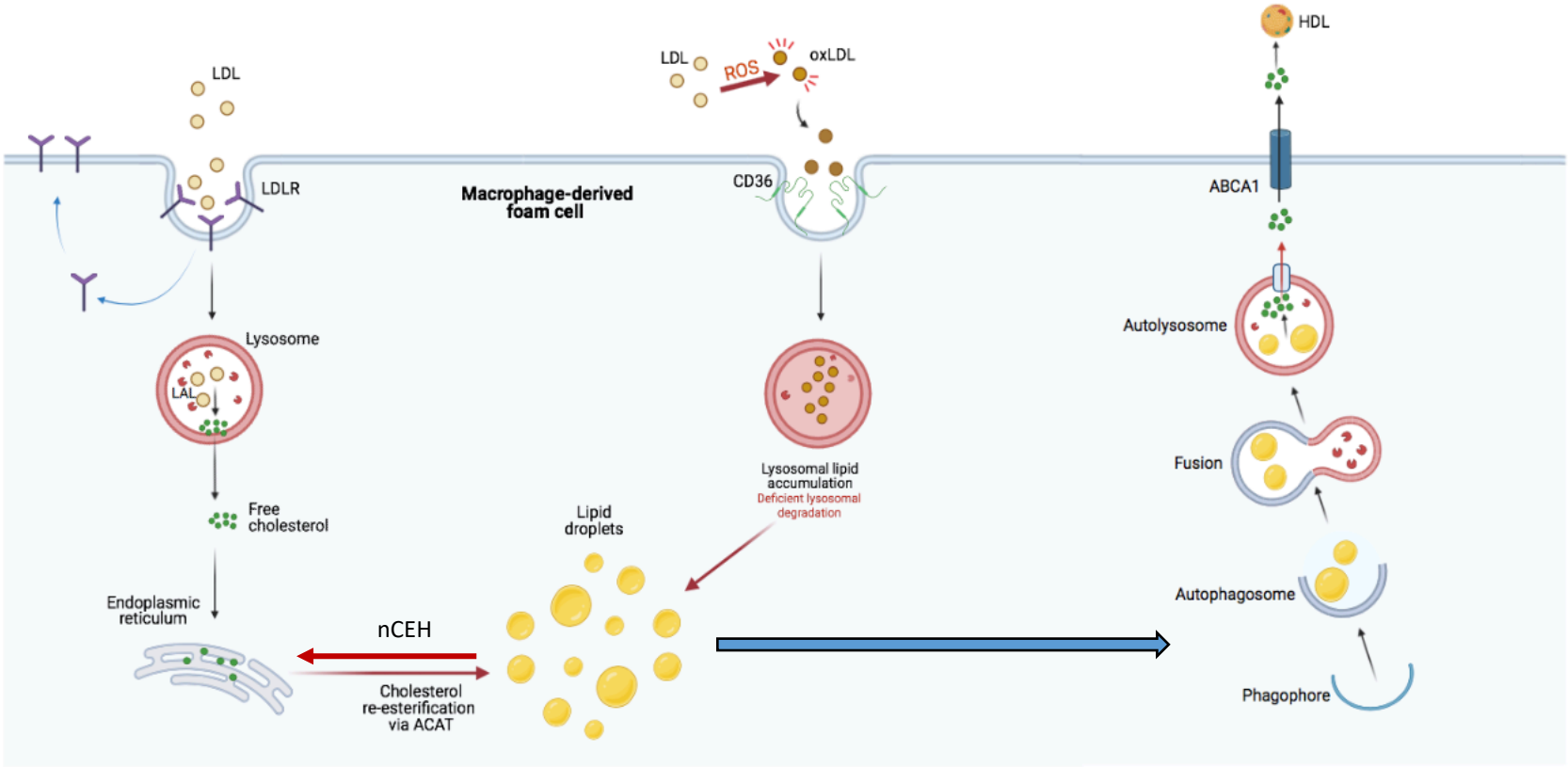


Figure 1-3: Cholesterol metabolism in macrophage-derived foam cells.

LDLR plays a critical role in regulating cholesterol homeostasis in plasma by intaking LDL particles into the cell to generate free cholesterol to maintain cellular function. This process is highly regulated to maintain optimum levels of cholesterol uptake. However, oxLDL is taken up via scavenger receptors such as CD36 expressed on the surface of macrophages. This is an unregulated process causing excessive accumulation of oxLDL in lysosomes that is stored in lipid droplets. Excessive lipid droplet formation is characteristic of a foam cell phenotype. ACAT is required to convert free cholesterol that is not required by the cell for storage as lipid droplets whereas nCEH is needed for lipid droplet catabolism. Free cholesterol is also generated by the process of lipophagy whereby lipid droplets are engulfed by autphagosomes for lysosomal breakdown to generate free cholesterol that is effuxed out the cell via ABC transporters such as ABCA1 and transported to HDL (Diagram self-illustrated using Biorender).

1.5.3. The cellular identity and phenotypic characteristics of foam cells

Accumulated studies have demonstrated the concept of lipid-driven inflammation as the central tenet in the development of atherosclerosis. With foam cells being the hallmark of atherogenesis, evidence has largely focused on foam cell biology as the central regulator of lipid-driven inflammation. It is evident that modified LDL and its retention plays a major role in driving inflammation within the vessel wall and uptake by macrophages can alter their phenotypic and functional behaviour. However, till today the precise function and identify of lipid associated macrophages (foam cells) remains actively debated making it difficult to isolate these cells as a pure population from tissue.

More recently the use of single-cell transcriptomic analysis has been used to dissect the cellular composition of atherosclerotic plaque both in mouse and human revealing a spectrum of macrophages which goes beyond the simplified M1 and M2 polarisation states. Consistently across these studies they have identified a population of lipid associated macrophages associated with high levels of TREM2 gene expression. These cells show enrichment for gene signatures associated with lipid metabolism, cholesterol efflux and oxidative stress – all of which are reminiscent of a foam cell phenotype. (Lin et al., 2019, Kim et al., 2018, Cochain et al., 2018, Song et al., 2020). However, contradictory to the perceived notion of foam cell behaviours, these TREM2^{hi} macrophages lack an inflammatory signature. In murine atherosclerotic plaque, foamy macrophages (TREM2^{hi}) demonstrated a dramatically reduced expression of inflammatory genes such as IL-1β and TNF-α compared to intimal non-

foamy macrophages (Kim et al., 2018). Parallel to these findings, foam cells derived from peritoneal macrophages have also shown to exhibit a so called ‘deactivated’ phenotype with a suppression of pro-inflammatory genes (Spann et al., 2012). An additional interesting observation of these intimal foam cells was the expression of genes associated with osteoclastogenesis suggesting a role of TREM2^{hi} macrophages in atherosclerotic lesion calcification (Cochain et al., 2018). There are a number of studies that have highlighted the importance of TREM2 expression in driving lipid homeostasis in macrophages and its role in acting as a key regulator in foam cell formation (Jaitin et al., 2019, Damisah et al., 2020). Deletion of TREM2 was associated with enhanced foam cell death and reduction in plaque size, suggesting TREM2 poses as a potential therapeutic target in the treatment for atherosclerosis (Patterson et al., 2023). These findings have raised the question as to whether foam cells themselves are actively pro-inflammatory in nature or whether they require external cross-cellular signalling in order contribute to inflammation during atherosclerosis disease progression.

The major disadvantage of these transcriptomic studies is the fact that they have merely captured a single snapshot of plaque at a given point in time and have failed to capture the cellular composition of plaque and the genomic profile of foam cells at different stages of disease. Although interestingly Dib et al, recently discovered an additional population of lipid associated macrophages in plaque that express high levels of perilipin-2 (PLIN2) and TREM1 (PLIN2^{hi}/TREM1^{hi}). In contrast to TREM2^{hi} foamy macrophages, these PLIN2^{hi}/TREM1^{hi} population exhibit a transcriptional signature that is associated with lipid accumulation and inflammation and likely contribute to atherogenic monocyte recruitment due to increased expression of

chemokines CCL2 and CCL7. They demonstrated in this study that in fact the commonly identified TREM2^{hi} foam cells are not in a static transcriptional state but can transition towards a PLIN2^{hi}/TREM1^{hi} pro-inflammatory phenotype and that this transition is triggered by TLR2 signalling (Dib et al., 2023). Thus, it is likely that cellular cross talk between cells within plaque may trigger the release of intrinsic TLR2 ligands that facilitate switching of anti-inflammatory TREM2^{hi} foam cells into an activated pro-inflammatory state (PLIN2^{hi}/TREM1^{hi}). Such ligands may include modified lipoproteins that can be recognised by TLR2 and TLR4 and have been shown to contribute to foam cell formation (Seimon et al., 2010, Stewart et al., 2010). To conclude, it is evident that the characterisation and identification of foam cells is more complex than expected, since they exhibit multiple activation states that is driven by endogenous signals within plaque and this is not only dependent on plaque localisation but also the stage of disease progression.

1.6. Polyunsaturated fatty acids (PUFAs) and their role in inflammation

1.6.1. Omega-6 and omega-3 PUFAs

Polyunsaturated fatty acids (PUFAs) are essential lipids that from an integral component of membrane phospholipids and are precursors to a pool of bioactive lipid mediators that modulate inflammatory processes within the body. Among the most studied are the omega-3 PUFAs that include eicosapentaenoic acid (EPA) and docosahexaenoic acid (DHA) as well as omega 6 PUFAs including arachidonic acid (ARA) (Calder and Grimble, 2002, Michalak et al., 2016). Due to the body's inability to synthesise these lipids in the body, they are obtained naturally from dietary sources

rich in linoleic acid and α-linoleic acid. Via a series of elongation and desaturation steps linoleic acid is converted to ARA, and a-linoleic acid to EPA and DHA (Dyall, 2017).

PUFAs are notable for their ability to modulate immune cell function by giving rise to both pro-inflammatory and anti-inflammatory eicosanoids which are metabolised by key enzymatic pathways including cyclooxygenase (COX), lipid oxygenase (LOX) and cytochrome P450 (CYP450) (Dyall et al., 2022). The metabolism of omega-6 PUFAs, like ARA predominately result in the synthesis of pro-inflammatory metabolites including prostaglandins (PG), thromboxanes (TX) and leukotrienes (LT) which are generated in a cell-specific manner. Macrophages are a major source of prostaglandins, prostaglandin E_2 (PGE_2) and prostaglandin F_2 (PGF_2) which are both associated with systemic inflammation and vascular dysfunction (Calder and Grimble, 2002). Enhanced PGE_2 was linked with increased IL-6 production in murine models of chronic inflammation, and similarly PGF_2 production can stimulate release of IL-1β and TNF-α, promoting increased leukocyte recruitment to sites of inflammation (Williams and Shacter, 1997, Hinson et al., 1996, Anderson et al., 1996, Pang and Knox, 1997). Additionally, LTs such as LTB4 are widely known for their pro-inflammatory activities, including enhanced chemotaxis, cytokine production and activation of the inflammasome (Gagnon et al., 1989, Salina et al., 2020). Excessive amounts of omega-6 PUFA intake observed in modern western diets can ultimately drive low-grade inflammation and endothelial activation that contribute to development of chronic inflammatory diseases such as atherosclerosis (Dyall, 2017, DiNicolantonio and O'Keefe, 2018).

On the other hand, omega-3 PUFAs (EPA and DHA) derived from fish oil are precursors to anti-inflammatory mediators including SPMs such as resolvins, protectins and maresins and increased intake in omega-3 PUFAs have shown to suppress pro-

inflammatory effects and improve prognosis of numerous chronic inflammatory diseases (Grimble et al., 2002, Adkins and Kelley, 2010, Sethi et al., 2002, Kromhout et al., 1985, Mason et al., 2020). Several randomised control trials and epidemiological studies including the more recent Reduction of Cardiovascular Events with EPA Intervention Trial (REDUCE-IT) have shown evidence of a protective effect of omega-3 PUFAs in cardiovascular disease (He et al., 2004, Bucher et al., 2002, Yokoyama et al., 2007a, Bhatt et al., 2019, Sekimoto et al., 2023). Results from such studies have revealed an inverse relationship with coronary heart disease and overall sudden death in cardiovascular disease patients. However, not all studies agree with these findings and contradictions in results maybe be due to discrepancies in age and dosage administered to individuals across these studies (Jialal et al., 1999, Leng et al., 1998).

Although structurally similar, both EPA and DHA exhibit distinct physical and chemical properties. EPA monotherapy demonstrated a reduced the risk of nonfatal cardiovascular endpoints compared to EPA and DHA in combination or DHA alone (Khan et al., 2021). Additionally, EPA prevented endothelial dysfunction and stabilisation of plaque in *Apoe*$^{-/-}$ mice (Omura et al., 2001, Matsumoto et al., 2008). The precise mechanism of omega-3 PUFAs in cardiovascular disease is not entirely elucidated. However, several in vivo and in vitro research studies provide insight into possible mechanisms of action. Whilst DHA may be particularly effective in decreasing endothelial adhesion molecule expression, EPA was shown to inhibit the transformation of macrophages into foam cells in high fat diet fed mice (De Caterina et al., 1995, Nagatake et al., 2021). In another study, EPA was able to stimulate ABCA1-mediated cholesterol efflux from both human and murine macrophages in vitro (Dakroub et al., 2021, Moss et al., 2016). These findings suggest that a potential method utilised by EPA in protecting against cardiovascular disease may be through the inhibition of foam cell formation. Both

EPA and ARA competitively bind COX and LOX enzymes as a substrate to generate lipid metabolites, therefore the increased availability of EPA promotes the shift towards anti-inflammatory, pro-resolving lipid mediator generation. Hence, the overall ratio of omega-3 to omega-6 PUFA intake in the diet can influence the susceptibility to various chronic inflammatory disease (Dyall, 2017, DiNicolantonio and O'Keefe, 2018).

1.6.2. Specialised pro-resolving mediators (SPMs)

Resolution is identified as a critical stage during inflammation for the cessation of an acute inflammatory response and unresolved inflammation is the underlying cause for the onset of many chronic inflammatory diseases. Lipid metabolites derived from omega-3 PUFAs play an integral role during inflammatory resolution and modulating leukocyte behaviours. The use of liquid chromatography tandem mass spectrometry (LC-MS/MS) analysis over recent years has enabled the identification of SPMs which are a novel class of bioactive lipid mediators that are biosynthesised during inflammatory resolution. They are classified into four main groups: lipoxins, resolvins, maresins and protectins. The precursors for resolvins, maresins and protectins are the omega-3 PUFAs, EPA and DHA whereas lipoxins are generated from omega-6 PUFA, ARA. Functionally these SPMs are not immunosuppressive but actively regulate inflammation by reducing neutrophil infiltration, pro-inflammatory cytokine production and stimulating macrophage-mediated phagocytosis for the clearance of apoptotic cells, all of which are key stages of resolution.

Resolvins are generated in two structurally different forms classified as E-series (derived from EPA) and D-series (derived from DHA) resolvins. Resolvin E1 (RvE1) is associated with neutrophil transmigration and has been implicated as being athero-protective in murine models of cardiovascular disease (Serhan et al., 2000, Keyes et

al., 2010). Resolvin E2 (RvE2) is another member of the E-series resolving family, that decreases zymosan-induced neutrophil recruitment and is also secreted by apoptotic neutrophils during inflammatory resolution (Tjonahen et al., 2006, Dalli and Serhan, 2012). Apoptotic neutrophils also secrete RvD1, a member of the D-series of resolvins that demonstrates reduced pro-inflammatory cytokine production in peritoneal macrophages and stimulates M2 macrophage marker expression (Dalli and Serhan, 2012, Titos et al., 2011). A study has shown that RvD1 administration was able to promote plaque stabilisation by increasing the fibrous cap in *Ldlr*$^{-/-}$ mice. They also showed that a dysfunctional balance in pro-inflammatory and pro-resolving lipid mediators greatly impacts the stability in atherosclerotic lesions (Fredman et al., 2016).

The protectin family is predominantly biosynthesised from DHA and produced by macrophages and eosinophils. Neuroprotection D1 (NPD1) for example is associated with increased brain cell survival by promoting neuro-protective gene expression programs (Bazan, 2009). A recently discovered member of the protectin family, protectin-conjugates in tissue regeneration 1 (PTCR1), is implicated in ameliorating LPS-induced inflammation and multiple organ damage in a model of acute inflammation (Liu et al., 2020). Its expression is enhanced during inflammatory resolution, particularly in M2 macrophages where its expression is elevated compared to the M1 phenotype (Ramon et al., 2016). Maresins are also found to be enriched in macrophages and MaR1 in particular is found enriched in M2 macrophages where it contributes to macrophage efferocytosis and its tissue regeneration capabilities (Liu et al., 2022c). The role MaR1 in atherosclerosis has also been explored showing reduced TNF-α mediated monocyte adhesion and production of ROS (Chatterjee et al., 2014).

Whilst resolvins, protectins and maresins are derived from omega-3 PUFAs, lipoxins are biosynthesised from omega-6 PUFA, AA (Spite et al., 2014). In resolving inflammatory exudates, there is a switch in the production of pro-inflammatory leukotrienes and prostaglandins to that of lipoxins and other SPMs (Serhan et al., 2008). Inflammatory eicosanoids PGD_2 and PGE_2 initiate production of lipoxins such as lipoxin A_4 (LXA_4) during the resolution phase which signals to halt neutrophil infiltration to the site of inflammation (Serhan, 2005, Levy et al., 2001). Collectively, SPMs are potent lipid mediators that are active in the low picomolar and nanomolar range which open up novel avenues for the development of treatment strategies for chronic inflammatory diseases such as atherosclerosis where macrophages and lipid metabolism play a dominant role in disease manifestation.

1.7. Project aim

Macrophages and foam cells play an integral role in the pathogenesis of atherosclerosis, where they exist as a spectrum of different inflammatory and activation states. However, till today the characterisation of foam cells remains an active debate due to overlapping markers with other immune cells. Their functional properties are also uncertain due to conflicting evidence shown in recent transcriptomic studies as well as the technical difficulties associated with carrying out functional assays with foam cells *in vitro.* Whilst extensive studies have looked at the role of monocytes and macrophages in atherosclerosis, no studies to date have looked specifically at monocyte subsets and their impact on foam cell phenotypes during differentiation.

It was hypothesised that the distinct inflammatory characteristics which monocyte subsets exhibit would result in various foam cell phenotypes following differentiation of each monocyte subtype.

Therefore, the main aims of this study involved the following:

1. To investigate the phenotypic characteristics of foam cells by utilising flow cytometry since limited studies have been used looking at extensive multi-colour flow panels for human monocyte-derived foam cells.
2. Utilise transcriptomic analysis using bulk RNA sequencing and spatial transcriptomics in order to identify differences in the genetic profile of foam cells derived from different monocyte subsets and how their gene profile varies with disease severity and localisation.

3. To identify potential mediators that may drive the functional pro-inflammatory characteristics of foam cells via cellular crosstalk with vascular endothelium using in vitro co-culture based assays.

Chapter 2. MATERIALS AND METHODS

2.1. Ethical approval

All blood samples were obtained from healthy donors only which were required to be over the age of 18. Informed written consent was provided by all participants before collection of samples which was approved by the University of Birmingham local ethics committee (ERN_12-0079C).

2.2. Isolation of peripheral blood mononuclear (PBMCs) cells and neutrophils from whole blood

Human blood was collected in 9ml EDTA coated Vacuette® tubes (Greiner Bio-one) using the vacutainer blood collection set (BD Biosciences) via venepuncture. Peripheral blood mononuclear cells (PBMCs) and neutrophils were isolated from whole blood via density gradient separation. In a round bottom polypropylene tubes (Appleton woods), 2.5ml of Histopaque 1077 (Sigma Aldrich) was gently layered over 2.5ml of Histopaque 1119 (Sigma Aldrich) using a mixing needle (Henleys) and syringe. Whole blood (5ml) was then layered on top of the Histopaque 1077 and centrifuged at 800 g for 45 minutes at room temperature (RT) with no brake or acceleration.

The PBMC buffy coat located between the plasma layer and neutrophil layer was collected using pasture pipettes and diluted up to 15ml with ice cold MACS buffer (phosphate buffer solution without Ca^{2+} and Mg^{2+} (PBS -/-, Sigma Aldrich), 2mM (v/v) ethylenediaminetetraacetic acid (EDTA, Sigma Aldrich) and 0.5% (v/v) bovine serum albumin (BSA, Gibco). PBMCs were centrifuged at 300 g for 5 minutes to wash out the

density gradient before being resuspended in 1ml MACS buffer for cell counts which were performed using the Cellometer Auto T4 (Nexcelcom Bioscience).

Neutrophils were collected at the interface between Histopaque 1077 and Histopaque 1119 using a pasture pipette and transferred to a 15ml centrifugation tube. Neutrophils were topped up to 10ml with RT PBS with Ca^{2+} and Mg^{2+} (PBS +/+) for washing and centrifuged 300 g for 5 minutes. Cell pellets from each tube were pooled into a single 15ml tube using gentle pipetting to avoid activation and washed again in 10ml PBS (+/+) by centrifugation. PBS was aspirated and the cell pellet was resuspended in 1ml Ack lysing buffer (Gibco) for 2 minutes at RT to lyse red blood cells. Lysis buffer was then diluted with PBS (+/+) to 15ml and centrifuged at 300 g for 5 minutes. Following centrifugation, cells were resuspended in 1ml PBS (+/+) to perform cell counts. Neutrophils were observed under the microscope to ensure cells were not activated which was indicative by a circular morphology.

2.3. Monocyte isolation

$CD14^+$ (mixed monocytes), $CD14^+CD16^-$ (classical), and $CD14^+CD16^+$ (non-classical/intermediate) monocyte subsets were separated from PBMCs extracted from whole blood (see section 2.2) from healthy human donors (consented). Purification of monocyte subset isolation were all determined using flow cytometry analysis using CD14 and CD16 fluorescently conjugated antibodies as well as Zombie aqua fixable viability dye (Biolegend) to exclude dead cells (Table 2.1).

2.3.1. $CD14^+$ mixed monocyte isolation

For mixed monocyte isolation PBMCs were counted and resuspended in MACS buffer at a volume of 80ul per 10^7 cells followed by the addition of CD14 human

microbeads (Miltenyi) at 20ul per 10^7. Suspended cells were incubated at 4°C for 20 minutes before being positively selected using magnetic LS columns (Miltenyi) according to manufacturer's instructions. Briefly, LS columns were washed first with 2ml MACS buffer and cells were added directly to the column followed by three consecutive 1ml wash steps with MACS buffer. The negative fraction was discarded and positively selected $CD14^+$ monocytes were eluted from the column using 5ml MACS buffer and plunger. Monocytes were centrifuged and resuspended in 1ml MACS buffer to carry out cell counts.

2.3.2. $CD14^+$ $CD16^-$ monocyte isolation

$CD14^+CD16^-$ monocytes were isolated from PBMCs by first labelling PBMCs with CD16 human microbeads (Miltenyi) in MACS buffer at a concentration of 50μl per 50 $x10^6$ cells for 20 minutes at 4°C to deplete $CD16^+$ cells by passing them through a magnetic LD column (Miltenyi). LD columns were initially washed with 2ml MACS buffer before adding the cell suspension directly to the column. This was followed by two consecutive 1ml wash steps collecting all eluted $CD16^-$ cells (negative fraction). The $CD16^-$ cell population was then resuspended in CD14 human microbeads (Miltenyi) at 20μl per 10^7 at 4°C for 20 minutes. The cell suspension was positively selected using magnetic LS columns (Miltenyi) (as mentioned in section 2.3.1). The resulting $CD14^+CD16^-$ monocyte population were centrifuged and counted.

2.3.3. $CD14^+CD16^+$ monocyte isolation

$CD14^+CD16^+$ monocytes were isolated using the $CD16^+$ monocyte isolation kit (Miltenyi) according to instructions provided. Briefly, PBMCs were resuspended in 100μl of FCR block and 100μl of non-monocyte depletion cocktail (provided in kit) and

incubated at 4°C for 20 minutes. Non-monocytic cells were depleted by passing cells through an LD column as mentioned in section 2.3.2. The resulting flow through of cells were resuspended in 400μl MACS buffer and incubated with CD16 human microbeads (included in kit) at 4°C for 20 minutes. $CD16^+$ monocytes were then positively selected using as LS column (Miltenyi) (as mentioned in section 2.3.1) and eluted using 5ml MACS buffer, followed by cell counting.

2.4. Monocyte cell culture and differentiation into macrophages and foam cells

2.4.1. Culture of monocyte-derived macrophages

Isolated and counted monocytes were resuspended in pre-warmed 0.15% (v/v) BSA (Gibco) in RPMI (Gibco) at a concentration of 3.5 $x10^5$ cells per 500μl for a 24 well tissue culture plate (Falcon) or 1.5 $x10^5$ cells per 200μl in 8 well μ-slide chambers (Ibidi). Cells were seeded per well and left to adhere to plastic for 1 hr at 37 °C and 5% CO_2. Wells were then aspirated and replaced with fresh macrophage differentiation media constituting of RPMI 1640 (Gibco), 50ng/ml MCSF (Peprotech) and 10% fetal bovine serum (v/v) (FBS) (Sigma Aldrich) or 10% pooled human serum (v/v) (Sigma Aldrich) where specified. Alternatively, cells differentiated in human autologous serum (v/v) were cultured in M199 (Gibco), 10ng/ml epidermal growth factor (EGF) (Sigma Aldrich) and 10% autologous serum (v/v) from the corresponding donor which was heat-inactivated at 56°C for 20 minutes. Media was filter sterilised through 0.22μm filters. Cells were cultured 6 days with fresh media replacements every 2 days.

2.4.2. Polarisation of macrophages

Following 6 days of differentiation, monocyte-derived macrophages were polarised in macrophage differentiation media (see section 2.4.1) with low serum (5% FBS) stimulated with 100ng/ml lipopolysaccharide (LPS) (Sigma Aldrich) and 20ng/ml IFNγ (Peprotech) to induce an M1-like phenotype and with 20ng/ml interleukin-4 (IL-4) (Peprotech) for an M2-like phenotype. Cells cultured in unstimulated macrophage media were assumed to be in a resting, unpolarised macrophage state (M0).

2.4.3. Culture and treatment of monocyte-derived foam cells

Isolated monocytes were seeded for 1hr in 0.15% (v/v) BSA (Gibco) in RPMI (Gibco) at the appropriate densities in tissue culture plates as mentioned in section 2.4.1. Media was replaced with macrophage differentiation media (see section 2.4.1) supplemented with oxLDL (Generon) (unlabelled or fluorescent dil-labelled), acLDL (Generon) or maLDL (Generon) for foam cell formation. Cells were left to differentiate for 6 days at 37 °C and 5% CO_2 with fresh media changes every 2 days along with supplementation of modified LDL. Foam cell formation was determined by LDL uptake. Unlabelled LDL was detected via oil red o staining (see section 2.4.5) whereas fluorescent dil-labelled LDL was detected via flow cytometry analysis or confocal imaging via the PE laser.

For treatment conditions, (in addition to modified LDL), monocytes in culture were treated with EPA (5-25μg/ml) (Sigma Aldrich). Treatment conditions were also supplemented every 2 days with LDL for each media change. All lipids were handled using ultra-low retention pipette tips (Fisher scientific) and glass vials (Thermofisher) to avoid adhesion to plastic.

2.4.4. Reconstitution and storage of Eicosapentaenoic acid

Stock EPA (Sigma Aldrich) vials (10mg) were reconstituted in 330 μl of 100% ice-cold ethanol and vortexed thoroughly to give a final stock concentration of 100mM . The solution was then aliquoted into clear 300μl fixed insert glass vials (Thermoscientific) in 20 μl aliquots and stored under nitrogen gas to prevent oxidation. Briefly, a very gentle stream of nitrogen gas was flowed into each vial before immediately closing the vial and storing at -80°C for no longer than a month.

2.4.5. Oil red O staining

Oil red O stock solution was prepared from 3% (1.5g) (w/v) Oil Red O powder (Sigma Aldrich) dissolved in 100% isopropanol (50ml) and left to incubate overnight. The next day the Oil Red o stock solution was filtered through Whatman paper using a funnel. Stock solutions were kept at room temperature in the dark for up to 1 year.

Before staining a working solution of Oil Red o was prepared by diluting the required volume of Oil Red o stock solution 2:5 in ddH_2O which was filtered through a 0.22μm filter. Cultured macrophage and foam cells (in 24 well tissue-culture plates) (see section 1.3 for macrophage and foam cell culture) were initially washed with PBS (+/+) followed by fixation in 300 μl 2% (v/v/) formaldehyde solution for 20 minutes at RT. Fixative was aspirated and wells were washed twice with ddH_2O before adding 300 μl of 60% isopropanol solution (prepared using 100% (v/v) isopropanol diluted in ddH_2O) for 30 secs. The isopropanol solution was discarded and replaced with 300 μl of Oil Red O working solution. The plate was gently rotated for even distribution and incubated in the dark at RT for 20 minutes. The Oil Red O solution was aspirated, and wells were washed for an additional 30 secs with 60% (v/v/) isopropanol, followed by

rinsing of wells with 300 μl ddH_2O three times to remove excess staining. Finally, cells were kept in 500 μl PBS in the dark at 4 °C until ready for imaging. Oil Red O staining was detected using the fluorescent Cy5 λ laser on the EVOS (Thermofisher) microscope.

2.4.6. Analysis of uptake of oxLDL (dil-oxLDL)

Analysis of fluorescently labelled dil-oxLDL was performed using ImageJ software whereby channels were split into single colours and the raw integrated density was measured for each confocal microscopy image in the red channel. Then the raw integrated density was divided by the number of cells per field of view in each image determined using DAPI stain in the blue channel to obtain a reading for 'integrated density per cell'. The integrated density per cell was then averaged over 5 images to obtain a final reading per well.

2.4.7. Macrophage dissociation

Macrophages in each well were initially washed with PBS (-/-). Adherent macrophages were detached using either Accutase (10 minutes at 37°C; Gibco), Trypsin (10 minutes at 37 °C; Gibco), Cell dissociation buffer (20 minutes at 37°C; Gibco), 0.05mM (v/v) EDTA (20 minutes at 37 °C, Sigma Aldrich), MACS buffer (20 minutes at 37°C) or RT MACS buffer (20 minutes), followed by gentle scraping using mini cell scrapers (Cambridge Bioscience) to fully detach cells. Cells were then washed in MACS buffer and resuspended in 100μl PBS (-/-) for extracellular flow cytometry staining of fluorescently conjugated CD206 and CD86 cell surface markers (antibodies listed in Table 2.2) including Zombie aqua viability dye (see section 1.4.1 for extracellular flow cytometry staining).

2.5. Flow cytometry staining and analysis

All flow cytometry staining was performed in polypropylene FACS tubes (BD Biosciences) specifically designed for LSR Fortessa X-20 (BD Biosciences)

2.5.1. Extracellular antibody cell surface staining

Monocytes, detached macrophages and enzymatically harvested endothelial cells (using Accutase, see section 2.4.6) were initially resuspended in 100μl of MACS buffer and incubated for 10 minutes in FCR block (1:50; Miltenyi) at 4°C to prevent non-specific binding. Samples were topped up to 1ml with PBS (-/-) and centrifuged 300 g for 5 minutes (with break and acceleration) for washing. Cells were then resuspended in 100μl PBS (-/-) along with the addition of relevant antibodies and viability dye at the appropriate concentrations (Table 2.1-2.3) which were incubated at 4°C for 20 minutes in the dark. Following two further wash steps in 1ml PBS, cells were resuspended in 2% (v/v) formaldehyde for fixation for 15 minutes at 4°C in the dark. Finally, samples were washed and resuspended in 400μl PBS and were analysed using the 5-laser LSR Fortessa X-20 flow cytometer (BD Biosciences).

2.5.2. Intracellular CD68 antibody staining

For detection of intracellular markers, cells were washed twice with 1x permeabilisation buffer (BD Biosciences) diluted in dH_2O (1:10) after fixation to permeabilise cells. Wash steps after fixation were performed at 400g for 5 minutes. Cells were then resuspended in 1ml permeabilisation buffer for 15 minutes at RT followed by a further wash (in permeabilisation buffer). Fixed and permeabilised cells were incubated with CD68 antibody (1:100) (Biolegend) (see Table 2.2) diluted in 100μl of permeabilisation buffer at 4°C for 20 minutes in the dark. Staining was followed by

two wash steps (in 1ml permeabilisation buffer) before being resuspended in 400μl PBS (-/-) for flow cytometry analysis.

2.5.3. Flow cytometry staining procedure for macrophage characterisation

Adherent macrophages were initially harvested non-enzymatically by incubating cells in RT MACS buffer for 20 minutes followed by gentle scraping as detailed in section 2.4.6. Cells were initially blocked in FCR block (Miltenyi) followed by incubation with primary unconjugated Clever-1/Stabilin-1 antibody (1:100) (developed in-house) for 20 minutes at 4°C. Following two wash steps with MACS buffer, secondary anti-mouse Alexa-fluor 700 IgG1 (Biolegend) was added for a further 20 minutes at 4°C. After two additional washing steps, the cells were incubated in PBS (-/-) with the rest of the extracellular conjugated antibodies or relevant isotype controls, along with a viability dye listed in Table 2.2 for 20 minutes at 4°C in the dark. This was followed by cell fixation as mentioned in section 2.5.1. Finally, cells were permeabilised and stained for intracellular marker CD68 as detailed in section 2.5.2.

2.5.4. Flow cytometry analysis

Samples for flow cytometry analysis were acquired on the 5-laser LSR Fortessa X-20 flow cytometer (BD Biosciences) using FACSDiva (BD Biosciences) software to set up gating strategies. Data was exported from FACSDiva and imported into FlowJo (Version 10.8.1) software for analysis. Cells were detected based on size and granularity based on forward scatter (FSC) and side scatter (SSC) plots followed by doublet exclusion. Dead cells were excluded via positive staining for viability dye Zombie aqua. Subsequently, median fluorescence intensity (MFI) values and

percentage frequency of markers detected on each fluorescent channel was exported into a table and plotted on graph pad prism software.

Table 2-1 Flow cytometry antibody panel

Target	Fluorophore	Clone	Manufacturer	Dilution	Cat no:
CD68 (intracellular)	APC	Y1/82A	Biolegend	1:100	333810
CD80	BV786	L307.4	BD Biosciences	1:50	564159
CD86	BV605	IT2.2	Biolegend	1:50	305429
CD11c	PerCP-efluor 710	3.9	Thermofisher	1:100	46011642
CD36	BUV395	CB38	BD Biosciences	1:100	565422
Mertk	PE	590H11G1E3	Biolegend	1:100	367607
MHC II	FITC	L243	Biolegend	1:100	307604
CD204	BV421	U23-56	BD Biosciences	1:100	742438
CD206	PE-cyanine 7	15-2	Biolegend	1:100	321123
Zombie aqua dye	BV510	-	Biolegend	1:400	423101
StabilIn-1 (Primary)	Unconjugated	-	In-house	1:100	-
-	AF700 (Secondary)	RMG1-1	Biolegend	1:100	406631
CD14	PE-Texas Red	TuK4	Life technologies	1:50	MHCD1417
CD16	FITC	3G8	Biolegend	1:50	302006

Table 2-2 Isotype controls for flow cytometry panel

Isotype	Fluorophore	Clone	Manufacturer	Dilution	Cat no:
IgG2b κ	APC	MPC-11	Biolegend	1:400	400321
IgGk κ	BV786	X-40	BD Biosciences	1:50	563330
IgG2b κ	BV605	MPC-11	Biolegend	1:50	400349
IgG1 κ	PerCP-efluor 710	P3.6.2.8.1	Thermofisher	1:100	46471482
IgM κ	BUV395	G155-228	BD Biosciences	1:100	563866
IgG1 κ	PE	P3.6.2.8.1	Thermofisher	1:100	12471441
MHC II	FITC	MOP3-173	Biolegend	1:250	400208
IgG1 κ	BV421	X40	BD Biosciences	1:100	562438
IgG1 κ	PE-cyanine 7	MOPC-21	Biolegend	1:100	400125
IgG1	AF700 (Secondary)	RMG1-1	Biolegend	1:100	406631

2.6. Detection of protein in culture supernatants

2.6.1. Enzyme-linked immunoassay (ELISA)

To detect TNFα and IL-10 levels in macrophage and foam cell culture supernatants, the human TNFα and IL-10 DuoSet ELISA kits (Biotechne) was used according to manufacturer's instructions. The Ancillary reagent kit 2 (Biotechne) was used for supplemental supplies to perform the ELISAs. Supernatants were clarified by centrifuging at 1000g for 10 minutes to remove cellular debris before use. In brief, 96 well microplates were coated with capture antibody overnight. The next day wells were blocked with reagent diluent for 1 hour followed by three wash steps in wash buffer. Standards and supernatant samples were then incubated in coated plate for 2 hours at RT. Wells were washed and incubated with detection antibody for 2 hours at RT followed by further wash steps and addition of Streptavidin-HRP solution for 20 minutes in the dark. The wells were washed a final time, and this was followed by a further 20 minutes incubation in substrate solution at RT in the dark before stop solution was added and the plate was analysed using the Synergy HT plate reader (BioTek) at 450nm.

2.6.2. Cytokine array

Monocyte, macrophage and foam cell supernatants were screened for cytokines using a cytokine array analysis according to manufacturer's instructions (Abcam). Briefly, cytokine membranes were blocked for 30 minutes followed by incubation with pooled supernatant samples (pooled from 6-8 experiments) overnight at 4 °C with gentle rotation. The next day, membranes were washed with wash buffer

and incubated with biotin-conjugated anti-cytokine cocktail (1:2000 dilution) for 2 hrs at RT under gentle rotation. Membranes were washed once again and Streptavidin-HRP (1:1000) solution was added to the membranes for 2 hrs under gentle rotation. Following, final wash steps, detection buffer was added to the membranes for 2 minutes at RT. Excess detection buffer was removed and membranes were exposed using the Odyssey Fc imaging system (Li-Cor Biosciences). Densitometry analysis was performed using ImageJ to quantify cytokine intensity.

2.7. In *vitro* static transmigration assay

2.7.1. Expansion and cryopreservation of endothelial cell

Human dermal blood endothelial cells (HDBEC; Promocell) stock vials were initially thawed at 37°C in a water bath and transferred to a T25 tissue culture flask (Falcon) containing prewarmed Endothelial Cell Basal Medium MV (Promocell) supplemented with Foetal calf Serum (FCS; 5%, v/v), Endothelial Cell Growth Supplement (ECGF; 0.4%, v/v), Epidermal Growth Factor (EGF; 10ng/ml) and Hydrocortisone (1μg/ml) (provided in media supplement pack; Promocell). Cells were allowed to reach 90% confluency before expanding through 4 passages followed by freeze down in Cryo-SFM freezing media (Promocell) and storage in liquid nitrogen.

2.7.2. Endothelial cell culture

Cryopreserved HDBEC (Promocell) stored at passage 4 were defrosted at 37 °C in a water bath and transferred to a T25 tissue culture flask containing prewarmed complete HDBEC media consisting of Endothelial Cell Basal Medium MV (Promocell) supplemented with FCS (5%, v/v), ECGF (0.4%, v/v) and Epidermal Growth Factor (EGF; 10 ng/ml) (provided in media supplement pack; Promocell) without

Hydrocortisone. Cells were left to culture at 37 °C with 5% CO_2 for 48 hrs to reach 90% confluency before seeding.

For seeding in 12 well tissue culture plates, HDBEC (in T25 flask) were washed with warm 0.5 mM (v/v) EDTA followed by enzymatic detachment using 0.05 % (v/v) Trypsin (Gibco) for 1 min at 37 °C. Cells were allowed to full detach by gently tapping the flask. Neutralisation media composed of Medium-199 (M199; Gibco) and 20% (v/v) FBS was quickly added to neutralise the Trypsin. Cells were transferred to a 15 ml centrifuge tube and centrifuged 300g for 5 minutes. Media was aspirated and cells were resuspended in 1ml complete HDBEC media (Promocell) for cell counting. Volume of media was adjusted to give a final concentration of 2 $x10^5$ cells/ml which was added per well of a 12 well tissue culture plate. HDBEC were allowed to form a monolayer for 24 hrs prior to stimulation the next day incubated at 37 °C with 5% CO_2.

2.7.3. Preparation of macrophage and foam culture supernatants of endothelial cells stimulation

Macrophage and foam cells were generated in 24 well tissue culture plates as mentioned previously in section 2.3. After 6 days of differentiation wells were washed three times with warm RPMI 1640 (Gibco) to remove excess modified LDL and replaced with fresh macrophage differentiation media (see section 2.3.2). Cells were left to culture for a further 24 hrs at 37 °C with 5% CO_2.

2.7.4. Endothelial cell stimulation

For HDBEC stimulation, existing media was aspirated from each well (cultured for 24 hrs) and replaced with cell supernatants generated from macrophage and foam cell cultures in section 1.8.3. Macrophage differentiation media only was used as a

negative control whereas TNF-α (100U/ml; Biotechne) was used as a positive control. HDBEC was stimulated for 4 hrs at 37 °C with 5% CO_2. before performing static transmigration assays.

2.7.5. Static transmigration assay

During HDBEC stimulation, neutrophils were isolated from whole blood from healthy donors as previously described (see section 2.2) and resuspended in warm 0.15% (v/v) BSA in M199 at a concentration of $1x10^6$ cells/ml. Following the 4 hr timepoint for stimulation, each well of HDBEC was washed twice with warm 0.15% (v/v) BSA in M199 followed by the addition of $1x10^6$ neutrophils per well. Immediately, cells were left to incubate undisturbed at 37 °C with 5% CO_2 for 7 minutes to allow for cell adhesion and transmigration. For imaging, wells were then washed twice to remove unbound neutrophils and fixed in 2% (v/v) glutaraldehyde (Sigma Aldrich) solution prepared in ddH_2O for 10 minutes at room temperature. The glutaraldehyde was aspirated, and each well was washed twice before imaging in PBS (+/+). Images were taken at five different fields of view using a phase contrast Olympus IX70 microscope (Olympus) at x20 magnification. Images were analysed based on cell adherence and transmigration. Total adhered cells were calculated and expressed as cells per mm^2 and transmigrated cells as a percentage of total adhered neutrophils (Figure 2-1).

2.7.6. Dissociation of endothelial cells for staining

For flow cytometry staining of HDBEC prior to detachment from plastic, wells were washed with warm PBS (+/+) (after the 7 minutes transmigration incubation period) and incubated with 200μl FCR block (1:5) diluted in PBS (+/+) for 10 minutes

for blocking. Fluorescently conjugated antibodies for VCAM-1, ICAM-1, E-selectin and viability dye Zombie aqua (Table 2.1) was then added directly to the wells containing FCR block solution and were left to incubate at 4°C for 20 minutes in the dark. Contents of the well was then transferred to labelled FACS tubes (Falcon) and immediately Accuatase (Gibco) solution was added to each well and left to incubate at 37 °C for 2 minutes. Accutase was neutralised with PBS (-/-) and pipetted up and down gently to detach stained HDBEC from plastic. Detached cells were transferred to corresponding FACS tubes and centrifuged 300g for 5 minutes. Cells pellets were aspirated and washed twice in PBS (-/-) before fixing in 2% (v/v) formaldehyde solution for 15 minutes. Following additional wash steps, cells were resuspended in 400µl PBS (-/-) before analysis was performed on the LSR Fortessa X-20 (BD Biosciences).

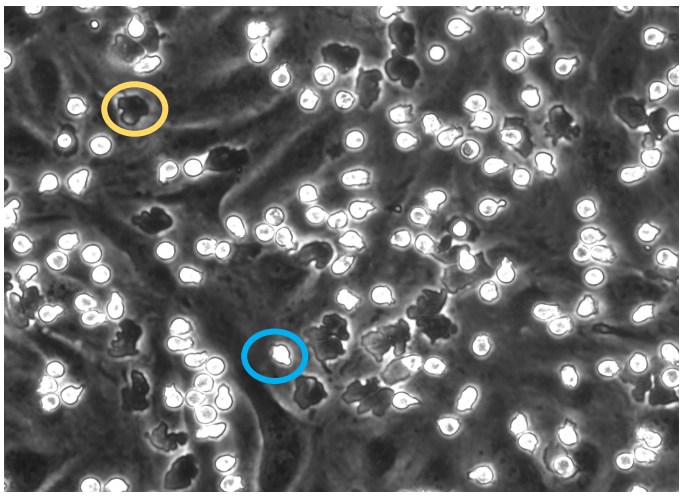


Figure 2-1: Analysis of adhered and transmigrated neutrophils in static migration assays.

In each well five random fields of interest were imaged using a phase contrast microscope and cells were quantified based on their appearance being phase bright considered (circled in blue) as adhered of phase dark being transmigrated cells (circled in yellow).

2.8. Co-culture assays

2.8.1. Monocyte culture and differentiation in transwell inserts

$CD14^+CD16^-$ monocytes were isolated from PBMCs (as mentioned in section 1.2 and 1.3) and seeded on the inside of 24 well, 0.4μm pore, high density transwell inserts (Falcon) placed into each well of a 24 well tissue culture plate. Cells were seeded at 1.5 x 10^5 cells per 200μl in macrophage differentiation media supplemented with unlabelled oxLDL (Generon) for foam cell formation. A further 400μl of media was placed at the bottom of the transwell insert. Monocytes were left to differentiate for 6 days at 37°C in 5% CO_2 with media changes every two days on both top and bottom of the transwell.

2.8.2. Seeding endothelial cells on transwell insets to establish co-cultures

HDBEC was trypsinised from T25 flasks and counted as described previously (see section 1.9.2). Cells were resuspended in complete HDBEC media without phenol red (Promocell). Following 6 days of monocyte differentiation, transwell inserts were washed in warm PBS (+/+) three times (both top and bottom) before inverting and seeding 0.6 x 10^5 HDBEC on the top of each transwell insert for 45 minutes in a sterile humidified chamber at 37°C in 5% CO_2. Following HDBEC adhesion, transwell inserts with co-cultured cells were placed into fresh 24 well tissue culture plates (Falcon) containing complete HDBEC media without phenol red (Promocell) both top and bottom of the inserts and were left to culture for 24 hours at 37°C in 5% CO_2.

2.8.3. Sample collection of lipidomic analysis

Following 24-hour co-culture of macrophage/foam cell and endothelial cells, supernatants were collected and centrifuged at 1000g for 10 minutes to remove cellular

debris. Supernatants were then transferred to cryovials and snap frozen in liquid nitrogen along with individual transwell inserts. Vials and transwells were stored at -80°C for storage until analysis.

2.8.4. Immunofluorescence staining of transwell filters

To detect HDEBC monolayer formation, transwells were washed in PBS (+/+) and fixed with 2% (v/v) formaldehyde for 15 minutes at RT. Using a disposable scalpel (Swann-Morton, transwell filters were gently cut out and placed on a glass microslide (HDEBC facing up) and blocked with 1% (v/v) BSA (Gibco) in PBS solution (PBSA) for 30 minutes. The filter was then incubated for 30 minutes with anti-human CD31 antibody (1:100) conjugated to PE (Biolegend) diluted in PBSA. Slides were washed three times and mounted with Vectorshield Antifade Mounting Media with DAPI (Vector Laboratories) with a glass coverslip sealed with clear nail varnish, ready for imaging using the LSM 780 Confocal microscope (Zeiss).

2.9. Lipidomics

LC-MS/MS analysis was performed at Queen Mary University of London in Professor Jesmond Dalli's lab. All samples for LC-MS/MS analysis were extracted using solid phase extraction (SPE) columns. Initially frozen co-culture supernatants were thawed on ice followed by the addition of 2ml methanol to 1ml of each sample in a falcon tube. Deuterium- labelled internal standards were also added to each sample which were placed at -20°C for 45 mins to allow them to precipitate. Samples were then centrifuged at 3000g for 5 mins and supernatants were collected in glass vials and transferred to the TurboVap Evaporator to evaporate methanol to less than 1ml

using nitrogen gas in order to limit oxidation of lipid mediators. Evaporation was performed in a 37°C water bath with a nitrogen gas flow rate set to no more than 15 psi. Supernatants were centrifuged again at 3000g for 5 mins at 4°C to be ready for extraction. Samples were then diluted with acidified ddH_2O and loaded onto C18 SPE columns which were washed with neutral ddH_2O and hexane. Methyl formate was added to each column to elute the samples which were dried with a stream of nitrogen gas followed by resuspension in 50ul of methanol and ddH_2O at a 1:1 ratio. Samples were centrifuged 3000g for 5 mins and supernatants were collected and transferred to 1.5ml Eppendorf tubes. Tubes were centrifuged again at 17, 000g for 5 mis and supernatants transferred to glass vials ready for LC-MS-MS profiling.

For lipid mediator profiling the QTrap 5500 (Sciex) LC-UV-MS/MS system was used equipped with the Agilent HP1100 binary pump and diode-array detector. Calibration curves were obtained using authentic lipid mediator mixtures. Quantification was carried out based on peak area of the multiple reaction monitoring (MRM) transition and calibration curve for each compound. All data analysis was carried out using Analyst Quantitative tool.

2.10. Real-time quantitative polymerase chain reaction (RT-qPCR)

2.10.1. RNA extraction

RNA extraction from monocytes and cultured macrophages and foam cells were performed using the RNeasy kit (Qiagen) according to manufacturer's instructions. RLT lysis buffer was added to cell pellets or directly to cultured cells in wells before scraping and transferring to RNAase free eppendorf tubes. Cell pellets were thoroughly

vortexed before adding 70% (v/v) ethanol to each sample. Samples were then transferred to RNA easy spin columns and centrifuged at 8000g for 1 minute. All centrifuge steps were performed at this speed unless indicated. Flow through was disposed and RW1 buffer was added to each column and centrifuged again. Each sample was then incubated with DNase solution (1 part DNase and & parts RDD buffer; Qiagen) for 15 minutes at RT. RW1 solution was added again and samples were centrifuged followed by addition of buffer RPE and an additional spin step with flow through being disposed of each time. The addition of RPE was repeated and spun down but for 2 minutes this time. RNA easy spin columns were transferred to new collections tubes and spun dry for 5 minutes to dry the membrane. RNase free water was finally added to each column (34 μl) and ran through twice with spin steps lasting for 1 minutes each to elute the RNA. Quantity of was RNA was measured using the Nanodrop 2000. Samples were stored at -80°C until cDNA conversion.

2.10.2. cDNA conversion

RNA was converted to cDNA using a High-Capacity cDNA Reverse Transcription Kit (Applied Biosystems) according to manufacturer's instructions. A mastermix was made up consisting of 2 μl 10x RT buffer, 2 μl 10x Random Primers, 0.8μl of 25x dNTP mix, 3.2 μl of RNase free water and 1 μl of Multiscribe™ Reverse Transcriptase (Applied Biosystems) per 10 μl of RNA sample. RNAseOUT inhibitor (1 μl) (Thermofisher) was also added to the mastermix to prevent RNA degradation. The reverse transcription process was performed using a thermocycler, whereby samples were heated 25°C for 10 minutes, 37°C for 120 minutes and 85°C for 5 minutes, before being held at 4°C. cDNA samples were stored -20°C until required for real-time polymerase chain reaction (RT-qPCR) analysis.

2.10.3. Quantitative RT-qPCR

RT-qPCR for quantifying gene expression was performed in MicroAmp® Optical 384-Well Reaction Plates (Applied Biosystems). Each reaction comprised of 5.5μl TaqMan™ Gene Expression Master Mix, 3.9 μl of RNase free water, 0.6μl of gene specific TaqMan™ Gene Expression Assay (FAM) primers and 0.5μl of cDNA sample (see section 1.13.2). Plates were sealed using MicroAmp™ Optical Adhesive Film (Applied Biosystems) and centrifuged 300g for 3 minutes. Quantification was performed using the Quant Studio™ 5 384-well Block (Thermofisher) at 50°C for 2 minutes, followed by 95°C for 10 minutes, 95°C for 15 seconds and finally 60°C for 1 minute for a total of 40 cycles.

An average CT value was obtained by calculating the mean of three technical replicates with readings > 35 cycles being omitted from analysis. To plot relative expression (2- ΔCT) the ΔCt values were obtained by subtracting Ct values for housekeeping genes from Ct values of gene of interest. Fold change (2- ΔΔCT) was calculated by comparing ΔCt from experimental samples with ΔCt values from experimental controls.

2.11. Bulk RNA-sequencing

2.11.1. Preparation of sequencing libraries

Following RNA isolation, RIN (RNA integrity values) were measured using the High Sensitivity RNA ScreenTape® (Agilent) prior to performing sequencing. RIN scores ranged from 1-10 with 10 being 10 being the highest integrity and 7 being the threshold score to carry samples forward for sequencing. All samples had RIN scores

>7 and were processed by University of Birmingham Genomics service. Library prep was performed using the Lexogen QuantSeq 3‘ mRNA-Seq Library Prep Kit FWD (Illumina) followed by quality checks carried out using the Agilent TapeStation DNA 1000 tape (Aligent) and DNA HS Qubit™ (Fisher Scientific). The final RNA sequencing libraries were sequencing using the NovaSeq 6000 (Illumina).

2.11.2. RNA sequencing analysis

All sequenced data files were generated in .fastq format and quality of reads were checked using FASTQC packages in Rstudio. Trimming was performed using BBDuk to remove adapter sequences, poly A tails and low quality bases. FASTQC analysis was performed again post trimming to assess improvement in read quality. STAR aligner was used to map sequenced reads to the human genome. Prior to this, the genome index was generated using from the ‘Homo_sapiens.GRCh38.dna Subread.primary_assembly’ human genome file and corresponding annotation file, ‘Homo_sapiens.GRCh38.101’ obtained from the ensemble website. FeatureCounts was then used to generate a matrix of row counts of each of the genes across all samples. Genes that had 5 reads or less in the analysis were eliminated.

2.11.3. Analysis of differentially expressed genes

Differential gene expression (DEG) and pathway analysis was all performed using the iDEP integrated web application for bulk RNAseq analysis. The gene counts table generated with featureCounts was uploaded to iDEP and subsequent normalisation and analysis was performed. Data was normalised using variable stabilising transformation (VST) and the default filter of 0.5 counts per million (CPM) was used to filter out genes with low read counts. DEG analysis was performed using

the DESeq2 package. Enrichment analysis of DEGs was performed based on Gene Ontology (GO) databases. All heatmaps, PCA and MA plots were generated with the iDEP online application. iDEP is freely accessible at:

http://bioinformatics.sdstate.edu/idep/

2.12. Spatial transcriptomics

2.12.1. GeoMX Whole Transcriptome Atlas (WTA) assay

Formalin-fixed paraffin-embedded (FFPE) Human coronary artery tissue sections were provided by Claudio Mauro's group, University of Birmingham. Staining and GeoMX WTA assay was performed at Propath UK. FFPE tissue sections were processed following GeoMX Digital Spatial Profiler (DSP) slide preparation user manual. Briefly, prior to deparaffinisation, slides were baked at 60°C for 30 mins then cooled to RT. Deparaffinisation and antigen retrieval was performed using the Leica Biosystems BOND RX system using the BOND RX version 6.0 software. In site hybridisation was carried out for WTA designed to target 19,505 RNA targets. For this 200ul of hybridisation solution was added to each slide followed by the addition of a Grace Bio-labs HybriSlip. Slides were inserted into a hybridisation chamber and incubated at 37°C overnight. Stringent washes were performed in 4x SSC and 100% formamide. This was followed by staining for morphology markers for visualisation which are fluorescent antibodies against: CD31, CD45, CD4 and nuclear marker (SYTO83-AF532). Once stained and probed with WTA reagents, slides were loaded into the GeoMX DSP machine to be scanned and ROIs were selected. Slides were scanned at 20x magnification and ROIs were selected based on T cell positive areas

for both adventitia layer and the plaque regions as well as control non-T cell areas. The sequencing library was constructed by photocleavage of DNA oligos which were collected into 96-well plates for each area of interest (AOI) and quantified with Nanostring nCounter technology. PCR was performed on the collected aspirates from individual AOIs and purified using AMPure XP beads (Beckman Coulter). Libraries were sequenced using the Illumina platform and Fastq files were generated for analysis.

2.12.2. GeoMX RNA data quality control (QC)

Data analysis was performed using the GeoMX Data Analysis Suite. Initially two rounds of QC were performed to remove data of low quality and low reads. First, technical QC was carried out to flag segments with less than 1000 raw reads and less than 80% raw reads aligned. Additionally, segments were flagged if the negative probe (used to measure technical background noise in WTA panel) count geomean was less than 10, suggesting if the background signal is too low, it may indicate that signal of targeted RNA probes are also too low. Segments with nuclei counts of less than 200 were also excluded. Next, biological probe QC was performed that excluded probes from target count calculation in all segments if it failed the Grubbs test in >=20% of segments. Finally, data was filtered to keep targets with expression >=10% segments above threshold value which was set as being higher than the limit of quantification. If the value is greater than the limit of quantification, then I are confident it is expressed above background levels. Data was normalised using quartile 3 (Q3) normalisation which divides counts in a segment by the 3rd quartile value for that segment and subsequently multiplies that value by the geometric mean of the 3rd quartile values across all segments.

2.12.3. GeoMX DSP data analysis

Each segment was annotated based on localisation, disease severity and immune infiltration. All data visualisations including heatmaps, PCA plots, box plots and volcano plots were generated using the GemoMX DSP data analysis suite software which were further modified using custom R scripts. Data was selected filtered based on annotated factors and further segmented based on level of CD68 and CD11c expression. For pathway analysis the gene set enrichment analysis (GSEA) package from Bioconductor was implemented using pathway groups from the Reactome database. Statistical analysis was performed using the linear mixed model test.

2.13. Statistical analysis

All data was plotted, and statistical analyses performed using Graphpad Prism software (version 8.4.2). Data are presented as ± standard error mean (SEM) unless otherwise stated. Differences between two groups were analysed using t-test and differences between more than one group using one-way anova or two way anova if more comparing multiple parameters. Post-hoc tests were applied to the data sets where appropriate and normality tests were initally performed to determine whether to carry out parametric or non-parametric statistical tests. In all cases a p value of ≤ 0.05 was considered as statistically significant.

Chapter 3. IN VITRO CHARACTERISATION OF HUMAN MONOCYTE-DERIVED MACROPHAGES

3.1. Introduction

The generation of MDM in culture is widely used as an *in vitro* model for human macrophages. The addition of specific polarising agents can be used to model the various phenotypic states of macrophages which exhibit distinct characteristics based on surface molecule expression, gene expression and secretory profiles. More recent studies have demonstrated the complexity of macrophage polarisation by revealing additional phenotyic states that go beyond the simplified M1-M2 paradigm, which in fact represent two extremes of a continuous spectrum of macrophage activation states that are constantly changing in accordance to their environmental signals (Mosser and Edwards, 2008, Munoz-Rojas et al., 2021, Xue et al., 2014, Martinez and Gordon, 2014). Thus, one can refer to the phenotypic profile to be more 'M1-like' or 'M2-like' depending on their functional properties at a specific point in time. It is important to note that these macrophage subsets often have overlapping properties and expression of markers, although their levels of expression may vary.

Defining macrophage subsets can be achieved using different techniques. Multi-coloured flow cytometry is a particularly powerful technique that enables the definition and study of immune cells by detecting relative expression of multiple surface proteins on an individual cell at the same time (Maecker and McCoy, 2010). However, the characterisation of adherent cells via flow cytometry analysis is especially

challenging due to compromised cell membranes and poor cell yields when attempting to obtain single cell suspensions (Malheiro et al., 2017). Macrophages being highly adherent cells, in addition to being auto-fluorescent, are particularly difficult to harvest and assay. Hence the use of extensive poly-chromatic panels for macrophage flow cytometry analysis is challenging (Bourdely et al., 2022).

In this chapter, I designed an 11-colour flow cytometry panel for the characterisation of human MDMs in culture. When designing multi-colour panels, it is important to consider the biological expression of cell surface markers for appropriate selection of fluorochrome conjugates and to ensure appropriate compensation matrices can be applied. I observed macrophage polarisation over selected time periods and applied our macrophage flow panel to these cells in order define the various macrophage subsets and verify our panel design.

3.2. Results

3.2.1. Isolation and purification of monocyte subsets

Methodological advances have enabled multiple techniques for cell purification from whole blood. The isolation of monocytes can be typically achieved by plastic adherence or more commonly, magnetic bead separation for the isolation of specific subsets. To isolate $CD14^{+}CD16^{-}$ (classical) and $CD14^{+}CD16^{+}$ (non-classical and intermediate) monocyte subsets from whole blood PBMCs I used positive magnetic selection by using anti-CD14 and anti-CD16 microbeads which bind to cells of interest. Bead bearing cells are then passed through a column in a magnetic field where they are retained. After removal of the magnetic field, cells can be eluted form the column with wash buffer.

To test eluted cells for purity, isolated monocyte subsets were stained for anti-CD14 and anti-CD16 with fluorescently conjugated antibodies for flow cytometry analysis, and dead cells were excluded using zombie aqua fixable viability dye (Biolegend). Significant lymphocyte contamination was observed following magnetic bead isolation (as shown in the FSC and SSC plots in Figure 3.1A), so monocytes were further enriched by adherence to tissue-culture plastic, whereby non-adherent and non-monocytic cells were removed by washing after 1 hour of seeding prior to further differentiation (Figure 3.1B). Flow cytometry gating strategies confirmed higher levels of CD14 on the classical monocytes compared to the non-classical/intermediate subset. CD16 expression showed a reciprocal pattern of expression, with enrichment on the non-classical/intermediate population and negative expression on the classical monocytes as expected (Figure 3.1A and C). Generally, percentage purity levels were greater with classical monocyte isolation (greater than 90%) presenting with the least

contamination (Figure 3.1D/F). Overall, surface expression of both markers confirmed the identity of isolated monocyte subsets prior to further differentiation and use in *in vitro* culture assays (Figure 3.1E).

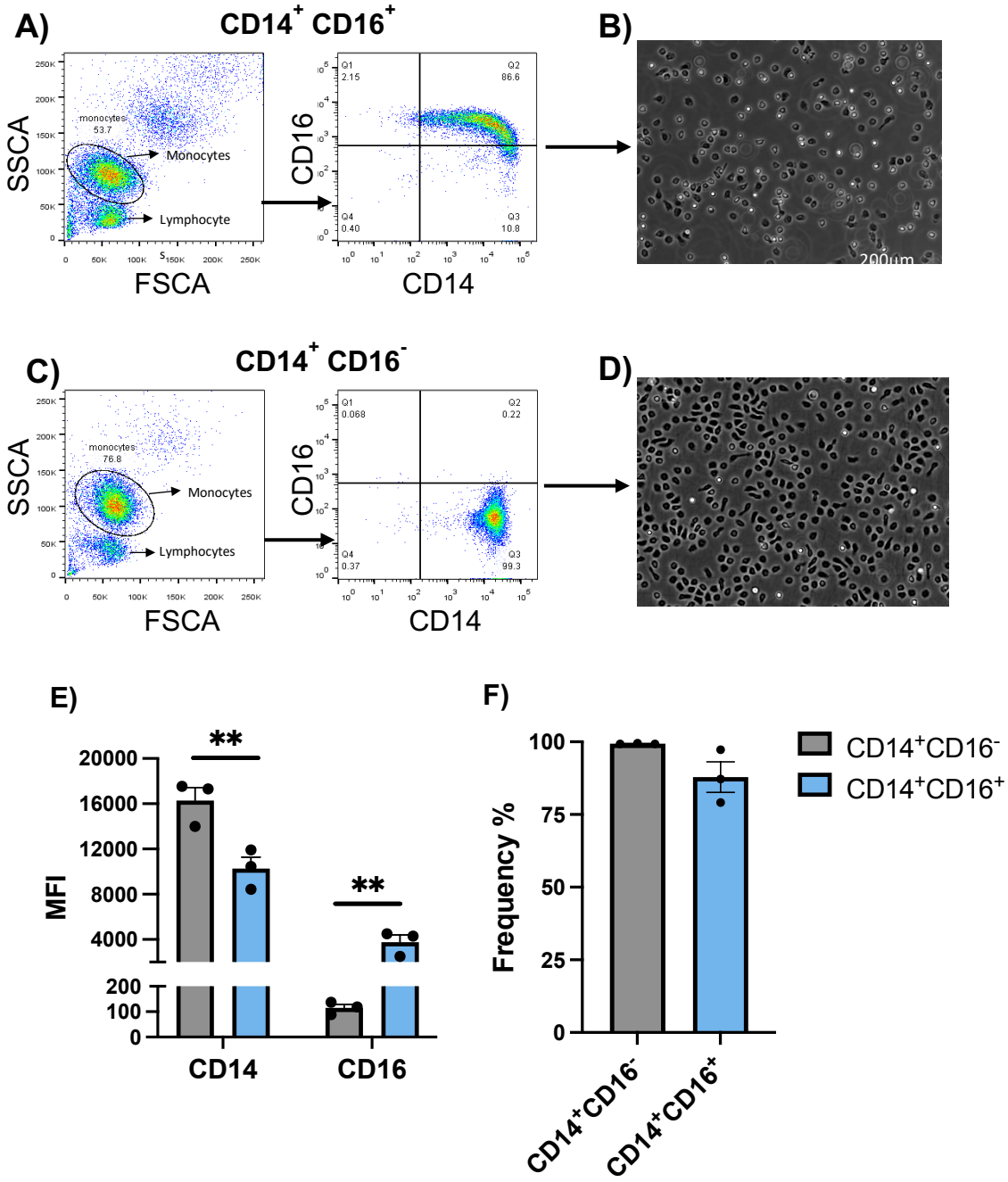


Figure 3-1 Purification of CD14⁺CD16⁻ and CD14⁺CD16⁺ monocyte subsets

CD14⁺CD16⁻ and CD14⁺CD16⁺ monocytes were isolated via magnetic bead separation. **(A, C)** Purity of subsets were determined by flow cytometry analysis by staining with anti-CD14 and anti-CD16 antibodies. **(B, D)** For additional purification, monocytes were cultured on tissue culture-treated plates for 1hr to allow adhesion to plastic, followed by removal of non-adhesive, non-monocytic (lymphocytes) cells **E)** Median fluorescence intensity (MFI) of CD14 and CD16 antibody expression and **F)** frequency (%) of subsets was determined. Data are mean ± SEM (n=3, biological replicate). Statistical analysis performed using unpaired t-test, *=$p<0.05$. Scale bars = 200µm.

3.2.2. Monocyte-derived macrophage differentiation in autologous serum vs MCSF

Several methods can be applied for the differentiation of monocytes to macrophages *in vitro* and these can result in various morphological differences in mature macrophages. Here I compared the morphology of MDMs derived using two commonly used methods, culture in autologous serum with recombinant human EGF or culture in foetal calf serum containing recombinant human MCSF and FBS, the aim being to select an appropriate *in vitro* model for further assays that presented with reduced inter-donor variability in morphology.

For *in vitro* monocyte differentiation, $CD14^{+}CD16^{-}$ monocytes were isolated and differentiated to macrophages in culture for 6 days with either 10% autologous serum and EGF or recombinant MCSF and 10% FBS, with media replenishment and phase contrast images taken every 2 days (Figure 3.2). Differentiated macrophages on day 6 were analysed for morphological differences including measurement of area (μm^2) and circularity. I found that MCSF-differentiated macrophages had a greater surface area on average than those cultured in autologous serum and EGF (Figure 3.3A and C). The circularity index for MCSF-differentiated macrophages was also greater indicating that macrophages cultured in autologous serum were more elongated and demonstrated greater heterogeneity and irregularity in cell shape (Figure 3.3B and D). I also found that monocytes grown in autologous serum did not survive in culture for the majority of our healthy donors with significant cell death observed by day 2 and the cells that did survive had greater morphological variation between donors. Thus, I selected recombinant MCSF as our method for macrophage differentiation for all

subsequent work as this technique proved to be more robust in the context of cell survival and morphological uniformity.

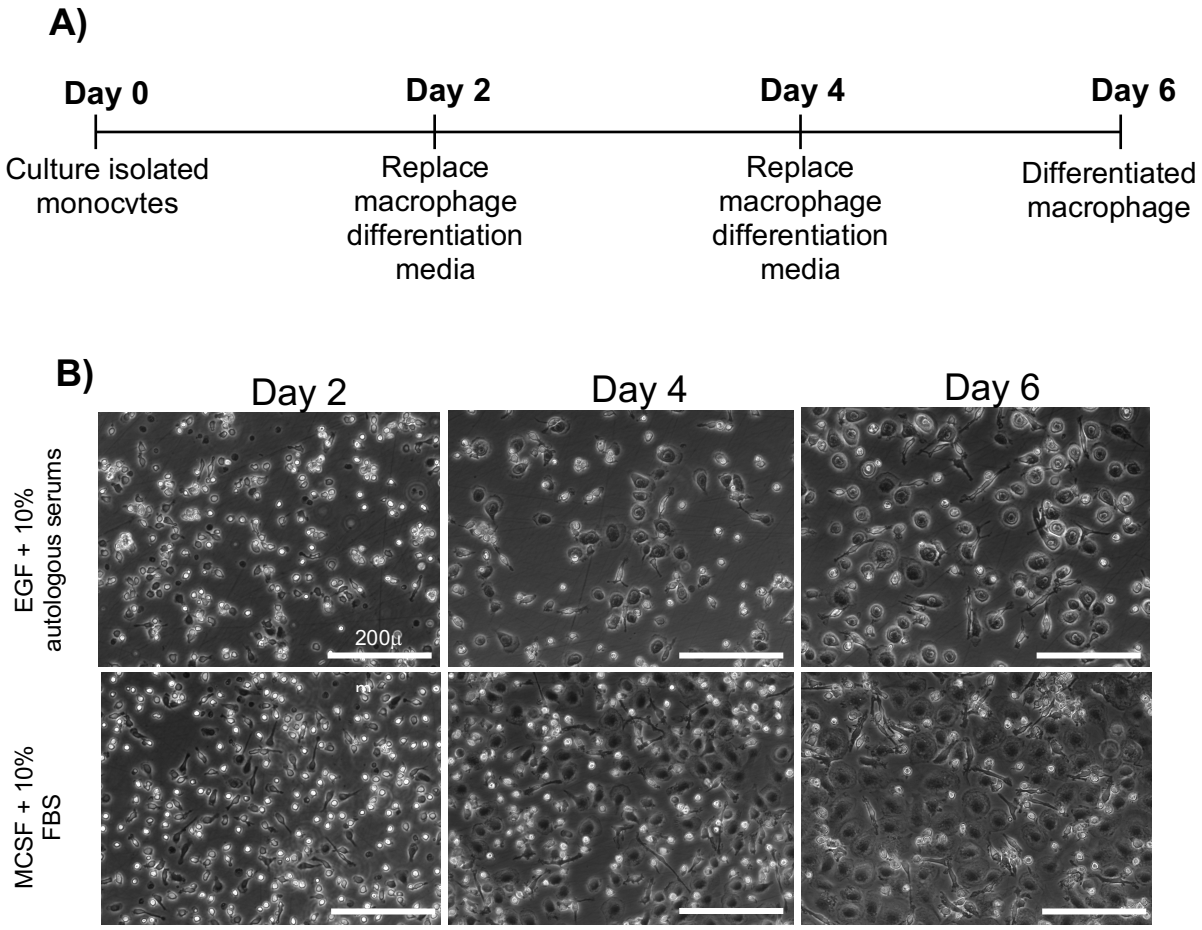


Figure 3-2 Macrophage differentiation in autologous serum vs MCSF

(A) Timeline of monocyte derived macrophage differentiation over the course of 6 days. **(B)** Phase contrast images showing morphology of macrophage differentiation at days 2, 4 and 6 cultured with recombinant human EGF (10ng/ml) + 10% autologous serum or recombinant human MCSF (50 ng/ml) + 10% FBS (n=2). Scale bars = 200μm

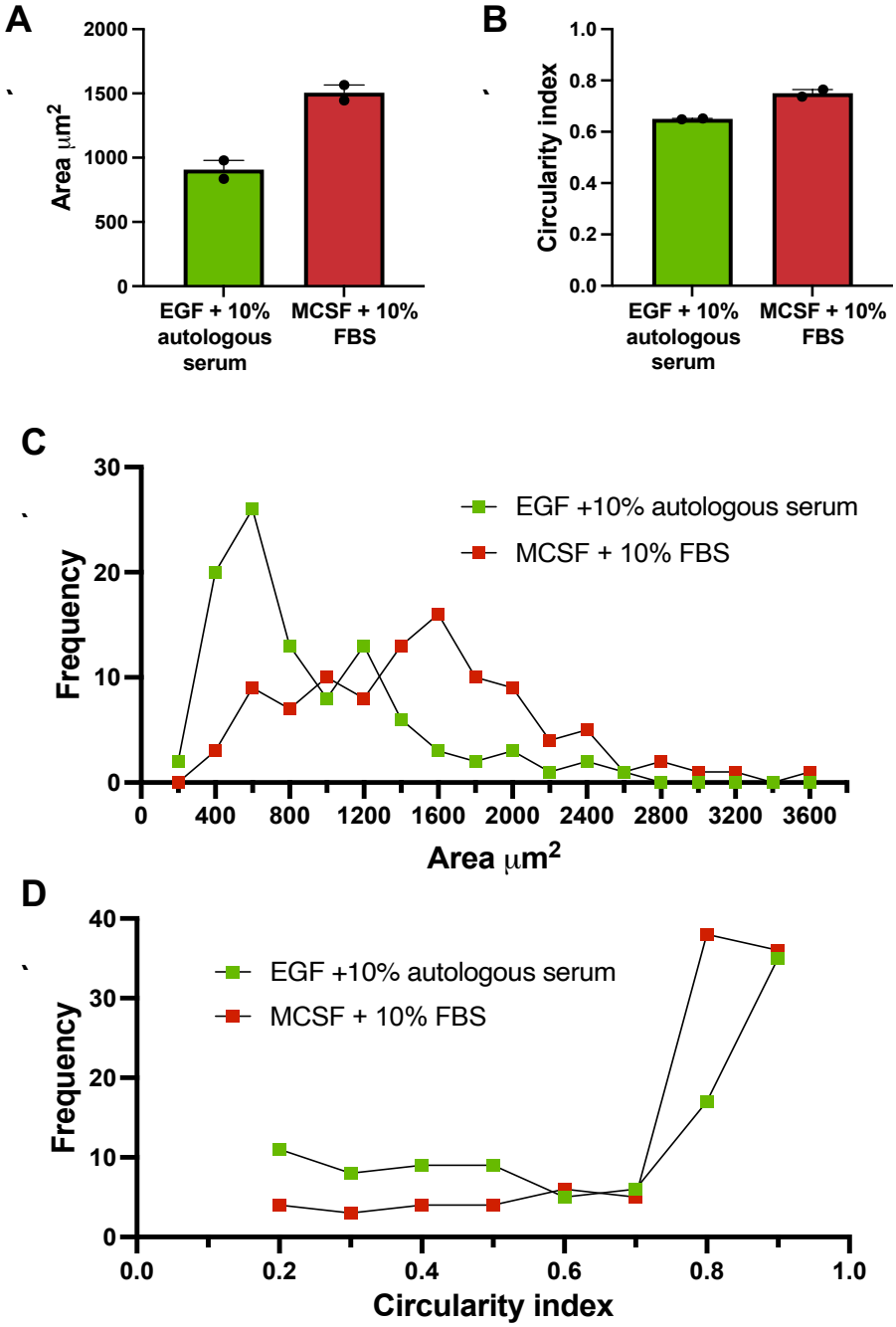


Figure 3-3 Size and circularity index of day 6 macrophages differentiated with autologous serum vs MCSF

$CD14^{+}CD16^{-}$ monocytes were isolated from whole blood PBMCs and differentiated into macrophages for 6 days either with recombinant human EGF (10ng/ml) + 10% autologous serum or recombinant human MCSF (50 ng/ml) + 10% FBS. Average **(A)** Size (μm^2) and **(B)** circularity index of macrophages at day 6 was measured from phase contrast images using image J for a total of 100 cells per sample from 5 different fields of view. **(C)** Frequency of distribution for size and **(D)** circularity index shown between the different culture conditions. Data are mean ± SEM (n=2, biological replicate).

3.2.3. Target selection for macrophage flow cytometry panel design

To investigate the phenotype of macrophages based on their surface marker expression, an extended flow cytometry panel was designed targeting various markers with the aim of defining macrophages and their subtypes as well as measuring scavenger receptor expression (listed and defined in Table 3.1.) A total of 10 targets were selected with the addition of a viability dye to exclude dead cells to enable us to characterise macrophage based on their phenotypic state. The rationale for selection with appropriate citations are also listed in Table 3.1.

Table 3-1 List of targets for flow cytometry panel and functional relevance

Group	Target	Function	References
Macrophage marker	CD68	A glycoprotein that is expressed highly by macrophages and functionally plays a role in various inflammatory and auto-immune responses	(Chistiakov et al., 2017)
	CD11c	An integrin that promotes recruitment and migration of monocytes/macrophages with evidence of increased expression on macrophage-derived foam cells	(Sadhu et al., 2007)
Scavenger receptors	CD36	A scavenger receptor expressed on monocyte/macrophages and is known to specifically bind Ox-LDL	(Nicholson et al., 1995)
	CD204/MSR1	A scavenger receptor expressed monocytes/macrophages that is primarily known to mediated Ac-LDL uptake	(Goldstein et al., 1979b)
	CLEVER-1/Stabilin-1	A scavenger receptor shown to bind Ox-LDL and MA-LDL in hepatic macrophages	(Rantakari et al., 2016)
M1-like marker	CD80	A key co-stimulatory marker expressed transiently on macrophages and binds to CD28 on the surface of T cells to promote or downregulate their activation (acts in conjunction with CD86)	(Jimenez-Uribe et al., 2019, Thiel et al., 2009)
	CD86	A key co-stimulatory marker expressed constitutively on macrophages and binds to CD28 on the surface of T cells to promote or downregulate their activation (acts in conjunction with CD80)	(Thiel et al., 2009)
	HLA-DR/MHC II	A surface receptor responsible for antigen presentation. Down regulation of HLA-DR has been shown to contribute to M2-like macrophage polarisation	(Unuvar Purcu et al., 2022)
M2-like marker	CD206	A C-type lectin expressed primarily on M2-like but not on M1-like macrophages and plays a role in phagocytosis during inflammatory resolution	(Porcheray et al., 2005)
Phagocytosis marker	MerTK	A tyrosine kinase that is key for macrophage phagocytosis during an inflammatory response	(Scott et al., 2001)

3.2.4. Fluorophore selection for selected targets in flow panel

Fluorophores were specifically selected to minimise spectral overlap using Thermofisher's spectral viewer. This enabled visualisation of emission spectra of fluorophores in combination or separated according to specific excitation lasers (Figure 3.4). It is recommended to avoid the selection of fluorophores with high spectral overlap on antigen targets that are co-expressed on a single cell based on the gating strategy (Figure 3.5). However, due to majority of the markers in our panel being co-expressed on macrophages, I selected a combination of fluorophores that were well separated with the aim of having little spectral overlap.

Depending on fluorophore brightness and predicted target abundance, individual fluorophores were paired with selected targets accordingly, with consideration for commercial availably of antibody conjugates. Ideally, targets with higher predicted expression were paired with fluorophores that were less bright whereas brighter fluorophores were paired with targets of low abundance on macrophages to avoid saturation and enable better detection upon analysis (Table 3.2).

3.2.5. Indirect labelling of stabilin-1 antibody with fluorescently labelled antibody

Since the Stabilin-1 antibody (generated in house) in our flow cytometry panel was unconjugated I selected an appropriate fluorescently labelled secondary antibody (anti-mouse Alexa-fluor 700) to confirm binding to Stabilin-1.and subsequent use in our macrophage panel. Staining of $CD14^{+}CD16^{-}$ MDMs with secondary only or both

primary and secondary antibodies was carried out to detect binding. Flow cytometry analysis confirmed the detection of Stabilin-1 via indirect staining with our selected secondary anti-mouse Alexa-fluor 700 antibody as I observed a two-fold increase in MFI compared to the secondary only control (Figure 3.6)

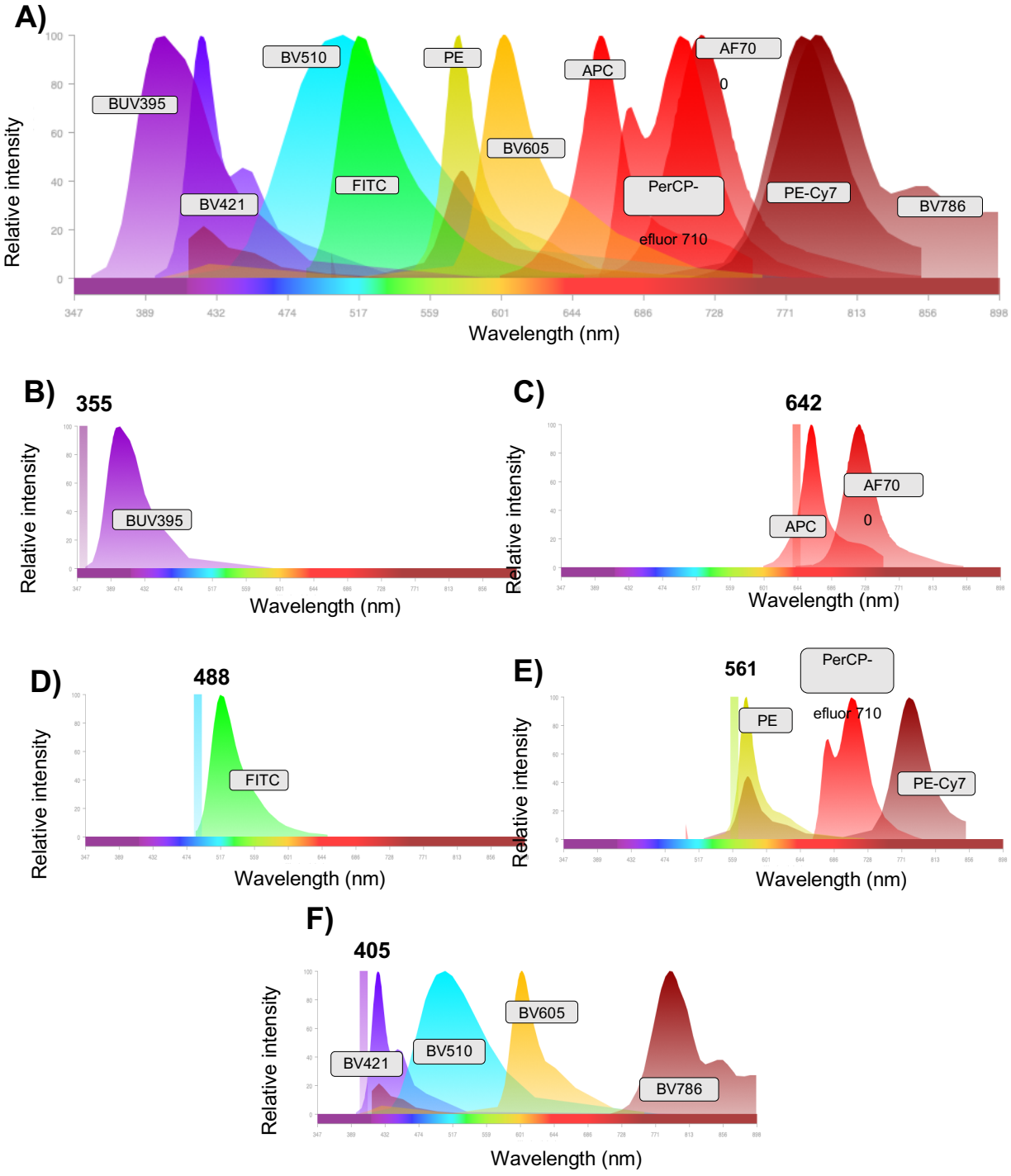


Figure 3-4 Emission spectra of fluorochrome for 11-colour macrophage flow cytometry panel

Relative intensity of each fluorochrome **A)** combined and separated by excitation laser: **B)** 355, **C)** 642, **D)** 488, **E)** 561, **F)** 405

Table 3-2 Relative fluorochrome brightness and predicted target abundance

Laser	Fluorophore	Relative fluorochrome brightness	Target	Predicted target abundance on macrophages
UV (355)	BUV395	Moderate	CD36	Moderate
Violet (405)	BV421	Very bright	CD204/MSR1	Low
	BV786	Bright	CD80	Low
	BV605	Bright	CD86	Moderate
	BV510	Moderate	Zombie aqua	Permeant in dead cells
Blue (488)	FITC	Moderate	HLA-DR/MHC II	Moderate
	efluor-710	Very bright	CD11c	Moderate
	PE-Cy7	Very Bright	CD206	Low
Yellow (561)	PE	Bright	MerTK	Moderate
Red (642)	APC	Bright	CD68	High
	Alexa fluor 700	Dim	Stabilin-1/CLEVER-1	Moderate

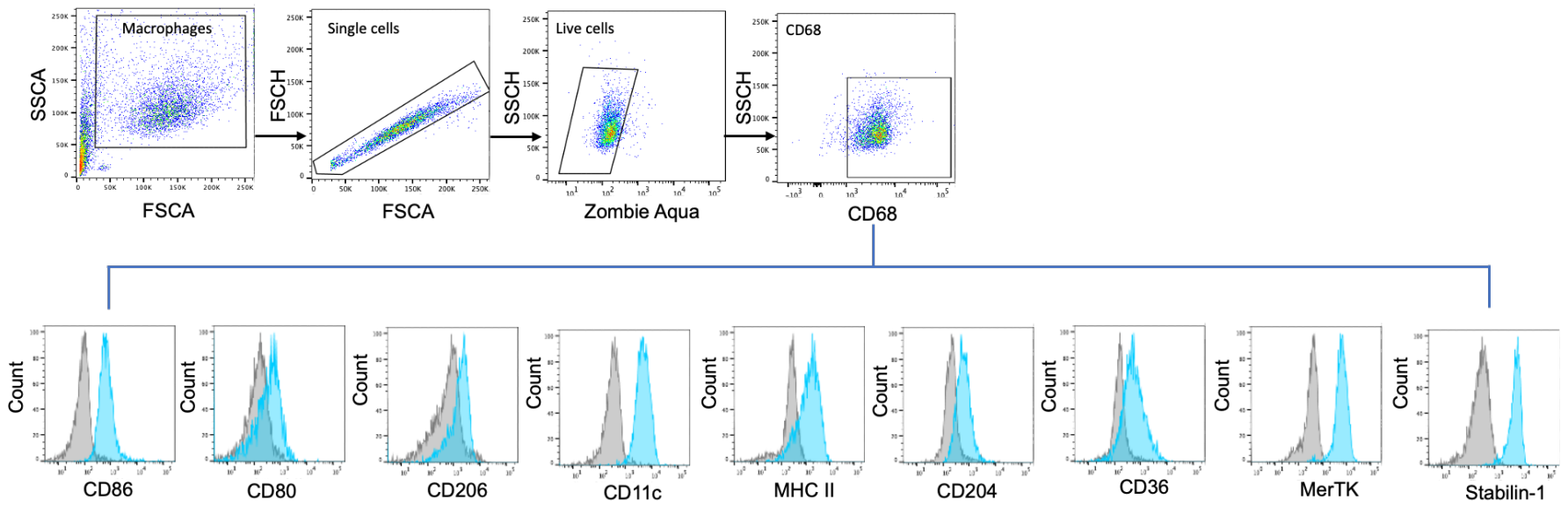


Figure 3-5 Gating strategy for macrophage flow cytometry panel

Macrophages were detached from tissue culture plate and cells were stained with our 11-colour flow cytometry panel. Firstly, macrophages were identified based on the forward and side scatter plots followed by doublet exclusion. Live cells were selected to exclude false artefacts imposed by dead cells. CD68 positive macrophages were then selected from the live population followed by gating on the rest of our panel markers (CD86, CD80, CD206, CD11c, MHC II, CD204, CD36, MerTK and Stabilin-1) to determine MFI values.

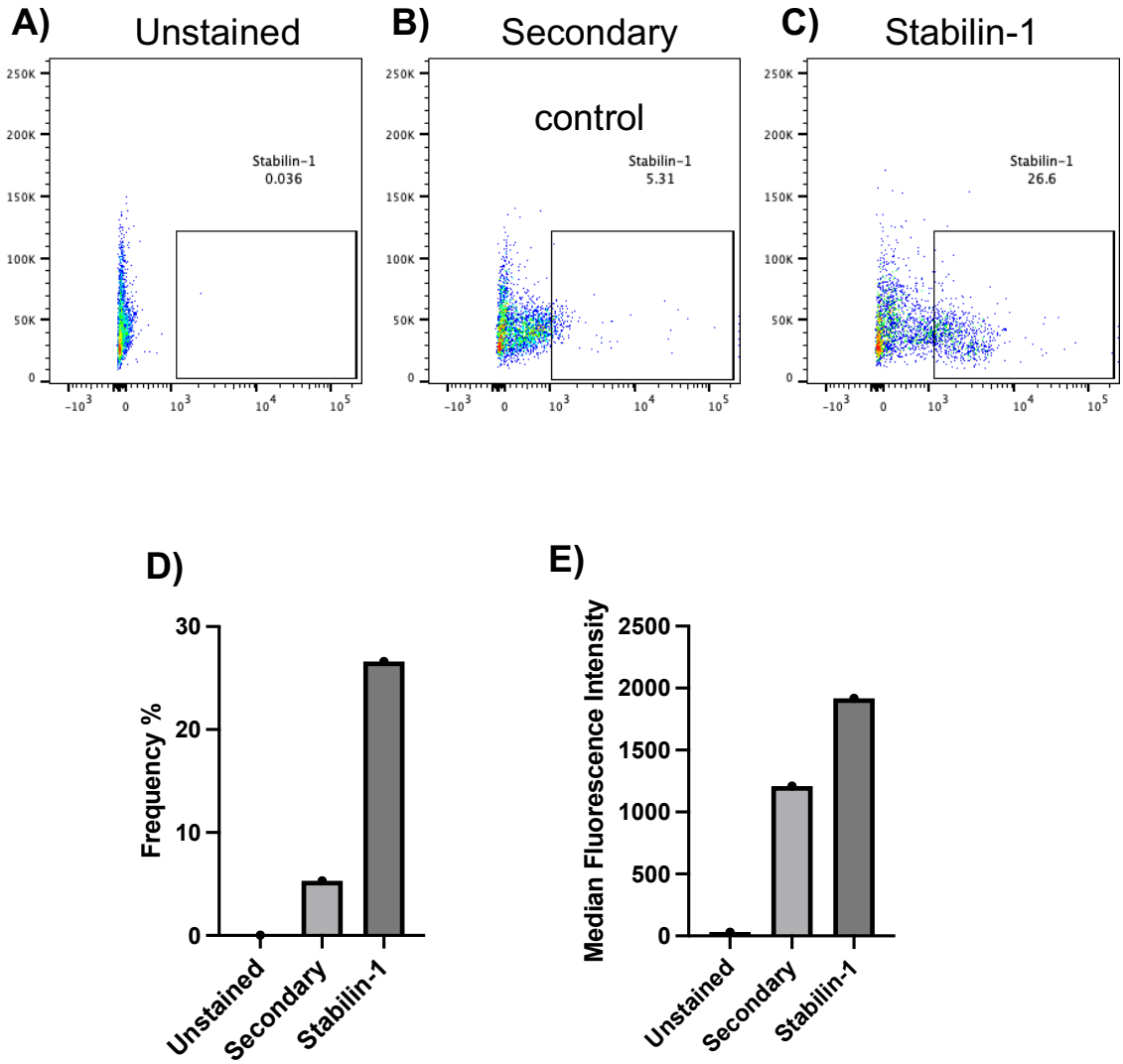


Figure 3-6 Gating strategy to confirm binding of primary unconjugated Stabilin-1 antibody to Alexa-fluor 700 fluorescently labelled secondary antibody.

Monocyte-derived macrophages cultured till day 6 were harvested using MACS buffer and were stained with either secondary antibody only (anti-mouse conjugated to Alexa-fluor 700) or primary unconjugated Stabilin-1 antibody (10 μg/ml) followed by secondary antibody to confirm binding. Flow cytometry plots for **(A)** unstained, **(B)** secondary control and **(C)** Stabilin-1 antibody stained cells are shown. **(D)** Percentage frequency and **(E)** median fluorescence intensity (MFI) was assessed, (n=1).

3.2.6. Single antibody stain analysis

The avoidance of reduced data resolution in multi-colour flow cytometry panels due to spectral overlap can be a challenge. To determine whether spectral overlap had an impact on our entire macrophage panel I stained detached $CD14^{+}CD16^{-}$ MDMs individually with each antibody as well as the entire panel of antibodies combined. I compared changes in fluorescence intensity between individual antibodies and the combined panel to determine whether the selected antibody signal was being compromised by the fluorescent emission of other antibodies in the panel.

For anti-CD86, anti-CD204, anti-CD206 and anti-CD68 minimal to no change in MFI expression was observed in single stained vs whole panel staining, suggesting negligible reduction in sensitivity for antibodies on these channels (Figure 3.7). However, for anti-CD11c, anti-CD36, anti-CD80, anti-Stabilin-1, anti-MerTK and anti-HLA-DR, a decrease in MFI was clear, signifying a reduction in sensitivity in these channels as a result of spectral overlap (Figure 3.8).

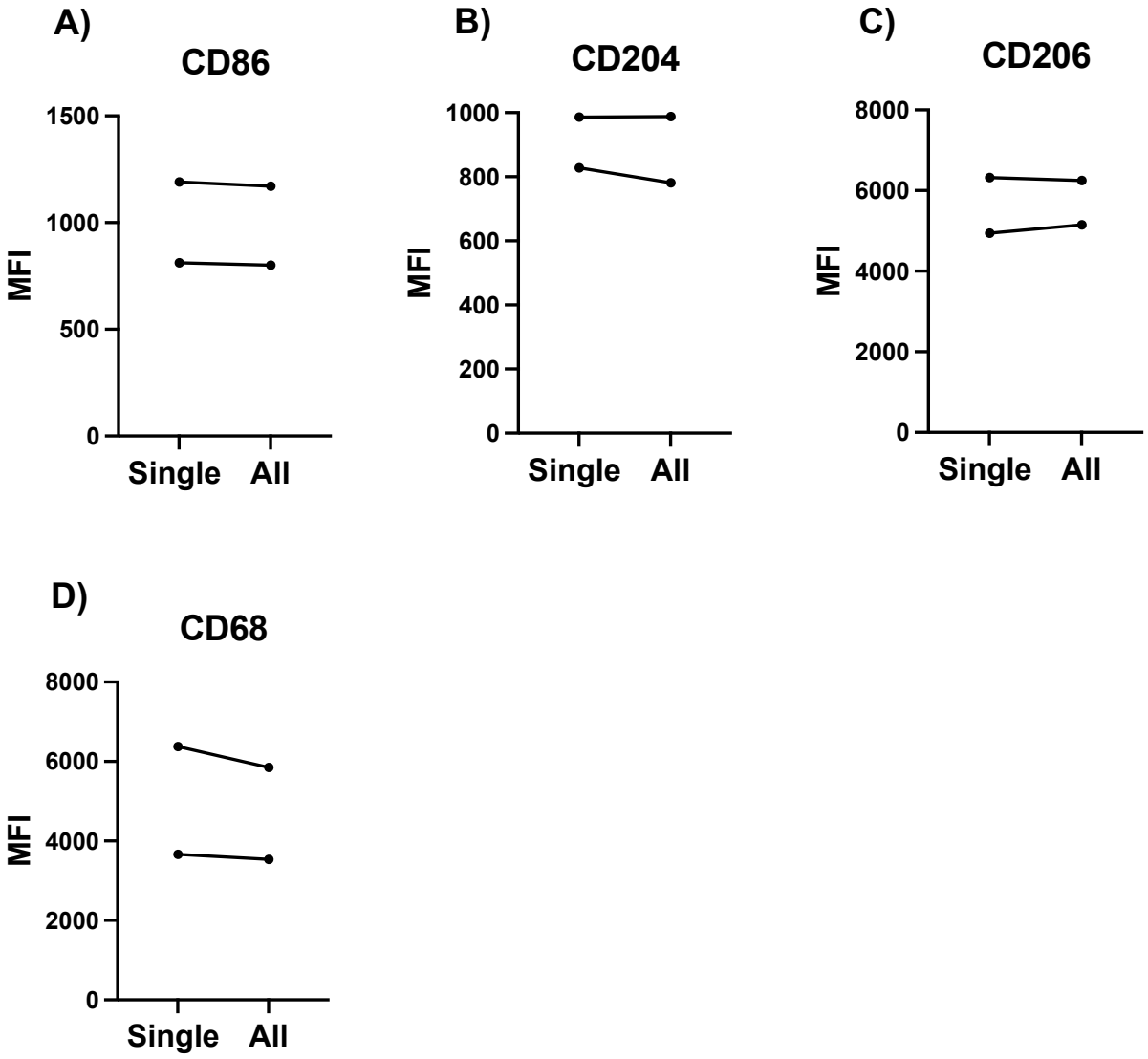


Figure 3-7 Median fluorescence intensity of macrophages stained individually with anti-CD86, anti-CD204, anti-CD206, anti-CD86 or in combination with all antibodies in the panel

$CD14^{+}CD16^{-}$ monocytes (from healthy donors) (n=2) were isolated from whole blood PBMCs and differentiated into macrophages for 6 days. Macrophages were harvested and stained individually with **(A)** anti-CD86, **(B)** anti-CD204, **(C)** anti-CD206, **(D)** anti-CD68 or with all relevant antibodies described in Table 2.1. Staining was performed alongside their corresponding isotype controls to determine correct gating via flow cytometry analysis. Median fluorescence intensity (MFI) plotted, n=2, biological replicate.

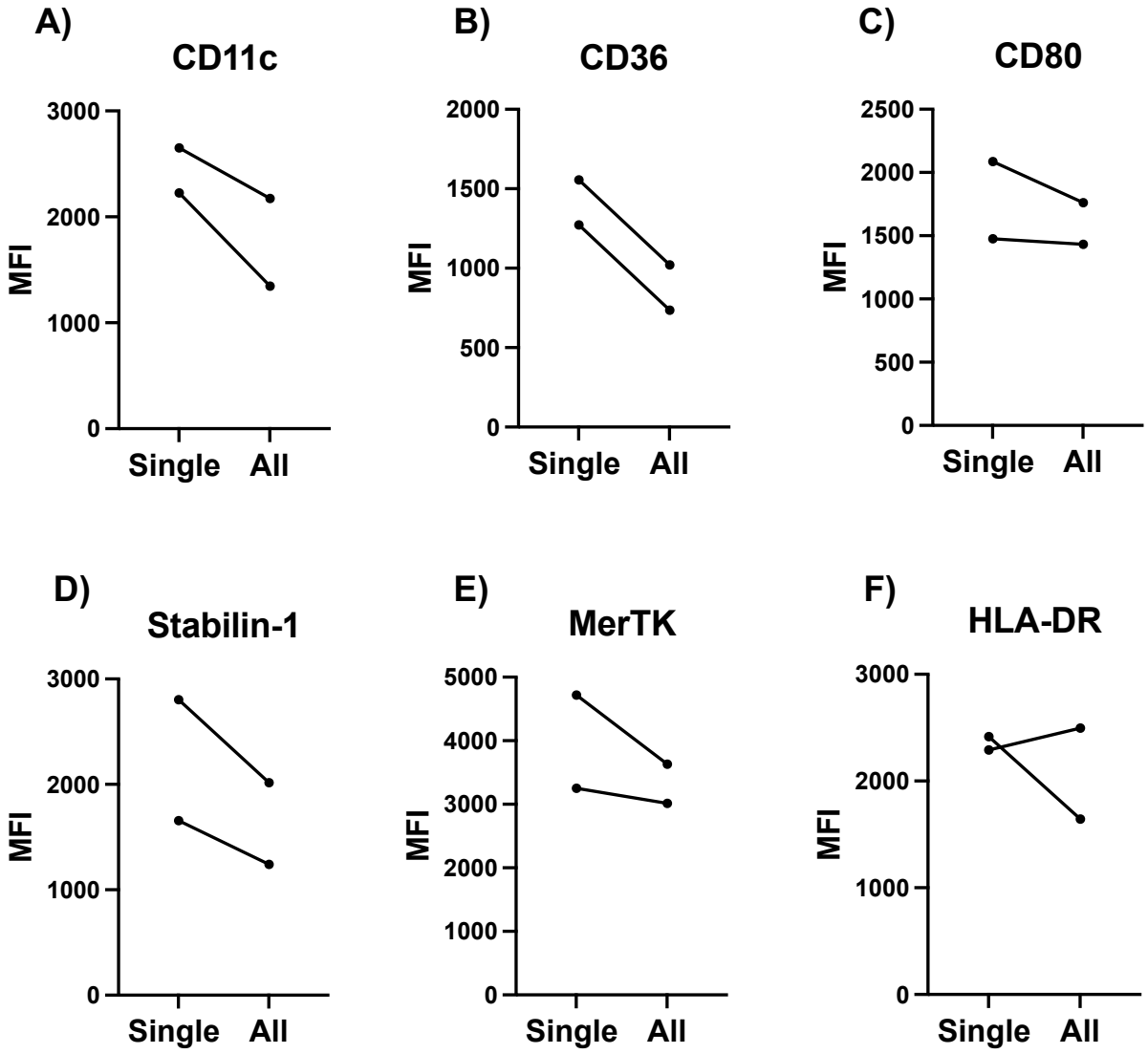


Figure 3-8 Median fluorescence intensity of macrophages stained individually with anti-CD11c, anti-CD36, anti-CD80, anti-Stabilin-1, anti-MerTK, anti-HLA-DR or in combination with all antibodies in the panel

$CD14^{+}CD16^{-}$ monocytes (from healthy donors) (n=2) were isolated from whole blood PBMCs and differentiated into macrophages for 6 days. Macrophages were harvested and stained individually with **(A)** anti-CD11c, **(B)** anti-CD36, **(C)** anti-CD80, **(D)** anti-Stabilin-1 **(E)** MerTK, **(F)** HLA-DR or with all relevant antibodies described in Table 2.1. Staining was performed alongside their corresponding isotype controls to determine correct gating via flow cytometry analysis. Median fluorescence intensity (MFI) plotted, n=2, biological replicate.

3.2.7. The effects of macrophage detachment methods on surface protein expression

Due to the highly adherent nature of human macrophages in cell culture, harvesting these cells from tissue culture treated polystyrene plates has the disadvantage of significant cell death or impaired surface protein expression (Malheiro et al., 2017, Glazer et al., 2010). I looked to identify a suitable method for macrophage detachment for flow cytometry analysis with minimal loss of protein expression by comparing both enzymatic (Trypsin and Accutase) and non-enzymatic techniques (cell dissociation buffer, EDTA and MACS buffer). I looked at the expression and frequency of CD86 and CD206 (a marker that is readily cleaved) macrophage markers on $CD14^{+}CD16^{-}$ MDMs.

The expression (MFI) and frequency of CD86 was unaffected by the various detachment methods (Figure 3.9 A-B), however both CD206 expression (MFI) and frequency was significantly reduced with Trypsin treatment, suggesting cleavage of the surface protein which has been reported by previous studies (Figure 3.9 C-D). Other methods did not show dramatic differences in signal. Ultimately, I selected MACS buffer at room temperature for our preferred method of detachment., although the differences observed were marginal compared to the other methods, the use of MACS buffer at RT demonstrated superior performance in maintaining CD86 and CD206 surface marker expression.

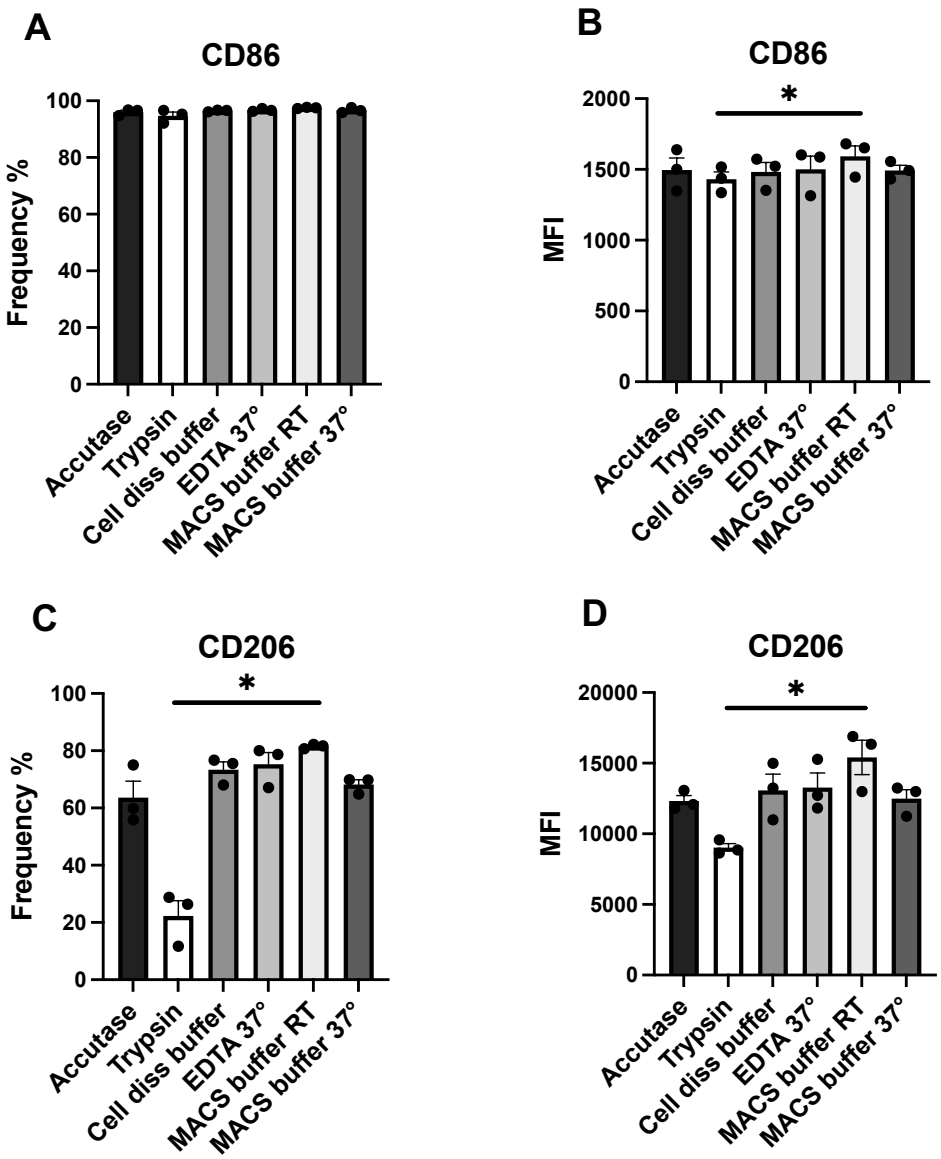


Figure 3-9 Frequency and median fluorescence intensity of CD86 and CD206 surface markers following detachment from plastic using various dissociation methods

$CD14^{+}CD16^{-}$ monocytes were isolated from whole blood PBMCs and differentiated into macrophages for 6 days in 24-well tissue-cultured treated plates. Macrophages in corresponding wells were treated with various dissociation methods: Accutase (10 mins at 37 °C), Trypsin (10 mins at 37 °C), Cell dissociation buffer (20 mins at 37 °C) 0.05 mM EDTA (20 mins at 37 °C), MACS buffer (20 mins at 37 °C) or RT MACS buffer (20 mins) followed by gentle cell scraping. Macrophages were stained for anti-CD86 and anti-CD206 antibodies or flow cytometry analysis. Percentage frequency and median fluorescence intensity (MFI) was plotted for both **(A-B)** CD86 and **(B)** CD206. Data are mean ± SEM (n=3, biological replicate). Statistical analysis performed using non-parametric Friedmans test with Dunn's post-hoc test for comparisons between each condition, *=$p<0.05$.

3.2.8. Time course for macrophage polarisation to macrophage subtypes

Macrophages can assume differential characteristics due their plasticity and their phenotypic outcome is highly dependent on the microenvironment including tissue of origin (Raggi et al., 2017, Zhang et al., 2021, Stout et al., 2005). Distinguishing between the different macrophage subsets is typically achieved by analysing differences in surface marker expression and inflammatory mediator secretion (Tabas and Bornfeldt, 2016, Zhang et al., 2021).

In order to validate our flow panel, I carried out flow cytometry staining using our full panel of antibodies (see table 3.2) to distinguish and define M0 (naïve), M1 and M2-like macrophage phenotypes derived from $CD14^{+}CD16^{-}$ monocytes. Classically M1 macrophage express high levels of CD80 and CD86 (co-stimulatory markers) whilst M2 macrophages are more enriched for CD206 and MerTk expression. Since the length of stimulation can greatly affect protein expression, I performed a time course for macrophage polarisation to establish an appropriate stimulation time for the characterisation of macrophage subtypes for utilisation in further assays.

After 6 days in culture, MDMs were polarised for 24, 48 and 72 hours using LPS and IFNγ for M1 macrophages and IL-4 for M2 macrophages and supernatants were collected for TNF-α ELISA analysis to confirm the different polarisation states. As expected, pro-inflammatory M1 macrophages demonstrated a drastic increase in secreted levels of TNF-α compared to both M0 and M2 macrophages and this appeared to peak at 24hrs and decrease slightly over the extended time period for stimulation (Figure 3.10). Additionally, flow cytometry analysis confirmed a higher expression of CD80 on M1 macrophages and CD206 (M2-like marker) on the M2

macrophages which was visually demonstrated in the gating strategy (Figure 3.11). These differences were evident at 24-hour stimulation but were significant at both 48- and 72-hour stimulations. Additional co-stimulatory markers such as such CD86 were elevated on M1 macrophages as expected, whereas expression of M1 markers such as HLA-DR started to diminish post 24-hour polarisation (fFigure 3.12).

The expression of pan macrophage markers CD68 and CD11c showed minimal differences between macrophage subtypes although I observed a slight increase in CD11c in M2 macrophages post 24-hour stimulation. On the other hand, the phagocytic marker, MerTK was expressed significantly higher in M0 and M2 macrophages compared to the M1 macrophages as anticipated based on existing studies and these changes were consistent over the stimulation time course (Figure 3.13).

I also looked at the expression of several scavenger receptors as part of our panel and observed greater CD36 expression on M2 macrophages compared to the M1 subset as predicted, which increased with time. CD204 and Stabilin-1 expression however remained consistent across the different macrophage subsets with no differences observed over the time course (Figure 3.14). Collectively, our analysis demonstrates successful polarisation of macrophages into the different subsets that can be distinguished using specific markers in our flow cytometry panel, with differences being present at 24-hour macrophage stimulation.

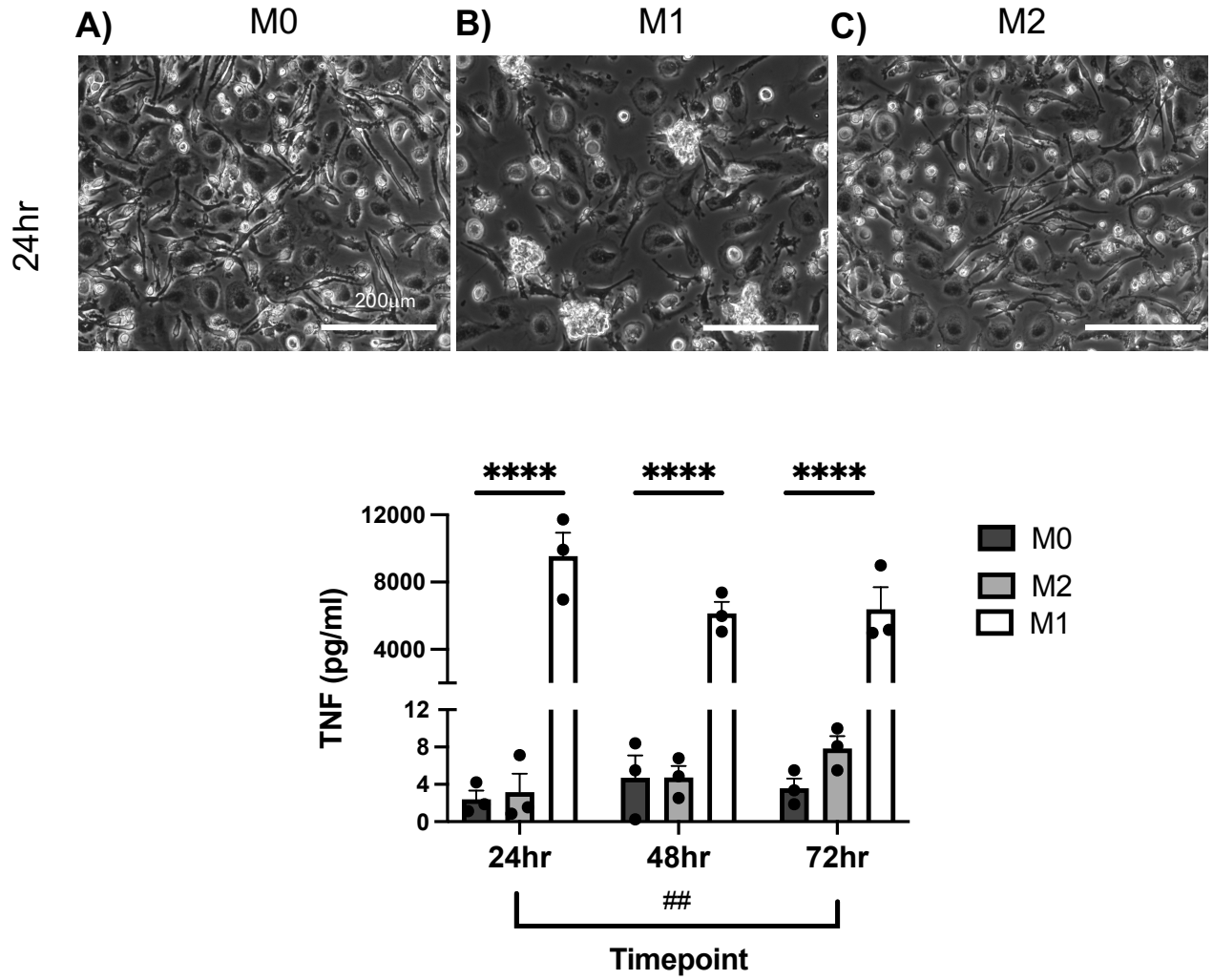


Figure 3-10 TNF-α secretion from macrophages polarised towards an M1 and M2 phenotype

$CD14^{+}CD16^{-}$ monocyte-derived macrophages (on day 6) were left untreated (M0 macrophage) or were polarised to M1 macrophages with 100 ng/ml LPS and 20 ng/ml IFN- γ or M2 macrophages with 20 ng/ml IL-4 for 24 hrs. Cell-culture supernatants were collected after each timepoint. Phase contrast images were taken displaying macrophage morphology (shown for 24 hr polarisation) **(A-C)** and TNF-α ELISA concentrations (pg/ml) were measured via ELISA **(D).** Data are mean ± SEM (n=3, biological replicate). Statistical analysis performed using two-way repeated measures ANOVA with Dunnetts post-hoc test compared to the M0 group, ****=p<0.0001, ##=p<0.01. Scale bars = 200μm.

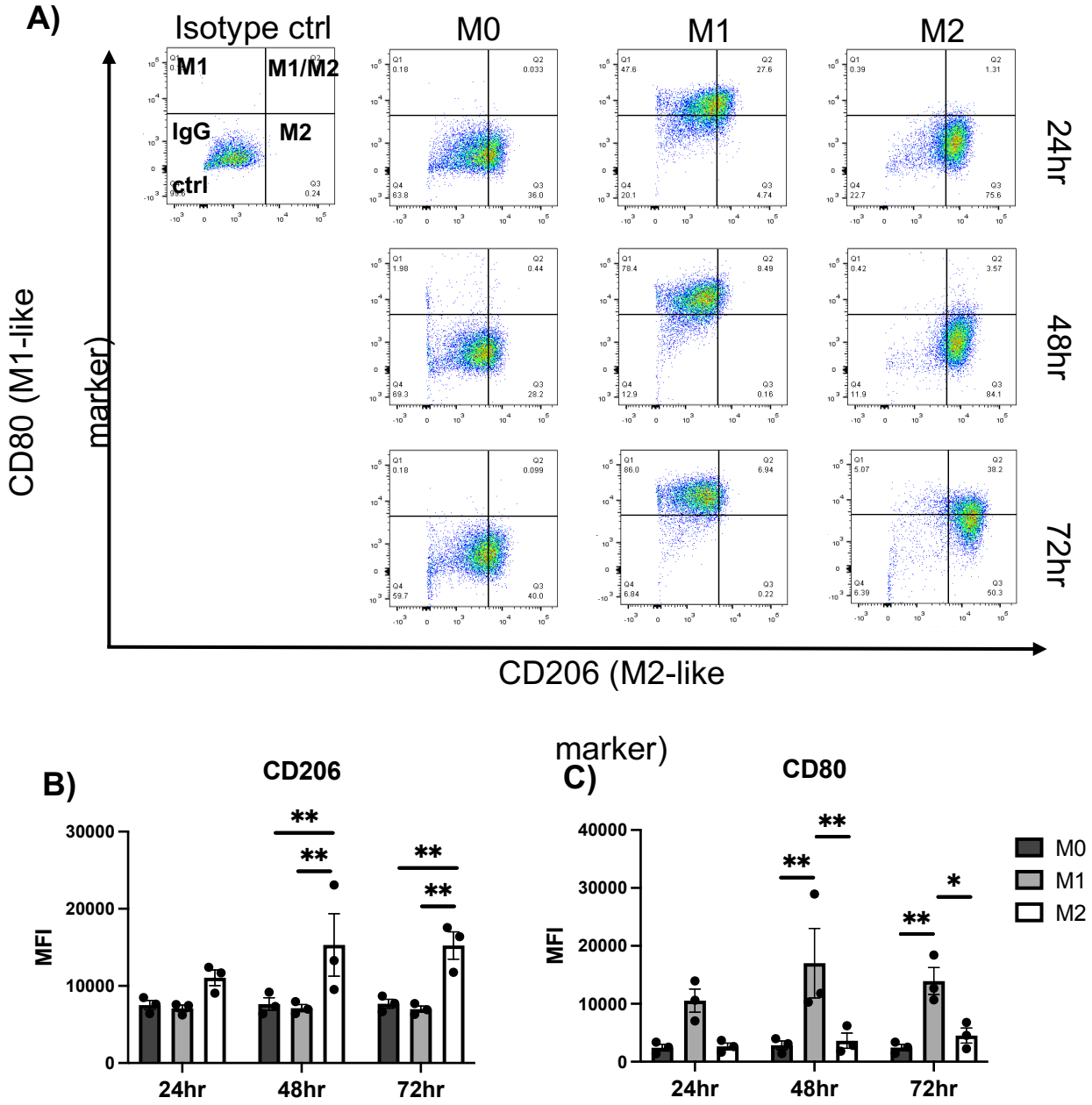


Figure 3-11 Flow cytometry analysis of macrophages for anti-CD206 and anti-CD80 antibodies on M0, M1 and M2 macrophage phenotypes.

$CD14^{+}CD16^{-}$ monocytes were isolated from whole blood PBMCs and differentiated into macrophages for 6 days. On day 6, macrophage were left untreated (M0) or were polarised to M1 macrophages with 100 ng/ml LPS and 20 ng/ml IFN- γ or M2 macrophages with 20 ng/ml IL-4 for 24, 48 or 72 hrs. Cells were dissociated and stained for all antibodies in the flow cytometry panel described in Table 2.1. (A) Gating strategy for M1 and M2 macrophage polarisation demonstrated by visualising expression of CD80 (M1 marker) and CD206 (M2 marker) across the different timepoints. Median fluorescence intensity (MFI) was plotted for (B) CD206 and (C) CD80. Data are mean ± SEM (n=3, biological replicate). Statistical analysis performed using two-way repeated measures ANOVA test with Tukey post-hoc test, *=p<0.05, **=p<0.01.

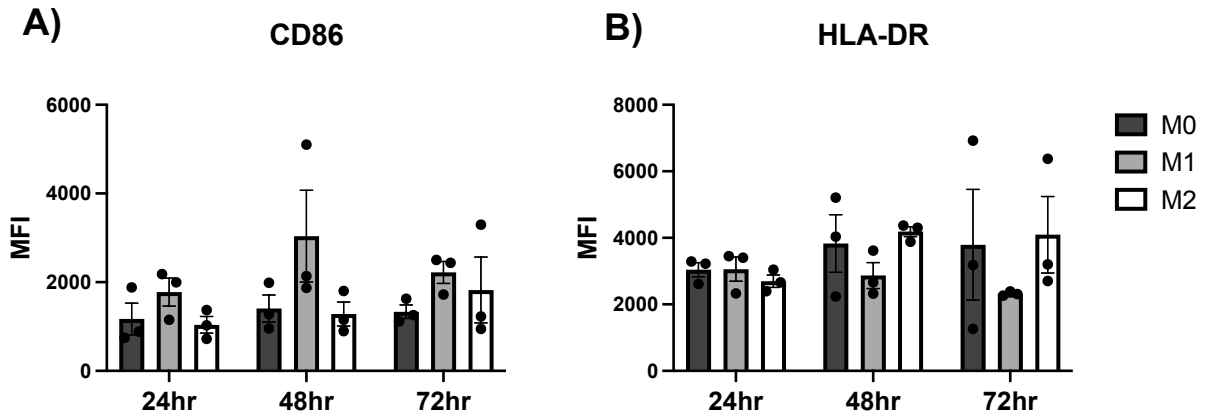


Figure 3-12 Flow cytometry analysis of M1-like macrophage markers on M0, M1 and M2 macrophage phenotypes.

$CD14^{+}CD16^{-}$ monocytes were isolated from whole blood PBMCs and differentiated into macrophages for 6 days. On day 6, macrophage were left untreated (M0 macrophage) or were polarised to M1 macrophages with 100 ng/ml LPS and 20 ng/ml IFN- γ or M2 macrophages with 20 ng/ml IL-4 for 24, 48 or 72 hrs. Cells were dissociated and stained for all antibodies in the flow cytometry panel described in Table 2.1. Median fluorescence intensity (MFI) was plotted for **(A)** CD86 and **(B)** HLA-DR. Data are mean ± SEM (n=3, biological replicate). Statistical analysis performed using two-way repeated measures ANOVA test with Tukey post-hoc test.

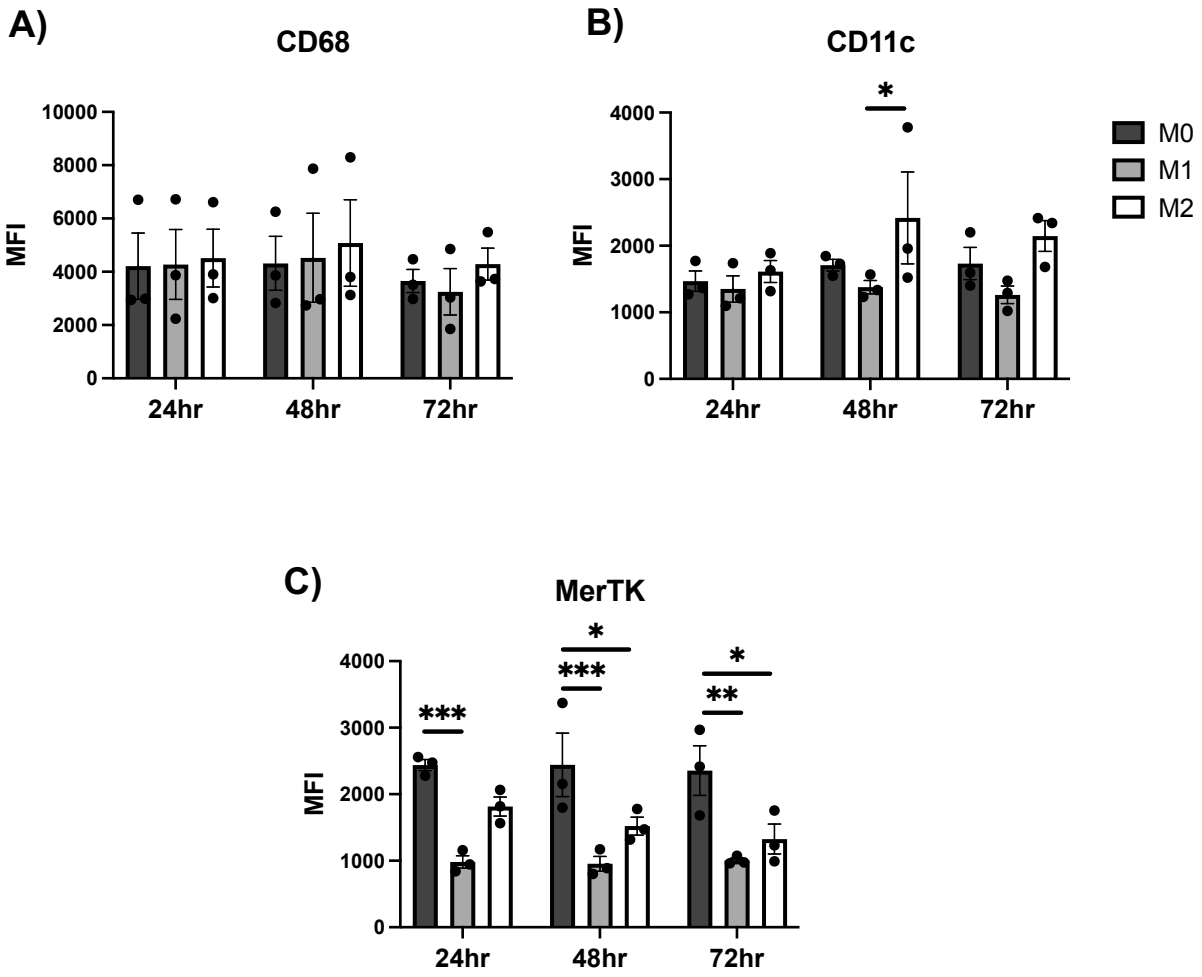


Figure 3-13 Flow cytometry analysis of anti-CD68, anti-CD11c and anti-MerTK macrophage markers on M0, M1 and M2 macrophage phenotypes.

$CD14^{+}CD16^{-}$ monocytes were isolated from whole blood PBMCs and differentiated into macrophages for 6 days. On day 6, macrophage were left untreated (M0 macrophage) or were polarised to M1 macrophages with 100 ng/ml LPS and 20 ng/ml IFN- γ or M2 macrophages with 20 ng/ml IL-4 for 24, 48 or 72 hrs. Cells were dissociated and stained for all antibodies in the flow cytometry panel described in Table 2.1. Median fluorescence intensity was plotted for **(A)** CD68, **(B)** CD11c and **(C)** MerTK. Data are mean ± SEM (n=3, biological replicate). Statistical analysis performed using two-way repeated measures ANOVA test with Tukey post-hoc test, *=$p<0.05$, **=$p<0.01$, ***=$p<0.001$.

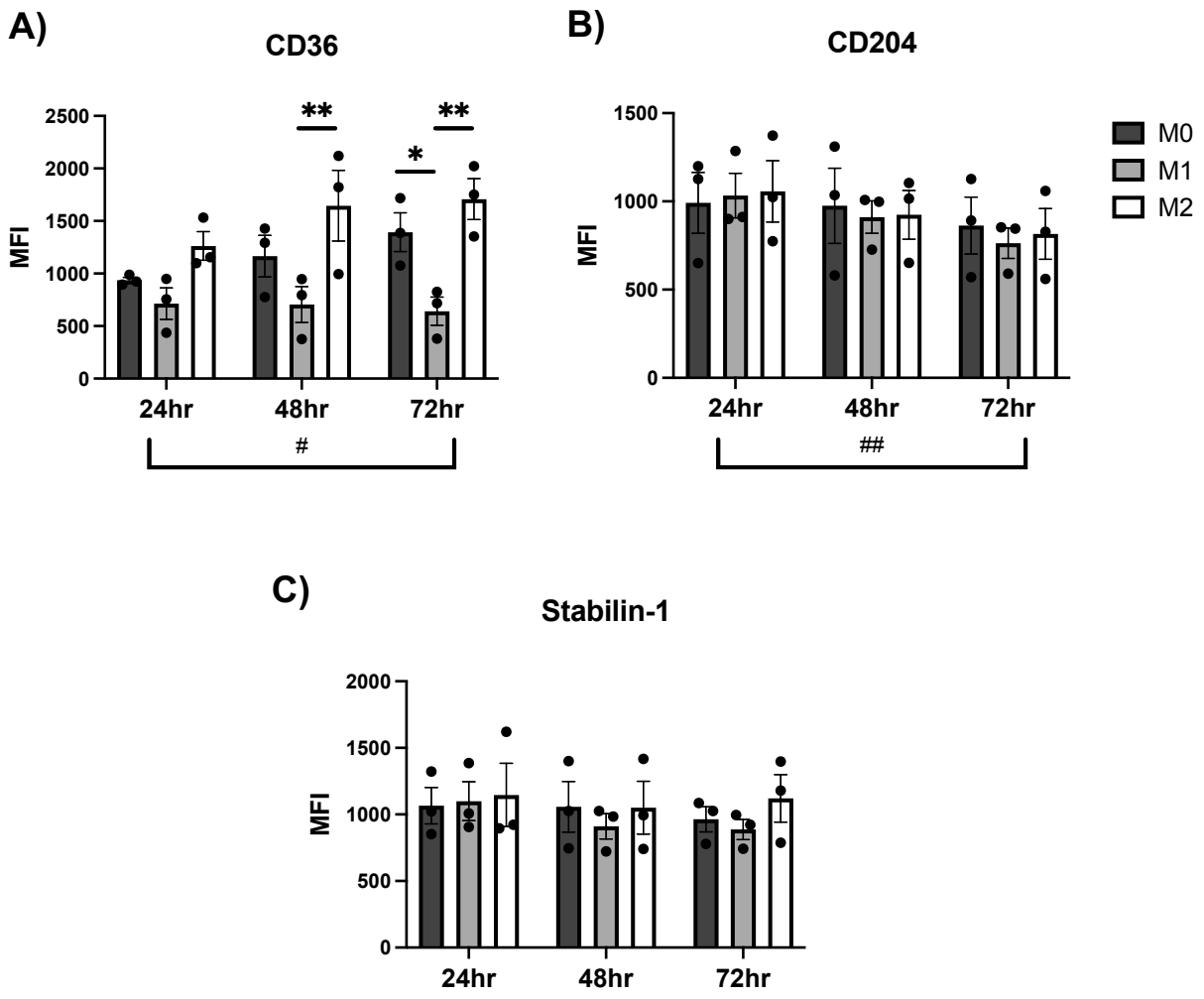


Figure 3-14 Flow cytometry analysis of scavenger receptors on M0, M1 and M2 macrophage phenotypes.

$CD14^{+}CD16^{-}$ monocytes were isolated from whole blood PBMCs and differentiated into macrophages for 6 days. On day 6, macrophage were left untreated (M0 macrophage) or were polarised to M1 macrophages with 100 ng/ml LPS and 20 ng/ml IFN- γ or M2 macrophages with 20 ng/ml IL-4 for 24, 48 or 72 hrs. Cells were dissociated and stained for all antibodies in the flow cytometry panel described in Table 2.1. Median fluorescence intensity was plotted for **(A)** CD36, **(B)** CD204 and **(C)** Stabilin-1. Data are mean ± SEM (n=3, biological replicate). Statistical analysis performed using two-way repeated measures ANOVA test with Tukey post-hoc test, *=$p<0.05$, **=$p<0.01$, #=$p<0.05$, ##=$p<0.01$.

3.3. Discussion

Macrophages and their various phenotypes (M0, M1 and M2) can be characterised based on their extracellular and intracellular marker expression, which is typically defined using two or three markers. Technological advancements in flow cytometry, coupled with the expanding knowledge of our immune system has enabled the design of larger more complex flow cytometry panels providing a powerful platform for more in-depth characterisation of immune cells on a single-cell basis. Flow cytometry analysis of macrophages in particular is complicated due to their highly adherent nature making it difficult to obtain viable, single-cell suspensions. Here I have designed and optimised an extensive 11-colour flow cytometry panel for the characterisation of cultured human MDMs that have been polarised over various time points with the aim of detecting phenotypic changes in macrophages exposed to various biological stimulants. I have optimised our protocol for the differentiation of macrophages in culture using recombinant MCSF and selected a suitable non-enzymatic method for cell detachment whilst maintaining surface protein expression for flow cytometry analysis.

3.3.1. Optimisation of MDM culture

Primary human macrophages are difficult to obtain from tissue due to poor yields and low viability, hence the use of primary peripheral monocytes as precursors for macrophage differentiation in culture is widely used to model tissue macrophages. Several studies have investigated different methods of monocyte isolation that can have an impact on their functional behaviour (Elkord et al., 2005, Lyons et al., 2007). By using positive magnetic bead separation, I demonstrated that I was able to isolate

highly purified populations of $CD14^{+}CD16^{-}$ and $CD14^{+}CD16^{+}$ monocytes subsets, confirmed via flow cytometry. Compared to negative selection, positive selection methods have been shown to yield greater MDM purity levels with low platelet contamination, whilst also maintaining their phagocytic abilities (Nielsen et al., 2020, Zhou et al., 2012). However, there are also studies reporting that positive selection of monocytes may lead to impaired cellular functionality in the context of cytokine production, adhesion as well as reduced sensitivity to LPS stimulation, which have been shown to be preserved with negative sorting. Hence, it is important to take these factors into consideration when performing downstream functional assays with these cells (Bhattacharjee et al., 2017, Hornschuh et al., 2022).

Further differentiation of isolated monocytes into macrophages can be achieved by exposing monocytes to different culture conditions resulting in macrophages with varying morphological differences that can have on impact on their functional behaviour. Maturation of monocytes in autologous serum is routinely used in some studies to preserve the individual traits of the blood donor (Musson, 1983, W.D., 1977, Krautter et al., 2020). However, I observed unacceptable levels of donor variability in cell viability in culture, with approximately 1 in 3 donors showing substantial adhesion and differentiation over the duration of the experiment. However, the addition of recombinant MCSF in cultures has been deemed superior for monocyte differentiation, due to increased cell survival, proliferation, and maturation as demonstrated (Tushinski et al., 1982, Brugger et al., 1991, Safi et al., 2016, Jin and Kruth, 2016). I found that macrophages from all donors survived and differentiated in the presence of MCSF with 10% FBS. Interestingly, these cells were on average, greater in size which is typically an indication of macrophage maturation, whereas autologous serum differentiated

macrophages were smaller in size, potentially indicating a lesser effect in monocyte to macrophage trans-differentiation, as previously reported similarly by Safi *et al,* who observed lower CD68 expression on mature macrophages cultured in autologous serum compared with MCSF (Safi et al., 2016).

Two main morphotypes are typically observed in macrophage cell culture, that is rounded egg-shaped cells or an elongated spindle-like morphology, both of which have been reported to have distinct phenotypic characteristics. It is suggested that rounded cells have higher lipid content and have superior efferocytosis abilities compared to those of an elongated phenotype (Eligini et al., 2013, Franzoni et al., 2017). Whilst I observed a mixture of morphotypes in both macrophage cultures, I found recombinant MCSF (with 10% FBS) differentiated macrophages to have a higher circularity index. For this study, functional characteristics of macrophages in our cultures were not compared, which was mainly due to the poor viability observed with monocytes cultured in autologous serum and EGF for the majority of our donors, which I assume to be due to the inter-donor variation in serum constituents. Thus, it would be ideal to measure levels of MCSF within autologous serum, prior to culture in the future to determine variation in monocyte survival. Although the use of autologous serum is more physiologically relevant to the donor, I found the use of recombinant MCSF with 10% FBS provided a robust and consistent method for MDM differentiation, as the presence of MCSF is essential for the survival and differentiation of monocytes in culture (Becker et al., 1987, Brugger et al., 1991).

3.3.2. The design and validation of a flow cytometry panel for macrophages

For the characterisation of macrophages in our experiments, I established an extensive eleven-colour flow cytometry panel that enabled the detection of multiple

markers simultaneously on a single cell both intracellularly and extracellularly. Currently there are limited studies published on human macrophage flow cytometry analysis using large polychromatic panels, due to the inherent adherent and autofluorescent nature of these cells.

The first step in designing our flow cytometry panel required the selection of appropriate fluorophores that presented with minimal spectral overlap. This is to avoid issues with excessive compensation which can ultimately lead to loss of data resolution, particularly with dimly expressed antigens (Bhowmick et al., 2021, Holmberg-Thyden et al., 2021). However, compensation is almost unavoidable especially with large multicolour panels, hence careful selection of fluorophores with best spectral separation was required to increase the accuracy of detecting our markers. Assigning fluorophores to each marker was based on expected antigen density on macrophages determined from data in the existing literature and fluorophore brightness index published online by antibody manufacturers. To exclude non-specific binding the corresponding isotype-matched controls were also used. It was important that the correct matching isotype controls were used to define an accurate level of background staining to the test antibody (Maecker and Trotter, 2006).

Investigating the compatibility of antibodies in the panel as a collective was assessed by comparing whole panel staining to single stains. Loss in the sensitivity of some channels was detected compared to single stains which is a consequence of extensive flow cytometry panels. This means that the greater the number of fluorescent markers, the greater the probability of compromising the resolution of target antigens (Ferrer-Font et al., 2021, Nguyen et al., 2013). Resolution can also be affected by autofluorescence which macrophages are notoriously known for (Njoroge et al., 2001).

In an attempt to minimise autofluorescence, dead cells were excluded using a viability marker as well as the use of unstained controls to determine levels of autofluorescence and avoid selection of false positive populations (Zamai et al., 1993, Li et al., 2012). Compared to conventional flow cytometry, advanced spectral flow cytometry technology now has the ability to define autofluorescence as its own individual parameter and improve the accuracy of fluorescence detection. It can be utilised for future applications for macrophage flow cytometry (Ferrer-Font et al., 2021).

3.3.3. Characterisation of macrophage phenotypes

Distinct M1 and M2 macrophage subsets can be generated *in vitro* by polarisation using specific activating agents. Pro-inflammatory M1-like macrophages are generated by treating macrophages with LPS and IFNγ. Pro-resolving, anti-inflammatory M2-like macrophages are typically generated with IL-4 treatment (Krautter et al., 2020, Cao et al., 2019). Data from our flow cytometry panel was in strong agreement with data from existing literature.

Since all macrophages are innately positive for the markers in our panel (at varying levels), it was irrational to plot percentage positive cells and instead I measured fluorescence intensity. TNF-α levels in cell-culture supernatants were determined via ELISA to confirm polarisation. I also found that polarising macrophages in vitro over a specific time course can affect their level of expression of some markers, and this varied across the different markers as reported similarly by Purcu *et al* in human MDMs.

As expected, LPS and IFNy stimulated macrophages displayed an M1 phenotype with an increase in prototypical M1 markers, CD80 and CD86. Both are

costimulatory molecules that drive T cell activation via their engagement with the CD28 T cell receptor and their expression levels are shown to correlate with increased atherosclerotic plaque vulnerability (Meletta et al., 2016, Buono et al., 2004). Whilst CD86 levels varied little over the polarisation time course, CD80 expression increased significantly after 24 hr and peaked at 48 hrs compared to both M2 and unstimulated macrophages, after which, levels of CD80 diminished indicating a possible shift to an M2 like phenotype. Levels of pro-inflammatory TNF-α secretion in culture followed a similar trend, demonstrating decreased levels with prolonged M1 macrophage stimulation as reported previously (Unuvar Purcu et al., 2022). These observations maybe a reflection of the dynamic changes in macrophage activation states, highlighting that polarised macrophages are not confined to a fixed phenotypic state throughout their evolution as they are not terminally differentiated (Little et al., 2014, Khallou-Laschet et al., 2010, Munoz-Rojas et al., 2021).

Purcu *et al* (Unuvar Purcu et al., 2022) have indicated that 12 hr stimulation is the optimal stimulation time for CD86 expression on M1 macrophages, suggesting that perhaps after this time frame CD86 expression levels plateau as I observed with our data. The expression of MHC II is also required for T cell activation via presentation of peptide antigens that bind surface T cell receptors. M1 macrophages are typically associated with higher expression of MHC II compared to the M2 phenotype as demonstrated in both human MDMs and murine macrophages (Ahmed and Ismail, 2020, Wang et al., 2020, Buchacher et al., 2015). I observed no differences in its expression between the different macrophage subsets and in fact, I saw a decrease in the intensity of MHC II expression in M1 macrophages after 24 hrs which was similarly observed by Liu *et al* in murine macrophages (Liu et al., 2022b). This suggests that a

lesser stimulation time may be optimal for its expression as shown by Purcu *et al* (Unuvar Purcu et al., 2022*)*.

Impaired efferocytosis in M1 macrophages is widely documented in the literature - a process involving the phagocytosis of apoptotic cells driven by surface MerTK expression (Wanke et al., 2021, Rahman et al., 2010, Pastore et al., 2019). It is noted that MerTK is consistently expressed more abundantly on M2 macrophages, specifically the M2c subtype, thus making them more efficient in apoptotic cell clearance during inflammatory resolution (Zizzo et al., 2012, Bi et al., 2019). In atherosclerotic plaque, the build of necrotic cellular debris is a clear representation of this phenomenon due to the enrichment of M1 macrophages in advanced lesions in areas considered most unstable (de Gaetano et al., 2016, Mohd Idrus et al., 2021). The CD36 scavenger receptor also plays a role in phagocytosis through is affinity for apoptotic cells, and its expression is downregulated in response to M1 macrophage activation (Pennathur et al., 2015). I mirrored these observations in our results demonstrating suppressed expression of both phagocytosis markers on M1 macrophages using our flow cytometry panel. Since CD36 is also a scavenger receptor for Ox-LDL, M2 macrophages are shown to be more susceptible to foam cell formation than their pro-inflammatory counterparts (van Tits et al., 2011). Additional scavenger receptors such as CD204 and Stabilin-1 and pan-macrophage markers CD68 and CD11c however showed minimal change between macrophage subsets.

CD206 mannose receptor expression and its mRNA levels are upregulated in response to IL-4 treatment and is considered a marker for alternatively activated M2-like macrophages, in particular the M2a subtype which is believed to express the highest level of the receptor compared to other M2-like phenotypic categories in both

murine and human macrophages (Porcheray et al., 2005, Stein et al., 1992, Unuvar Purcu et al., 2022, Li et al., 2022). Similarly, to Purcu *et al* I observed increasing levels of CD206 expression with extended stimulation times, although for the purpose of our study I did not subcategorise these M2 macrophages further into M2a, M2b, M2c and M2d subsets.

Based on our observations, it is evident that optimal expression of individual markers is highly dependent upon stimulation times, and this varies between each antigen. Overall, I found that 24hr stimulation time was sufficient to clearly distinguish between the different macrophage subsets and this time frame is typically used in polarised macrophage studies *in vitro* (Malheiro et al., 2017, Li et al., 2022). In summary, in this chapter I have demonstrated a clear strategy for MDM culture and characterisation via flow cytometry analysis using an extensive polychromatic panel which may be utilised to provide a comprehensive assessment of inflammatory and pro-resolution macrophage phenotypes.

3.3.4. Summary of results

- The differentiation of monocyte to macrophages in culture was more robust and consistent in terms of survival and cellular morphology between donors when cultured with recombinant MCSF and 10% FBS
- I designed and validated a 11-colour flow cytometry panel to distinguish between M1 and M2-like human macrophage subtypes
- The expression level of extracellular markers on human MDMs was highly dependent on the length of time for stimulation using M1 and M2 macrophage stimulants.

Chapter 4. HUMAN MONOCYTE-DERIVED FOAM CELL FORMATION AND CHARACTERISATION

4.1. Introduction

Foam cells being one of the major drivers of atherosclerosis are evident at all stages of plaque development, starting with the very early stages of fatty streak initiation. The current paradigm for foam cell formation proposes that monocytes recruited into the subintimal space undergo a period of differentiation into macrophages, during which scavenger receptors, predominantly CD36, are upregulated to facilitate the gradual assimilation of oxLDL (Javadifar et al., 2021, Seo et al., 2015, Bobryshev, 2006, Moore et al., 2013). However, monocytes also express scavenger receptors for oxLDL on their surface which induce transcriptional changes during receptor activation thus, making it possible that the diseased arterial environment may polarise these monocytes towards a foam cell phenotype, directly upon recruitment (Piechota et al., 2012).

In additional to oxidation, LDL can undergo alternative modifications such as acetylation and malondialdehyde modification, although oxLDL is known to be the most prominent stimuli for foam cell formation as modifications such as acLDL are rarely found *in vivo* (Goldstein et al., 1979b, Lougheed et al., 1999, Holvoet et al., 1998,

Schrijvers et al., 2007). This leads to reduced affinity of LDL for its complementary LDL receptor and greater affinity for scavenger receptors (Holvoet et al., 1995). The exact identity and characterisation of foam cells remains a challenge due to almost identical expression profiles with macrophages, making it difficult to decipher between the two cell types amongst the heterogenous cellular landscape within plaque (Lavine, 2023, Bonacina et al., 2023). More recently genomic and proteomic analyses, performed in both human and murine atherosclerotic regions, have associated foam cells with an anti-inflammatory and lipid metabolising transcriptional profile (Spann et al., 2012, Kim et al., 2018, Fernandez et al., 2019). Yet this novel phenotype associated with foam cells remains a subject of debate due to these cells being so poorly defined both in in vitro and in vivo studies. Whether these foam cell characteristics are also monocyte subset dependent has not been studied and will be explored in this chapter by investigating both protein and gene expression profiles of foam cells and macrophages derived from human $CD14^{+}CD16^{-}$ and $CD14^{+}CD16^{+}$ monocytes. Monocytes exist in circulation as three main subsets; classical monocytes which I refer here as $CD14^{+}CD16^{-}$ (C) cells, as well as non-classical and intermediate monocytes that I collectively refer to as $CD14^{+}CD16^{+}$ (NC) non-classical cells throughout this chapter. Both non-classical and intermediate populations were pooled due to very low numbers of intermediate monocytes being present in circulation, in addition to the ambiguity and technical difficulties in separating the two subsets.

4.2. $CD14^+CD16^-$ (classical) monocytes assimilate oxLDL more readily than $CD14^+CD16^+$ (non-classical) monocytes

To investigate monocyte specific differences in oxLDL uptake I isolated both $CD14^+CD16^-$ and $CD14^+CD16^+$ monocyte subsets and cultured them in the presence of fluorescent DiI-labelled oxLDL for 6 days followed by flow cytometry analysis for the detection of stored oxidised lipid. Uptake of DiI-oxLDL was evident with both subsets although to a significantly greater extent with $CD14^+CD16^-$ (classical) monocytes (Figure 4.1A). $CD14^+CD16^-$ monocytes were also accompanied by greater expression levels of CD36 scavenger receptor on their surface compared to their $CD14^+CD16^+$ (non-classical) counterpart (Figure 4.1B). Levels of oxLDL accumulation also appeared to gradually increase over the course of 6 days of culture, with $CD14^+CD16^-$ monocytes (Figure 4.1C-D), which may reflect the steady increase in CD36 receptor expression during monocyte-to-macrophage differentiation (Huh et al., 1996).

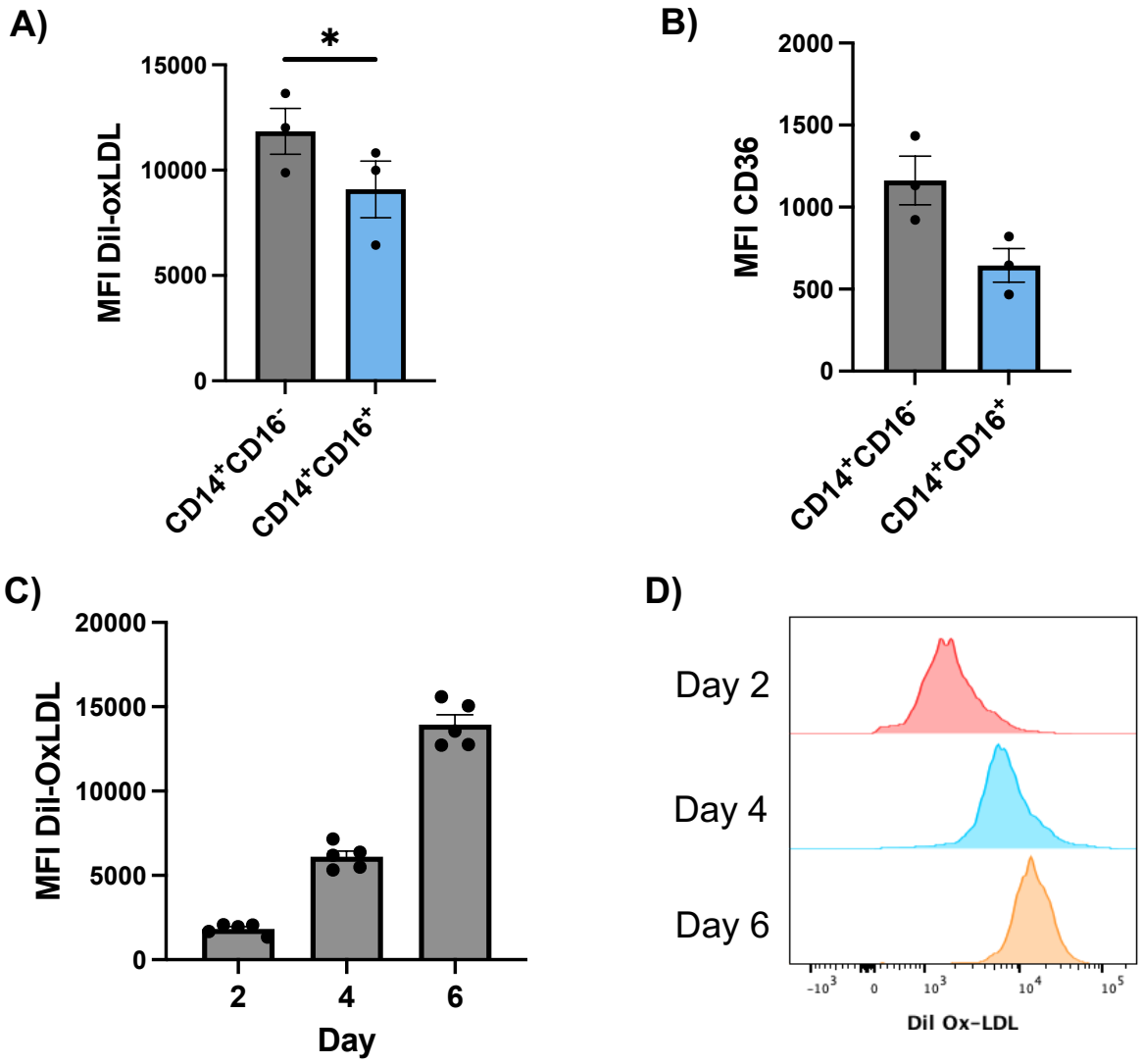


Figure 4-1: Dil-OxLDL uptake in $CD14^+CD16^-$ vs $CD14^+CD16^+$ monocyte-derived macrophages.

$CD14^+CD16^-$ and $CD14^+CD16^+$ monocytes were isolated via magnetic bead separation and differentiated into macrophages in culture for 6 days with or without Dil-labelled oxLDL. Monocytes were treated with dil-oxLDL on day 0 of culture and on day 6 cells were harvested from tissue culture plates and stained for CD36 antibody. **(A)** Dil-oxLDL and **(B)** CD36 expression was detected via flow cytometry analysis. **(C-D)** A time course for dil-oxLDL uptake by $CD14^+CD16^-$ (classical) monocytes over the course of 2,4 and 6 days was determined via flow cytometry analysis. Data are mean ± SEM (n=3-5, biological replicate). Statistical analysis performed using unpaired t-test, *=$p<0.05$.

4.3. Monocytes have an increased pro-inflammatory cytokine profile compared to macrophages and foam cells

Since foam cells strongly support inflammation during atherosclerosis (Javadifar et al., 2021), I investigated the cytokine profile of foam cells compared with macrophages and monocytes to determine potential foam cell specific cytokines that may drive such inflammatory events. Here I compared foam cells and macrophages derived from both $CD14^+CD16^-$ and $CD14^+CD16^+$ monocyte subsets. Initially, concentrations of pro-inflammatory TNF-α secretion were measured in culture supernatants revealing a significant increase in TNF-α levels with $CD14^+CD16^+$ monocytes (with monocytes being referred to as day 2 post culture). Although these differences were gradually lost upon differentiation into macrophages and foam cells over the course of 6 days with minimal differences observed upon addition of oxLDL (Figure 4.2A-C).

I investigated further by comparing a wide range of cytokines using a semi-quantitative cytokine array on cell culture supernatants taken from monocytes, macrophages, and foam cells. In this case only $CD14^+CD16^-$ monocytes were used to generate the different cell types as they have the ability to generate foam cells more readily as demonstrated earlier. The heatmap shows the relative expression levels of cytokines released by each cell population. Expression profiles were almost identical between macrophages and foam cells with a down regulation in pro-inflammatory genes such as IL-1β and IL-6 compared to monocytes (Figure 4.3). Thus, I recurrently observe a concomitant loss in the pro-inflammatory cytokine profile of monocytes upon differentiation into foam cells.

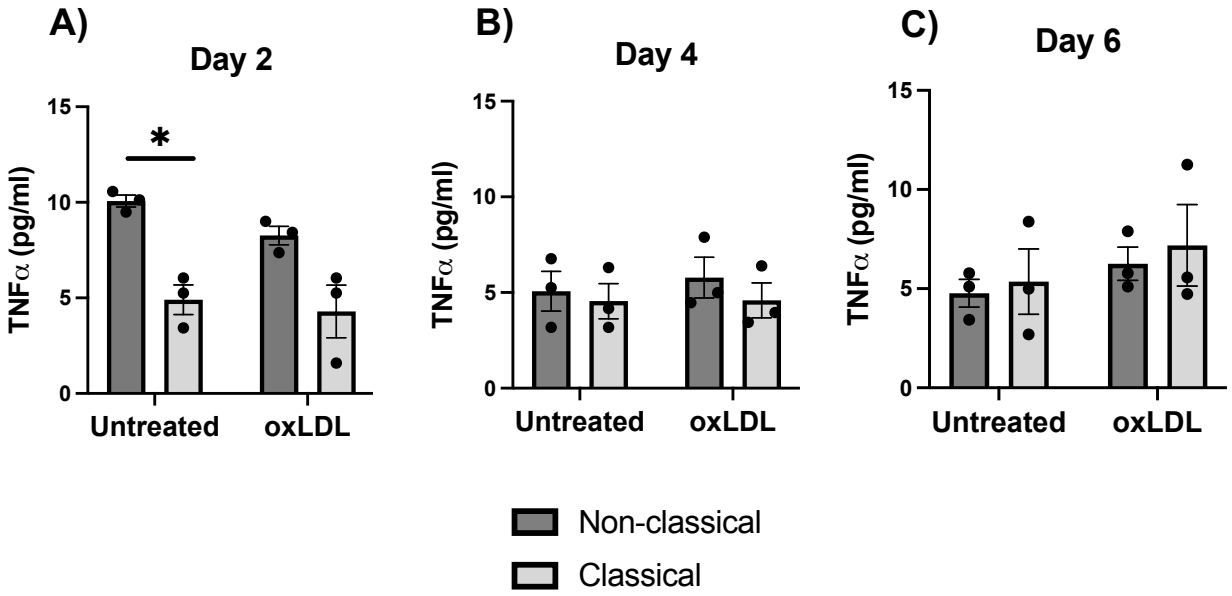


Figure 4-2: TNF secretion from untreated and oxLDL treated monocyte subsets upon differentiation

$CD14^{+}CD16^{-}$ and $CD14^{+}CD16^{+}$ monocytes were isolated via magnetic bead separation and cultured in the absence (for macrophage differentiation) or presence of oxLDL (for foam cell formation). Cell culture supernatants were collected every 2 days for TNFα ELISA analysis with cells being replaced with fresh media (with or without oxLDL supplementation) TNFα (pg/ml) levels were measured for cells cultured at **(A)** day 2, **(B)** 4 and **(C)** 6 throughout the course of monocyte differentiation. Data are mean ± SEM (n=3, biological replicate). Statistical analysis performed using unpaired t-test, *=$p<0.05$.

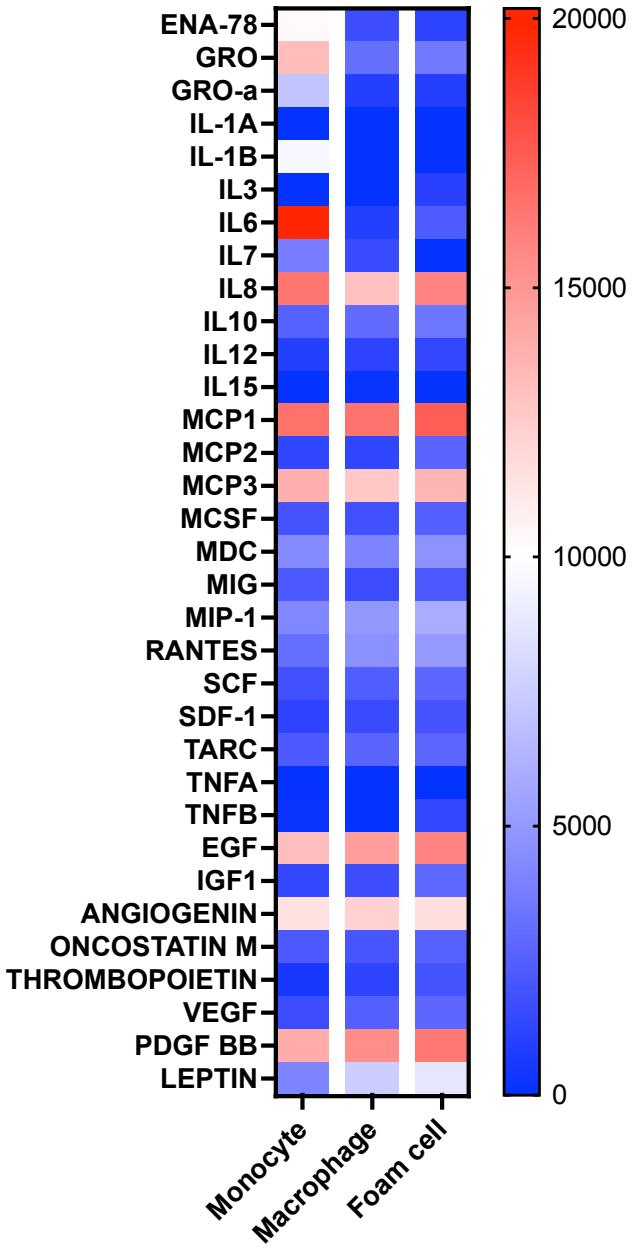


Figure 4-3: Upregulation of pro-inflammatory cytokines in culture supernatants from monocytes compared to macrophages and foam cells

$CD14^{+}CD16^{-}$ monocytes were isolated via magnetic bead isolation. Monocytes were either cultured in the absence (for macrophage differentiation) or presence of oxLDL (for foam cell formation) for 6 days. Cell culture supernatants were collected at day 2 of cell culture for monocytes and collected at day 6 for macrophages and foam cells (treated with oxLDL) following complete differentiation. Cell culture supernatants pooled from 4 donors were subjected to a cytokine array for analysis of secreted cytokines in culture. Relative expression is presented as a heatmap.

4.4. Bulk RNA sequencing (RNA-seq) analysis of monocytes, macrophages and foam cells derived from $CD14^+CD16^-$ (classical) and $CD14^+CD16^+$ (non-classical) monocyte subsets

Recent genome-wide transcriptomic studies have investigated the genetic variations in macrophages and lipid-associated macrophages in plaque; however, no studies to-date have looked at macrophage and foam cell characteristics derived from specific monocyte subsets. Here I directly compared differential gene expression profiles of monocytes, macrophages and foam cells derived from human $CD14^+CD16^-$ (classical) and $CD14^+CD16^+$ (non-classical) monocyte subsets via bulk RNA-sequencing (RNAseq). The aim was to explore any monocyte subset-specific differences in the gene expression atlas of foam cells that may ultimately indicate differences in their functional behaviour.

4.4.1. Bulk RNAseq experimental design and data transformation

For the bulk RNAseq experimental set up (Figure 4.4), human $CD14^+CD16^-$ and $CD14^+CD16^+$ monocyte subsets were isolated from healthy whole blood donors using magnetic bead isolation and cultured on tissue culture plastic for an additional level of purification to remove contaminating lymphocytes which was followed by RNA extraction. The same monocyte subsets were also cultured for 6 days for macrophage differentiation and foam cell formation with the addition of 25 μg/ml oxLDL. This was followed by RNA extraction on day 6 which was processed for bulk-RNA sequencing (Figure 4.4).

Following library preparation and sequencing, raw FASTA files were processed for quality control analysis using FASTQC and MultiQC software and sequences were aligned to the human genome using STAR aligner to generate a gene expression counts table using Subreads Featurecounts. Data was normalised using variable stabilising transformation (VST) and total read counts per million for each sample was plotted. The distribution of the transformed data was plotted, displaying minimal differences between sample mean and sample median (Figure 4.5A-B).

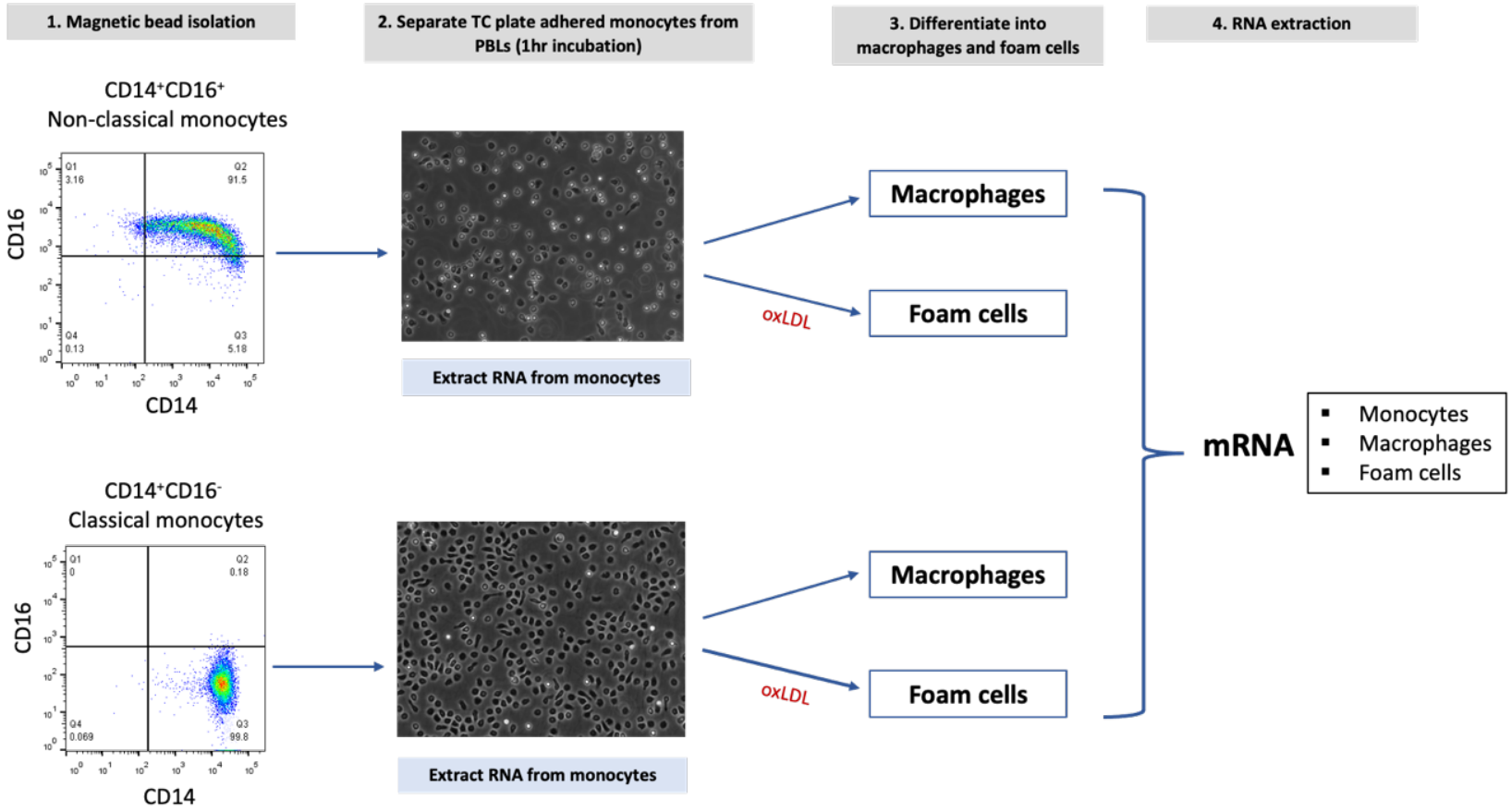


Figure 4-4: Schematic diagram of monocyte, macrophage and foam cell mRNA sample collection for bulk-RNAseq.

$CD14^{+}CD16^{-}$ classical and $CD14^{+}CD16^{+}$ non-classical monocytes were isolated via magnetic bead separation and purity was determine via flow cytometry analysis for CD14 and CD16 expression. Monocytes were further purified via adhesion to tissue-culture plastic (TC) for 1 hr for peripheral blood lymphocyte (PBL) removal, followed by mRNA extraction for bulk-RNAseq analysis. Monocyte subsets were also cultured for differentiation into macrophage or foam cells with the addition of 25 μg/ml oxLDL for 6 days. On day 6 mRNA was collected for bulk-RNAseq analysis as shown in schematic diagram.

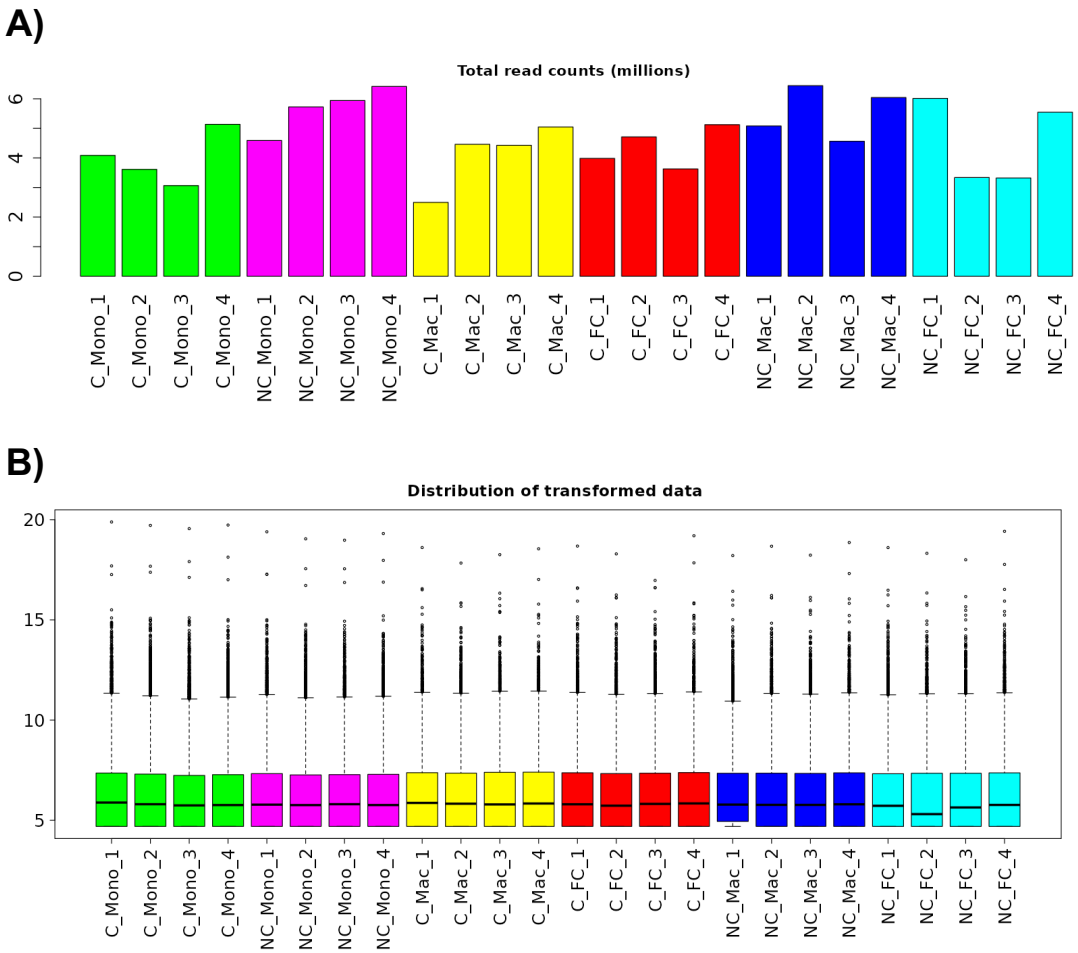


Figure 4-5: Total read counts and distribution of transformed bulk-RNAseq data for monocytes, macrophages and foam cells.

Bulk-RNAseq was performed on mRNA from monocytes, macrophages and foam cells derived from $CD14^{+}CD16^{-}$ and $CD14^{+}CD16^{+}$ monocytes subsets. Sequences were aligned to the human genome using STAR aligner followed by the generation of a gene expression counts table using Subread FeatureCounts which was used for analysis using iDEP software. Data was subject to variable stabilising transformation (VST) for normalisation. **(A)** Total counts per million and **(B)** distribution of transformed data was plotted. C_Mono = classical monocytes, NC_Mono = non-classical/intermediate monocytes, C_FC = classical monocyte-derived foam cells, C_Mac = classical monocyte-derived macrophage, NC_FC = non-classical/intermediate monocyte-derived foam cells, NC_Mac = non-classical/intermediate monocyte-derived macrophage. Sample size per group is n=4, biological replicate.

4.4.2. Differential gene expression between $CD14^+CD16^-$ and $CD14^+CD16^+$ monocyte subsets

I initially looked at only comparing the genomic profile of both classical ($CD14^+CD16^-$) and non-classical ($CD14^+CD16^+$) monocyte subsets. Principal component analysis (PCA) showed that both monocyte subsets formed distinct clusters as expected (Figure 4.6). Differential gene expression analysis revealed 430 genes being upregulated in non-classical monocytes (NC_Mono) compared to classical (C_Mono) monocytes and a downregulation of 677 genes displayed in an MA plot (Figure 4.7A-B). The list of the top 30 upregulated and downregulated genes were plotted showing a higher expression of genes such as CCR2 in classical monocytes as expected (Table 4.1-4.2). K means clustering analysis revealed that genes associated with the non-classical monocytes were highly enriched in pathways associated with regulating and promoting immune responses whereas in classical monocytes this included enrichment of pathways such as immune cell activation and cellular responses to metabolic processes (Figure 4.8A-B). These results agree with earlier studies showing similar trends, which demonstrates that our data has captured the known biological functions of monocyte subsets (Vallania et al., 2021).

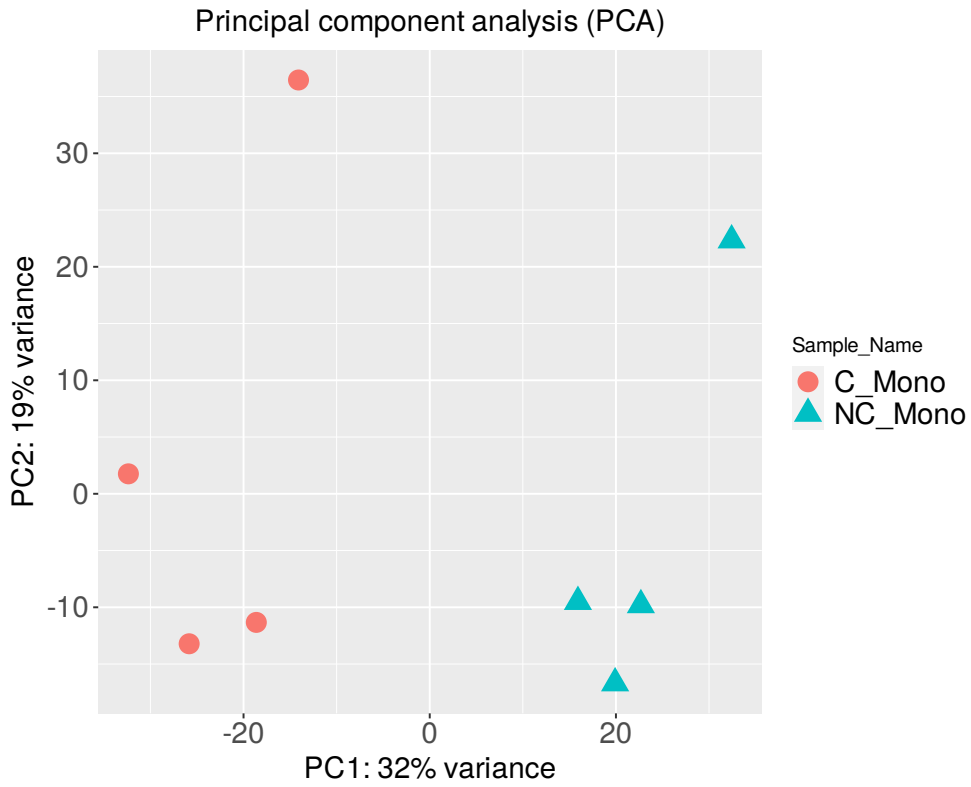


Figure 4-6: Classical, $CD14^{+}CD16^{-}$ (C) and Non-classical $CD14^{+}CD16^{+}$ (NC) monocytes cluster distinctly

Bulk-RNAseq was performed on mRNA from monocytes, macrophages and foam cells derived from $CD14^{+}CD16^{-}$ and $CD14^{+}CD16^{+}$ monocytes subsets. Gene counts were subject to variance stabilisation transformation (VST) on monocyte samples only with foam cell and macrophage samples removed from data set. **(A)** Principle component analysis (PCA) 1 and 2 were plotted and **(B)** C_Mono = classical monocytes, NC_Mono = non-classical/intermediate monocytes Sample size per group is n=4, biological replicate.

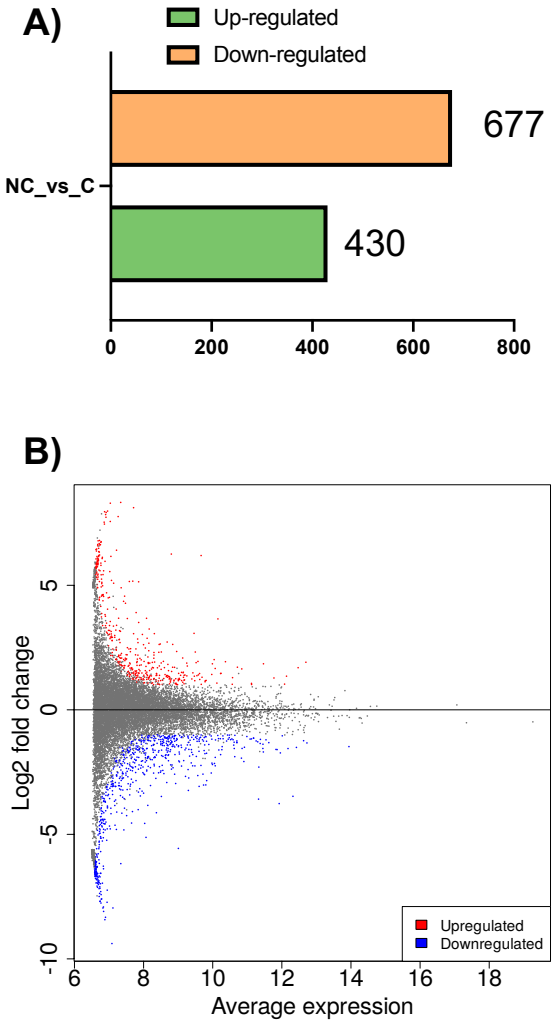


Figure 4-7: Differentially expressed gene (DEGs) between classical and non-classical monocyte subsets

Bulk-RNAseq was performed on mRNA from monocytes, macrophages and foam cells derived from $CD14^{+}CD16^{-}$ and $CD14^{+}CD16^{+}$ monocytes subsets. Gene counts were subject to variance stabilisation transformation (VST) on monocyte samples only with foam cell and macrophage samples removed from data set. **(A)** Number of differentially expressed genes (DEGs) that were up-regulated and down-regulated between classical $CD14^{+}CD16^{-}$ (C) and non-classical $CD14^{+}CD16^{+}$ (NC) monocyte subsets were plotted. **(B)** MA plots showing log2 fold change vs average gene expression between classical $CD14^{+}CD16^{-}$ non-classical $CD14^{+}CD16^{+}$ monocyte subsets. Genes upregulated depicted in red whilst genes downregulated depicted in blue. C_Mono = classical monocytes, NC_Mono = non-classical/intermediate monocytes. Sample size per group is n=4, biological replicate.

Table 4-1: Top 30 downregulated genes in non-classical monocytes compared to classical monocytes

	Symbol	log2 Fold Change	Adj.Pval	Ensembl gene ID
Downregulated	PADI2	-9.3851295	2.81E-11	ENSG00000117115
	CCR2	-8.3296945	8.56E-08	ENSG00000121807
	SYN2	-7.9575516	5.17E-06	ENSG00000157152
	KCNJ15	-7.9560608	2.08E-08	ENSG00000157551
	MTARC1	-7.7271528	2.65E-07	ENSG00000186205
	MTUS2	-7.6818542	4.59E-04	ENSG00000132938
	TMEM121B	-7.3705759	4.79E-04	ENSG00000183307
	FKBP1B	-7.2988647	1.07E-04	ENSG00000119782
	NIPAL4	-7.2412823	7.59E-06	ENSG00000172548
	STEAP3	-7.0776224	9.82E-03	ENSG00000115107
	STX16-NPEPL1	-7.0154228	2.56E-03	ENSG00000254995
	CATIP	-6.9817578	1.91E-03	ENSG00000158428
	SLC22A4	-6.9606745	1.27E-04	ENSG00000197208
	GJB6	-6.9413893	1.19E-03	ENSG00000121742
	CRLF2	-6.9019972	2.78E-03	ENSG00000205755
	RD3L	-6.8672125	1.57E-03	ENSG00000227729
	BPI	-6.8665101	5.16E-03	ENSG00000101425
	SERPINB10	-6.8071507	5.79E-03	ENSG00000242550
	TEX14	-6.763144	1.64E-02	ENSG00000121101
	TRIM16	-6.6957681	8.41E-03	ENSG00000221926
	GCSAML	-6.6537841	2.26E-02	ENSG00000169224
	IL31RA	-6.6509475	3.68E-02	ENSG00000164509
	ZBTB32	-6.629647	2.10E-02	ENSG00000011590
	SPRY1	-6.6038148	6.47E-02	ENSG00000164056
	CFAP99	-6.5774942	6.80E-02	ENSG00000206113
	PTGFRN	-6.5626305	8.10E-04	ENSG00000134247
	IL20RB	-6.555769	7.01E-02	ENSG00000174564
	LGALS12	-6.528997	7.63E-02	ENSG00000133317
	SERPINI2	-6.5287337	3.11E-02	ENSG00000114204
	BMP8B	-6.526502	2.64E-02	ENSG00000116985

Table 4-2: Top 30 upregulated genes in non-classical monocytes compared to classical monocytes

	Symbol	log2 Fold Change	Adj.Pval	Ensembl gene ID
Up-regulated	CABP4	8.29658053	1.99E-09	ENSG00000175544
	C1QB	7.98002923	1.08E-07	ENSG00000173369
	KLRD1	7.95531381	7.29E-06	ENSG00000134539
	GPR174	7.92392132	1.02E-06	ENSG00000147138
	ADD2	7.83981982	2.14E-06	ENSG00000075340
	PPM1N	7.75927924	3.71E-09	ENSG00000213889
	KNDC1	7.73236749	1.02E-06	ENSG00000171798
	GUCY1B1	7.56235012	1.95E-07	ENSG00000061918
	CCNE1	7.53493619	1.83E-05	ENSG00000105173
	PPP1R16B	7.45806694	6.89E-06	ENSG00000101445
	KIF5C	6.80044644	2.35E-03	ENSG00000168280
	PDGFRB	6.78596782	8.07E-03	ENSG00000113721
	TNFSF18	6.75180283	4.43E-04	ENSG00000120337
	HYLS1	6.72289132	6.17E-04	ENSG00000198331
	DCP1B	6.67772706	6.39E-03	ENSG00000151065
	CYP4F22	6.63939998	1.26E-02	ENSG00000171954
	ERCC5	6.62969669	1.06E-03	ENSG00000134899
	IL2RB	6.62065126	2.21E-03	ENSG00000100385
	GSTA4	6.48493412	1.23E-02	ENSG00000170899
	ACY3	6.4559166	4.62E-02	ENSG00000132744
	CD3E	6.43419152	5.12E-02	ENSG00000198851
	TMEM53	6.35239274	8.50E-03	ENSG00000126106
	SFTPD	6.33226762	4.04E-03	ENSG00000133661
	CDKN1C	6.25415615	3.97E-14	ENSG00000129757
	MYZAP	6.21671684	1.05E-02	ENSG00000263155
	ENHO	6.19596213	7.01E-03	ENSG00000168913
	FCGR3A	6.19429969	7.63E-68	ENSG00000203747
	RHOBTB2	6.16135445	2.23E-06	ENSG00000008853
	TTC34	6.15838527	3.36E-02	ENSG00000215912
	PARP15	6.15180584	7.93E-03	ENSG00000173200

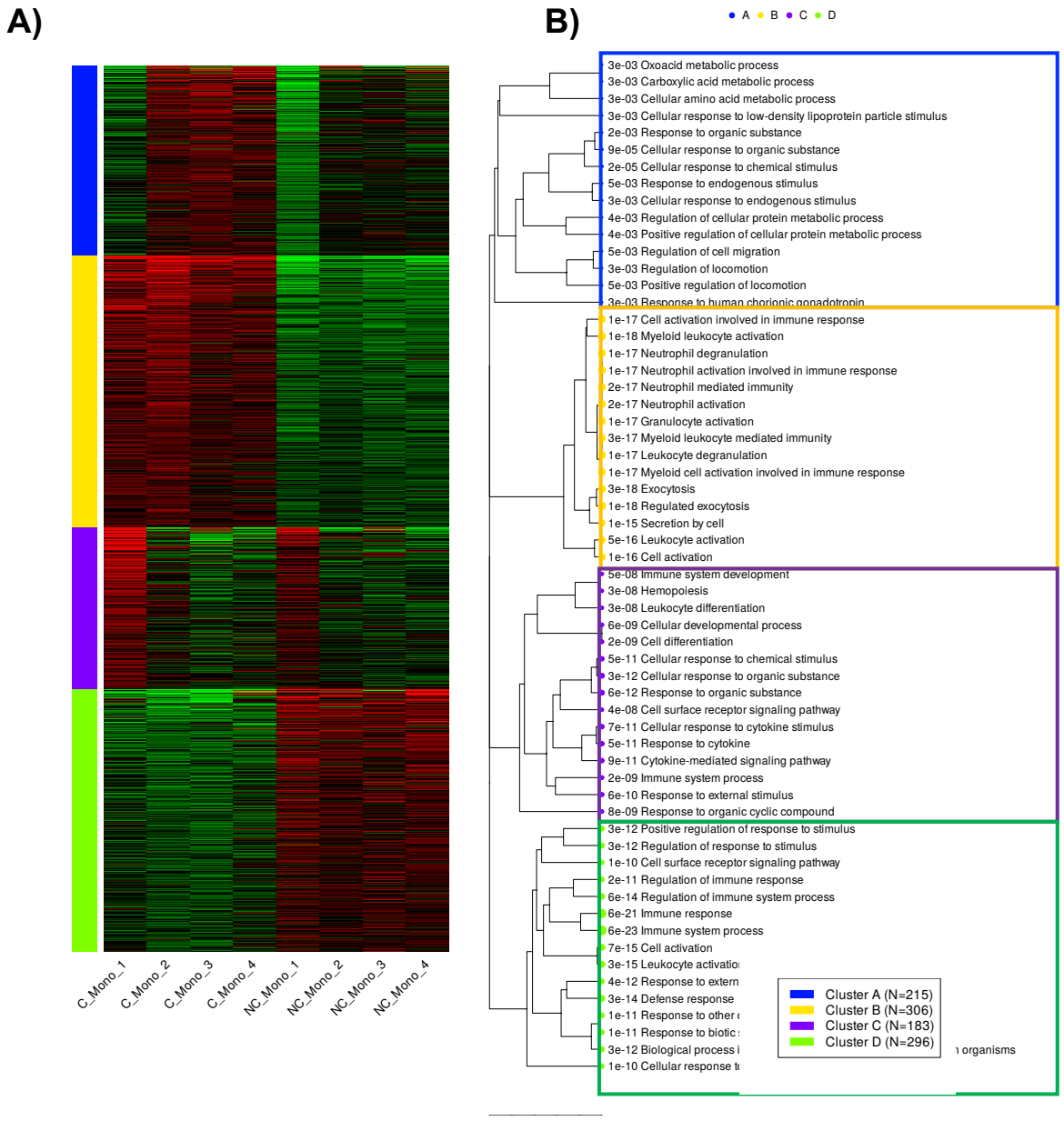


Figure 4-8: K means clustering of top 1000 genes in CD14^{+}CD16^{-} and CD14^{+}CD16^{+} monocytes subsets

Bulk-RNAseq was performed on mRNA from monocytes, macrophages and foam cells derived from CD14^{+}CD16^{-} and CD14^{+}CD16^{+} monocytes subsets. Gene counts were subject to variance stabilisation transformation (VST) on monocyte samples only with foam cell and macrophage samples removed from data set**. (A)** K-means unsupervised clustering was plotted in a heatmap for the clustering of top 1000 genes into **(B)** 4 groups (coloured a-d) based on the expression pattern across monocyte subsets including classical CD14^{+}CD16^{-} (C_Mono) and non-classical/intermediate CD14^{+}CD16^{+} (NC_Mono) monocyte subsets. Normalised relative expression levels are expressed on the heatmap as a gradient with highly expressed genes in red and lowly expressed genes in green. C_Mono = classical monocytes, NC_Mono = non-classical monocytes. Sample size per group is n=4, biological replicate.

4.4.3. Monocyte subsets cluster distinctly from foam cells and macrophages

To explore changes in gene expression between monocytes, macrophages and foam cells, principal component analysis (PCA) was performed revealing monocytes being distinctly clustered to macrophages and foam cells. The monocytes themselves also clustered individually based on the subset origin being either $CD14^{+}CD16^{-}$, classical (C) and $CD14^{+}CD16^{+}$, non-classical (NC). However, foam cells and macrophages did not cluster independently of one another, regardless of monocyte subset origin, demonstrating very similar expression transcriptomic signatures (Figure 4.9A). This was confirmed by performing unsupervised hierarchical clustering which was visualised using an enrichment tree (Figure 4.9B).

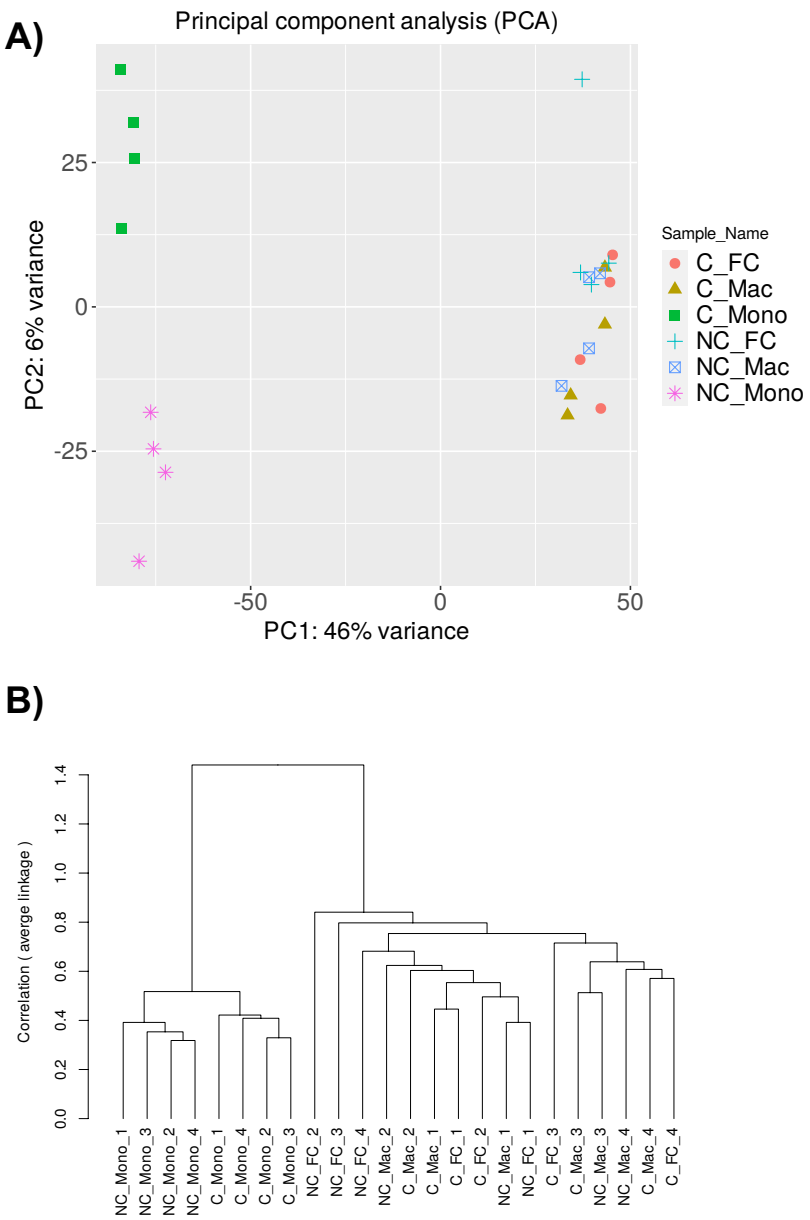


Figure 4-9: Foam cells and macrophages cluster together, distinctly from monocytes

Bulk-RNAseq was performed on mRNA from monocytes, macrophages and foam cells derived from $CD14^{+}CD16^{-}$ and $CD14^{+}CD16^{+}$ monocytes subsets. Gene counts were subject to variance stabilisation transformation (VST). **(A)** Principle component analysis (PCA) 1 and 2 were plotted and coloured by monocytes (Mono), macrophage and foam cells derived from $CD14^{+}CD16^{-}$ (C) and $CD14^{+}CD16^{+}$ (NC) monocyte subsets as shown in the key. **(B)** Hierarchical clustering tree depicts the correlation between the different cell types. C_Mono = classical monocytes, NC_Mono = non-classical monocytes, C_FC = Classical monocyte-derived foam cells, C_Mac = classical monocyte-derived macrophage, NC_FC = Non-classical monocyte-derived foam cells, NC_Mac = non-classical monocyte-derived macrophage. Sample size per group is n=4, biological replicate.

4.4.4. Monocytes display a pro-inflammatory transcriptomic signature compared to macrophages and foam cells

Differential gene expression between monocytes, macrophages and foam cells was also observed by plotting the top 50 variably expressed gene in a heatmap (Figure 4.10). Notably, monocytes displayed an increased expression of pro-inflammatory genes compared to macrophages and foam cells including S100A12, S100A8, CXCL8, TREM1 and IL-1β. Whereas macrophages and foam cells expressed high levels of genes associated with lipid metabolism such as APOE and APOC1 as well as matrix metalloproteinases MMP1 and MMP9. Interestingly TREM2 expression was also greater on macrophage and foam cells – a gene typically associated with inflammatory resolution (Han et al., 2023).

Furthermore, K-means clustering analysis revealed that genes upregulated on monocytes were associated with inflammatory responses, leukocyte, and cell activation as well as response to cytokine. On the other hand, foam cells and macrophages particularly demonstrated upregulation of genes associated with tissue remodelling - a characteristic feature of macrophages as well as lipid metabolising pathways identified in the heatmap as plasma lipoprotein particle clearance and triglyceride metabolic processes (Figure 4.11A-B).

Overall, these outcomes corroborate our earlier findings from our cytokine array analysis, highlighting the fact that monocytes have a greater pro-inflammatory signature compared to macrophages and foam cells, suggesting a shift towards a more anti-inflammatory signature upon monocyte differentiation.

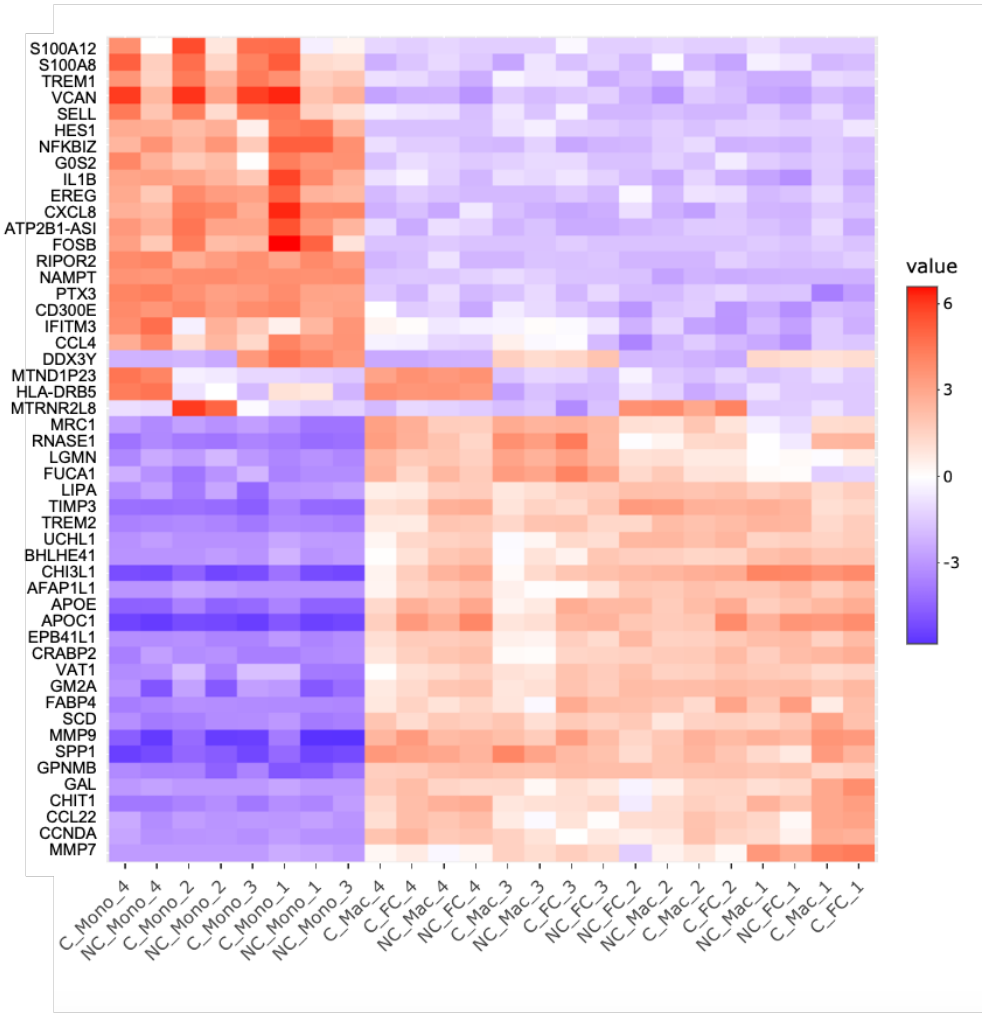


Figure 4-10: Top 50 variably expressed genes of monocytes, macrophages and foam cells.

Bulk-RNAseq was performed on mRNA from monocytes, macrophages and foam cells derived from $CD14^{+}CD16^{-}$ and $CD14^{+}CD16^{+}$ monocytes subsets. Gene counts were subject to variance stabilisation transformation (VST). Top 50 most variably expressed genes were plotted as a heatmap for monocytes, macrophages, and foam cells derived from $CD14^{+}CD16^{-}$ (C) and $CD14^{+}CD16^{+}$ (NC) monocyte subsets. C_Mono = classical monocytes, NC_Mono = non-classical monocytes, C_FC = Classical monocyte-derived foam cells, C_Mac = classical monocyte-derived macrophage, NC_FC = Non-classical monocyte-derived foam cells, NC_Mac = non-classical monocyte-derived macrophage. Sample size per group is n=4, biological replicate.

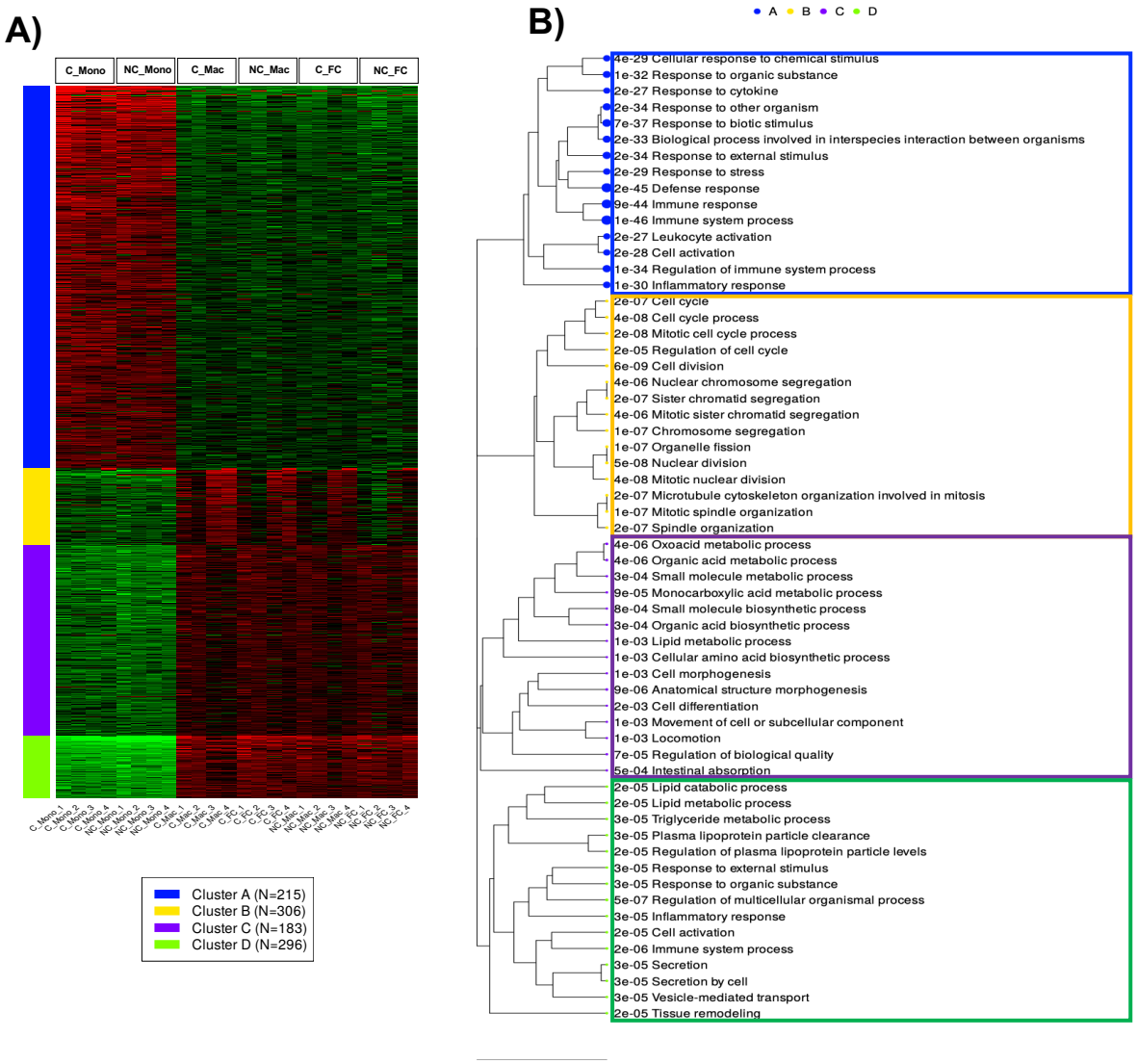


Figure 4-11: K means clustering of top 1000 genes in of monocytes, macrophages and foam cells.

Bulk-RNAseq was performed on mRNA from monocytes, macrophages and foam cells derived from $CD14^{+}CD16^{-}$ and $CD14^{+}CD16^{+}$ monocytes subsets. Gene counts were subject to variance stabilisation transformation (VST). **(A)** K-means unsupervised clustering was plotted in a heatmap for the clustering of top 1000 genes into **(B)** 4 groups (coloured a-d) based on the expression pattern across samples labelled as monocytes (Mono), macrophage (Mac) and foam cells (FC) derived from $CD14^{+}CD16^{-}$ (C) and $CD14^{+}CD16^{+}$ (NC) monocyte subsets. Normalised relative expression levels are expressed on the heatmap as a gradient with highly expressed genes in red and lowly expressed genes in green. C_Mono = classical monocytes, NC_Mono = non-classical monocytes, C_FC = Classical monocyte-derived foam cells, C_Mac = classical monocyte-derived macrophage, NC_FC = Non-classical monocyte-derived foam cells, NC_Mac = non-classical monocyte-derived macrophage. Sample size per group is n=4, biological replicate.

4.4.5. Foam cells and macrophages generated from classical and non-classical monocytes show very similar transcriptomic expression profiles

I then looked at comparing foam cells and macrophages exclusively by omitting the monocytes from the dataset to identify any subtle changes between both groups. By performing PCA analysis I observed no defined clustering between foam cells and macrophages regardless of their origin being from the classical or non-classical monocyte subset (Figure 4.12). According to the heatmap, minimal differences in gene expression was observed between macrophages and foam cells and it appeared they clustered according to donor and not cell type (Figure 4.13).

Differential gene expression analysis revealed minimal number of genes up- or down- regulated, particularly with classical monocyte derived macrophages and foam cells where only 4 genes were down-regulated in foam cells (Figure 4.14A-C). Genes upregulated in foam cells derived from non-classical monocytes were particularly associated with lipid metabolism including higher expression of ATP-binding cassette (ABC) transporter genes, ABCA1 and ACGG1 that promote cholesterol efflux, carboxylesterase 1 (CES1) which regulates cholesterol esterification, as well as PLIN2 which promotes lipid droplet formation and accumulation. Of interest, HMGCS1 was upregulated in foam cells derived from classical monocytes – a gene involved in the pathway for cholesterol biosynthesis, similarly demonstrating a lipid processing signature in foam cells. (Lists of genes listed in table 4.3-4.5). Gene enrichment analysis confirmed these findings whereby non-classical monocyte-derived foam cells displayed enhanced expression of genes associated with reverse cholesterol transport and lipid storage, which are reminiscent of a foam cell phenotype (Figure 4.15A-B).

This was accompanied by the downregulation of genes such as IL1R2 related to IL-1β receptor signalling as well as genes associated with cell cycle and proliferation indicating the reduced proliferative capacity of macrophages upon oxLDL accumulation.

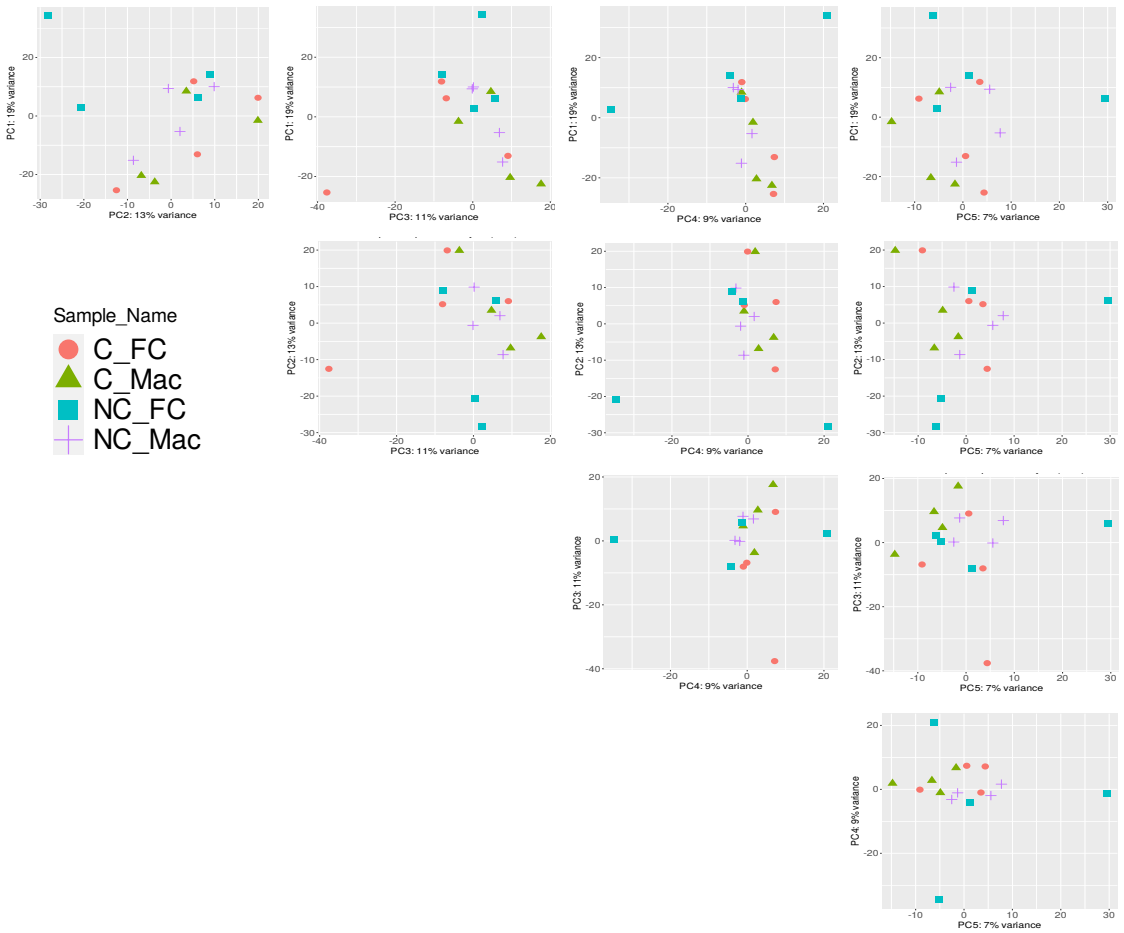


Figure 4-12: Foam cells and macrophages do not cluster distinctly based on cell type or cell origin.

Bulk-RNAseq was performed on mRNA from monocytes, macrophages and foam cells derived from $CD14^{+}CD16^{-}$ and $CD14^{+}CD16^{+}$ monocytes subsets. Gene counts were subject to variance stabilisation transformation (VST) and principle components analysis (PCA) plots were performed on foam cells and macrophages only with monocyte samples removed from data set. Principle component analysis (PCA) was performed and **(B)** pairsplots of top 5 PCs were generated with populations being coloured according to macrophages (Mac) and foam cells (FC) derived from $CD14^{+}CD16^{-}$ (C) and $CD14^{+}CD16^{+}$ (NC) monocyte subsets. C_FC = Classical monocyte-derived foam cells, C_Mac = classical monocyte-derived macrophage, NC_FC = Non-classical monocyte-derived foam cells, NC_Mac = non-classical monocyte-derived macrophage. Sample size per group is n=4, biological replicate.

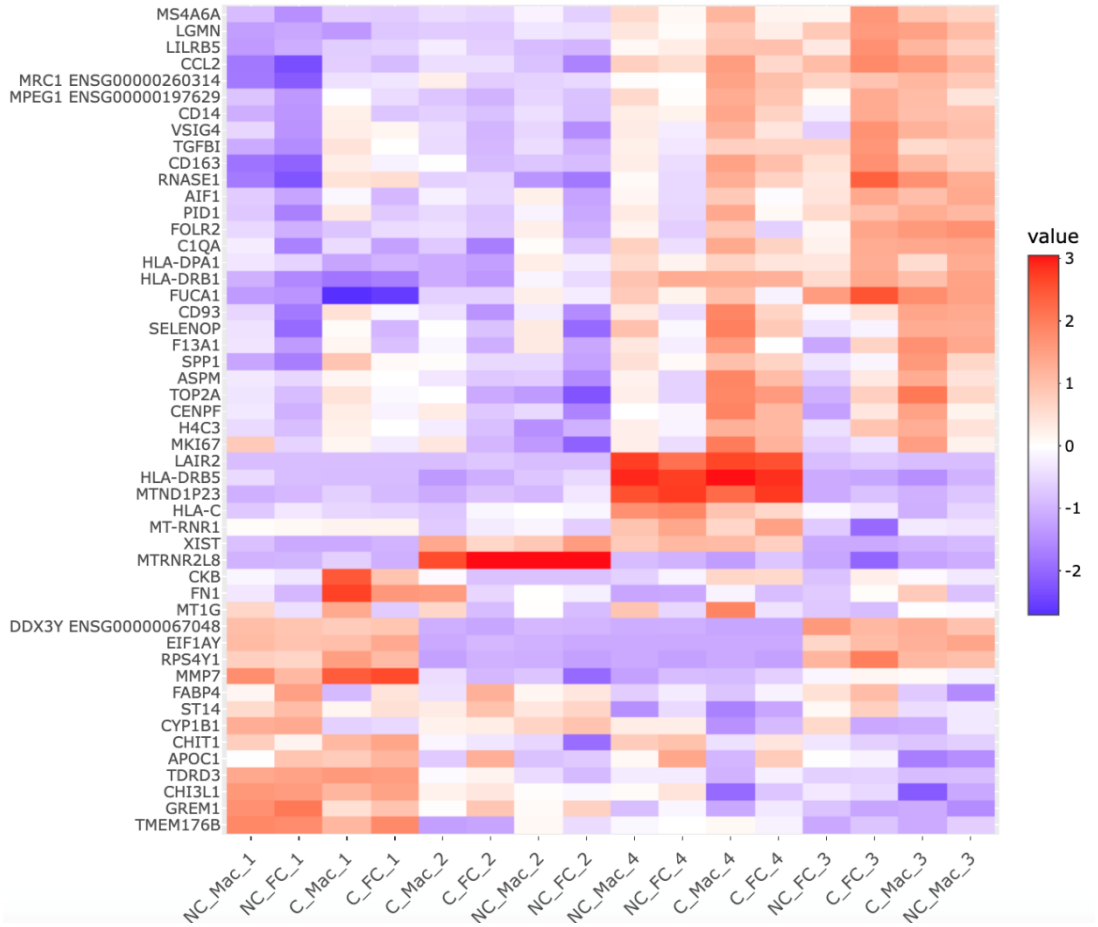


Figure 4-13: Top 50 variably expressed genes of foam cells and macrophages derived from $CD14^{+}CD16^{-}$ and $CD14^{+}CD16^{+}$ monocytes subsets

Bulk-RNAseq was performed on mRNA from monocytes, macrophages and foam cells derived from $CD14^{+}CD16^{-}$ and $CD14^{+}CD16^{+}$ monocytes subsets. Gene counts were subject to variance stabilisation transformation (VST). Top 50 most variably expressed genes were plotted as a heatmap for $CD14^{+}CD16^{-}$ (C) and $CD14^{+}CD16^{+}$ (NC) monocyte-derived macrophages (Mac) and foam cells (FC). C_FC = Classical monocyte-derived foam cells, C_Mac = classical monocyte-derived macrophage, NC_FC = Non-classical monocyte-derived foam cells, NC_Mac = non-classical monocyte-derived macrophage. Sample size per group is n=4, biological replicate.

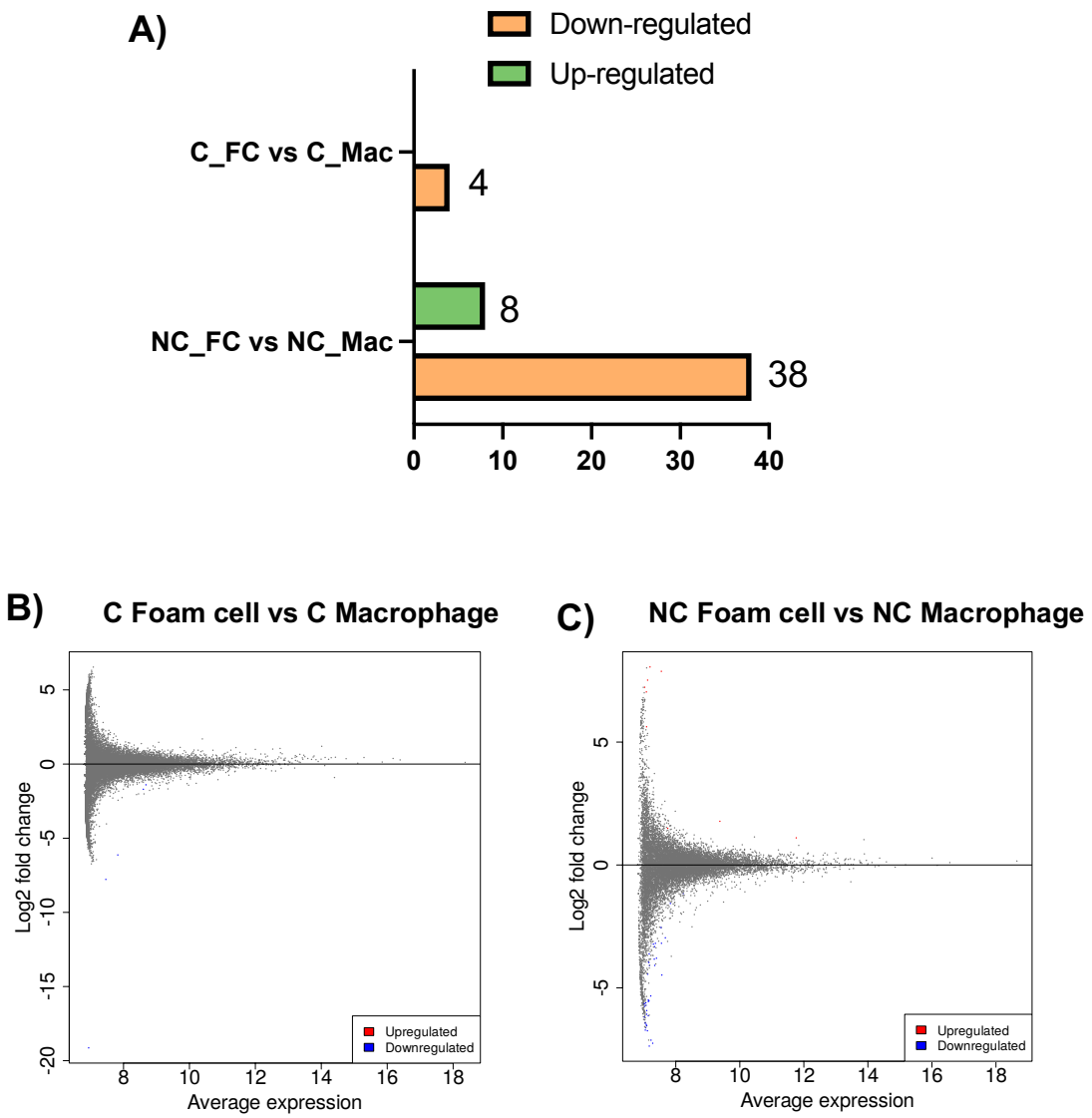


Figure 4-14: Differentially expressed gene (DEGs) between foam cells and macrophages derived from monocyte subsets

Bulk-RNAseq was performed on mRNA from monocytes, macrophages and foam cells derived from $CD14^{+}CD16^{-}$ and $CD14^{+}CD16^{+}$ monocytes subsets. Gene counts were subject to variance stabilisation transformation (VST) on foam cells and macrophages only with monocyte samples removed from data set**. (A)** Number of differentially expressed genes (DEGs) that were up-regulated and down-regulated between $CD14^{+}CD16^{-}$ (C) and $CD14^{+}CD16^{+}$ (NC) monocyte-derived foam cells and macrophages. MA plots showing log2 fold change vs average gene expression between **(B)** classical $CD14^{+}CD16^{-}$ monocyte-derived foam cells and macrophages as well as **(C)** non-classical $CD14^{+}CD16^{+}$ (NC) monocyte-derived foam cells and macrophages. Genes upregulated depicted in red whilst genes downregulated depicted in blue. C_FC = Classical monocyte-derived foam cells, C_Mac = classical monocyte-derived macrophage, NC_FC = Non-classical monocyte-derived foam cells, NC_Mac = non-classical monocyte-derived macrophage. Sample size per group is n=4, biological replicate.

Table 4-3: Top 30 down-regulated genes in $CD14^{+}CD16^{+}$ monocyte-derived foam cells compared to $CD14^{+}CD16^{+}$ monocyte derived macrophages

	Symbol	log2 Fold Change	Adj.Pval	Ensembl gene ID
Downregulated	SKA3	-7.3679683	1.23E-04	ENSG00000165480
	IL1R2	-7.2513228	4.44E-04	ENSG00000115590
	PDPN	-7.1260711	4.40E-04	ENSG00000162493
	DEPTOR	-6.7443446	2.33E-02	ENSG00000155792
	CDC25A	-6.6240652	4.07E-02	ENSG00000164045
	C21orf91	-6.4859115	1.23E-02	ENSG00000154642
	CHAC2	-6.4316917	8.06E-02	ENSG00000143942
	TMEM236	-6.415611	4.07E-02	ENSG00000148483
	OXCT1	-6.2958349	6.15E-02	ENSG00000083720
	TRIP13	-6.134775	1.13E-03	ENSG00000071539
	MARS2	-6.0725765	2.37E-02	ENSG00000247626
	CSPG4	-5.9227683	6.93E-02	ENSG00000173546
	TUFT1	-5.7501734	8.06E-02	ENSG00000143367
	NEK2	-5.7091979	4.41E-02	ENSG00000117650
	MBOAT2	-5.6674479	6.74E-02	ENSG00000143797
	ZNF671	-5.6645343	8.06E-02	ENSG00000083814
	FOSL1	-5.6097935	8.06E-02	ENSG00000175592
	ZNF775	-5.550222	4.41E-02	ENSG00000196456
	KBTBD6	-5.5332942	3.42E-02	ENSG00000165572
	BDH2	-5.4907401	1.72E-02	ENSG00000164039
	PCYOX1L	-5.3288445	1.23E-02	ENSG00000145882
	MT1G	-4.4776543	8.06E-02	ENSG00000125144
	ZNF783	-4.4420146	8.87E-02	ENSG00000204946
	DTL	-4.0882118	8.06E-02	ENSG00000143476
	DLGAP5	-4.0863176	4.41E-02	ENSG00000126787
	C17orf75	-3.9673647	8.06E-02	ENSG00000108666
	CDC20	-3.942106	8.87E-02	ENSG00000117399
	NUF2	-3.8304504	6.74E-02	ENSG00000143228
	INO80E	-3.7936319	5.74E-03	ENSG00000169592
	CDKN3	-3.6165508	8.06E-02	ENSG00000100526

Table 4-4: Top 8 up-regulated genes in $CD14^{+}CD16^{+}$ monocyte-derived foam cells compared to $CD14^{+}CD16^{+}$ monocyte derived macrophages

	Symbol	log2 Fold Change	Adj.Pval	Ensembl gene ID
	CES1	8.05526127	2.00E-02	ENSG00000198848
	ABCG1	7.87804522	3.15E-07	ENSG00000160179
	ZNF19	7.51953333	4.22E-02	ENSG00000157429
	MCC	7.22998902	4.67E-02	ENSG00000171444
	CCHCR1	5.62196262	4.35E-02	ENSG00000204536
	ABCA1	1.7771793	3.84E-03	ENSG00000165029
	KNSTRN	1.49232072	5.23E-02	ENSG00000128944
	PLIN2	1.10358514	8.06E-02	ENSG00000147872

Table 4-5: Top 4 down-regulated genes in $CD14^{+}CD16^{-}$ monocyte-derived foam cells compared to $CD14^{+}CD16^{-}$ monocyte derived macrophages

	Symbol	log2 Fold Change	Adj.Pval	Ensembl gene ID
	MT1H	-7.7773096	1.61E-03	ENSG00000205358
	MT1G	-6.1278953	3.46E-03	ENSG00000125144
	HMGCS1	-1.6995401	1.72E-02	ENSG00000112972
	FASN	-1.3996311	1.47E-03	ENSG00000169710

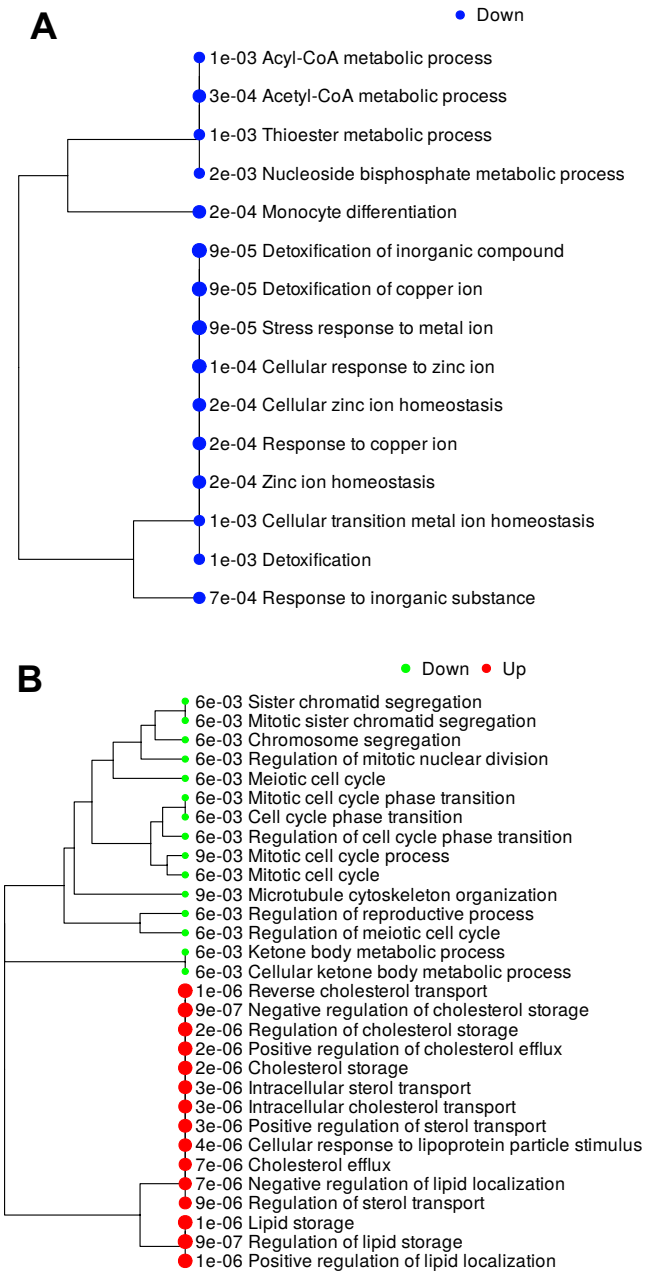


Figure 4-15 **Enrichment analysis of differentially expressed genes based on Gene ontology (GO) biological processes gene sets**

Bulk-RNAseq was performed on mRNA from monocytes, macrophages and foam cells derived from $CD14^{+}CD16^{-}$ and $CD14^{+}CD16^{+}$ monocytes subsets. Gene counts were subject to variance stabilisation transformation (VST) on foam cells and macrophages only with monocyte samples removed from data set**.** Enrichment tree of GO biological processes that were up or down regulated between **(A)** Classical, $CD14^{+}CD16^{-}$ (C) monocyte-derived foam cells relative to macrophages as well as **(B)** Non-classical $CD14^{+}CD16^{+}$ (NC) monocyte-derived foam cells relative macrophages. Sample size per group is n=4, biological replicate.

4.5. Foam cells are enriched for genes regulating cholesterol transport

Based on findings from our RNAseq data I observed a gradual loss in the inflammatory profile of monocytes upon differentiation into foam cells and these foam cells appeared to upregulate genes associated with lipid metabolism specifically in non-classical monocyte-derived foam cells. To validate this, I performed qPCR analysis on fundamental genes involved in cholesterol transport and lipid metabolism on foam cells derived from $CD14^+$ monocytes collectively. Notably, I looked at essential reverse cholesterol transporter genes, ABCA1 and ABCG1 that were also observed in our RNAseq dataset. I also investigated anti-inflammatory lipid-activated transcription factors, PPARα and PPARγ that regulate expression of lipid metabolism genes.

Both ABCA1 and ABCG1 were upregulated on foam cells relative to macrophages although the latter was not statistically significant (Figure 4.16A-B). This was similarly observed with PPARα and PPARγ showing significantly higher expression on foam cells with both transcription factors (Figure 4.16C-D). Collectively, our data indicate that foam cells adopt an anti-inflammatory, lipid metabolising phenotype which based on recent genome-wide studies is reminiscent of a foam cell phenotype.

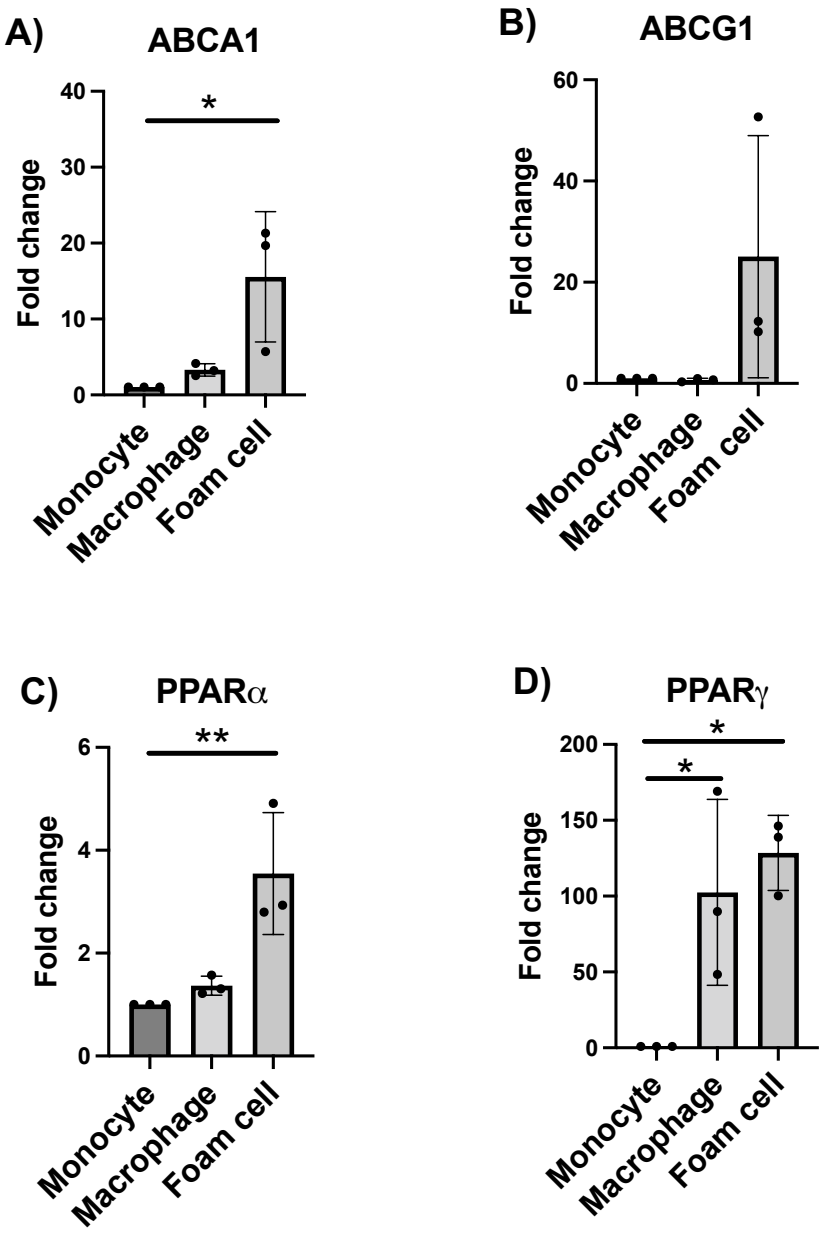


Figure 4-16: An increase in lipid metabolism genes in human monocyte-derived monocytes macrophages and foam cells

$CD14^+$ monocytes were isolated via magnetic bead separation. Monocytes were either cultured in the absence (for macrophage differentiation) or presence of oxLDL (for foam cell formation) for 6 days. RNA was extracted on day 2 for monocytes and on day 6 for macrophages and foam cells following complete differentiation. RNA was converted to cDNA followed by qPCR analysis for the following lipid processing genes: **(A)** ABCA1, **(B)** ABCG1, **(C)** PPARα and **(D)** PPARγ. Data are mean ± SEM (n=3, biological replicate). Statistical analysis performed using ordinary one-way ANOVA with Dunnetts multiple comparisons post-hoc test, *=p<0.05, **=p<0.01.

4.6. Characterisation of monocyte-derived foam cells via flow cytometry analysis

Having looked at the genomic profile of foam cells I then sought to identify potential differences at a protein level on foam cells both intracellularly and extracellularly. Up until this point I had only looked at characterising foam cells derived from oxLDL treatment. However, it is widely acknowledged the LDL can undergo several biochemical modifications in the subintimal space leading to the formation of additional forms of modified LDL including acLDL and maLDL that drive atherogenesis. Hence, I investigated the effects that such modifications can have on protein expression of human monocyte-derived foam cells and whether these foam cell subtypes can be characterised via flow cytometry.

4.6.1. Generation of foam cells derived from various forms of modified LDL

Earlier on in this chapter it had been shown that classical ($CD14^+CD16^-$) monocytes assimilate oxLDL to a greater extent than the non-classical ($CD14^+CD16^+$) subset and that this correlated with higher CD36 scavenger receptor expression. Thus, I used $CD14^+CD16^-$ monocytes in culture treated with oxLDL, acLDL or maLDL for foam cell formation (6 days) for the following set of experiments.

Compared to native LDL, modified LDL is endocytosed via the non-classical scavenger receptor pathway. To initially confirm uptake of each modified LDL I performed Oil Red O staining which demonstrated uptake of modified LDL across the three subtypes illustrated by accumulation of cholesterol stored in the form of lipid droplets detected by fluorescent microscopy (Figure 4.17A-D). Cell culture supernatants were then measured for TNFα and IL-10 cytokine levels. In line with our

data so far, all three foam cell subtypes appeared to have very similar inflammatory profiles to macrophages as levels of TNFα showed no significant change (Figure 4.17E). Interestingly however, I did observe a trend towards a decrease in IL-10 levels which was only significant with foam cells treated with acLDL (Figure 4.17F), although the levels detected in pg/ml were very low overall making it difficult to draw any conclusions.

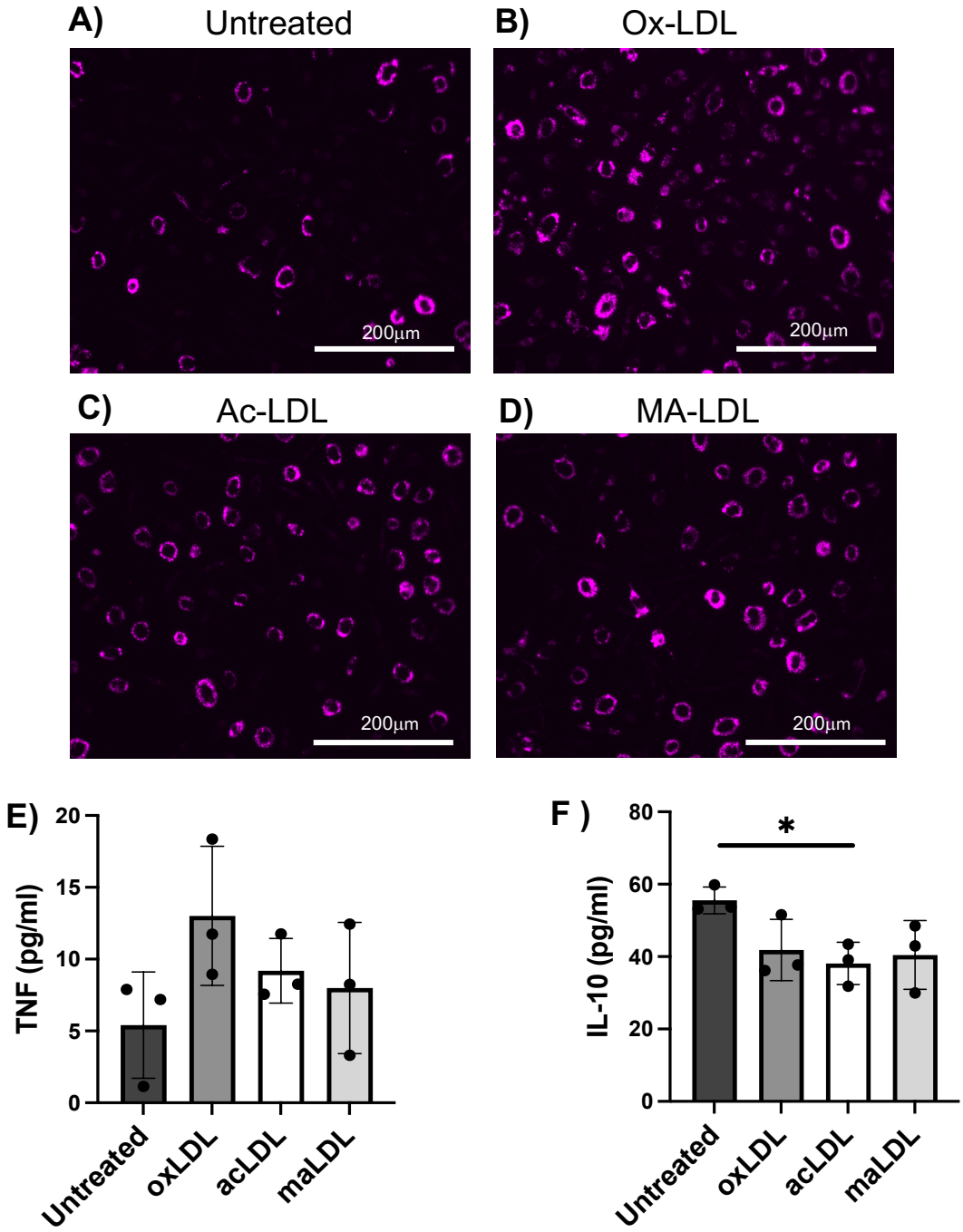


Figure 4-17: Cytokine profile of foam cells generated from ox-LDL, ac-LDL and ma-LDL.

$CD14^{+}CD16^{-}$ (classical) monocytes were cultured and differentiated with various modified forms of LDL including oxLDL, acLDL and maLDL for 6 days in 24 well tissue culture plates for foam cell formation. **(A-D)** On day 6, cell culture supernatants were collected and cells were stained with Oil-red o staining which was visualised using fluorescence microscopy. **(E, F)** TNF and IL-10 cytokine levels were detected in culture supernatants via sandwich ELISA. Data are mean ± SEM (n=3, biological replicate). Statistical analysis performed using one repeated measures ANOVA with Dunnetts post-hoc test compared to the untreated group, Scale bars = 200µm.

4.6.2. Characterisation of foam cell subtypes via flow cytometry

To characterise the various foam cell subtypes, I harvested the cells after 6 days in culture and stained them for flow cytometry analysis using our 11-colour macrophage panel design described in chapter 3. I looked to identify any differences in macrophage-specific markers including scavenger receptors and targets associated with M1-like and M2-like macrophages that may possibly be an indicator of foam cell subtypes being shifted towards a specific polarised macrophage phenotype.

Overall, I observed highly similar protein expression profiles between macrophages and foam cells, and this was consistent amongst foam cells derived from various modified forms of LDL. Classical macrophage-associated markers including CD68 and MerTk showed no significant changes (Figure 4.18A-B). Interestingly CD11c levels were significantly higher in foam cells generated from oxLDL and acLDL reported similarly in murine foamy macrophage within plaque (Figure 4.18C) (Kim et al., 2018). Based on our findings there appeared to be no indication of foam cells being skewed towards an M1 or M2-like phenotype with minimal differences in M1 macrophage markers, CD80, CD86 and HLA-DR and M2 marker CD206, although maLDL derived foam cells did present with reduced CD86 expression compared to macrophages (Figure 4.18D-G). Whilst the scavenger receptor CD204 is notable for its preferential uptake of acLDL and Stabilin-1 being a receptor for maLDL uptake, both receptors displayed no significant changes between macrophages and the various foam cell subtypes (Figure 4.18H-I). However, expression of the major scavenger receptor CD36 was increased on all foam cells, with it being significantly higher on acLDL and maLDL-treated foam cells (Figure 4.18J).

Broadly speaking, our analysis revealed that there was very limited difference in surface protein expression between macrophages and foam cells across the panel which is reflective of the historic data demonstrating the challenge in distinguishing foam cells from macrophages in vivo.

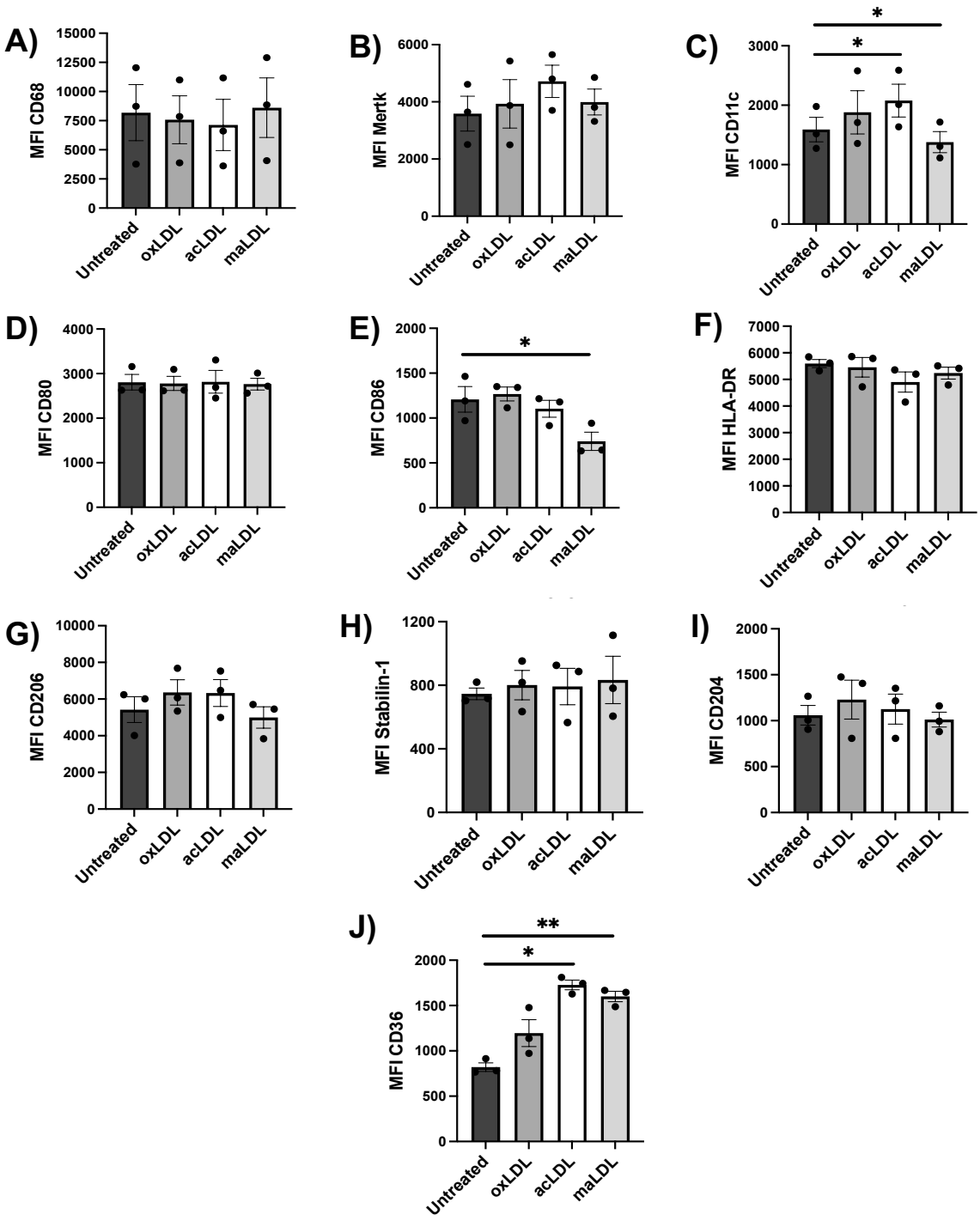


Figure 4-18: Flow cytometry analysis on foam cell phenotypes

$CD14^{+}CD16^{-}$ (classical) monocytes were cultured and differentiated with various modified forms of unlabelled LDL including oxLDL, acLDL and maLDL for 6 days in 24 well tissue culture plates for foam cell formation. On day 6 cells were harvested from tissue culture plastic and stained for flow cytometry analysis for all antibodies in the flow cytometry panel described in Table 2.1; chapter 3. Median fluorescence intensity (MFI) was plotted for **(A)** CD68, **(B)** CD11c, **(C)** MerTk **(D)** CD80, **(E)** CD86, **(F)** HLA-DR, **(G)** CD206, **(H)** CD36, **(I)** CD204 and **(J)** Stabilin-1. Data are mean ± SEM (n=3, biological replicate). Statistical analysis performed using one-way repeated measures ANOVA test with Dunnetts post-hoc test.

4.6.3. Foam cells generated from polarised macrophages demonstrate minimal differences in their phenotypic and secretory profile

Macrophages within in plaque are exposed to many stimuli, with oxLDL being one of them. This causes a dynamic shift in M1 and M2 macrophage polarisation with M1 macrophages dominating during plaque progression and typically corresponds to regions of plaque instability whereas M2 macrophages are concentrated in more stable regions (Barrett, 2020, Cho et al., 2013). Here, I investigated the effects of modified LDL on macrophage polarisation and how this may alter their inflammatory phenotype.

$CD14^{+}CD16^{-}$ MDMs were polarised on day 6 to an M1-like and M2-like phenotype as mentioned previously in chapter 3. The following day two sets of experiments were performed whereby for experiment one, polarising agents were removed and replaced with fresh complete macrophage culture media along with modified LDL (oxLDL, acLDL or maLDL) for 24 hrs (Figure 4.19A and C). The caveat to this experiment is that the removal of polarising stimulants has been reported to revert macrophage activation states back to resting state (M0-like stimulants) (Malheiro et al., 2017). Hence, for experiment two, macrophages were re-polarised by giving a second round of polarising stimulants in addition to modified LDL in attempt to maintain their M1- and M2-like phenotype (for 24 hrs) (Figure 4.19B and C). Naïve macrophages were treated with media without any stimulants. On day 8 cell culture supernatants were collected to assess their cytokine profiles and cells were harvested for flow cytometry analysis using our macrophage panel (see chapter 3).

Previously, from our in vitro experiments, human monocyte derived M1 macrophages secreted TNF-α at levels greater than 5000 pg/ml after 24hrs stimulation

with LPS and IFNy. However, relatively low levels of TNF-α secretion were observed on day 8 from both M1 and M2 macrophages after having polarising stimulants removed and being treated with modified LDL alone suggesting that macrophages tend to revert back to their original activation state upon removal of the original polarising stimuli. When cells were re-challenged with polarising agents, TNF-α levels remained relatively low, with minor insignificant increases detected. The addition of various forms of modified LDL appeared to have minimal effects on the pro-inflammatory TNF-α cytokine profile of M0, M1 and M2 macrophages (Figure 4.20A-C).

Additionally, flow cytometry analysis revealed no significant differences in target antigen expression (CD68, CD11c, MerTK, CD80, CD86, MHC II, CD206, CD35, CD204 and Stabilin-1) across M0, M1 and M2 macrophages treated with either modified LDL alone or with the addition of a second round of polarising agents (re-polarisation) compared to untreated macrophages (Figure 4.20-23) (Table 4.6). Collectively, this data reiterates that fact that foam cells and macrophages have very similar expression profiles, suggesting the addition of modified LDL has minimal effects on altering the protein and cytokine profile of macrophage subtypes in vitro.

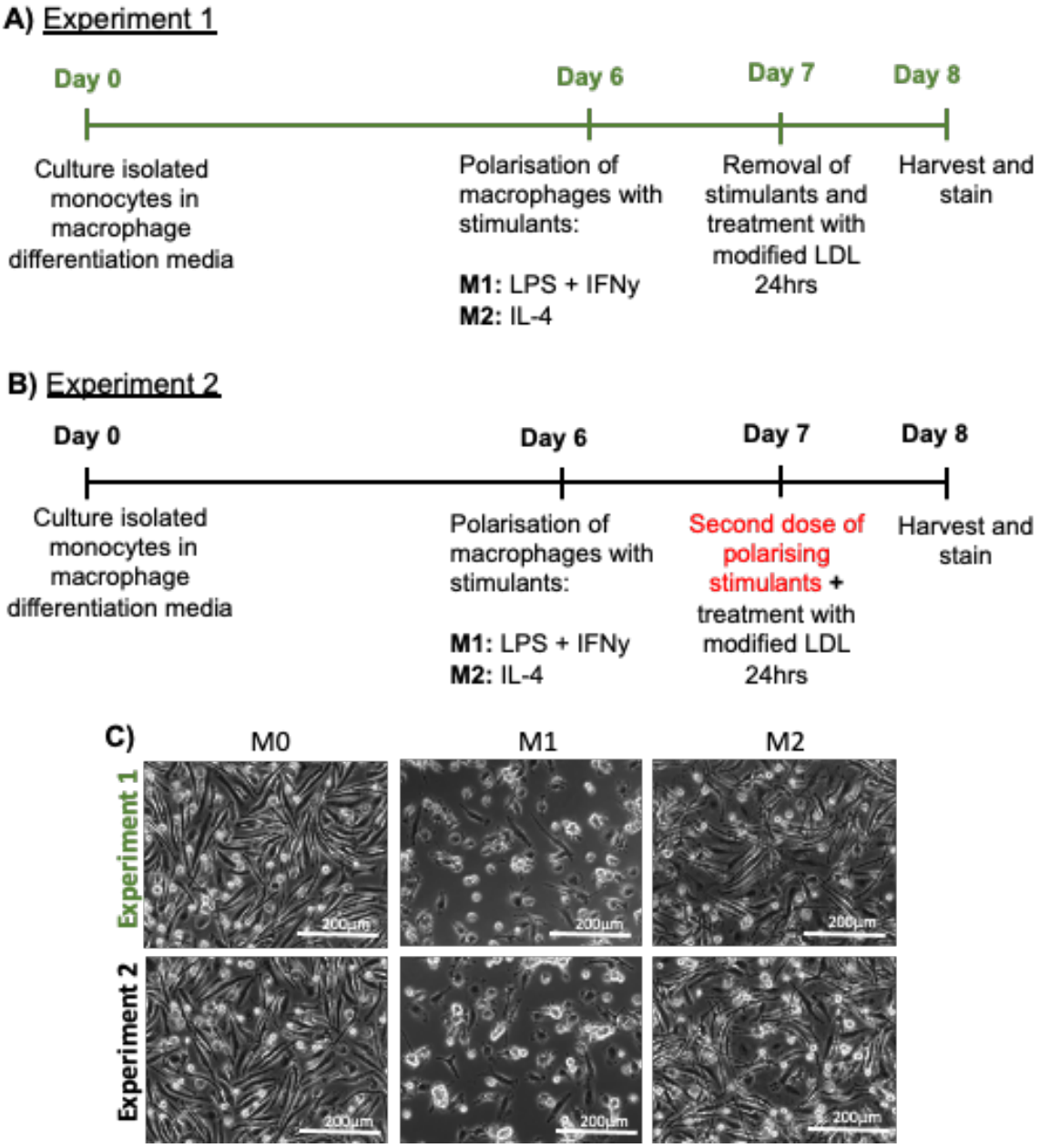


Figure 4-19: Experimental design for macrophage polarisation and treatment with modified forms of LDL

Timelines showing experimental design for polarisation of macrophages whereby on day 6 M1 macrophages were polarised with 100 ng/ml LPS and 20 ng/ml IFN- γ, M2 macrophages with 20 ng/ml IL-4 and M0 macrophages with complete culture media only for 24 hrs. This was followed by **(A)** 24hr treatment with modified forms of LDL (experiment 1) or **(B)** a second dose of polarising agents in conjunction with LDL treatment (experiment 2). **(C)** Phase contrast images showing morphology of foam cells treated with oxLDL derived from M0, M1 and M2 macrophages. Images taken at the experimental endpoint. Scale bars = 200μm.

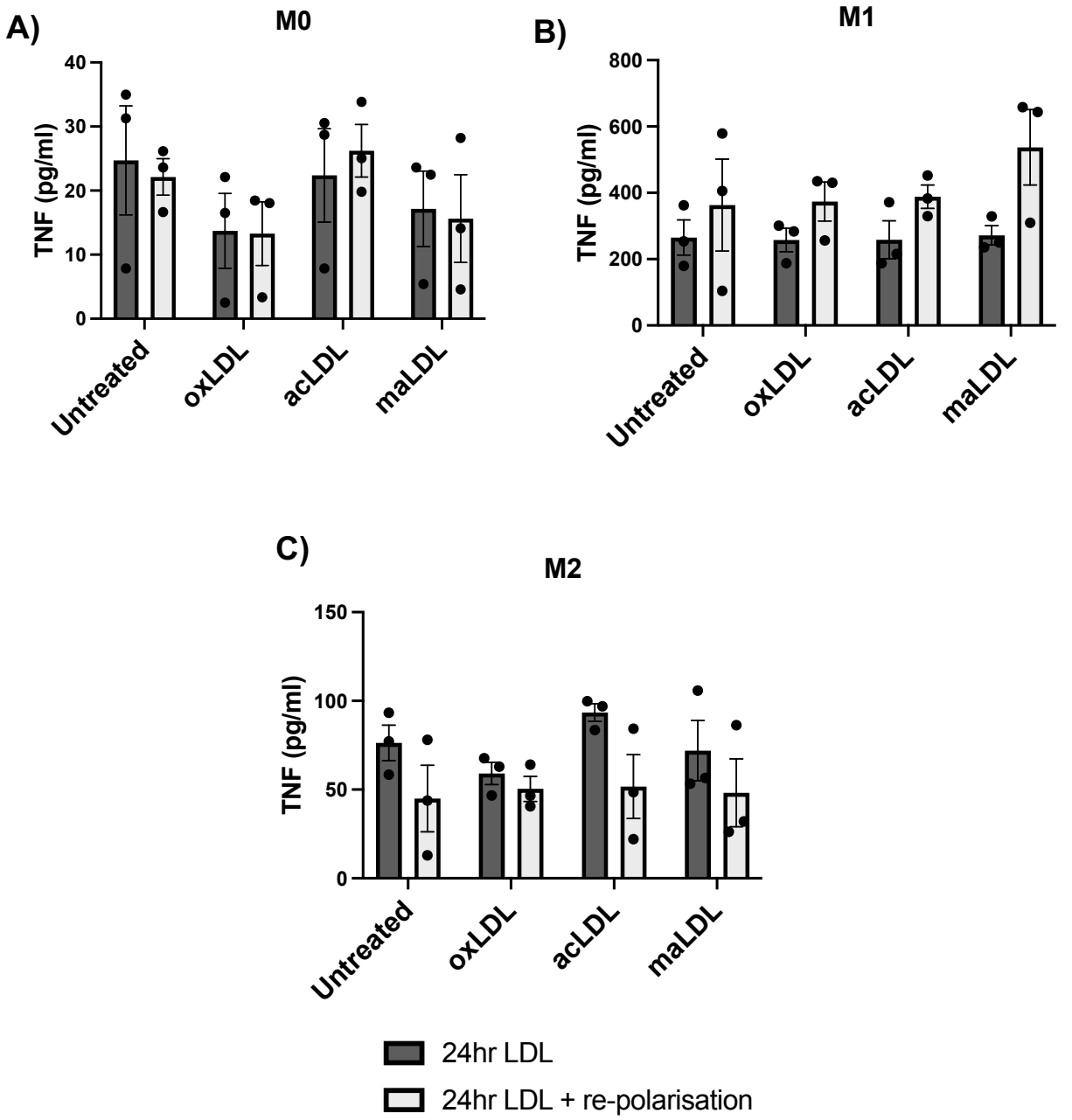


Figure 4-20: TNF secretion profile of foam cells derived from polarised macrophages.

$CD14^{+}CD16^{-}$ (classical) monocytes were cultured and differentiated for 6 days followed by polarisation to M0, M1 and M2 macrophages. On day 7 cells were treated for 24hrs with oxLDL (24hr LDL) or a second dose of polarising agents in conjunction with oxLDL treatment (24hr LDL + re-polarisation). On day 8 cell culture supernatants were collected and subject to TNF ELISA analysis (pg/ml) for **(A)** M0, **(B)** M1 and **(C)** M2 macrophage-derived foam cells. Data are mean ± SEM (n=3, biological replicate). Statistical analysis performed using the non-parametric Mann-Whitney test to compare 24hr LDL vs 24hr LDL + re-polarisation as well as two-way repeated measures ANOVA with Sidak's multiple comparisons post-hoc test for comparison between LDL treatments.

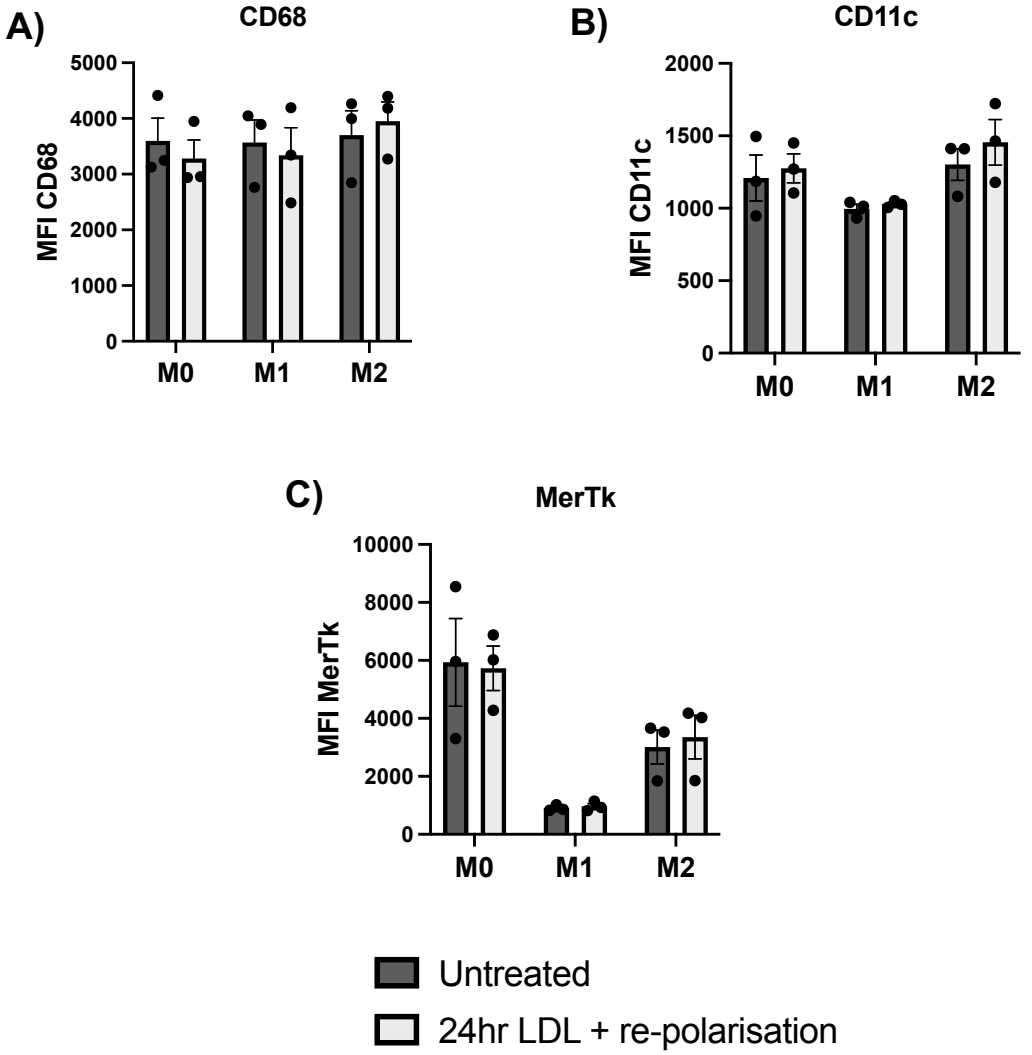


Figure 4-21: Flow cytometry analysis of anti-CD68, anti-CD11c and anti-MerTK macrophage markers on foam cells derived from polarised macrophages.

$CD14^{+}CD16^{-}$ (classical) monocytes were cultured and differentiated for 6 days followed by polarisation to M0, M1 and M2 macrophages. On day 7 cells were treated for 24hrs with second dose of polarising agents in conjunction with oxLDL treatment (24hr LDL + re-polarisation). On day 8 cells were harvested and were stained for flow cytometry analysis for all antibodies in the flow cytometry panel described in Table 2.1; chapter 3. Median fluorescence intensity (MFI) was plotted for **(A)** CD68, **(B)** CD11c and **(C)** MerTk. Data are mean ± SEM (n=3, biological replicate). Statistical analysis performed using the non-parametric Mann-Whitney test to compare 24hr LDL vs 24hr LDL + re-polarisation.

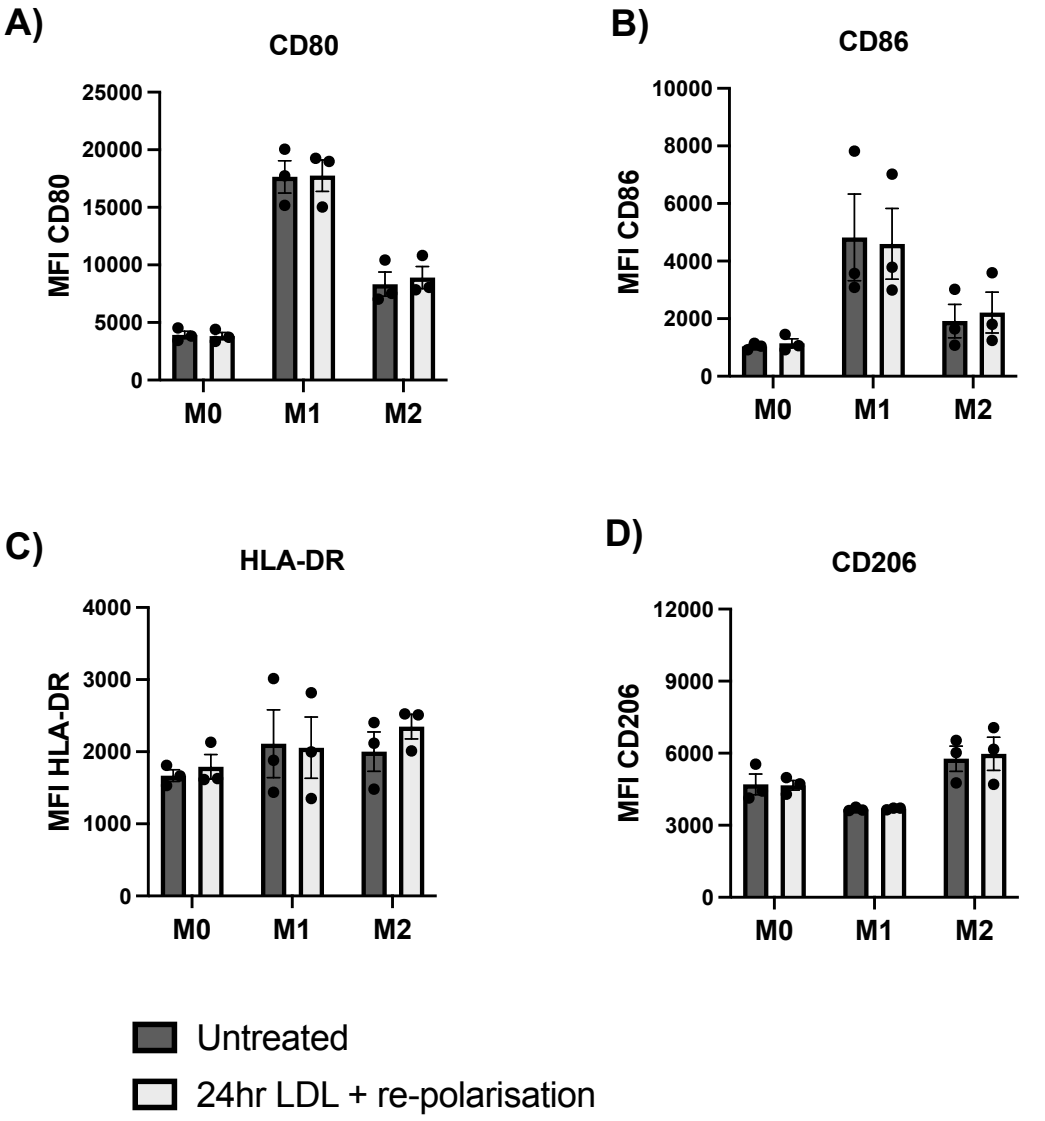


Figure 4-22: Flow cytometry analysis of anti-CD80, anti-CD86, anti-MHC II and anti-CD206 macrophage markers on foam cells derived from polarised macrophages.

$CD14^{+}CD16^{-}$ (classical) monocytes were cultured and differentiated for 6 days followed by polarisation to M0, M1 and M2 macrophages. On day 7 cells were treated for 24hrs with second dose of polarising agents in conjunction with oxLDL treatment (24hr LDL + re-polarisation). On day 8 cells were harvested and were stained for flow cytometry analysis for all antibodies in the flow cytometry panel described in Table 2.1; chapter 3. Median fluorescence intensity (MFI) was plotted for **(A)** CD80, **(B)** CD86, **(C)** HLA-DR and **(D)** Cd206. Data are mean ± SEM (n=3, biological replicate). Statistical analysis performed using the non-parametric Mann-Whitney test to compare 24hr LDL vs 24hr LDL + re-polarisation.

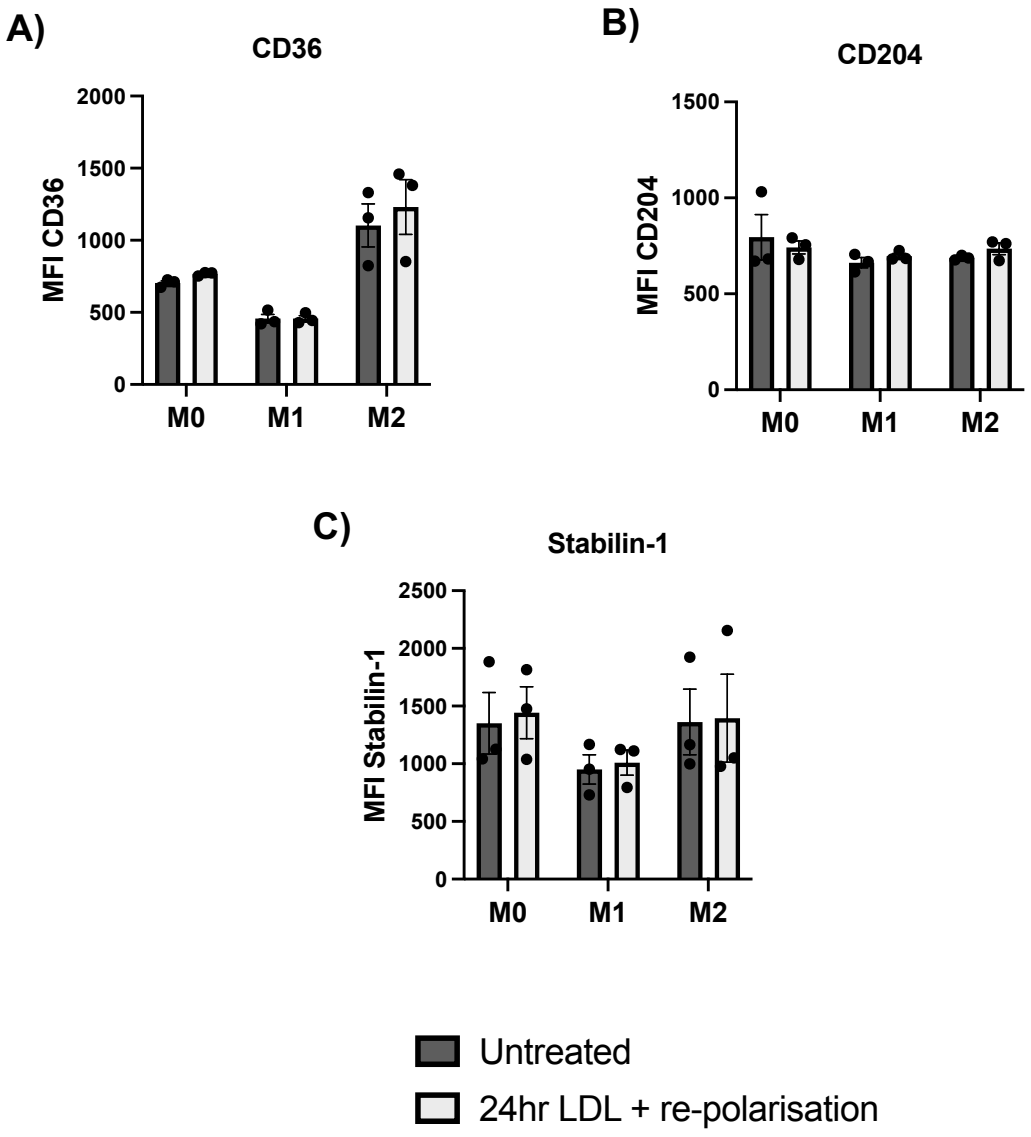


Figure 4-23: Flow cytometry analysis of anti-CD36, anti-CD204, and anti-Stabilin-1 macrophage markers on foam cells derived from polarised macrophages.

$CD14^{+}CD16^{-}$ (classical) monocytes were cultured and differentiated for 6 days followed by polarisation to M0, M1 and M2 macrophages. On day 7 cells were treated for 24hrs with second dose of polarising agents in conjunction with oxLDL treatment (24hr LDL + re-polarisation). On day 8 cells were harvested and were stained for flow cytometry analysis for all antibodies in the flow cytometry panel described in Table 2.1; chapter 3. Median fluorescence intensity (MFI) was plotted for **(A)** CD36 and **(B)** CD204 and **(C)** Stabilin-1. Data are mean ± SEM (n=3, biological replicate). Statistical analysis performed using the non-parametric Mann-Whitney test to compare 24hr LDL vs 24hr LDL + re-polarisation.

4.7. Discussion

Recent studies looking at immune cell composition in both human and murine atherosclerotic plaque have identified a heterogenous population of cells that has enabled greater resolution of the cellular landscape during atherosclerotic disease progression (Lavine, 2023). The precise identity of foam cells remains actively debated as their expression profiles are very similar to macrophages, thus making it difficult to isolate these cells exclusively from tissue without cross-contamination. The use of novel transcriptomic technologies has benefited our understanding of these lipid-associated macrophages (Bonacina et al., 2023). The aim of this chapter was to gain a comprehensive insight into the characterisation of foam cells by focusing also on the impact of monocyte origin in attempt to gain a better understanding of foam cell biology. I did this by utilising both flow cytometry analysis and bulk RNAseq in order to observe changes both at protein and gene level. Our findings were very similar to existing studies demonstrating very similar profiles based on protein expression and transcriptomic signatures with foam cells being presented with a down-regulated inflammatory profile and the upregulation of genes involved with lipid processing.

4.7.1. Monocytes display a pro-inflammatory signature that is gradually lost upon differentiation

Plaque macrophages are largely derived from a heterogenous population of recruited monocytes into the subintimal layer of the inflamed vessel wall. Whilst the current paradigm suggests monocytes undergo differentiation before assimilating oxLDL, I demonstrated that in fact human monocytes are capable of scavenging oxLDL before fully differentiating into macrophages at day 2 and that uptake is greater with $CD14^{+}CD16^{-}$ classical monocytes compared to their $CD14^{+}CD16^{+}$ non-classical

counterpart. This is likely due to increased surface expression of primary scavenger receptor, CD36 on $CD14^{+}CD16^{-}$ monocytes, - a distinguishing feature reported in numerous studies both at gene and protein level (Gren et al., 2015, Mukherjee et al., 2015, Wong et al., 2011, Tallone et al., 2011) . However, this did not reach statistical difference in our findings which most likely is a result of our $CD14^{+}CD16^{+}$ population being combination of non-classical and intermediate monocytes. Intermediate monocytes typically express much higher CD36 expression than the non-classical monocytes, thus contributing to an unexpectedly higher MFI as opposed to that observed with non-classical monocytes alone (Mukherjee et al., 2015). Together, with the enhanced migratory nature of classical monocytes, this subset serves as prime candidate for increased susceptibly to foam cell formation. In contrast, Marcovecchio *et al* revealed the opposite trend, with murine $Ly6C^{-}$ (non-classical) monocytes demonstrating a preferential uptake of oxLDL in comparison to $Ly6C^{+}$ (classical) monocytes in western-diet fed mice. It has been reported here that CD36 in non-classical monocyte not only plays a role in scavenging oxLDL but also facilitates in patrolling the endothelium, suggesting an atheroprotective role for CD36 in this subset in mice (Marcovecchio et al., 2017). Whether these opposing observations are species specific requires further investigation.

Due to overlapping evidence being reported on the roles of $CD14^{+}CD16^{-}$ and $CD14^{+}CD16^{+}$ in atherosclerosis, the precise role of these subsets is not yet clearly defined (Idzkowska et al., 2015). There are also existing conflicts in studies regarding the inflammatory nature of these monocyte subsets with some studies reporting classical monocytes to be more pro-inflammatory (Swirski et al., 2007, Tacke et al., 2007, Gautier et al., 2009). However, in response to inflammatory stimuli, non-classical

monocytes clearly show greater secretion of pro-inflammatory cytokines including TNF-α, IL-6 and IL-1 and have been shown to expand in inflammatory disease (Hofer et al., 2019). I found that $CD14^{+}CD16^{+}$ (non-classical/intermediate) monocytes trended towards a more pro-inflammatory phenotype in steady state based on an increases in TNF-α levels as well as increased expression of genes associated with cell activation, cellular responses to cytokine stimulus and leukocyte activation.

Whilst both monocyte subsets showed distinct transcriptomic profiles from one another via clear separation in PCA plots, I observed a gradual loss of distinction between the two subsets upon differentiation into macrophage and foam cells shown via bulk RNAseq analysis, indicating that $CD14^{+}CD16^{-}$ and $CD14^{+}CD16^{+}$ monocytes develop similar characteristics when differentiated into macrophages. It is generally believed that classical monocytes give rise to 'inflammatory' macrophages and non-classical monocytes differentiate into macrophages of a less inflammatory phenotype (Nahrendorf et al., 2007, Woollard and Geissmann, 2010, Iqbal et al., 2016). However, M2-like non-inflammatory macrophages can also be derived from classical monocytes in the context of allergic inflammation, highlighting the fact that the microenvironment ultimately determines the phenotypic polarisation of monocytes which cannot be recapitulated in our in vitro studies using cells in isolation (Egawa et al., 2013, Yang et al., 2014, Richards et al., 2013). For the purpose of this study, no functional assays were performed to clarify potential behavioural differences between the different macrophage and foam cell populations.

Preliminary data in our lab have shown that functionally monocytes have a greater capacity to activate endothelium compared to macrophages due to increased secondary leukocyte capture under flow conditions, thus considering them more pro-

inflammatory in nature. Likewise, I observed that monocytes overall had a greater enrichment of genes associated with leukocyte activation and inflammatory responses compared to both macrophages and foam cells based on transcriptomic data which reflect such functional behaviours. Among the list of upregulated pro-inflammatory genes included S100A8 and S100A9, which both contribute to increased leukocyte recruitment and cytokine production and are widely known to be differentially expressed in peripheral blood monocytes and MDMs (Beitnes et al., 2012, Rugtveit et al., 1996). Yet this pro-inflammatory phenotype appeared to dissipate upon differentiation confirming a reduction in pro-inflammatory gene signature in macrophages and foam cells. These observations were mirrored in our cytokine array analysis demonstrating a diminished pro-inflammatory cytokine profile with monocyte differentiation. Similar conclusions have been derived from studies within the gut reporting a gradual loss in the pro-inflammatory capacity of monocytes with differentiation into resident and MDMs (Bujko et al., 2018, Bernardo et al., 2018). Collectively I have shown that monocytes in their inflammatory state can scavenge oxLDL and that this pro-inflammatory response is down-regulated upon differentiation into foam cells and macrophages.

4.7.2. Foam cells display an anti-inflammatory and lipid metabolising profile

Transcriptomic studies have primarily utilised single-cell RNA sequencing (scRNAseq), bulk RNAseq analysis and mass cytometry to identify several myeloid specific clusters corresponding to macrophages at various activation states (Fernandez et al., 2019, Winkels et al., 2018, Kim et al., 2018, Lin et al., 2019, Cochain et al., 2018, Depuydt et al., 2020). Uniformly, they have identified a population of resident-like aortic macrophages, inflammatory macrophages and lipid-accumulated

foamy macrophages that exhibit differential gene expression profiles. The distinguishing feature on foam cell-like populations was the elevated expression levels of the TREM2 gene reflected in both murine and human plaque (Cochain et al., 2018, Lin et al., 2019, Depuydt et al., 2020). In this study I similarly observed a gradual increase in TREM2 expression on foam cells with monocyte differentiation. In addition to its role in cell survival and its involvement in neuroinflammation, TREM2 has recently emerged as a significant player in lipid metabolism, whereby TREM2-deficient mice presented with fewer lipid droplets in myeloid cells upon exposure to cholesterol (Gouna et al., 2021, Khantakova et al., 2022). Thus, enrichment of TREM2 in foam cells may contribute to the characteristic accumulation of cholesterol-filled lipid droplets observed in macrophages.

These studies also reported an increase in lipid processing genes that regulate cholesterol uptake and efflux in TREM2^{hi} foamy macrophages. This included ABC transporters and PPAR signalling pathway genes (Depuydt et al., 2020, Kim et al., 2018, Cochain et al., 2018, Xu and Yang, 2023). Similarly, I also observed increased expression of ABC transporter genes, ABCA1 and ABCG1 which was only evident in macrophages derived from non-classical monocytes. These genes are typically induced by PPARs and I confirmed this via qPCR analysis demonstrating a simultaneous increase in PPARα and PPARγ in foam cells (Chinetti et al., 2001). Such genes may be upregulated in response to excessive influx of oxLDL-derived cholesterol that become trapped within the cell in the form of lipid droplets (Javadifar et al., 2021, Wang et al., 2019a). Evidence for this was supported by the increased levels of lipid-droplet associated gene, PLIN2 that I observed in these foam cells,

whereby overexpression of this gene typically corelates with reduced cholesterol efflux in macrophages (Saliba-Gustafsson et al., 2019, Larigauderie et al., 2004).

Previous studies have demonstrated pro-inflammatory characteristics of foam cells through their interaction with TLRs and oxLDL and activation of the NLRP3 inflammasome (Zhang et al., 2014, Liu et al., 2014). However, based on recent findings, there is a current paradigm shift in the field, suggesting foam cells are not inevitably pro-inflammatory but instead maybe considered to be anti-inflammatory (Thomas et al., 2015a, Depuydt et al., 2020). In fact, macrophages are considered more pro-inflammatory than foam cells and Depuydt et al identified two subsets of these pro-inflammatory macrophages expressing IL-1β and TNFα in human atherosclerotic plaque (Depuydt et al., 2020, Kim et al., 2018). This is supported by Reschen et al, displaying evidence of the degradation of pro-inflammatory genes in human macrophages upon oxLDL exposure (Reschen et al., 2015). In contrast, $TREM2^{high}$ foamy macrophage were associated with low levels of inflammatory genes such as IL-1β and TNFα (Kim et al., 2018). In line with this, I found down-regulated expression of interleukin 1 receptor type II (IL1R2) (a high affinity receptor for mature IL-1β) in foam cells derived from non-classical monocytes only, indicating reduced pro-inflammatory IL-1β signalling in foam cells (Ding et al., 2023).

These findings indicate that foam cells exhibit a genomic profile characterised by lipid metabolism and anti-inflammatory traits. This paradoxical observation challenges the longstanding association of foam cells with promoting inflammation (Thomas et al., 2015a). I demonstrate here that this phenotype is specifically associated in foam cells derived from non-classical monocytes in our study. Whilst classical monocytes may assimilate oxLDL more readily, it may be that non-classical

monocytes react more aggressively to pro-inflammatory stimuli such as oxLDL, leading to greater differential gene expression that is indicative of a foam cell phenotype. Interestingly, it has been shown that Ly6C^{high} monocytes are mostly found in healthy aortas whereas Ly6C^{low} non-classical monocytes are the dominant monocyte population in diseased atherosclerotic plaque, suggesting a pro-atherogenic role for these cells (Winkels et al., 2018). Whether these observations are translational in humans would require further investigation.

4.7.3. Characterisation of foam cell subtypes and their effect on macrophage polarisation states

Whilst oxLDL has predominantly been indicated in atherosclerotic lesions, several other forms of modified LDL such as acLDL and maLDL have been reported from early studies that permit cholesterol accumulation (Griffin et al., 2005, Schuh et al., 1978, Goldstein et al., 1979b). Several studies have reported differences between foam cell subtypes showing that modified LDL ligands traffic to different lysosomal compartments resulting in varying degrees of cholesterol accumulation within the cell and that the degradation and uptake of modified LDL ligands differ (Wang et al., 2007, Lougheed et al., 1999). Although few if any studies have attempted to characterise these foam cell subtypes based on protein expression, due to challenges in generating pure populations of foam cells and to their highly adherent nature in vitro. By applying flow cytometry analysis on in vitro cultured foam cells, our data revealed minimal differences in intracellular and extracellular protein expression between foam cell subtypes. In fact all three subtypes displayed very similar profiles to macrophages, mirroring the data observed at a genomic level.

Distinguishing features observed between macrophages and foam cells included higher CD36 expression. It is noted that that uptake of various forms of modified LDL varies, whereby high affinity uptake of oxLDL, acLDL and maLDL are all attributable to specific scavenger receptors (Kunjathoor et al., 2002, Lougheed et al., 1999, Moore and Freeman, 2006). Candidate receptors for oxLDL include CD36, CD68, MARCO, LOX-1, whereas for SRA (CD204) is considered the prototypical receptor for majority of acLDL uptake demonstrated in SRA-knockout mouse (Moore and Freeman, 2006, Jay et al., 2015, Lougheed et al., 1997). However, I observed no significant differences in CD204 expression between human macrophages and foam cells derived from acLDL. Similarly, I observed no significant changes with stabilin-1 expression on maLDL-derived foam cells since stabilin-1 deficiency has been associated with abrogated maLDL uptake in hepatic macrophages (Rantakari et al., 2016). Notably, CD36 expression was elevated on all foam cell subtypes, indicating its prominent role in the uptake of all three forms of modified LDL in human macrophages. This contradicts the findings observed in studies involving mice and cell lines (Lougheed et al., 1997, Rantakari et al., 2016, Podrez et al., 2000). It is possible that the various forms of modified LDL may compete for scavenger receptor binding based on their affinity to CD36 and that the absence of CD36 may be indispensable for their uptake (Kunjathoor et al., 2002, Sparrow et al., 1989). Previous data in our lab (unpublished) is indicative of this showing that blocking CD36 abrogated majority of oxLDL uptake in human macrophages, however this has yet to be repeated with both acLDL and maLDL.

In addition, I also observed increased CD11c expression on foam cells compared to macrophages which was significant with acLDL and maLDL subtypes.

Whilst CD11c is typically associated as a dendritic cell marker, macrophages also co-express high levels of CD11c (particularly alveolar and intestinal macrophages), which contributes to the ongoing inability to distinguish accurately between DCs and macrophages in tissue due to extensive overlap in expression (Merad et al., 2013, Bain and Mowat, 2014, Bernardo et al., 2018, Misharin et al., 2013). Parallel with our findings, its expression is found on mature macrophages in atherosclerotic lesions and more recently its expression has been linked with foamy macrophages in murine atherosclerotic plaque and BMDM-derived foam cells (Kim et al., 2018, Koltsova et al., 2013, Wu et al., 2009, Bisgaard et al., 2016). Whether it contributes to the functional role of foam cells during atherogenesis is unknown. Based on our results, it is evident that macrophages and foam cells consistently exhibit very similar profiles based on protein expression also. However our findings suggest CD36 and CD11c expression may be used as potential markers to distinguish between them. Further analysis would be required in order to find distinguishing features between the different foam cell subtypes.

4.7.4. The impact of modified LDL on the polarisation state of macrophages

During atherogenesis M1 macrophages are typically associated with plaque progression and M2 macrophages with plaque stability and regression. Previously, it has been shown that exposure to oxLDL can modify the inflammatory response of macrophages (Ohlsson et al., 1996, Alique et al., 2015). Murine BMDMs and THP-1 cells demonstrated enhanced LPS-induced pro-inflammatory cytokine secretion with prior exposure to oxLDL (Mikita et al., 2001, Groeneweg et al., 2006). Here I looked to investigate the impact of oxLDL, acLDL and maLDL on human MDM polarisation states and whether uptake ultimately modifies macrophage phenotypes.

Based on their cytokine profiles, it appears that the removal of polarising stimuli after 24 hours led a loss in macrophage polarisation states due to a drastic reduction in TNFα levels detected in M1 macrophages (greater than tenfold) compared to levels detected immediately after 24 hour stimulation (demonstrated in chapter 3). It seems as if they revert back an M0-like state which was also similarly reported by Malheiro *et al* where they observed a loss in M1 and M2 macrophage protein expression with cytokine removal (Malheiro et al., 2017) Yet, I found that adding a second round of polarising agents post 24 hours made minimal differences in cytokine levels. This reiterates the fact that macrophages acquire optimal times for stimulation after which expression of phenotypic markers begin to decline (detailed in chapter 3) (Unuvar Purcu et al., 2022). Further to this I observed no differences in TNFα and IL-10 levels upon exposure to modified LDL between the 3 macrophage subsets indicating that modified LDL uptake has little effect on modulating cytokine levels in cultured MDMs.

Interestingly M2 macrophages have been shown to accumulate oxLDL more rapidly compared to M1 macrophages. This is supposedly driven by the enrichment of scavenger receptors on their surface which I similarly observed with higher CD36 and stabilin-1 expression on the M2 macrophages compared to the M1 phenotype, although there appeared to be no significant change upon exposure to modified LDL. (van Tits et al., 2011, Bisgaard et al., 2016, Isa et al., 2011). This trend was mirrored across the rest of the markers in our flow cytometry panel where I observed no changes in protein expression with modified LDL treatment across the macrophage subsets.

Overall, in this chapter I demonstrated little to no changes in the genomic, cytokine and protein expression profile of macrophages upon exposure to modified LDL. Once again, these findings are reflective of the majority of studies demonstrating

significant overlap in macrophage and foam cell phenotypes. Yet, one may argue that perhaps phenotypic changes in foam cells are not being captured due to the length of time of our foam cells in culture since the lifespan of macrophages in plaque is typically extensive, lasting up to several months long (Murphy and Tall, 2014, Robbins et al., 2013). Interestingly Nogeic′ *et al* demonstrated that prolonged cultured of human monocyte-derived foam cells at 30 days was able to functionally elicit pro-inflammatory responses as well as express significantly higher expression of CD36 scavenger receptor and CD86 M1 macrophage marker compared to macrophages alone (Nogieć et al., 2020). Thus, our model of 8 days may not truly reflect the cumulative effects of modified LDL uptake over prolonged periods of time which realistically occurs during chronic disease.

4.7.5. Summary of results

- Classical monocytes are able to assimilate oxLDL more readily than their non-classical counterpart which may correspond to higher CD36 scavenger receptor expression
- Monocytes demonstrate a greater pro-inflammatory transcriptomic profile compared to macrophages and foam cells as monocytes exhibit higher expression levels of pro-inflammatory genes. This pro-inflammatory phenotype appears to dissipate upon differentiation into macrophages and foam cells i*n vitro*
- Foam cells display an anti-inflammatory and lipid metabolising transcriptomic profile which appears to be more prominent in foam cells derived from non-classical monocytes

- Foam cells derived from various forms of modified LDL exhibit similar protein expression profiles detected via flow cytometry.
- Elevated CD11c and CD36 expression on foam cells may be used to distinguish these lipid-laden cells from macrophages
- Various forms of modified LDL (oxLDL, acLDl and maLDL) appeared to have minimal effect on the polarisation states of MDMs

Chapter 5. SPATIAL TRANSCRIPTOMIC PROFILING OF HUMAN CORONARY ARTERIAL PLAQUE TISSUE

5.1. Introduction

In the previous chapter I investigated differences in the protein and genomic signature of foam cells and macrophages in vitro.Whilst, studying these cells in isolation is routinely performed in atherosclerosis research, in reality the immune landscape in the plaque is more heterogenous, whereby intercellular interactions between immune cells orchestrate disease pathogenesis (Fernandez et al., 2019, Lavine, 2023, Bonacina et al., 2023). Thus, our studies in vitro looking at foam cells and macrophages in isolation most likely fails to recapitulate the inter-cellular interactions that may influence their phenotype and behaviour in vivo during the disease state (Mahdinia et al., 2023). Hence, I employed novel spatial transcriptomics technology using the GeoMx Digital Spatial Profiler (DSP) to carry out immunoprofiling of human coronary arterial plaque tissue. This novel technology has the added advantage of providing spatial and temporal assessments of proteomic and genomic immune profiles within tissue (Hernandez et al., 2022). Arterial tissue sections were taken from patients with atherosclerosis at different stages of disease severity which also allowed us to look into potential changes in the immune landscape with disease progression to identify potential biomarkers of disease severity. I specifically made an

attempt to look at changes in the expression profiles of macrophage and foam cells within plaque as they are the predominant immune cells responsible for disease manifestation.

5.2. Experimental design and rational for spatial transcriptomic profiling

Although the experimental design was not tailored specifically for our research question, I was able to utilise the raw data to investigate potential differences in the gene expression profiles of macrophage and foam cell markers during disease progression at distinct anatomical sites of coronary artery tissue. The experiment workflow consisted of initially staining human coronary artery tissue sections with immunofluorescent antibodies which in this case were CD45 for immune cells, CD4 for T cells and SYT013 for a nuclear stain. This was followed by staining with DSP barcoded RNAscope probes for human whole transcriptome analysis (WTA). Sections were imaged and selective ROIs were chosen for sequencing for WTA (Figure 5.1-5.2).

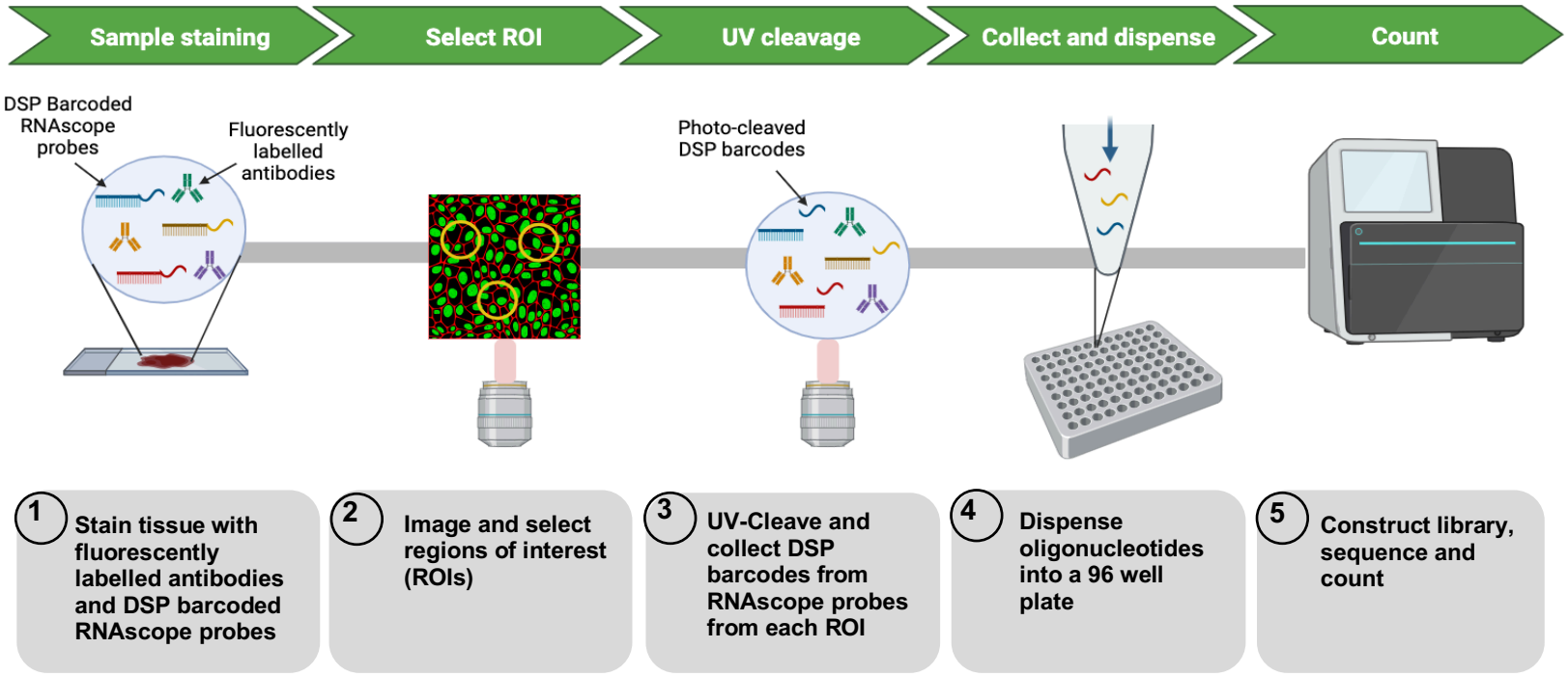


Figure 5-1: Schematic diagram of digital spatial profiling (DSP) assay workflow using nanostring GeoMX DSP.

1) Tissue sections are labelled with fluorescently labelled antibodies for specific markers for tissue localisation followed by staining with RNAscope photo-cleavable DSP barcoded probes to detect RNA. 2) Tissue section is then imaged using a fluorescent microscope and specific regions of interest (ROIs) are selected for profiling. 3-4) UV-light is then used to cleave DSP barcodes from RNA probes which are collected from specific ROIs and dispensed in a 96-well plate, where each well corresponds to a pool of photocleaved probes from a single ROI 5) Collected barcoded probes are then counted using an illumina sequencer (Diagram self-illustrated using Biorender).

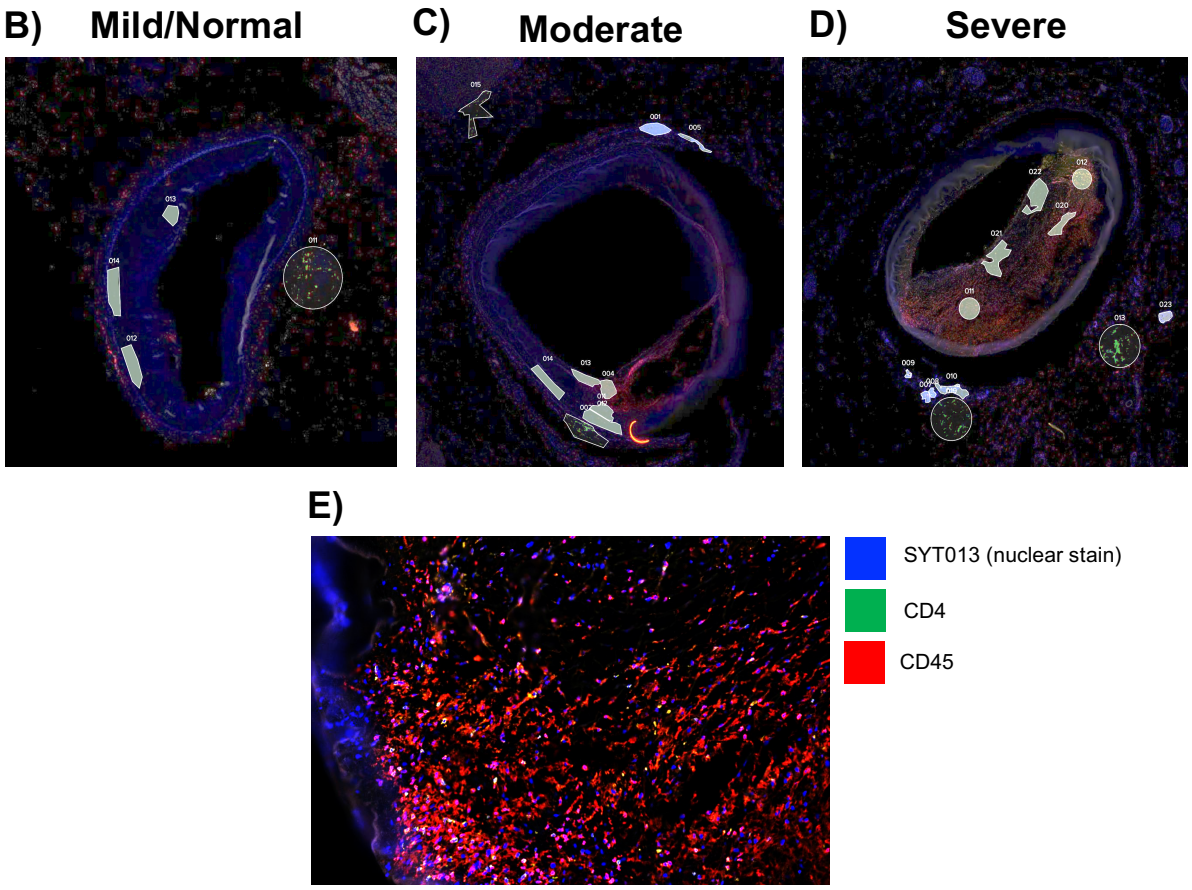


Figure 5-2: Microscopy images of fluorescently labelled human coronary artery tissue sections with selected ROIs for GeoMX digital spatial profiling (DSP).

Human coronary artery sections of varying disease severity; **(A)** mild/normal, **(B)** moderate and **(C)** severe were stained with fluorescently labelled antibodies including **(E)** SYTO13 for nucleic acid stain (blue), CD4 for T cells (green) and CD45 for immune cells (red) followed by RNAscope photo-cleavable DSP barcoded probes for whole transcriptome analysis (WTA). Sections were then imaged and specific regions of interest (ROIs) were selected (as shown in images) whereby circular ROIs refer to areas corresponding to arterial tertiary lymphoid organs.

5.3. The rationale for spatial transcriptomic data analysis

The raw sequenced data were processed for quality control and normalised before downstream analysis was performed using the GeoMx DSP data analysis suite software. Since the experiment was originally designed to look at CD4 T cells, I had to adjust our analysis workflow to meet the needs of our research investigation which was to look at differential gene expression of macrophages and foam cells in regions within atherosclerotic plaque at different disease states.

Initially, unsupervised hierarchical clustering was performed demonstrating that for the most part genes were clustered according to tissue localisation based on the generated heatmap (Figure 5.3). Since the tissue was not stained specifically using a macrophage marker, I selected ROIs that were $CD45^+$ to ensure I was focusing on regions containing immune cells. Further to this, based on existing literature and findings from our in vitro studies I based our downstream analysis using CD68 mRNA as a marker for macrophages and CD11c (ITGAX) mRNA which from our data was elevated on foam cells at a protein level and has been reported in parallel in previous studies (Kim et al., 2018, van der Kooij et al., 1997). Trem2 expression to also found to be closely associated with foam cells as I have demonstrated in the previous chapter, however I failed to detect sufficient levels in this transcriptomic dataset (Depuydt et al., 2020, Cochain et al., 2018, Kim et al., 2018). As T cells are amongst the most abundant cells in plaque, I found CD68 gene expression correlated with greater expression in $CD4^+$ ROIs compared to $CD4^-$ ROIs, although expression of CD11c (ITGAX) was more variable (Figure 5.4).

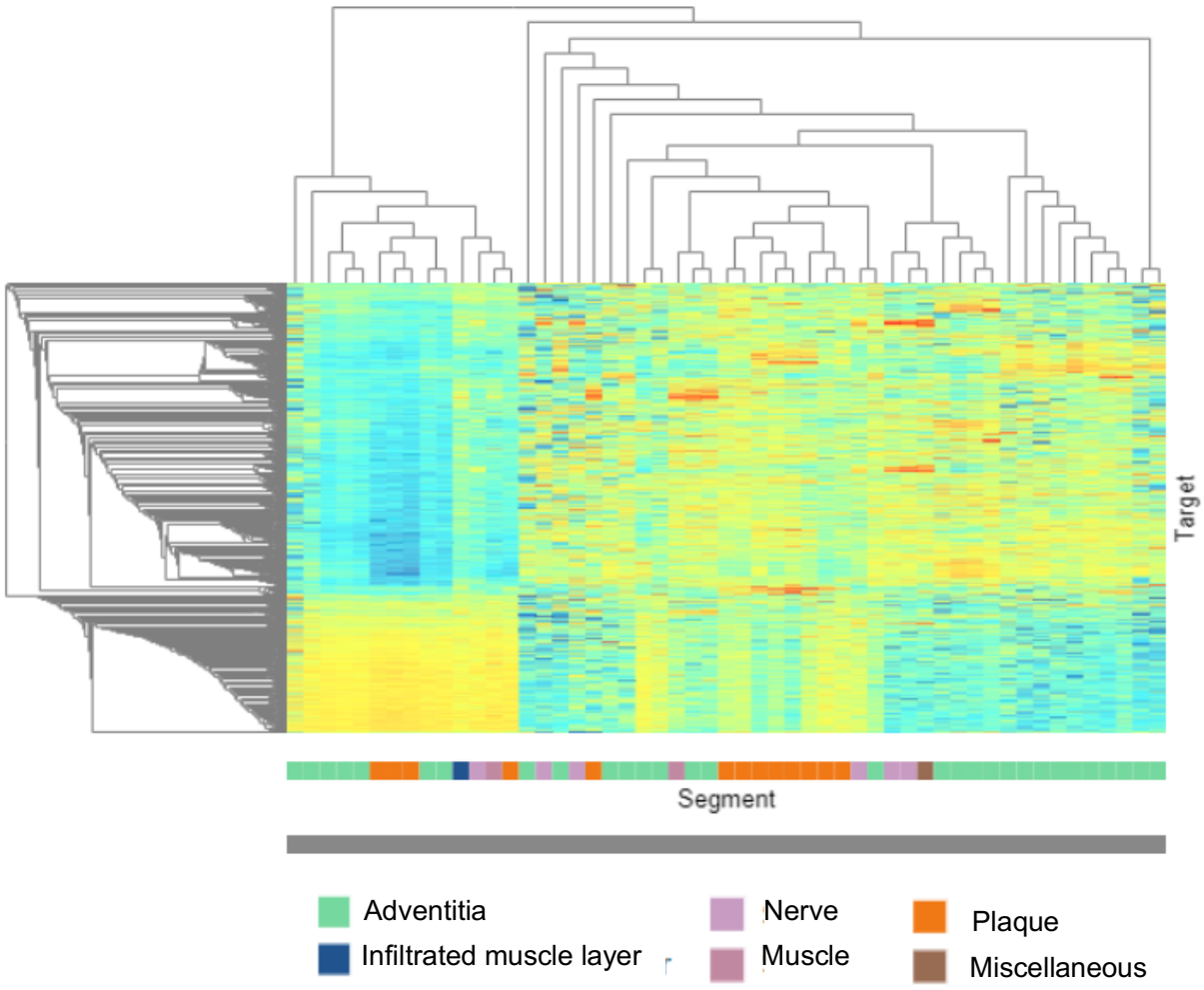


Figure 5-3: Unsupervised hierarchical clustering of genes according to localisation in coronary artery tissue sections

Human coronary artery sections of varying disease severity were analysed using the GeoMX DSP for whole transcriptome analysis (WTA). Using the GeoMX DSP data analysis suite software, unsupervised hierarchical clustering was performed based on tissue localisation as labelled in key; adventitia, infiltrated muscle layer, nerve, muscle, plaque, miscellaneous (unlabelled regions). Data presented as a heatmap.

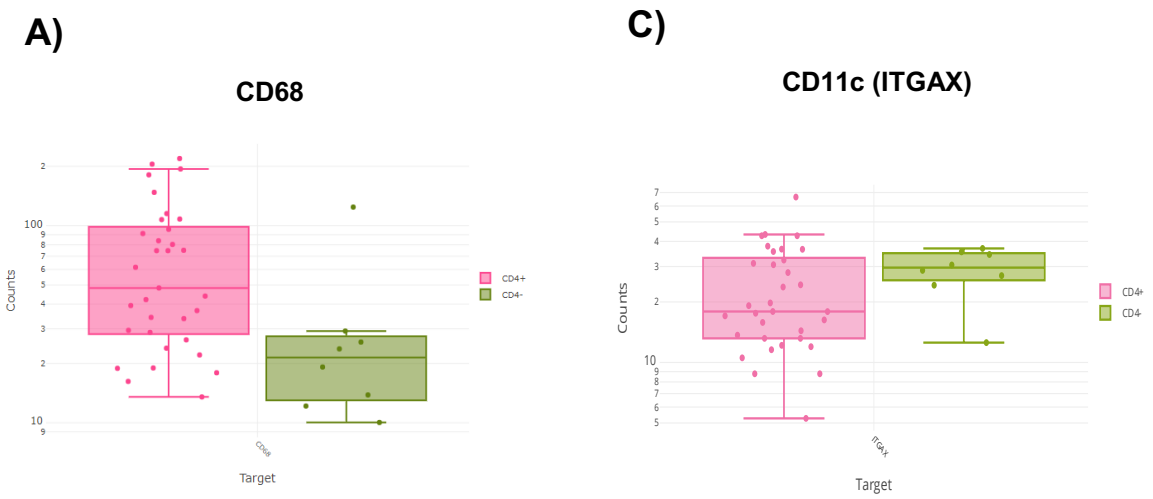


Figure 5-4: Box plot of CD68 and ITGAX (CD11c) gene counts in CD45+CD4+ vs CD45+CD4- ROIs

Human coronary artery sections of varying disease severity were analysed using the GeoMX DSP for whole transcriptome analysis (WTA). Gene expression of **(A)** CD68 and **(B)** ITGAX (CD11c) was plotted in CD45+ CD4+ (pink) and CD45+ CD4- ROIs (green). Gene expression counts were normalised based on quartile three (Q3) normalisation. Data plotted are ± SD.

5.4. Spatial CD68 gene expression in coronary artery tissue

I then sought to investigate the expression of CD68 (macrophage marker) within tissue in attempt to look at its changes with disease severity and localisation. The distribution of CD68 gene expression according to disease severity was variable. CD68 expression was appeared to be greater in mild and normal regions of tissue, although in ROIs of moderate and severe disease expression was highly variable with some ROIs expressing high counts for CD68 (Figure 5.5A-B). Overall CD68 expression was shown to be greater in regions of plaque tissue. However, one must take into account the dissimilar number of ROIs for the different factors (tissue localisation and disease severity) which may skew data outcomes (Figure 5.5C-D).

Since, the original experimental design did not include a CD68 antibody I split ROIs based on $CD68^{high}$ vs $CD68^{low}$ expression in attempt to select regions that are likely to be truly positive for CD68 (macrophages) based on relative expression. A range of macrophage-associated genes (based on the macrophage flow cytometry panel mentioned in chapter 3) were then investigated for their expression in $CD68^{high}$ and $CD68^{low}$ ROIs in the tissue sections including (Figure 5.6A-B). These genes were generally elevated in $CD68^{high}$ regions as expected with majority of these differences being statistically significant with an FDR < 0.01 as visualised in the form of a volcano plot (except for ITGAX, and ABCG1). The top 15 genes elevated in $CD68^{high}$ ROIs were also plotted showing significantly high expression in complement factors (C1QA, C1QB and C1QC) as well as CD14, all of which are indicative of a macrophage phenotype (Figure 5.6C-D). Pathway enrichment analysis was performed on both groups whereby statistically significant pathways of interest were identified. This revealed an up-regulation of pathways in $CD68^{high}$ ROIs associated with innate macrophage functions

such as MHC II antigen presentation, regulation of complement cascade and binding and uptake of ligands by scavenger receptors (Park et al., 2022). I also observed an increase in IL-4 and IL-13 signalling that are classically required for activation of M2 macrophage polarisation (Scott et al., 2023) (Figure 5.6E) (Table 5.1). Together these findings are suggestive of $CD68^{high}$ regions being enriched with macrophages due to their gene expression profiles and suggests that such regions are enriched mainly in plaque as anticipated.

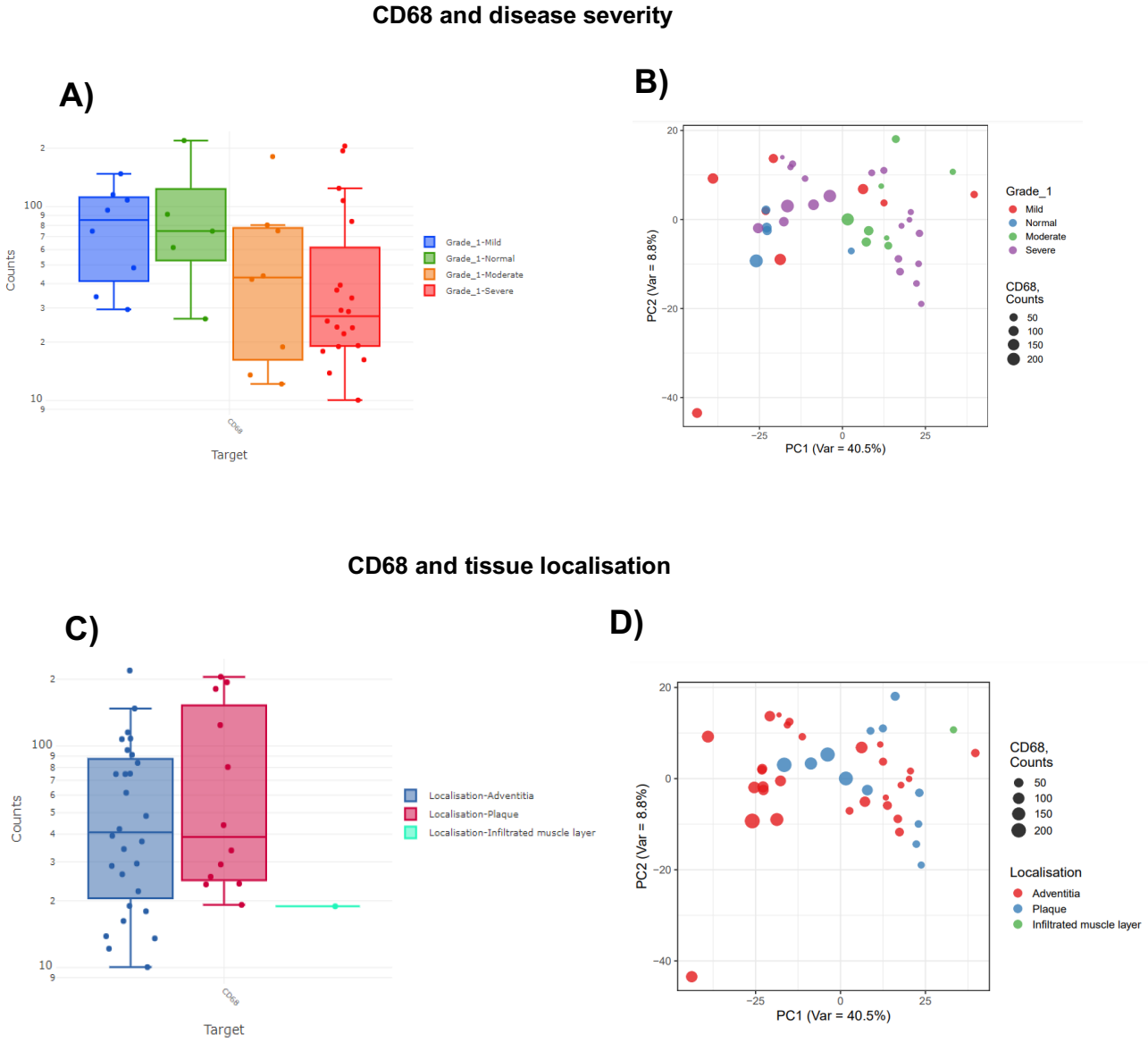


Figure 5-5: The variation in CD68 gene expression in coronary artery tissue based on disease severity and tissue localisation

Human coronary artery sections of varying disease severity were analysed using the GeoMX DSP for whole transcriptome analysis (WTA). CD68 gene expression was visualised as box plots and PCA plots according to **(A,B)** disease severity graded according to being mild, normal, moderate or severe and **(C, D)** tissue localisation in adventitia, plaque or infiltrated muscle layer. Gene expression counts were normalised based on quartile three (Q3) normalisation. Data plotted are ± SD.

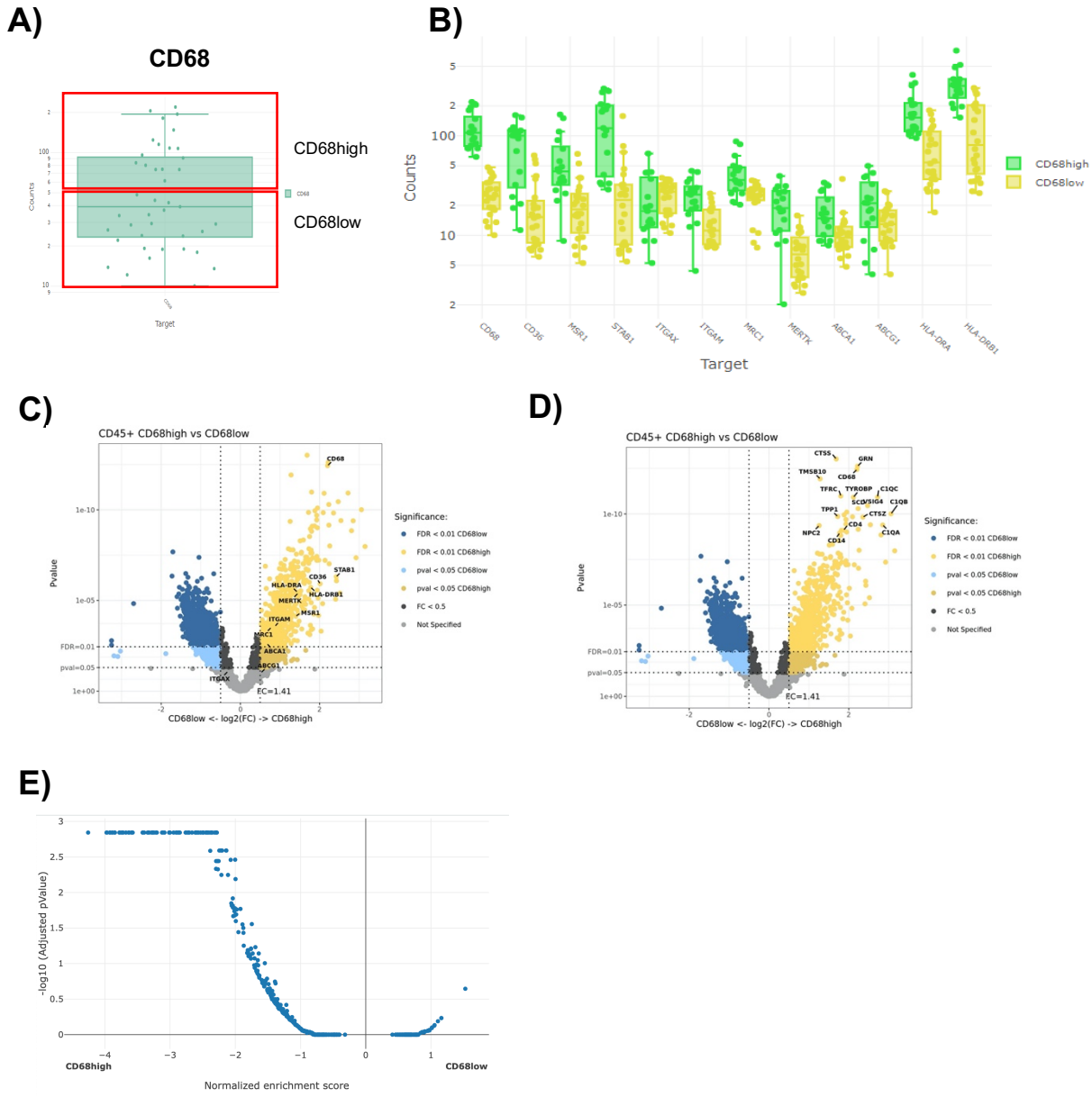


Figure 5-6: Gene expression in coronary artery tissue in CD68high vs CD68low ROIs

Human coronary artery sections of varying disease severity were analysed using the GeoMX DSP for whole transcriptome analysis (WTA). **(A)** ROIs in tissue sections were labelled according to CD68high vs CD68low gene expression. **(B)** Pan macrophage markers were plotted in box plots for CD68high (green) vs CD68low (yellow) ROIs. Volcano plots were plotted to identify **(C)** top 15 statistically significant up-regulated genes (labelled) with an FDR <0.01 as well as **(D)** expression of pan macrophage markers (labelled) in CD68high vs CD68low ROIs. **(E)** Pathway analysis was performed to observe pathway enrichment obtained from the online Reactome database with '–log adjusted p value' on the y-axis and 'normalised enrichment score' on the x-axis. Gene expression counts were normalised based on quartile three (Q3) normalisation.

5.5. Spatial CD11c (ITGAX) gene expression in coronary artery tissue

I performed a similar set of analysis based on CD11c (ITGAX) gene expression which I proposed as a potential foam cell marker in coronary artery tissue sections, based on previous findings in the literature and our flow cytometry analysis (chapter 4) (Kim et al., 2018). Similarly, CD11c (ITGAX) was not included as an antibody stain in the original experimental design. Interestingly, CD11c (ITGAX) expression was much higher on moderate to severe disease ROIs and this coincided with greater expression in regions of plaque (Figure 5.7). ROIs were also split according to $CD11c^{high}$ and $CD11c^{low}$ expression with the aim of selecting regions consisting of cells truly positive for CD11c (ITGAX) expression which I hypothesised as being potentially foam cell positive (Figure 5.8A). Our panel of macrophage-associated genes demonstrated minimal significant differences between $CD11c^{high}$ and $CD11c^{low}$ ROIs, with only significantly higher expression found with STAB1 and CD36 scavenger receptor expression (with an FDR <0.01) surprisingly on $CD11c^{low}$ areas (Figure 5.8B and D). Caution was taken when interpreting the data as CD11c is also widely known as a dendritic cell marker, thus distinguishing between foam cells and dendritic cells posed as a great challenge.

By exploring the top 15 significantly expressed genes in $CD11c^{high}$ and $CD11c^{low}$ ROIs, I failed to detect markers that were uniquely associated with foam cells or a macrophage phenotype and instead, observed significant expression of genes such as CD72 and ADA2 that overlap with both macrophages and dendritic cells (Suzuki et al., 2008, Watanabe et al., 2021). Interestingly CLEC10A expression was significantly expressed in $CD11c^{low}$ regions which is a marker specific for CD1c+ dendritic cells (Wesa and Galy, 2001) (Figure 5.8C). Further to this, pathway analysis, demonstrated

an enrichment of genes associated with IL-12 signalling in CD11c^{low} ROIs, a cytokine produced prominently by dendritic cells. This was accompanied by the up-regulation of pathways associated with amino acid metabolism and cellular responses to starvation such as autophagy all of which are characteristics that are typically defective in foam cells (Figure 5.8E) (Table 5.2) (Robichaud et al., 2022, Zaric et al., 2020). Whether the CD11c^{high} regions correspond to foam cells or dendritic cell enriched areas remains obscure due to the nature of the experimental design.

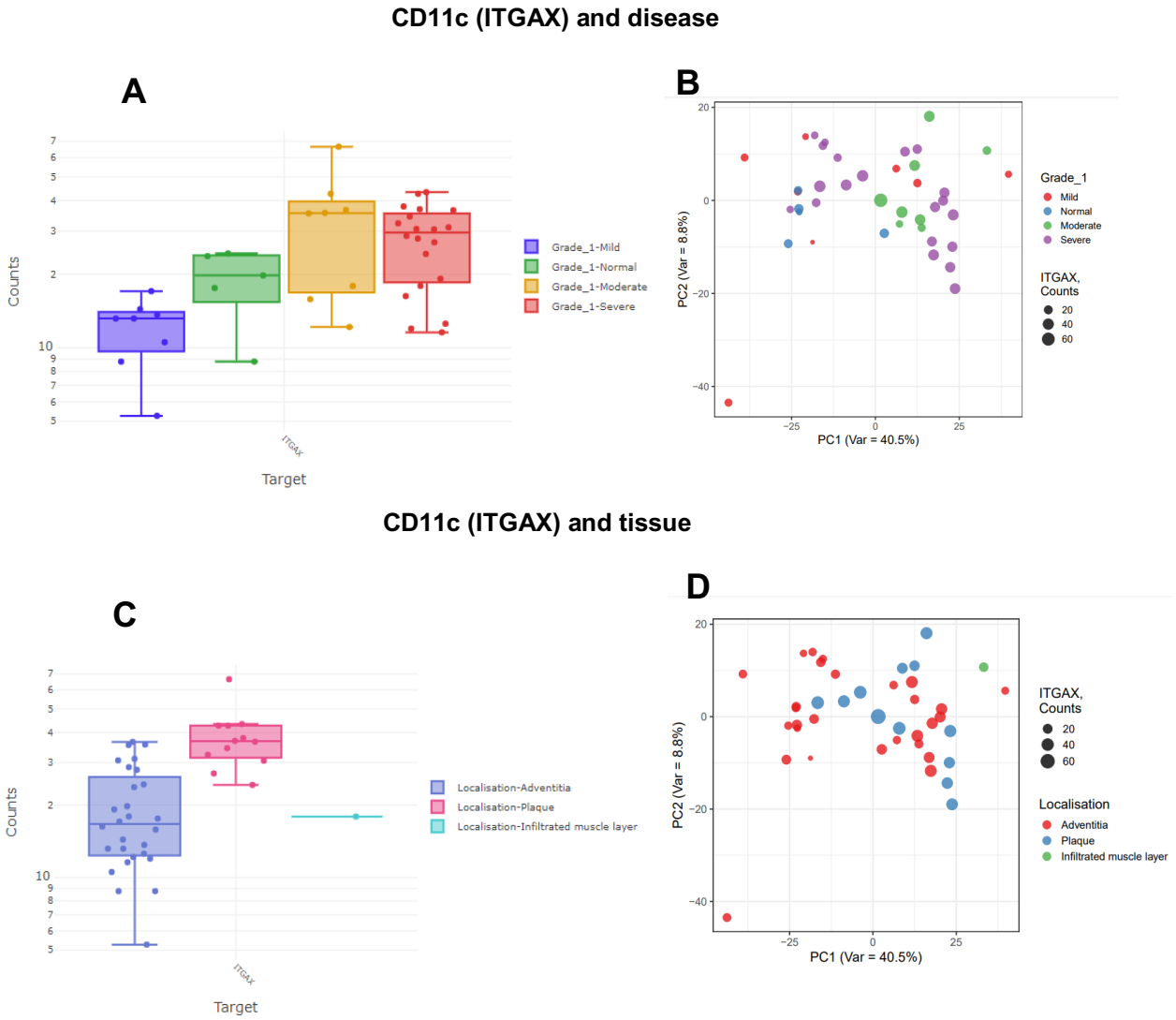


Figure 5-7: The variation in ITGAX (CD11c) gene expression in coronary artery tissue based on disease severity and tissue localisation

Human coronary artery sections of varying disease severity were analysed using the GeoMX DSP for whole transcriptome analysis (WTA). ITGAX (CD11c) gene expression was visualised as box plots and PCA plots according to **(A,B)** disease severity graded according to being mild, normal, moderate or severe and **(C, D)** tissue localisation in adventitia, plaque or infiltrated muscle layer. Gene expression counts were normalised based on quartile three (Q3) normalisation. Data plotted are ± SD.

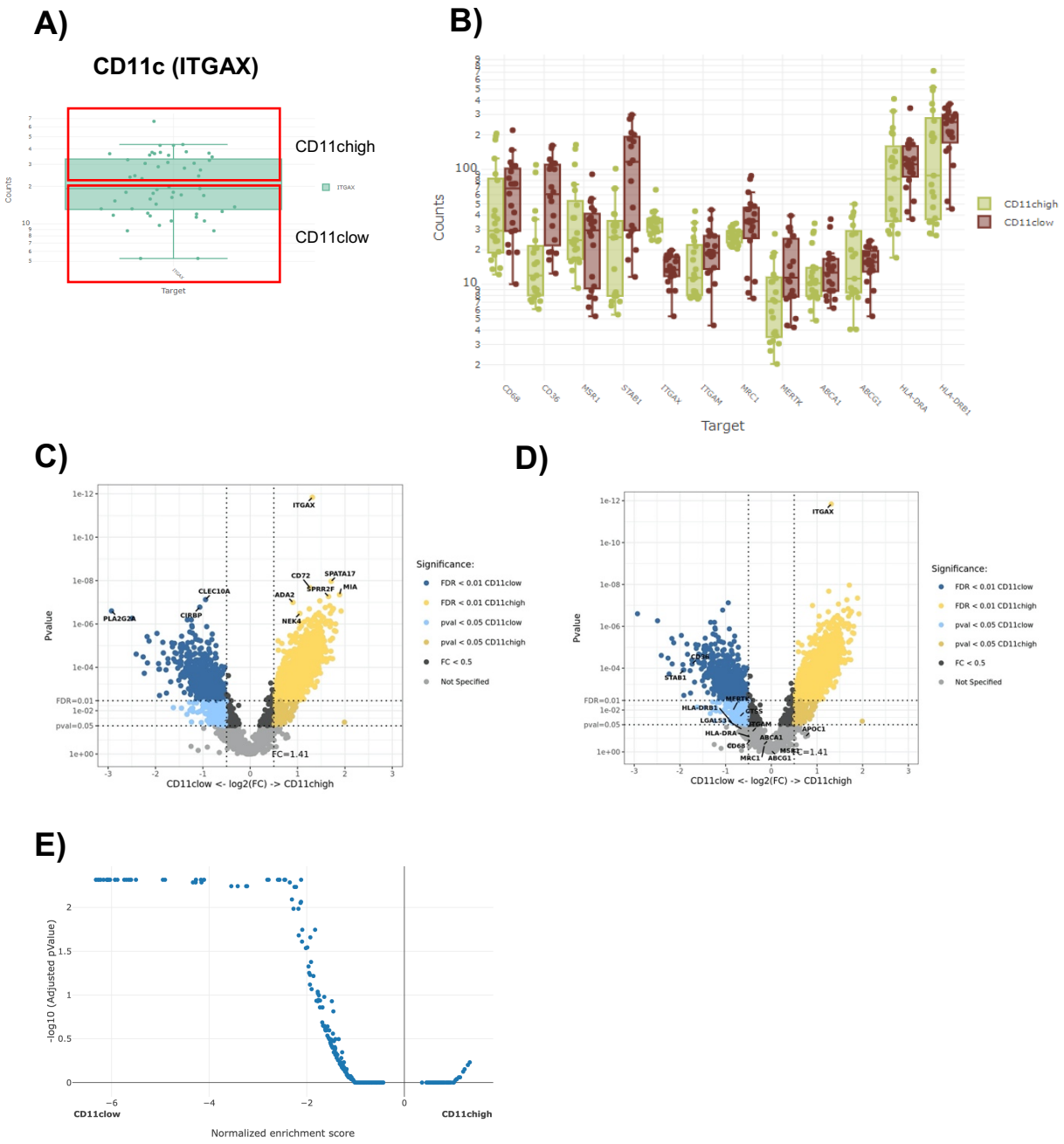


Figure 5-8: Gene expression in coronary artery tissue in CD11chigh vs CD11clow ROIs

Human coronary artery sections of varying disease severity were analysed using the GeoMX DSP for whole transcriptome analysis (WTA). **(A)** ROIs in tissue sections were labelled according to CD11chigh vs CD11clow gene expression. **(B)** Pan macrophage markers were plotted in box plots for CD11chigh (green) vs CD11clow (yellow) ROIs. Volcano plots for were plotted to identify **(C)** top 10 statistically significant up-regulated genes (labelled) with an FDR <0.01 as well as **(D)** expression of pan macrophage markers (labelled) in CD11chigh vs CD11clow ROIs. **(E)** Pathway analysis was performed to observe pathway enrichment obtained from the online Reactome database with '–log adjusted p value' on the y-axis and 'normalised enrichment score' on the x-axis. Gene expression counts were normalised based on quartile three (Q3) normalisation.

Table 5-1: Pathways that are downregulated in CD68^{high} ROIs

Symbol	Normalised enrichment score in CD68^{high}	p value	Adj p value
Plasma lipoprotein assembly, remodelling, and clearance	-2.752033016	0.00017668	0.00143627
Interleukin-4 and Interleukin-13 signalling	-2.76202145	0.00017215	0.00143627
Platelet activation, signalling and aggregation	-2.850643691	0.00016878	0.00143627
Regulation of Complement cascade	-2.865126153	0.00017768	0.00143627
Metabolism of amino acids and derivatives	-3.00040985	0.00016714	0.00143627
ECM proteoglycans	-3.014325935	0.000174	0.00143627
Binding and Uptake of Ligands by Scavenger Receptors	-3.123158023	0.00017724	0.00143627
Platelet degranulation	-3.2838964	0.00016858	0.00143627
MHC class II antigen presentation	-3.322171268	0.00017235	0.00143627

Table 5-2: Pathways that are downregulated in CD11c^{low} ROIs

Symbol	Normalised enrichment score in CD11c^{low}	p value	Adj p value
Selenoamino acid metabolism	-6.0639176	0.00027465	0.00482996
Cellular response to starvation	-5.5010353	0.00028818	0.00482996
Metabolism of amino acids and derivatives	-4.9059098	0.00030931	0.00482996
Platelet degranulation	-2.5914763	0.00025927	0.00482996
Interleukin-12 signaling	-2.3044627	0.00068228	0.00810386
Platelet activation, signaling and aggregation	-2.116453	0.00030516	0.00482996
Innate Immune System	-2.2211457	0.00047438	0.00583494
Regulation of Complement cascade	-2.8079607	0.00022242	0.00482996

5.6. Spatial gene expression analysis specifically in plaque ROIs within human coronary artery tissue

As foam cells reside specifically within the plaque, I shifted our focus specifically on plaque ROIs only, that were selectively filtered using the GeoMx DSP analysis suite software. The aim was to identify plaque-specific changes in gene expression in macrophages or foam cells based on CD68 and CD11c (ITGAX) expression. Regions of moderate and severe plaque demonstrated very similar transcriptomic profiles with no significant differences in gene expression (FDR > 0.01) (Figure 5.9A-B). The top 30 negatively enriched pathways of moderate and severe plaques were listed on Table 5.3 showing reduced amino acid metabolism and response to cellular starvation mechanisms in moderate plaque ROIs – features that are typically expected in advanced atherosclerotic disease (Figure 5.9C) (Zaric et al., 2020).

Preliminary data in our lab has suggested CD68 expression is diminished on macrophages with oxLDL uptake. Whether foam cells are characterised as the $CD68^{low}$ regions was investigated. By dissecting plaque ROIs according to $CD68^{high}$ and $CD68^{low}$ expression, I observed an enrichment of macrophage-associated genes in $CD68^{high}$ plaque regions although these differences did not reach statistical difference (FDR < 0.01) (Figure 5.10A-B). Both LGALS3, a pro-inflammatory galectin and APOC1, an apolipoprotein that contributes to increased plasma triglyceride levels were significantly elevated in $CD68^{high}$ plaque ROI (Pillois et al., 2012, Lu et al., 2020). Similarly, pathway analysis was performed and of these pathways, $CD68^{high}$ plaque ROIs were positively enriched for genes involved in cellular responses to starvation and metabolism of amino acids. Interestingly I also observed an enrichment of genes associated with GTP hydrolysis in $CD68^{high}$ regions compared to $CD68^{low}$ regions – a

pathway typically required for efficient macrophage phagocytosis, proliferation and survival (Figure 5.10C) (Table 5.4) (Tzircotis et al., 2011). Whilst these pathways are typically defective in foam cells, whether the $CD68^{low}$ ROIs truly correspond to a foam cell phenotype is inconclusive. I was unable to compare $CD11c^{high}$ vs $CD11c^{low}$ regions within plaque as surprisingly all regions of plaque were $CD11c^{high}$.

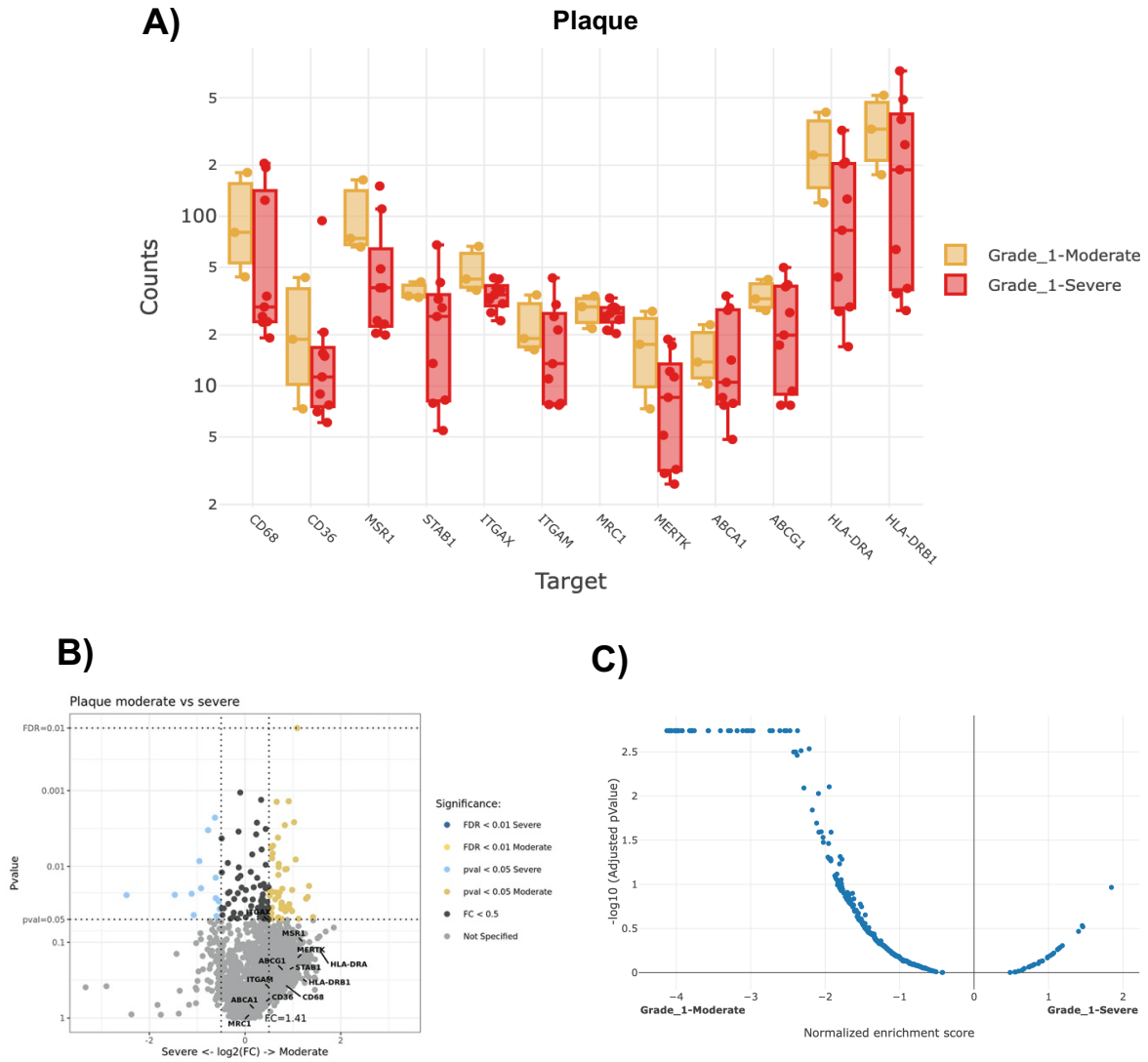


Figure 5-9: Gene expression within plaque ROIs of coronary artery tissue that are of varying disease severity

Human coronary artery sections of varying disease severity were analysed using the GeoMX DSP for whole transcriptome analysis (WTA) and ROIs in plaque regions were selected only. **(A)** Pan macrophage markers were plotted in box plots for ROIs that were segmented according to plaque that were of moderate or severe disease severity grading. **(B)** Volcano plot was plotted to identify statistically significant up-regulated genes (labelled) with an FDR <0.01 as well as expression of pan macrophage markers (labelled) in moderate vs severe diseased plaque ROIs. **(C)** Pathway analysis was performed to observe pathway enrichment obtained from the online Reactome database with '–log adjusted p value' on the y-axis and 'normalised enrichment score' on the x-axis. Gene expression counts were normalised based on quartile three (Q3) normalisation.

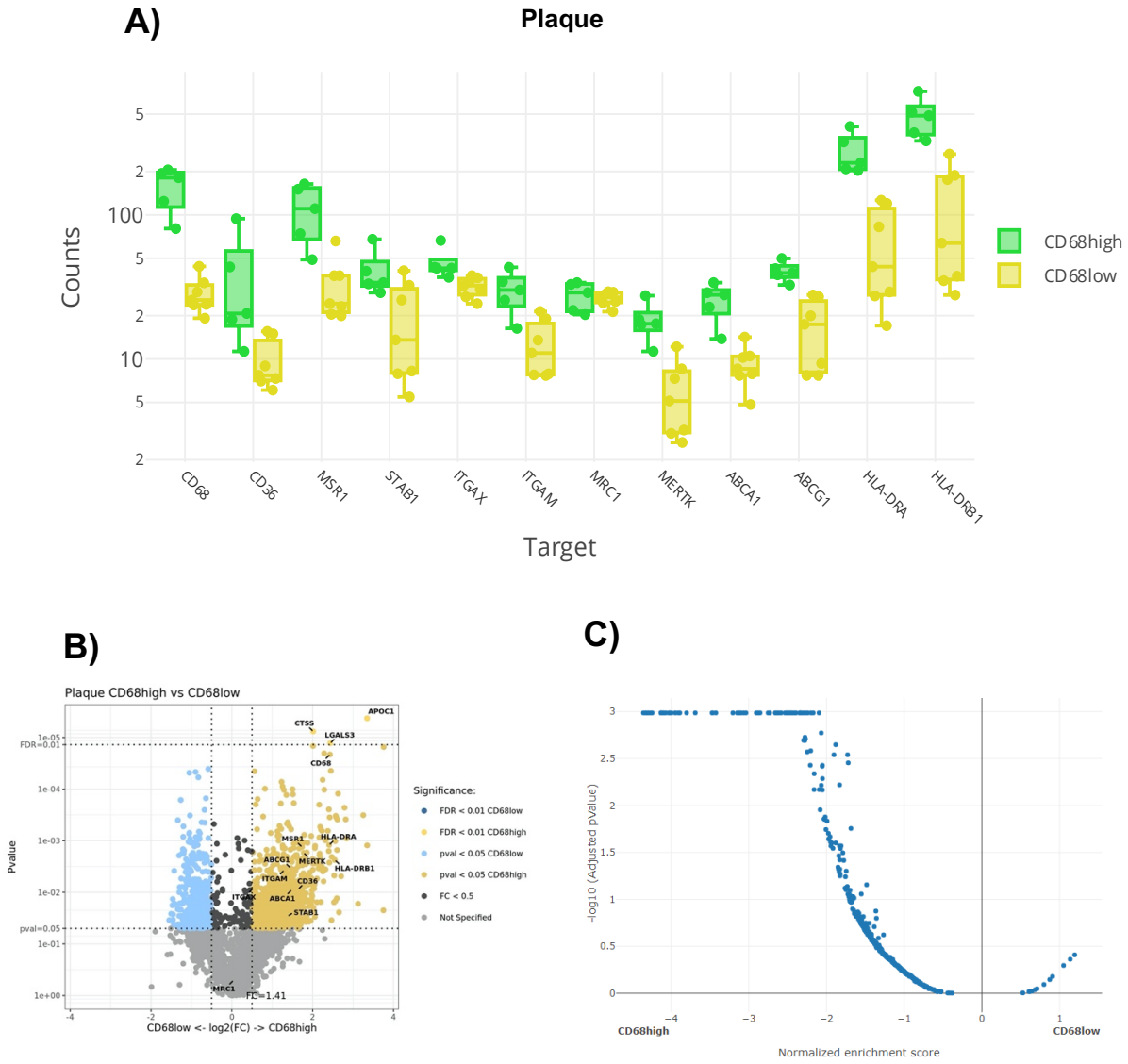


Figure 5-10: Gene expression within plaque of coronary artery tissue within ROIs that are CD68high and CD68low

Human coronary artery sections of varying disease severity were analysed using the GeoMX DSP for whole transcriptome analysis (WTA) and ROIs in plaque regions were selected only. **(A)** Pan macrophage markers were plotted in box plots for ROIs that were segmented according to plaque regions that were CD68high and CD68low **(B)** Volcano plot was plotted to identify statistically significant up-regulated genes (labelled) with an FDR <0.01 as well as expression of pan macrophage markers (labelled) in CD68high vs CD68low expression plaque ROIs. **(C)** Pathway analysis was performed to observe pathway enrichment obtained from the online Reactome database with '–log adjusted p value' on the y-axis and 'normalised enrichment score' on the x-axis. Gene expression counts were normalised based on quartile three (Q3) normalisation.

Table 5-3: Pathways that are downregulated in plaque ROIs of moderate disease severity

Symbol	Normalised enrichment score in moderate plaque	p value	Adj p vlaue
Formation of a pool of free 40S subunits	-4.127057577	0.000118441	0.001818023
L13a-mediated translational silencing of Ceruloplasmin expression	-4.097040045	0.000117661	0.001818023
Response of EIF2AK4 (GCN2) to amino acid deficiency	-4.095027172	0.000119133	0.001818023
Eukaryotic Translation Elongation	-4.083094239	0.000119789	0.001818023
Peptide chain elongation	-4.06279141	0.000120019	0.001818023
Selenocysteine synthesis	-4.06279141	0.000120019	0.001818023
Nonsense Mediated Decay (NMD) independent of the Exon Junction Complex (EJC)	-4.019716315	0.000119789	0.001818023
GTP hydrolysis and joining of the 60S ribosomal subunit	-4.018450084	0.000117661	0.001818023
Viral mRNA Translation	-4.006194076	0.000120048	0.001818023
Eukaryotic Translation Initiation	-3.99209779	0.000116918	0.001818023
Cap-dependent Translation Initiation	-3.99209779	0.000116918	0.001818023
Selenoamino acid metabolism	-3.973595922	0.000118793	0.001818023
Eukaryotic Translation Termination	-3.966629501	0.000120163	0.001818023
SRP-dependent cotranslational protein targeting to membrane	-3.927870613	0.000117398	0.001818023
Influenza Infection	-3.91803568	0.000116117	0.001818023
Major pathway of rRNA processing in the nucleolus and cytosol	-3.821198308	0.000117661	0.001818023
Cellular response to starvation	-3.809124472	0.000115861	0.001818023
Influenza Viral RNA Transcription and Replication	-3.790669546	0.00011805	0.001818023
rRNA processing in the nucleus and cytosol	-3.788505076	0.000116918	0.001818023
Nonsense-Mediated Decay (NMD)	-3.787674748	0.000118203	0.001818023
Nonsense Mediated Decay (NMD) enhanced by the Exon Junction Complex (EJC)	-3.787674748	0.000118203	0.001818023
rRNA processing	-3.757324993	0.000116822	0.001818023
Translation	-3.572025561	0.000111111	0.001818023
Regulation of expression of SLITs and ROBOs	-3.565826075	0.000115075	0.001818023
Metabolism of amino acids and derivatives	-3.406143234	0.00011212	0.001818023
Signaling by ROBO receptors	-3.299224064	0.000113109	0.001818023
Formation of the ternary complex, and subsequently, the 43S complex	-3.270692369	0.000128074	0.001818023
Translation initiation complex formation	-3.18283726	0.000126871	0.001818023
Activation of the mRNA upon binding of the cap-binding complex and eIFs, and subsequent binding to 43S	-3.18283726	0.000126871	0.001818023
Neutrophil degranulation	-3.10683706	0.00010618	0.001818023

5.7. Discussion

Given that the experimental design was not specifically tailored to our research question it is difficult to draw firm conclusions from this dataset. Although here I have demonstrated the power and the potential of utilising novel spatial transcriptomic technology in identifying changes in gene expression based on the spatial profile of the cell within human coronary arterial tissue. I also had the additional advantage of looking at how these changes differ based on disease severity in humans in this study. Collectively, such technology can be utilised to identify potential biomarkers of disease during early disease onset and progression towards more advanced disease.

This study was specifically designed to focus on $CD4^+$ T cells within coronary arteries. As well as macrophages and foam cells being highly enriched in atherosclerotic plaque, interestingly, more recent studies using single cell RNA sequencing have identified T cells as the predominant leukocyte population within advanced plaque, with majority of the T cell population corresponding to the CD4 subset (Winkels and Wolf, 2021). These activated T cells appear to be specific to oxLDL which is the known stimuli for foam cell formation and subsequent inflammatory events during atherosclerosis (Hinkley et al., 2023, Stemme et al., 1995). Based on our analysis, CD68 expression (specific for macrophages), positively correlated with CD4 T cell positive ROIs, suggesting both cell types are in close vicinity enabling communication between the innate and adaptive arm of immunity during inflammation.

Due to the lack of CD68 antibody used in the initial tissue staining stage, I based CD68 expression on $CD68^{high}$ expressing ROIs, which according to gene expression and pathway analysis exhibit macrophage-like properties such as significant expression of complement factors and enrichment of MHC II antigen presentation

genes. Subsequent downstream analysis revealed a trend towards an enrichment of CD68 in mild atherosclerotic disease compared to severe disease ROIs. Whether CD68 expression changes with advanced atherosclerosis due to oxLDL uptake in macrophages is unclear as macrophages slowly adopt a foam cell phenotype with disease progression (Gui et al., 2022). Preliminary data in our lab is indicative of this showing CD68 expression to be downregulated in macrophages upon oxLDL accumulation, yet I failed to observe this on a protein level in vitro via flow cytometry in chapter 4. Perhaps, more extended culture times for foam cell formation is required for in vitro to observe true changes in protein and gene expression since foam cells and macrophage typically exist in plaque for an extended length of time typically lasting months (Nogieć et al., 2020).

Based on tissue localisation, I observed a great deal of variation for CD68 expression with a trend towards greater enrichment in regions of plaque compared to adventitia as expected, since macrophages are amongst the most predominant immune cells in plaque (Hou et al., 2023, Lin et al., 2021, Cochain et al., 2018). The adventitia is a dynamic environment which plays a key role in development of the neointima in the early stages of atherosclerosis (Milutinovic et al., 2020, Maiellaro and Taylor, 2007). However, the distribution of ROIs was not equal across the different areas of tissue and would be ideal to improve the study design if repeated.

In attempt to compare CD68+ macrophage expression to foam cells, I utilised CD11c as a potential foam cell marker based on previous transcriptomic data analysis (Kim et al., 2018). As I have highlighted in the previous chapter, there is a pronounced difficulty in identifying foam cell specific markers due to the highly similar expression profiles between macrophages and foam cells. Thus, our analysis is only based on the

assumption that CD11c is expressed more highly on foam cells relative to macrophages, although the inherent overlap with dendritic cells posed a challenge. CD11c was clearly enriched in severe disease and specifically within plaque ROIs, which is a trend typically expected of foam cells as they are the major driver of atherosclerosis disease progression (Javadifar et al., 2021, Yu et al., 2013). Yet one must be aware that dendritic cells are also present in plaque and are potent activators of adaptive immunity (Alberts-Grill et al., 2013, Yilmaz et al., 2004, Zernecke, 2015). Evidence has shown that they too can also engulf modified LDL, adopting a foam cell like appearance (Nickel et al., 2009). Whether the CD11chigh ROIs correspond to macrophage derived foam cells cannot be certain based on the study design. Although when comparing both CD11cl^{low} and CD11c^{high} ROIs, I observed an enrichment in several pathways corresponding to a dendritic cell-like phenotype in CD11c^{low} ROIs including enrichment of Il-12 signalling and CLEC10A expression – a marker for a specific subset of CD1c+ dendritic cells that are predominantly involved in CD4+ T cell priming (Heger et al., 2018, Wesa and Galy, 2001).

Foam cells are associated with defects in the autophagy pathway resulting in poor lipid droplet metabolism (Ouimet et al., 2011). They also linked with aberrant amino acid metabolism leading to pro-atherogenic amino acids being released that can alter accumulation of cholesterol and triglyceride levels in macrophages (Zaric et al., 2020). Both pathways were less enriched in the CD11c^{high} segments, compared to the CD11c^{low}, that resembles features of a foam cell phenotype. This may be indicative that CD11c^{low} ROIs are more enriched in dendritic cells and that foamy macrophages correspond to the CD11c^{high} population. Again, without initial CD11c antibody staining,

one cannot make any definite conclusions, but simply make educated speculations based on the analysis.

Similarly, when I performed downstream analysis within plaque regions specifically, I observed no significant changes in gene expression in moderate to severe tissue. Hence, identifying a biomarker for disease severity was not feasible in this case. This may be due to the low number of ROIs selected for plaque in the study design and additional regions would ideally need to be selected for our study to identify variation across the entire region of plaque.

Further analysis looking at $CD68^{high}$ and $CD68^{low}$ expression within plaque revealed significantly higher expression of genes such as LGALS3, APOC1 and CTSS in $CD68^{high}$ regions, all of which are pro-atherogenic genes. LGALS3 is known for its contribution to exacerbating inflammation in several malignant diseases and overexpression has been reported in the aorta of human atherosclerotic regions and hypercholesterolemic mice (Varasteh et al., 2021, Papaspyridonos et al., 2008). It is also typically associated as a marker of activated macrophages suggestive of $CD68^{high}$ macrophages attaining a pro-inflammatory phenotype within plaque (Lu et al., 2020). APOC1 being the smallest of the apolipoprotein family, regulates triglyceride metabolism, and increased expression has been associated with high plasma triglyceride levels and accelerated development of atherosclerosis in individuals with chronic inflammation (Pillois et al., 2012, Westerterp et al., 2007). Finally, CTSS (cathepsin S) expression has been strongly linked with atherosclerosis with evidence showing co-localisation specifically with pro-inflammatory macrophages (Luo et al., 2018, Hughes et al., 2016). Whilst the specific mechanism of CTSS in atherosclerosis is unknown, studies have indicated this is possibly through its ability to increase antigen

presentation (Borghese and Clanchy, 2011). Thus, from these observations I can postulate that CD68^{high} macrophages within plaque appear to take on an activated pro-inflammatory phenotype and contribute to irregular lipid metabolism that may ultimately contribute to advanced plaque formation. Dissecting this further and looking at changes in the expression of these genes with severity of disease would be of further interest.

As mentioned, there were significant limitations to this study as it was not designed for our specific research interest. In future, to tailor this study for our research would invoke initially staining tissue for CD68, CD11c and perhaps Trem2 antibodies to distinguish between macrophages and foam cells within plaque tissue. Further downstream analysis could then be more precisely filtered by selecting truly positive CD68 cells and potentially foam cells to investigate changes in gene expression based on localisation as well I disease severity.

5.7.1. Summary of results

- Spatial transcriptomics of human coronary arterial tissue at mild, moderate and severe disease states was performed where we identified CD68 and CD11c enriched ROIs for macrophage and foam cells expression
- CD68 expression was used a macrophage marker which was found to be most enriched in regions of plaque tissue where they appear to exhibit a grater pro-inflammatory gene profile
- CD11c was used as a foam cell marker where it was also found to be enriched in plaque ROIs, most specifically in the severe disease state

Chapter 6. INVESTIGATING THE INFLAMMATORY PHENOTYPE OF FOAM CELLS IN VITRO

6.1. Introduction

In the previous chapters, the focus was primarily on the characterisation of foam cells based on protein and gene expression, demonstrating that foam cells display an anti-inflammatory lipid metabolising gene profile. However, our lab has generated preliminary data showing that functionally, oxLDL derived foam cells display a pro-inflammatory phenotype by promoting activation of the endothelium resulting in secondary leukocyte capture. As the gatekeepers to tissue, during inflammation activation of the endothelium serves as one of the initial stimuli for the development of atherosclerotic disease, allowing for the penetration of oxLDL and transmigration of leukocytes into the intimal layer of the artery, which facilitates downstream foam cell formation (Cahill and Redmond, 2016, Botts et al., 2021). Thus, the interaction between foam cells and endothelium signifies a critical juncture in the progression of the disease (Westhorpe et al., 2012). In this chapter I investigate the pro-inflammatory functional phenotype of foam cells in vitro both when in monoculture and in co-culture with vascular endothelium and explore possible mechanisms of action that drive this phenotype through cytokine and lipidomic analysis.

Whilst statins are typically used as gold standard lipid lowering treatment for atherosclerosis, not all patients respond to statin treatment and it is often administered as a therapeutic drug whereas looking at prophylactic means of preventing atherosclerosis is the key to limit disease manifestation and resulting acute coronary events (Tian et al., 2012, Aprotosoaie et al., 2022). Given the increasing connection between omega-3 polyunsaturated fatty acids (n-3 PUFAs) and their cardioprotective and anti-inflammatory properties, I investigated the role of eicosapentaenoic acid (EPA), a potent n-3 PUFA in modulating oxLDL uptake and foam cell-mediated inflammation through its derivation of anti-inflammatory eicosanoids and specialised pro-resolving mediators (SPMs) – both of which are lipid mediators of inflammation (Yagi et al., 2017, James et al., 2000, Mason et al., 2020).

6.2. Foam cells activate endothelium minimally in monoculture

Given that foam cells are associated with inflammatory disease progression, I looked to investigated whether factors secreted by foam cells generated in monoculture were able to activate endothelium to a greater extent than factors released from macrophages that ultimately lead to greater leukocyte recruitment (Javadifar et al., 2021, Gui et al., 2022). Foam cells were generated from $CD14^{+}CD16^{-}$ (classical monocytes) monocytes treated with oxLDL as this subset of monocytes are more susceptible to foam cell formation as demonstrated earlier in chapter 4. Supernatants from cultured foam cells and macrophages were used to treat HDBEC for 4 hours followed by the addition primary isolated neutrophils to observe their ability to adhere to and transmigrate through stimulated endothelium, captured in a static transmigration assay. Activation of endothelium is typically signified by the upregulation of adhesion molecules and selectins, hence I also measured expression of ICAM-1, VCAM-1 and E-selectin on endothelium via flow cytometry analysis (Iiyama et al., 1999, Wragg et al., 2014).

Following 4 hours of endothelial treatment and 7 mins of neutrophil transmigration, cells were fixed and imaged to capture total neutrophil adhesion and transmigration. TNFα, a potent pro-inflammatory stimulus, was used as a positive control which demonstrated significant levels of neutrophil adhesion and transmigration (>35%). However, both macrophage and foam cell supernatants showed little to no adhesion and transmigration of neutrophils (Figure 6.1). Flow cytometry analysis of adhesion molecules revealed increased susceptibility of antigen cleavage with enzymatic detachment. Thus, comparing the staining profiles both post- and pre-detachment with accutase demonstrated strikingly dissimilar profiles whereby

fluorescence signals were significantly diminished for ICAM-1, VCAM-1 and E-selectin with staining post detachment (Figure 6.2). Therefore, staining was performed directly in culture plates before harvesting with accutase to preserve surface antigen expression.

Percentage positive cells and median fluorescence intensity (MFI) expression levels for all three markers (ICAM-1, VCAM-1 and E-selectin) showed no differences between macrophages and with oxLDL treatment (foam cells), highlighting that supernatants from foam cells in mono-culture were insufficient in activating endothelium for neutrophil adhesion and transmigration in the inflammatory context (Figure 6.3).

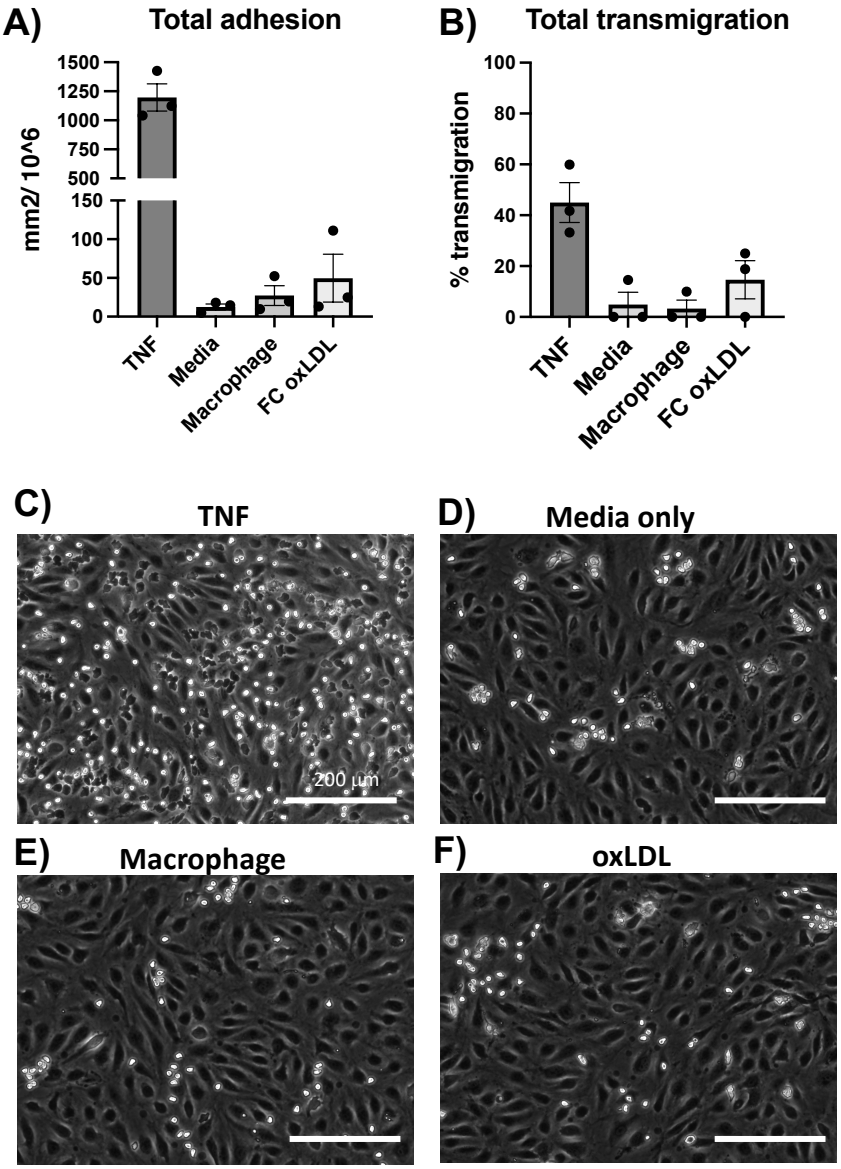


Figure 6-1: Endothelial activation using macrophages and foam cell mono-culture supernatants

$CD14^{+}CD16^{-}$ monocytes were isolated via magnetic bead isolation and differentiated into macrophages or foam cells with oxLDL (25ug/ml) for 6 days. Day 6 culture supernatants from macrophage and foam cell mono-cultures were used to treat HDBEC for 4 hours. TNF-a (100U/ml) and media only controls were also used to stimulate HDBEC for 4 hours. Static transmigration assay was then performed using primary human isolated neutrophils ($1x10^{6}$ /ml) which were added to the stimulated HDBEC for 7 mins at 37°. Cells were fixed and imaged for 5 random fields of interest to assess **(A)** neutrophil adherence and **(B)** transmigration. **(C-F)** Representative images of endothelium with adhered neutrophils were taken. Data are mean ± SEM (n=3, biological replicate). Statistical analysis performed using unpaired t-test comparing macrophage and foam cell oxLDL treatment to media only control. Scale bars = 200µm.

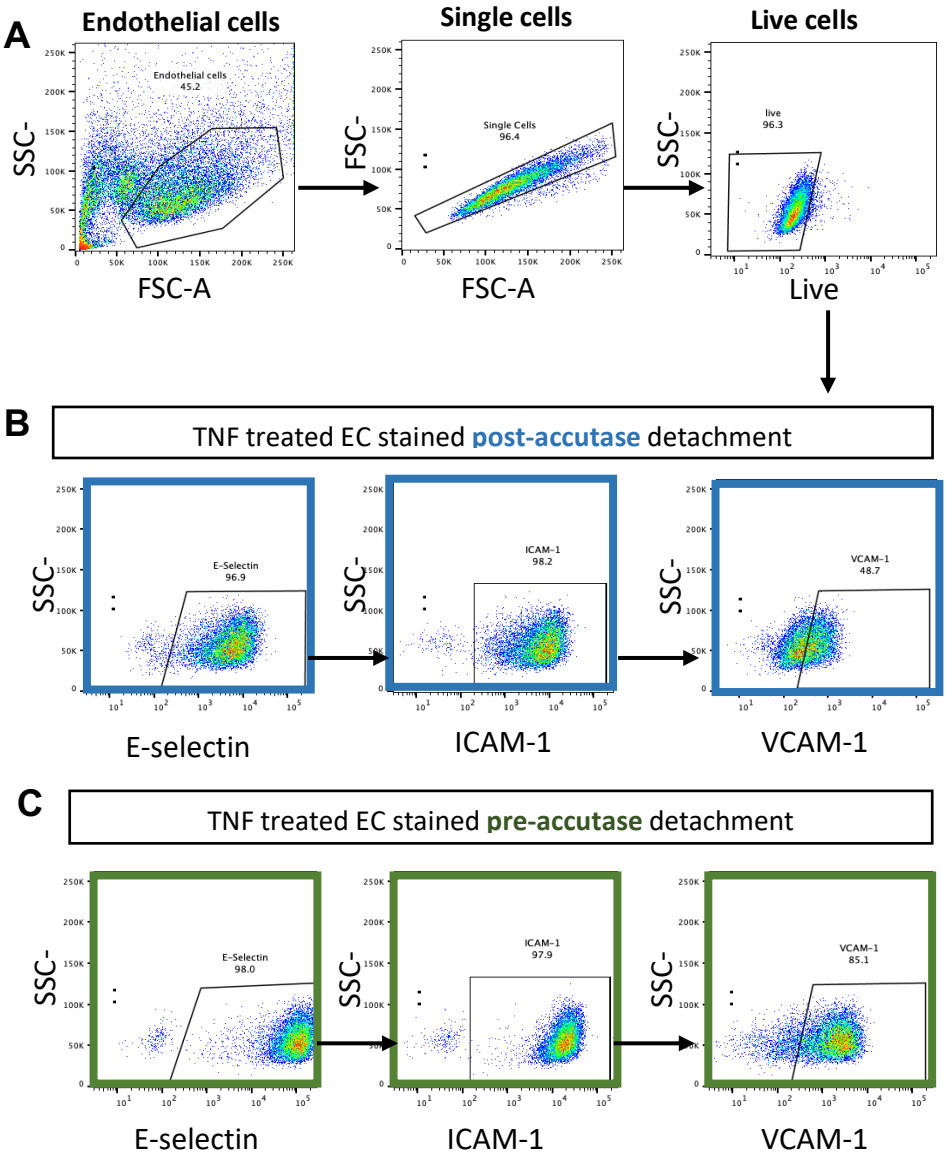


Figure 6-2: Flow cytometry staining and analysis of endothelium pre- and post-enzymatic detachment

Static transmigration assay was performed using primary human isolated neutrophils ($1x10^6$ /ml) which were added to the stimulated HDBEC for 7 mins at 37°. Cells were either stained for flow cytometry analysis after accutase detachment or stained directly in cultured wells before accutase detachment to minimise antigen cleavage. Cells were stained for E-selectin, ICAM-1 and VCAM-1 and analysed via flow cytometry. Endothelial cells were gated according to **(A)** FSC/SSC profiles (forward scatter/side scatter) followed by doublets and dead cell exclusion using a viability dye (zombie aqua). Endothelial cells were then gated for positive expression of individual markers **(B)** post-accutase and **(C)** pre-accutase detachment. Data are mean ± SEM (n=3, biological replicate).

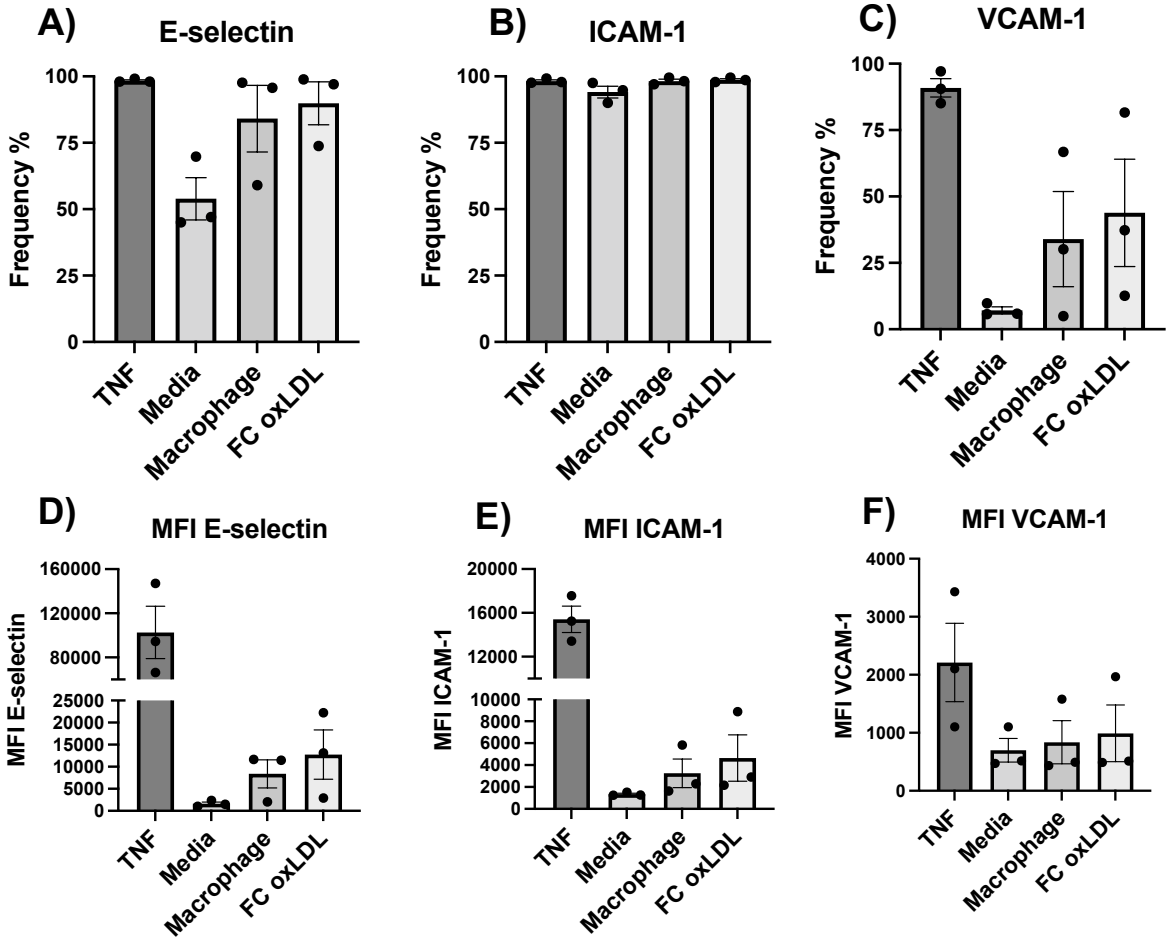


Figure 6-3 Expression of endothelial activation markers following treatment with macrophage and foam cell mono-culture supernatants

$CD14^{+}CD16^{-}$ monocytes were isolated via magnetic bead isolation and differentiated into macrophages or foam cells with oxLDL (25ug/ml) for 6 days. Day 6 culture supernatants from macrophage and foam cell mono-cultures were used to treat HDBEC for 4 hours. TNF-a (100U/ml) and media only controls were also used to stimulate HDBEC for 4 hours. Static transmigration assay was then performed using primary human isolated neutrophils ($1x10^{6}$ /ml) which were added to the stimulated HDBEC for 7 mins at 37° after which HDBEC were stained for E-selectin, ICAM-1 and VCAM-1. Cells were stained directly in wells followed by accutase detachment and analysed via flow cytometry analysis for **(A-C)** MFI and **(D-F)** frequency for target antibodies. Data are mean ± SEM (n=3, biological replicate). Statistical analysis performed using unpaired t-test comparing macrophage and foam cell oxLDL treatment to media only control.

6.3. Rationale for investigating the secretory profile of foam cell and endothelial (EC) co-cultures

I have shown that foam cells cultured alone do not exhibit a pro-inflammatory secretory profile based on its ability to activate endothelium. Yet, preliminary data in our lab has shown that foam cells co-cultured with endothelium are able to promote secondary leukocyte capture to a greater extent to macrophages alone, demonstrating an increased pro-inflammatory functional phenotype. Here, I investigated the functional mechanism of action of this phenotype by investigating the secretory profile of supernatants from foam cell and EC co-cultures via both ELISA and lipidomics analysis.

6.3.1. Experimental design for co-culture assays

The experimental set up for our co-culture assays involved initially culturing $CD14^{+}CD16^{-}$ monocytes within transwell inserts and allowing them to differentiate for 6 days with the addition of oxLDL for foam cell formation. On day 6, culture inserts were inverted and ECs were cultured on the alternate side of the transwells for 24 hours to enable monolayer formation (Figure 5.4A). Confirmation of macrophage and foam cell adherence to transwell filters was determined using DAPI staining and endothelial monolayer formation visualised using CD31 staining (Figure 6.4C-E).

Following 24 hour co-culture, culture supernatants were collected and either snap frozen for lipidomics analysis or analysed for TNFα levels via ELISA. Levels of TNFα level appeared to be very low, with levels mostly lying below the lower ELISA standard (15.6 pg/ml) for all treatment conditions including foam cell and EC co-cultures (Figure 6.4B). This suggests that the functional inflammatory phenotype

observed with foam cells is most likely not cytokine driven and may be driven by alternative inflammatory mediators.

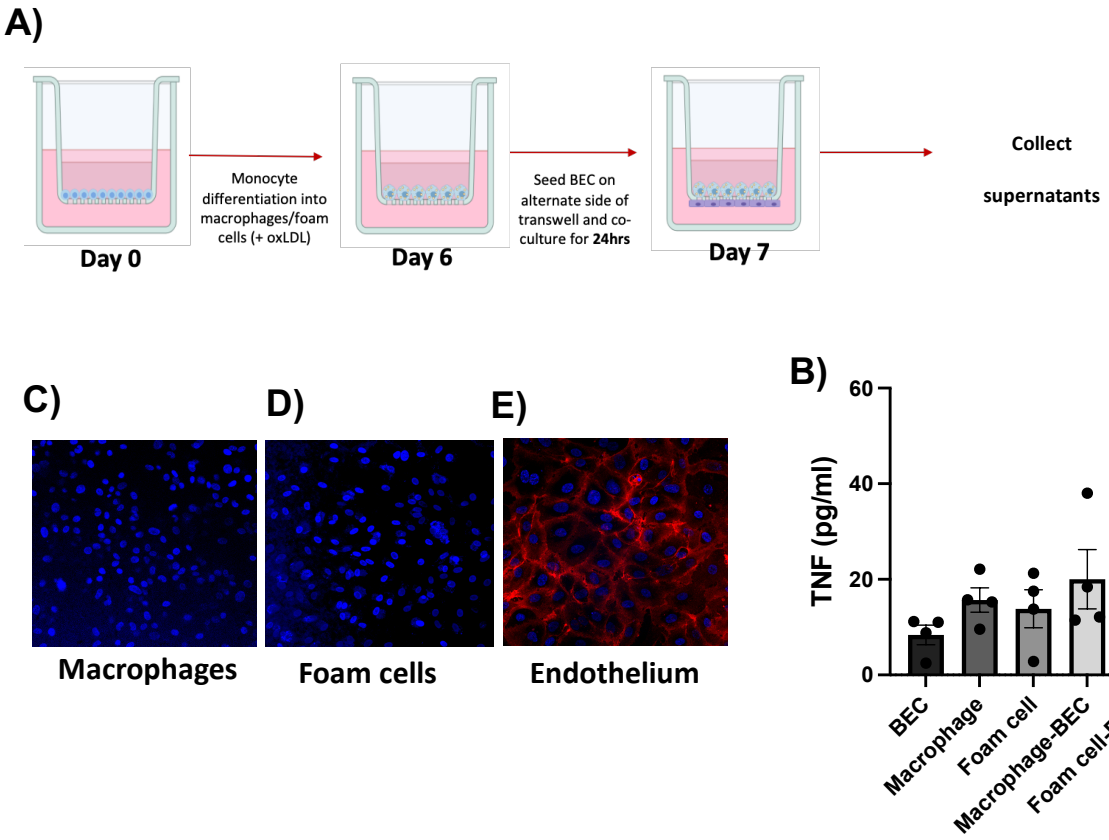


Figure 6-4 Co-culture of endothelium with macrophages and foam cells

(A) $CD14^{+}CD16^{-}$ monocytes were isolated via magnetic bead isolation and differentiated into macrophages or foam cells with oxLDL (25ug/ml) for 6 days in 24-well transwell inserts. On day 6, HDBEC were cultured on the alternate side of the transwell for 24 hours to establish co-cultures. Supernatants were collected on day 7 and analysed for **(B)** TNF-a levels via ELISA. Transwell filters were cut out and stained for DAPI nuclear stain to confirm the presence of **(C)** macrophages and **(D)** foam cells followed by **(E)** CD31 staining to confirm HDBEC monolayer formation on the alternative side of the transwell. Data are mean ± SEM (n=4, biological replicate). Statistical analysis performed using non-parametric Friedmans test with Dunn's post-hoc test for comparisons between each condition, *=$p<0.05$.

6.3.2. Lipidomics analysis of foam cell-EC co-culture supernatants

As well as cytokines, lipid mediators including eicosanoids and SPMs are also potent regulators of inflammation and leukocyte function (Yamaguchi et al., 2022, Dennis and Norris, 2015). I carried out lipidomics analysis via LC-MS-MS on co-culture supernatants to determine levels of secreted pro-inflammatory lipid mediators and anti-inflammatory SPMs that may be altering the inflammatory phenotype of foam cells when in culture with endothelium. I compared foam cells and macrophages both in monoculture and in co-culture and the top 15 lipid mediators were plotted in a VIP plot. I observed enrichment of several resolvins in foam-cell co-culture compared to foam cells alone including RvE2, RvD2 and RvE1, whilst RvE3 appeared to be downregulated in foam cell-EC co-cultures compared to macrophage-EC co-cultures. Additionally, SPMs elevated in foam cell-EC co-cultures included maresins and lipoxins such 5S-15s-diHETE, LXB4 and MCTR1 which were more enriched compared to macrophage-EC co-cultures or foam cells alone (Figure 6.5 and 6.6).

Of particular interest in our study was the observational increase in pro-inflammatory prostaglandins in foam cell-EC co-cultures including prostaglandin E2 (PGE2), prostaglandin F2a (PGF2a) and prostaglandin D2 (PGD2). PGF2a is hormone that plays a critical role in the initiation of labour, causing contraction of the uterus lining – a process classified as a natural inflammatory response, whereas PGD2 and PGE2 are a potent inflammatory mediators associated with increased vascular permeability, leukocyte activation and migration (Xu et al., 2015, Gomez et al., 2013, Park et al., 2006, Rittchen and Heinemann, 2019). From the data PGE2 and PGD2 appears to be enriched in foam cell-EC co-cultures compared to foam cells alone suggesting the interaction between both cells is required to upregulate expression of such pro-

inflammatory lipid mediators. PGF2a was also found to be enriched on foam cells in co-culture compared to in monoculture, although these levels appear to be more enriched in macrophage-endothelial cell co-cultures (Figure 5.6C-D). Overall, the results from lipidomic analysis suggest that prostaglandins may possibly be driving the functional pro-inflammatory phenotype observed in foam cell and EC co-cultures.

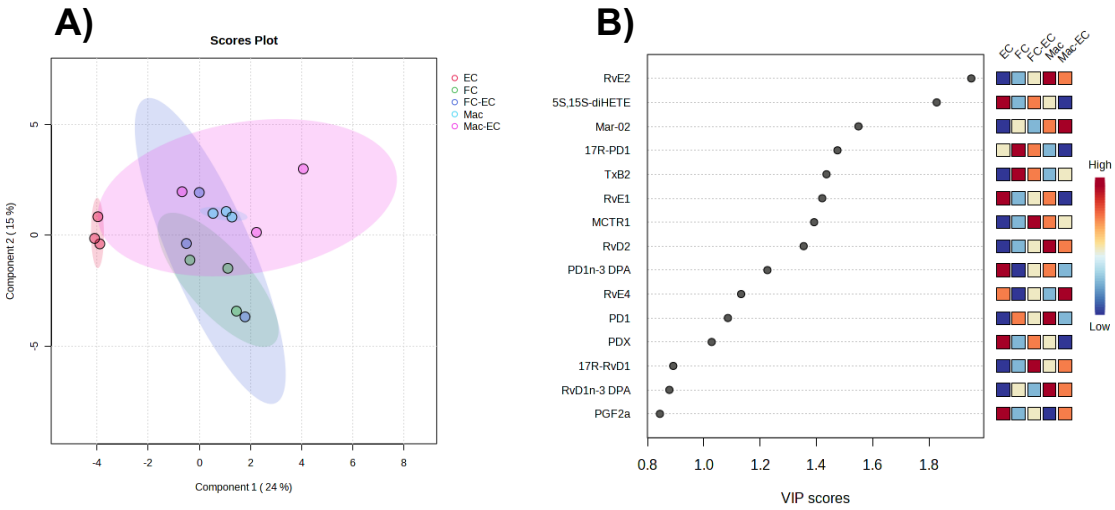


Figure 6-5: Biosynthesis of lipid mediators by macrophage and foam cells co-cultured with endothelium

$CD14^{+}CD16^{-}$ monocytes were isolated via magnetic bead isolation and differentiated into macrophages or foam cells with oxLDL (25ug/ml) for 6 days in 24-well transwell inserts. On day 6, HDBEC were cultured on the alternate side of the transwell for 24 hours to establish co-cultures. Supernatants were collected on day 7 and metabolipidomics analysis was performed using LC-MS/MS to identify and quantify pro-inflammatory lipid mediators and SPM biosynthesis. **(A)** A PCA plot was generated to visualise variation between treatment conditions as well as a **(B)** variable importance plot (VIP) plot listing top 15 variable lipid mediators. FC = foam cell, EC = endothelial cells and Mac = macrophage.

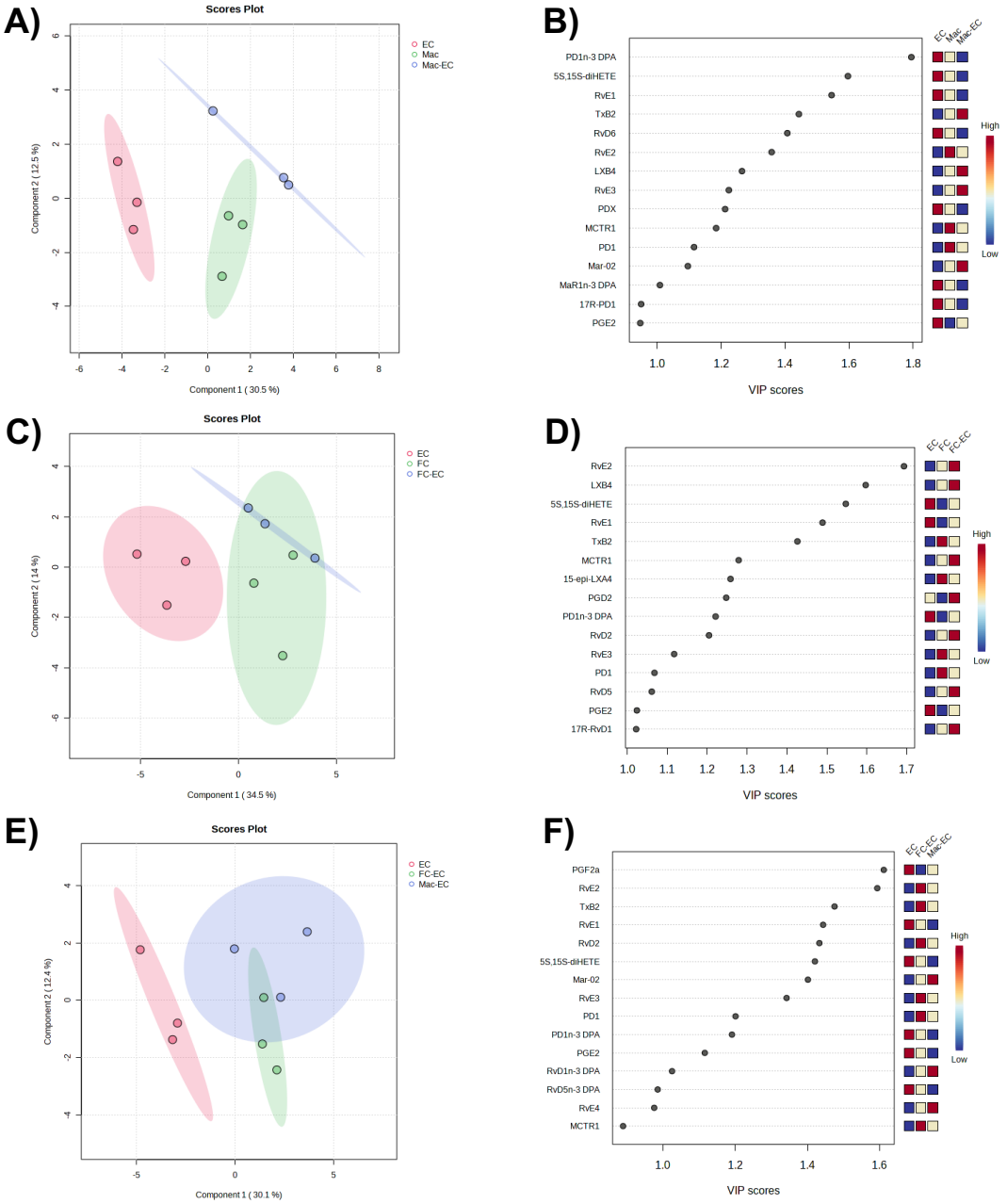


Figure 6-6: Biosynthesis of lipid mediators by macrophage and foam cells co-cultured with endothelium

$CD14^{+}CD16^{-}$ monocytes were isolated via magnetic bead isolation and differentiated into macrophages or foam cells with oxLDL (25ug/ml) for 6 days in 24-well transwell inserts. On day 6, HDBEC were cultured on the alternate side of the transwell for 24 hours to establish co-cultures. Supernatants were collected on day 7 and metabolipidomics analysis was performed using LC-MS/MS to identify and quantify pro-inflammatory lipid mediators and SPM biosynthesis. PCA plots were generated as well as a variable importance plot (VIP) plots listing top 15 variable lipid mediators between treatment conditions: **(A-B)** Mac vs Mac-EC **(C-D)** FC vs FC-EC **(E-F)** FC-EC vs Mac-EC. FC = foam cell, EC = endothelial cells and Mac = macrophage.

6.4. Effects of EPA on oxLDL uptake and foam cell formation

Several therapeutic strategies have been utilised with the aim of reversing foam cell formation, that include targeting the accumulation and metabolism of cholesterol within immune cells that invade the vascular intimal layer (Javadifar et al., 2021). Increasing interest has been focused on n-3 PUFAs (EPA and DHA) that have been linked with reduced occurrence of cardiovascular events based on respective epidemiological studies. EPA has been shown to reduce endothelial dysfunction and stabilise atherosclerotic plaque, although its mechanism of action is not yet fully understood (Sekimoto et al., 2023, Limbu et al., 2018, Thies et al., 2003). Here in our study I observed the effects of EPA on potentially reversing foam cells formation by investigating whether it can prevent oxLDL uptake in human MDMs.

For our foam cell model, I cultured $CD14^{+}CD16^{-}$ (classical monocytes) with dil-oxLDL for foam cell formation and treated them with either EPA or vehicle control (0.05% ethanol). On day 6, foam cells and macrophages were harvested and analysed via flow cytometry or confocal microscopy to detect dil-oxLDL uptake. In both cases I observed a slight reduction in oxLDL uptake based on fluorescence intensity, yet these differences were not significant (Figure 6.7). CD36 scavenger receptor expression levels were also measured via flow cytometry and qPCR analysis showing no significant differences with EPA treatment Figure 6.7B and 6.8A). Since ABC transporters have been shown to be elevated in foam cells (as demonstrated in chapter 4 via bulk RNA-seq), I looked at how EPA may modulate both ABCG1 and ABCA1 expression. Whilst ABCA1 levels remained similar across treatments, ABCG1 levels decreased with EPA treatment, although levels failed to reach statistical significance

(Figure 6.8B-C). Whether alternative concentrations of EPA may be effective have not been investigated.

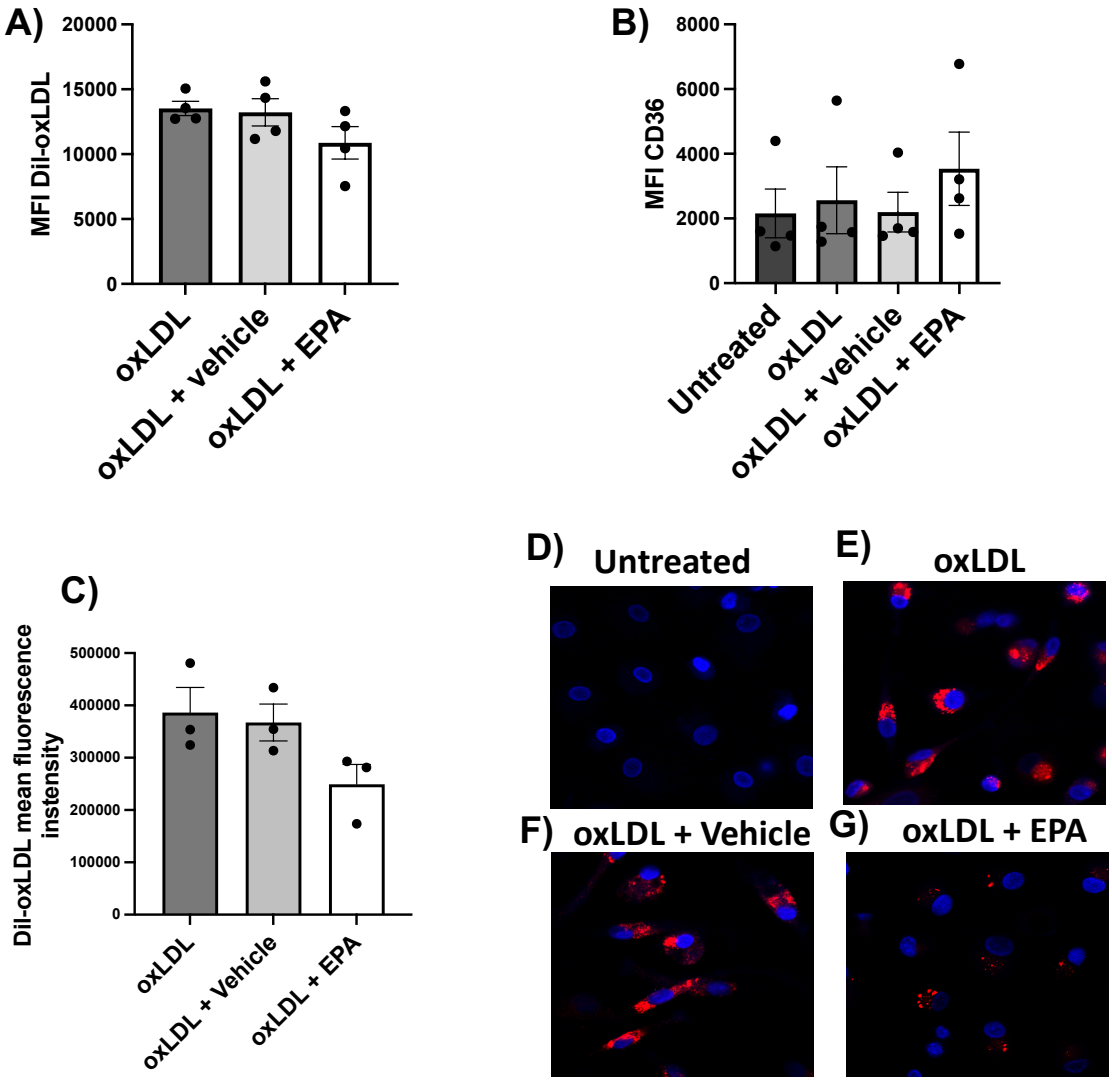


Figure 6-7: Effects of EPA on oxLDL uptake for foam cell formation

$CD14^{+}CD16^{-}$ monocytes were isolated via magnetic bead isolation and cultured with or without the addition of DiI-labelled oxLDL or vehicle control (0.5% ethanol) for foam cell formation. Flow cytometry analysis was used to detect **(A)** median fluorescence intensity (MFI) for DiI-oxLDL uptake as well as extracellular **(B)** CD36 scavenger receptor expression. **(C)** DiI-oxLDL uptake was also detected via confocal microscopy measuring mean fluorescence intensity. **(D-G)** Representative images of treatment groups were taken. Data are mean ± SEM (n=3-4, biological replicate). Statistical analysis performed using non-parametric Friedmans test with Dunn's post-hoc test for comparisons between each condition, *=$p<0.05$.

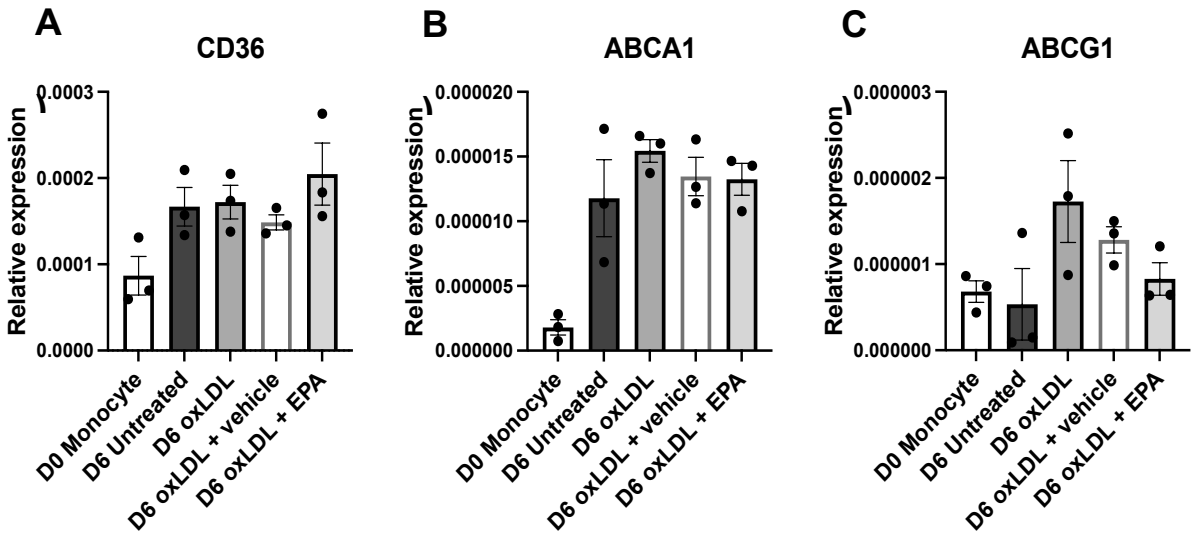


Figure 6-8: Effects of EPA on genes associated with cholesterol transport

$CD14^{+}CD16^{-}$ monocytes were isolated via magnetic bead isolation and cultured with or without the addition of oxLDL or vehicle control (0.5% ethanol) for foam cell formation for 6 days. mRNA was isolated from cultured cells on day 6 as well as on day 0 from monocytes taken from the same donor and analysed via RT-qPCR analysis to detect expression of the following genes: **(A)** CD36 **(B)** ABCA1 **(C)** ABCG1. Statistical analysis performed using non-parametric Friedmans test with Dunn's post-hoc test for comparisons relative to day 6 untreated macrophages (n=3, biological replicate).

6.5. Discussion

Foam cells play a crucial role in the development and progression of atherosclerosis and it is widely acknowledged that foam cells contribute to inflammatory events during disease manifestation (Yu et al., 2013, Javadifar et al., 2021). Yet single cell transcriptomic data and the data discussed in the previous chapter (chapter 4) conversely define foam cells to exhibit an anti-inflammatory genomic profile (Kim et al., 2018, Fernandez et al., 2019). Although functionally these foam cells appear to exhibit a pro-inflammatory phenotype when in co-culture which may not be cytokine driven but instead driven by pro-inflammatory lipid mediators such as prostaglandins as demonstrated in this chapter.

6.5.1. Foam cells in mono-culture vs co-culture

Atherosclerotic plaque are highly heterogenous structures both in composition and morphology. The complex network of cellular interactions within plaque includes inflammatory immune cells, vascular smooth muscle cells, endothelial cells as well cytokines and chemokines. Changes in their behaviour and cross talk ultimately exacerbates the pro-inflammatory microenvironment determining the fate of disease outcome (Bonacina et al., 2023, Mahdinia et al., 2023). Yet, studies looking at the role of foam cells in atherosclerosis are most usually performed in monoculture with models either utilising immortalised cell lines, BMDMs or human monocyte-derived macrophages, that often result in irregular outcomes across the difference cell types (Xu et al., 2010a, Nogiec et al., 2020, Luo et al., 2017). Such models fail to capture the cellular crosstalk and mimicry of multi-cellular interactions that impact foam cell behaviour within plaque.

Endothelial activation is a critical process for foam cell formation and as a result of aberrant lipid accumulation, foam cells in proximity can further perpetuate activation by impairing endothelial barrier function (Yang et al., 2017, Orekhov et al., 2020). Interestingly, preliminary data in our lab has shown that foam cells in co-culture with ECs can activate endothelium to a greater extent compared to macrophages and ECs in coculture by promoting secondary leukocyte capture under flow conditions, providing evidence of a pro-inflammatory functional phenotype exhibited by foam cells (Nogieć et al., 2020). In contrast, when I looked at foam cells in monoculture, their supernatants failed to activate endothelium, since little to no neutrophil adhesion and transmigration was observed in conjunction with minimal expression of adhesion receptors on the surface of endothelium following stimulation. This demonstrates that functionally, foam cells in isolation do not display pro-inflammatory characteristics which coincides with our bulk RNAseq data. In fact an inflammatory functional phenotype may only be adopted through cellular crosstalk with endothelium and additional surrounding cells within plaque. Evidence for this has been shown in in vitro studies confirming that oxLDL is able to stimulate expression of adhesion molecules on the surface of endothelium, to promote further leukocyte recruitment (Takei et al., 2001, Bonacina et al., 2023) (Jiang et al., 2022).

The precise mechanism by which foam cells drive endothelial activation and downstream inflammation is poorly understood. To investigate this, I generated foam cells in coculture with endothelium in attempt to mimic foam cell-EC crosstalk and I looked at the possible secretory factors that may be responsible for foam cell-driven inflammation. Surprisingly culture supernatants revealed little to no TNFα expression suggesting a possible alternate mediator being responsible for endothelial activation.

Whether different cytokines are involved has not been explored as part of this study. Although there is evidence that cytokines such as IL-1β are increased in response to oxLDL uptake and that this is driven by TLR signalling. Ultimately this shifts lipid-associated macrophages towards a pro-inflammatory state in atherosclerosis. Yet majority of these studies were performed in monoculture and did not observe the functional behaviour of these foam cells ex vivo. (Bekkering et al., 2014, Dib et al., 2023, Stewart et al., 2010).

Amongst the pathways that regulate macrophage and foam cell formation is the metabolism of fatty acids that serve as precursors for eicosanoids including prostaglandins and leukotrienes as well as anti-inflammatory SPMs such as resolvins and maresins – all of which are of great importance during inflammation as they alter the inflammatory state within the tissue microenvironment (Menegaut et al., 2019, Dalli and Serhan, 2012). By performing lipidomics analysis on foam cell-EC and macrophage-EC co-cultures I was able to define the lipid mediator profile released in supernatants based on cell-cell crosstalk. Surprisingly, I observed an elevation in several anti-inflammatory SPMs such as resolvins and maresins in foam cell-EC co-cultures relative to foam cells alone and macrophage-EC co-cultures. Contrary to the role of foam cells in atherosclerosis, resolvins such as RvD2 and RvE1 have been shown to reduce atherosclerosis in murine models of atherosclerosis (Bardin et al., 2022, Hasturk et al., 2015). The precise role of these resolvins in foam cell-EC cocultures is unclear would require further investigation.

Interestingly in our dataset I observed an increase particularly in the enrichment of prostaglandins in foam cell-EC cocultures. Prostaglandins are primarily associated with inflammatory sites of tissue damage and infection and key drivers of leukocyte infiltration (Yamaguchi et al., 2022, Sheppe and Edelmann, 2021). Both PGE2 and PGD2 were both elevated in foam-EC cocultures compared to foam cells alone and both are associated with inflammatory disease whereby PGE2 is a critical mediator of rheumatoid arthritis and PGD2 has been implicated in asthma and allergic inflammation (Park et al., 2006, Rittchen and Heinemann, 2019). Whether these prostaglandins are responsible for foam-cell driven pro-inflammatory responses in atherosclerotic disease is to be further explored based on this dataset. When comparing foam cell-EC and macrophage-EC cocultures, PGF2a was particularly higher in foam cell-EC cocultures. PGF2a plays a central role in the initiation and induction of labour which is considered a pro-inflammatory event due to the increase infiltration of immune cells and secretion of inflammatory cytokines (Xu et al., 2015). Elevated levels of this hormone have also been reported in murine models of atherosclerosis as well as in patients with rheumatoid and psoriatic arthritis (Yu et al., 2009, Basu et al., 2001). Collectively all three prostaglandins can be released by endothelial cells and ultimately contribute to the inflammatory state of the tissue microenvironment (Arnould et al., 2001, Perrot et al., 2020, Rittchen et al., 2020). Whether this interaction between endothelium and foam cells is responsible for driving foam cell mediated-inflammation requires further insight.

From this I can conclude that there are apparent differences in lipid mediator profiles between foam cells alone and in co-culture that may define the behavioural responses of foam cells in vivo. Yet as mentioned earlier, the plaque is a highly

heterogenous environment and it is important to take into account other immune cells that interact with macrophages and foam cells, including T cells that constitute majority of the immune cell composition in advanced plaque (Winkels and Wolf, 2021, Winkels et al., 2018). Further studies would be ideal to look at multi-cellular interactions and look at effects of prostaglandins on foam cells both in ex vivo and in vivo models.

6.5.2. The therapeutic potential of EPA in the treatment of atherosclerosis

Despite extensive research on atherosclerosis, current treatment strategies are insufficient to completely cure the disease (Libby et al., 2019, Aprotosoaie et al., 2022). N-3 PUFAs, EPA and DHA have widely been associated with increased health benefits due to their anti-inflammatory properties (Mason et al., 2020, Johansson et al., 2015, Tull et al., 2009). The outcome from several studies and randomised control trials have highlighted the link between the intake of n-3 PUFAs and the reduced risk of cardiovascular events and plaque stability, however their precise mechanism of actions remains obscure (Khan et al., 2021, Matsumoto et al., 2008, Wang et al., 2009, Kromhout et al., 2010). Both the REDUCE-IT trial and JELIS trial demonstrated a reduction in major cardiovascular events in patients treated with highly purified forms of EPA (Bhatt et al., 2020, Yokoyama et al., 2007b). Yet other studies using a combination of both EPA and DHA or DHA alone such as the ASCEND and VITAL trials have shown no cardiovascular benefits which may represent the inherent variation in the chemical and physical properties of both PUFAs (Manson et al., 2020, Khan et al., 2021).

In our in vitro experiments I focused specifically on EPA only and observed little to no changes in dil-oxLDL uptake in foam cells demonstrated both via both flow cytometry analysis and fluorescence microscopy. This suggests that EPA may not

directly inhibit foam cells formation through the inhibition oxLDL uptake but instead act by an alternative mechanism. Evidence has shown EPA to reverse foam cell formation by promoting ABCA1-mediated cholesterol efflux, with no changes to its actual gene expression with EPA treatment (Dakroub et al., 2021, Salehipour et al., 2010). Similarly, I also observed no changes in ABCA1 expression, yet I detected an apparent reduction in ABCG1 mRNA expression, reported similarly by Sarabi et al (Moradi Sarabi et al., 2014). The functional reason for this has not been reported in the literature and has not been explored further due to the time frame of this study.

Additional mechanisms by which EPA may exert its athero-protective effects include improved endothelial function (Sekimoto et al., 2023, Mason et al., 2018) and attenuated expression of adhesion receptors that reduce inflammatory immune cell transmigration (Chen et al., 2003, Tull et al., 2009). Such beneficial properties of EPA may be attributed to the local biosynthesis of anti-inflammatory eicosanoids and pro-resolving mediators that are directly derived from omega-3 PUFAs. For example, it is widely acknowledged that EPA acts as a competitive inhibitor with arachidonic acid for metabolism by COX to generate anti-inflammatory eicosanoids such as PGE3 as opposed to PGE2 derived from arachidonic acid (Siriwardhana et al., 2012, Pilkington et al., 2014). This shift in the eicosanoid profile, towards the production of less inflammatory mediators contributes to inflammatory resolving properties associated with EPA consumption. In addition, EPA also serves as precursor for the synthesis of SPMs such as EPA-derived resolvins (known as E-series resolvins). For example, RvE1 is an e-series resolvin associated with inhibition of the Nf-κb pathway in macrophages as well as reduced neutrophil infiltration (Xu et al., 2010b, Flesher et al., 2014, Li et al., 2020a). Thus, investigating the role of EPA in foam cell-EC co-culture

models would be of interest to investigate as an expansion of our current study. Since the pro-resolving effects of omega-3 PUFAs are regulated at multiple levels, direct treatment with anti-inflammatory lipid mediators rather than the parent omega-3 PUFA may be more potent in regulating inflammatory responses and may explain why anti-inflammatory effects of EPA are not always consistently observed across human studies (Spite et al., 2014). It is also of importance to note, that successful outcomes from reported clinical trials utilised highly purified forms of n-3 PUFAs (Bhatt et al., 2020, Yokoyama et al., 2007b). Due to inherent instability of EPA, it is highly prone to oxidation and degradation with exposure to temperature changes and light that may be affected during transportation and storage. Thus, purity levels of commercial EPA used in our study were inconsistent and can in fact produce adverse harmful effects in its oxidised form (Albert et al., 2013, Hsu and Yin, 2016).

Collectively, in this chapter I demonstrated the importance of studying cells utilising multi-cellular models in order to capture cell-cell interactions that cannot be recapitulated using cells in monoculture. By investigating the role of foam cells and endothelial cells together I were able to identify differences in the lipidomic profile both in co-culture and monoculture that may contribute to the pro-inflammatory functional phenotype of foam cells. Whilst the data presented here is very preliminary, it provides a foundation for further study into potential lipid mediators secreted as a result of foam cell-EC interactions that are responsible for driving pro-inflammatory events during atherosclerosis.

6.5.3. Summary of results

- The secretory profile of foam cells in monoculture do not display pro-inflammatory characteristics which is in line with their transcriptomic signature,

although when co-cultured with endothelium their display a pro-inflammatory secretory profile

- Foam cells co-cultured with ECs display a greater pro-inflammatory profile compared to macrophages and EC co-cultures based on their lipidomic profile where foam cell-EC cultures secreted greater levels of pro-inflammatory prostaglandins compared to macrophage-EC cultures
- EPA demonstrated minimal effect of oxLDL uptake in foam cells generated *in vitro*

Chapter 7. CONCLUDING REMARKS

In this study I explored the phenotypic and functional characteristics of foam cells by utilising multiple different avenues. Given the significant overlap of foam cell and macrophage signatures both at protein and gene level, distinguishing between both cell types in attempt to identify markers unique to foam cells proved to be a challenge. Collectively from this dataset I can conclude that increased surface levels of CD36 and CD11c expression can potentially be used as markers to distinguish between macrophages and foam cells, although this does not yet solve the issue of being able isolate pure foam cell populations from tissue digests.

The majority of our findings from our RNA-seq results coincided with that in the existing literature showing that foam cells exhibited an increased lipid metabolism and anti-inflammatory genomic profile and that these characteristics were similar regardless of foam cell originating from non-classical or classical monocytes in vitro (Kim et al., 2018, Cochain et al., 2018, Dib et al., 2023, Winkels et al., 2018). Whether this is also the case in vivo is unclear, since the constant evolution of the tissue microenvironment during disease progression and regression largely determines cellular behaviours in plaque (Mahdinia et al., 2023). In particular, TREM2 gene expression in lipid-associated macrophages was shown consistently across existing transcriptomics studies and detected similarly in our foam cell dataset suggesting a critical role of TREM2 expression in foam cell formation (Kim et al., 2018, Cochain et al., 2018, Dib et al., 2023, Patterson et al., 2023).

For the first time in this study, I demonstrate that functionally foam cells exhibit pro-inflammatory functional properties which contradict their anti-inflammatory genomic profile. Their pro-inflammatory behaviour appears to be largely dependent on their cellular crosstalk with vascular endothelial cells which appears not to be cytokine driven by initiated by lipid mediators, predominantly being prostaglandins. This highlights the fact studying cells in isolation often fails to capture the complex interactions between multiple cell types that can dictate cell function, differentiation status and response to stimuli. Lipid mediators play a crucial role during inflammation as they can dictate leukocyte behaviour and the inflammatory status within tissue (Yamaguchi et al., 2022). Thus, an expansion of this study would involve exploring further the role of lipid mediators on the pro-inflammatory functional behaviour of foam cells and perhaps whether SPMs can resolve this inflammatory phenotype in vitro.

By increasing our understanding of foam cell phenotype and behaviours, novel therapeutic targets can be developed to specifically target lipid-associated macrophages in plaque with the aim of reversing the foam cell phenotype or limit their progression and reduce the risk of cardiovascular disease.

References

Abbas, A., Aukrust, P., Russell, D., et al. 2014. Matrix metalloproteinase 7 is associated with symptomatic lesions and adverse events in patients with carotid atherosclerosis. *PLoS One,* 9**,** e84935.

Adkins, Y. & Kelley, D. S. 2010. Mechanisms underlying the cardioprotective effects of omega-3 polyunsaturated fatty acids. *J Nutr Biochem,* 21**,** 781-92.

Ahmed, I. & Ismail, N. 2020. M1 and M2 Macrophages Polarization via mTORC1 Influences Innate Immunity and Outcome of Ehrlichia Infection. *J Cell Immunol,* 2**,** 108-115.

Akhavanpoor, M., Gleissner, C. A., Akhavanpoor, H., Lasitschka, F., Doesch, A. O., Katus, H. A. & Erbel, C. 2018. Adventitial tertiary lymphoid organ classification in human atherosclerosis. *Cardiovasc Pathol,* 32**,** 8-14.

Al-Sharea, A., Lee, M. K., Moore, X. L., et al. 2016. Native LDL promotes differentiation of human monocytes to macrophages with an inflammatory phenotype. *Thromb Haemost,* 115**,** 762-72.

Albert, B. B., Cameron-Smith, D., Hofman, P. L. & Cutfield, W. S. 2013. Oxidation of marine omega-3 supplements and human health. *Biomed Res Int,* 2013**,** 464921.

Alberts-Grill, N., Denning, T. L., Rezvan, A. & Jo, H. 2013. The role of the vascular dendritic cell network in atherosclerosis. *Am J Physiol Cell Physiol,* 305**,** C1-21.

Alexander, K. A., Chang, M. K., Maylin, E. R., et al. 2011. Osteal macrophages promote in vivo intramembranous bone healing in a mouse tibial injury model. *J Bone Miner Res,* 26**,** 1517-32.

Alexopoulou, L., Holt, A. C., Medzhitov, R. & Flavell, R. A. 2001. Recognition of double-stranded RNA and activation of NF-κB by Toll-like receptor 3. *NATURE,* 413**,** 732-738.

Alique, M., Luna, C., Carracedo, J. & Ramírez, R. 2015. LDL biochemical modifications: a link between atherosclerosis and aging. *Food Nutr Res,* 59**,** 29240.

Allahverdian, S., Chehroudi, A. C., Mcmanus, B. M., Abraham, T. & Francis, G. A. 2014. Contribution of intimal smooth muscle cells to cholesterol accumulation and macrophage-like cells in human atherosclerosis. *Circulation,* 129**,** 1551-9.

Alon, R., Kassner, P. D., Carr, M. W., Finger, E. B., Hemler, M. E. & Springer, T. A. 1995. The integrin VLA-4 supports tethering anf rolling in flow on VCAM-1. *J Cell Biol,* 128**,** 1243-1253.

Alon, R. & Shulman, Z. 2011. Chemokine triggered integrin activation and actin remodeling events guiding lymphocyte migration across vascular barriers. *Exp Cell Res,* 317**,** 632-41.

Amarante-Mendes, G. P., Adjemian, S., Branco, L. M., Zanetti, L. C., Weinlich, R. & Bortoluci, K. R. 2018. Pattern Recognition Receptors and the Host Cell Death Molecular Machinery. *Front Immunol,* 9**,** 2379.

Ancuta, P., Rao, R., Moses, A., Mehle, A., Shaw, S. K., Luscinskas, F. W. & Gabuzda, D. 2003. Fractalkine preferentially mediates arrest and migration of CD16+ monocytes. *J Exp Med,* 197**,** 1701-7.

Anderson, G. D., Hauser, S. D., Mcgarity, K. L., Bremer, M. E., Isakson, P. C. & Gregory, S. A. 1996. Selective inhibition of cyclooxygenase (COX)-2 reverses

inflammation and expression of COX-2 and interleukin 6 in rat adjuvant arthritis. *J Clin Invest,* 97**,** 2672-9.
Andreeva, E. R., Pugach, I. M. & Orekhov, A. N. 1997. Collagen-synthesizing cells in initial and advanced atherosclerotic lesions of human aorta. *Atherosclerosis,* 130**,** 133-42.
Aprotosoaie, A. C., Costache, A. D. & Costache, Ii 2022. Therapeutic Strategies and Chemoprevention of Atherosclerosis: What Do We Know and Where Do We Go? *Pharmaceutics,* 14.
Aqel, N. M., Ball, R. Y., Waldmann, H. & Mitchinson, M. J. 1985. Identification of macrophages and smooth muscle cells in human atherosclerosis using monoclonal antibodies. *J Pathol,* 146**,** 197-204.
Araujo, A. V., Ferezin, C. Z., Rodrigues, G. J., et al. 2011. Prostacyclin, not only nitric oxide, is a mediator of the vasorelaxation induced by acetylcholine in aortas from rats submitted to cecal ligation and perforation (CLP). *Vascul Pharmacol,* 54**,** 44-51.
Archer, S. L., Huang, J. M. C., Hampl, V., Nelson, D. P., Shultz, P. J. & Weir, E. K. 1994. Nitric oxide and cGMP cuse vasorelaxation by activation of a charybdotoxin-sensitive K channel by cGMP-dependent protein kinase. *Physiology,* 91**,** 7583-7587.
Arnold, C. E., Gordon, P., Barker, R. N. & Wilson, H. M. 2015. The activation status of human macrophages presenting antigen determines the efficiency of Th17 responses. *Immunobiology,* 220**,** 10-9.
Arnould, T., Thibaut-Vercruyssen, R., Bouaziz, N., Dieu, M., Remacle, J. & Michiels, C. 2001. PGF(2alpha), a prostanoid released by endothelial cells activated by hypoxia, is a chemoattractant candidate for neutrophil recruitment. *Am J Pathol,* 159**,** 345-57.
Auffray, C., Fogg, D., Garfa, M., et al. 2007. Monitoring of blood vessels and tissues by a population of monocyes with patrolling behaviour. *Science,* 317**,** 666-670.
Bain, C. C. & Mowat, A. M. 2014. Macrophages in intestinal homeostasis and inflammation. *Immunol Rev,* 260**,** 102-17.
Bain, C. C., Scott, C. L., Uronen-Hansson, H., et al. 2013. Resident and pro-inflammatory macrophages in the colon represent alternative context-dependent fates of the same Ly6Chi monocyte precursors. *Mucosal Immunol,* 6**,** 498-510.
Bardin, M., Pawelzik, S. C., Lagrange, J., et al. 2022. The resolvin D2 - GPR18 axis is expressed in human coronary atherosclerosis and transduces atheroprotection in apolipoprotein E deficient mice. *Biochem Pharmacol,* 201**,** 115075.
Barker, R. N., Erwig, L. P., Hill, K. S., Devine, A., Pearce, W. P. & Rees, A. J. 2002. Antigen presentation by macrophages is enhanced by the uptake of necrotic, but not apoptotic, cells. *Clin Exp Immunol,* 127**,** 220-5.
Barrett, T. J. 2020. Macrophages in Atherosclerosis Regression. *Arterioscler Thromb Vasc Biol,* 40**,** 20-33.
Barringhaus, K. G., Phillips, J. W., Thatte, J. S., et al. 2004. Alpha4beta1 integrin (VLA-4) blockade attenuates both early and late leukocyte recruitment and neointimal growth following carotid injury in apolipoprotein E (-/-) mice. *J Vasc Res,* 41**,** 252-60.

Basu, S., Whiteman, M., Mattey, D. L. & Halliwell, B. 2001. Raised levels of F(2)-isoprostanes and prostaglandin F(2alpha) in different rheumatic diseases. *Ann Rheum Dis,* 60**,** 627-31.
Bazan, N. G. 2009. Neuroprotectin D1-mediated anti-inflammatory and survival signaling in stroke, retinal degenerations, and Alzheimer's disease. *J Lipid Res,* 50 Suppl**,** S400-5.
Becker, S., Warren, M. K. & Haskill, S. 1987. Colony-stimulating factor-induced monocyte survival and differentiation into macrophages in serum-free cultures. *The Journal of Immunology,* 139**,** 3703-3709.
Beitnes, A. C., Ráki, M., Brottveit, M., Lundin, K. E., Jahnsen, F. L. & Sollid, L. M. 2012. Rapid accumulation of CD14+CD11c+ dendritic cells in gut mucosa of celiac disease after in vivo gluten challenge. *PLoS One,* 7**,** e33556.
Bekkering, S., Quintin, J., Joosten, L. A., Van Der Meer, J. W., Netea, M. G. & Riksen, N. P. 2014. Oxidized low-density lipoprotein induces long-term proinflammatory cytokine production and foam cell formation via epigenetic reprogramming of monocytes. *Arterioscler Thromb Vasc Biol,* 34**,** 1731-8.
Belge, K. U., Dayyani, F., Horelt, A., et al. 2002. The proinflammatory CD14+CD16+DR++ monocytes are a major source of TNF. *J Immunol,* 168**,** 3536-42.
Bentzon, J. F., Otsuka, F., Virmani, R. & Falk, E. 2014. Mechanisms of plaque formation and rupture. *Circ Res,* 114**,** 1852-66.
Bernardo, D., Marin, A. C., Fernández-Tomé, S., et al. 2018. Human intestinal pro-inflammatory CD11chighCCR2+CX3CR1+ macrophages, but not their tolerogenic CD11c-CCR2-CX3CR1 - counterparts, are expanded in inflammatory bowel disease. *Mucosal Immunol,* 11**,** 1114-1126.
Bhatt, D. L., Miller, M., Brinton, E. A., et al. 2020. REDUCE-IT USA: Results From the 3146 Patients Randomized in the United States. *Circulation,* 141**,** 367-375.
Bhatt, D. L., Steg, P. G., Miller, M., et al. 2019. Cardiovascular Risk Reduction with Icosapent Ethyl for Hypertriglyceridemia. *N Engl J Med,* 380**,** 11-22.
Bhattacharjee, J., Das, B., Mishra, A., Sahay, P. & Upadhyay, P. 2017. Monocytes isolated by positive and negative magnetic sorting techniques show different molecular characteristics and immunophenotypic behaviour. *F1000Res,* 6**,** 2045.
Bhowmick, D., Van Diepen, F., Pfauth, A., Tissier, R. & Ratliff, M. L. 2021. A gain and dynamic range independent index to quantify spillover spread to aid panel design in flow cytometry. *Sci Rep,* 11**,** 20553.
Bi, Y., Chen, J., Hu, F., Liu, J., Li, M. & Zhao, L. 2019. M2 Macrophages as a Potential Target for Antiatherosclerosis Treatment. *Neural Plast,* 2019**,** 6724903.
Bisgaard, L. S., Mogensen, C. K., Rosendahl, A., Cucak, H., Nielsen, L. B., Rasmussen, S. E. & Pedersen, T. X. 2016. Bone marrow-derived and peritoneal macrophages have different inflammatory response to oxLDL and M1/M2 marker expression - implications for atherosclerosis research. *Sci Rep,* 6**,** 35234.
Bobryhev, Y. V., Ivanova, E. A., Chistiakov, D. A., Nikiforov, N. G. & Orekhov, A. N. 2016. Macrophages and Their Role in Atherosclerosis: Pathophysiology and Transcriptome Analysis. *BioMed Research International,* 2016**,** 1-13.

Bobryshev, Y. V. 2006. Monocyte recruitment and foam cell formation in atherosclerosis. *Micron,* 37**,** 208-22.
Bochem, A. E., Van Der Valk, F. M., Tolani, S., Stroes, E. S., Westerterp, M. & Tall, A. R. 2015. Increased Systemic and Plaque Inflammation in ABCA1 Mutation Carriers With Attenuation by Statins. *Arterioscler Thromb Vasc Biol,* 35**,** 1663-9.
Bonacina, F., Di Costanzo, A., Genkel, V., et al. 2023. The heterogeneous cellular landscape of atherosclerosis: Implications for future research and therapies. A collaborative review from the EAS young fellows. *Atherosclerosis,* 372**,** 48-56.
Borden, E. C., Sen, G. C., Uze, G., Silverman, R. H., Ransohoff, R. M., Foster, G. R. & Stark, G. R. 2007. Interferons at age 50: past, current and future impact on biomedicine. *Nat Rev Drug Discov,* 6**,** 975-90.
Borghese, F. & Clanchy, F. I. 2011. CD74: an emerging opportunity as a therapeutic target in cancer and autoimmune disease. *Expert Opin Ther Targets,* 15**,** 237-51.
Boring, L., Gosling, J., Cleary, M. & Charo, I. F. 1998. Decreased lesion formation in CCR2-/- mice reveals a role for chemokines in the initiation of atherosclerosis. *Nature,* 394**,** 894-7.
Botts, S. R., Fish, J. E. & Howe, K. L. 2021. Dysfunctional Vascular Endothelium as a Driver of Atherosclerosis: Emerging Insights Into Pathogenesis and Treatment. *Front Pharmacol,* 12**,** 787541.
Bourdely, P., Petti, L., Khou, S., et al. 2022. Autofluorescence identifies highly phagocytic tissue-resident macrophages in mouse and human skin and cutaneous squamous cell carcinoma. *Front Immunol,* 13**,** 903069.
Bradfield, P. F., Nourshargh, S., Aurrand-Lions, M. & Imhof, B. A. 2007. JAM family and related proteins in leukocyte migration (Vestweber series). *Arterioscler Thromb Vasc Biol,* 27**,** 2104-12.
Brown, G. D., Herre, J., Williams, D. L., Willment, J. A., Marshall, A. S. & Gordon, S. 2003. Dectin-1 mediates the biological effects of beta-glucans. *J Exp Med,* 197**,** 1119-24.
Brown, M. S. & Goldstein, J. L. 1986. A receptor-mediated pathway for cholesterol homeostasis. *Science,* 232**,** 34-47.
Brugger, W., Kreutz, M. & Andreesen, R. 1991. Macrophage colony-stimulating factor is required for human monocyte survival and acts as a cofactor for their termina differentiation to macrophage in vtiro. *Journal of Leukocyte Biology,* 49**,** 483-488.
Buchacher, T., Ohradanova-Repic, A., Stockinger, H., Fischer, M. B. & Weber, V. 2015. M2 Polarization of Human Macrophages Favors Survival of the Intracellular Pathogen Chlamydia pneumoniae. *PLoS One,* 10**,** e0143593.
Bucher, H., Hengstler, P., Schindler, C. & Meier, G. 2002. N-3 Polyunsaturated Fatty Acids in Coronary Heart Disease: A Meta-analysis of Randomized Controlled Trials. 112**,** 298-304.
Bujko, A., Atlasy, N., Landsverk, O. J. B., et al. 2018. Transcriptional and functional profiling defines human small intestinal macrophage subsets. *J Exp Med,* 215**,** 441-458.
Buono, C., Pang, H., Uchida, Y., Libby, P., Sharpe, A. H. & Lichtman, A. H. 2004. B7-1/B7-2 costimulation regulates plaque antigen-specific T-cell responses and

atherogenesis in low-density lipoprotein receptor-deficient mice. *Circulation,* 109**,** 2009-15.
Burger, P. C. & Wagner, D. D. 2003. Platelet P-selectin facilitates atherosclerotic lesion development. *Blood,* 101**,** 2661-6.
Burke, A. P., Farb, A., Malcom, G. T., Liang, Y. H., Smialek, J. & Virmani, R. 1997. Coronary risk factors and plaque morphology in men with coronary disease who died suddenly. *N Engl J Med,* 336**,** 1276-82.
Burstyn-Cohen, T. & Fresia, R. 2023. TAM receptors in phagocytosis: Beyond the mere internalization of particles. *Immunol Rev,* 319**,** 7-26.
Cahill, P. A. & Redmond, E. M. 2016. Vascular endothelium - Gatekeeper of vessel health. *Atherosclerosis,* 248**,** 97-109.
Calder, P. C. & Grimble, R. F. 2002. Polyunsaturated fatty acids, inflammation and immunity. *Eur J Clin Nutr,* 56 Suppl 3**,** S14-9.
Cao, X., Yakala, G. K., Van Den Hil, F. E., Cochrane, A., Mummery, C. L. & Orlova, V. V. 2019. Differentiation and Functional Comparison of Monocytes and Macrophages from hiPSCs with Peripheral Blood Derivatives. *Stem Cell Reports,* 12**,** 1282-1297.
Carlin, L. M., Stamatiades, E. G., Auffray, C., et al. 2013. Nr4a1-dependent Ly6C(low) monocytes monitor endothelial cells and orchestrate their disposal. *Cell,* 153**,** 362-75.
Caterina, R. D., Libby, P., Peng, H., et al. 1995. Nitic oxide decreases cytokine-induced endothelial activation. Nitrix oxide selectively reduces endothelial expression of adhesion molecules and proinflammatory cytokines. *J Clin Invest,* 96**,** 60-68.
Celi, A., Pellegrini, G., Lorenzet, R., Blasi, A. D., Ready, N., Furie, B. C. & Furie, B. 1994. P-selectin induces the expression of tissue factor on monocytes. 91**,** 8767-8771.
Chappell, D. C., Varner, S. E., Nerem, R. M., Medford, R. M. & Alexander, W. 1998. Oscillatory shear stress stimulates adhesion molecule expression in cultured human endothelium. *Circ Res,* 82**,** 532-539.
Chatterjee, A., Sharma, A., Chen, M., Toy, R., Mottola, G. & Conte, M. S. 2014. The pro-resolving lipid mediator maresin 1 (MaR1) attenuates inflammatory signaling pathways in vascular smooth muscle and endothelial cells. *PLoS One,* 9**,** e113480.
Chen, H., Li, D., Chen, J., Roberts, G. J., Saldeen, T. & Mehta, J. L. 2003. EPA and DHA attenuate ox-LDL-induced expression of adhesion molecules in human coronary artery endothelial cells via protein kinase B pathway. *J Mol Cell Cardiol,* 35**,** 769-75.
Chen, L., Deng, H., Cui, H., et al. 2018. Inflammatory responses and inflammation-associated diseases in organs. *Oncotarget,* 9**,** 7204-7218.
Chen, M., Masaki, T. & Sawamura, T. 2002. LOX-1, the receptor for oxidized low-density lipoprotein identified from endothelial cells: implications in endothelial dysfunction and atherosclerosis. *Pharmacol Ther,* 95**,** 89-100.
Chen, S., Saeed, A., Liu, Q., et al. 2023. Macrophages in immunoregulation and therapeutics. *Signal Transduct Target Ther,* 8**,** 207.
Chinetti, G., Lestavel, S., Bocher, V., et al. 2001. PPAR-alpha and PPAR-gamma activators induce cholesterol removal from human macrophage foam cells through stimulation of the ABCA1 pathway. *Nat Med,* 7**,** 53-8.

Chistiakov, D. A., Killingsworth, M. C., Myasoedova, V. A., Orekhov, A. N. & Bobryshev, Y. V. 2017. CD68/macrosialin: not just a histochemical marker. *Lab Invest,* 97**,** 4-13.
Cho, K. Y., Miyoshi, H., Kuroda, S., et al. 2013. The phenotype of infiltrating macrophages influences arteriosclerotic plaque vulnerability in the carotid artery. *J Stroke Cerebrovasc Dis,* 22**,** 910-8.
Chuntharpursat-Bon, E., Povstyan, O. V., Ludlow, M. J., et al. 2023. PIEZO1 and PECAM1 interact at cell-cell junctions and partner in endothelial force sensing. *Commun Biol,* 6**,** 358.
Cochain, C., Vafadarnejad, E., Arampatzi, P., et al. 2018. Single-Cell RNA-Seq Reveals the Transcriptional Landscape and Heterogeneity of Aortic Macrophages in Murine Atherosclerosis. *Circ Res,* 122**,** 1661-1674.
Collins, E. J., Cervantes-Silva, M. P., Timmons, G. A., O'siorain, J. R., Curtis, A. M. & Hurley, J. M. 2021. Post-transcriptional circadian regulation in macrophages organizes temporally distinct immunometabolic states. *Genome Res,* 31**,** 171-185.
Consuegra-Sanchez, L., Esteban-Luque, A. & Kaski, J. C. 2024. Modulating the phenotypic transition of vascular smooth muscle cells via LKB1, a new pharmacologic target to strike atherosclerosis? *Int J Cardiol,* 395**,** 131427.
Crola Da Silva, C., Lamerant-Fayel, N., Paprocka, M., Mitterrand, M., Gosset, D., Dus, D. & Kieda, C. 2009. Selective human endothelial cell activation by chemokines as a guide to cell homing. *Immunology,* 126**,** 394-404.
Cros, J., Cagnard, N., Woollard, K., et al. 2010. Human CD14dim monocytes patrol and sense nucleic acids and viruses via TLR7 and TLR8 receptors. *Immunity,* 33**,** 375-86.
Cunningham, K. S. & Gotlieb, A. I. 2005. The role of shear stress in the pathogenesis of atherosclerosis. *Lab Invest,* 85**,** 9-23.
Cunningham, P. S., Jackson, C., Chakraborty, A., Cain, J., Durrington, H. J. & Blaikley, J. F. 2023. Circadian regulation of pulmonary disease: the importance of timing. *Clin Sci (Lond),* 137**,** 895-912.
Cushing, S. D., Berliner, J. A., Valente, A. J., et al. 1990. Minimally modified low density lipoprotein induces monocyte chemotactic protein 1 in human endothelial cells and smooth muscle cells. *Proc Natl Acad Sci U S A,* 87**,** 5134-8.
Cybulsky, M. I., Iiyama, K., Li, H., et al. 2001. A major role for VCAM-1, but not ICAM-1, in early atherosclerosis. *J Clin Invest,* 107**,** 1255-62.
Dai, X., Ryan, G. R., Hapel, A. J., et al. 2002. Targeted disruption of the mouse colony-stimulating factor 1 receptor gene results in osteopetrosis, mononuclear phagocyte deficiency, increased primitive progenitor cell frequencies, and reproductive defects. *Blood,* 99**,** 111-120.
Dakroub, H., Nowak, M., Benoist, J. F., Noel, B., Vedie, B., Paul, J. L. & Fournier, N. 2021. Eicosapentaenoic acid membrane incorporation stimulates ABCA1-mediated cholesterol efflux from human THP-1 macrophages. *Biochim Biophys Acta Mol Cell Biol Lipids,* 1866**,** 159016.
Dalli, J. & Serhan, C. N. 2012. Specific lipid mediator signatures of human phagocytes: microparticles stimulate macrophage efferocytosis and pro-resolving mediators. *Blood,* 120**,** e60-72.

Damisah, E. C., Rai, A. & Grutzendler, J. 2020. TREM2: Modulator of Lipid Metabolism in Microglia. *Neuron,* 105**,** 759-761.
De Caterina, R., Cybulsky, M. A., Clinton, S. K., Gimbrone, M. A., Jr. & Libby, P. 1995. Omega-3 fatty acids and endothelial leukocyte adhesion molecules. *Prostaglandins Leukot Essent Fatty Acids,* 52**,** 191-5.
De Gaetano, M., Crean, D., Barry, M. & Belton, O. 2016. M1- and M2-Type Macrophage Responses Are Predictive of Adverse Outcomes in Human Atherosclerosis. *Front Immunol,* 7**,** 275.
Dennis, E. A. & Norris, P. C. 2015. Eicosanoid storm in infection and inflammation. *Nat Rev Immunol,* 15**,** 511-23.
Depuydt, M. a. C., Prange, K. H. M., Slenders, L., et al. 2020. Microanatomy of the Human Atherosclerotic Plaque by Single-Cell Transcriptomics. *Circ Res,* 127**,** 1437-1455.
Dib, L., Koneva, L. A., Edsfeldt, A., et al. 2023. Lipid-associated macrophages transition to an inflammatory state in human atherosclerosis increasing the risk of cerebrovascular complications. *Nat Cardiovasc Res,* 2**,** 656-672.
Dimmeler, S., Haendeler, J., Galle, J. & Zeiher, A. M. 1997. Oxidized low-density lipoprotein induces apoptosis of human endothelial cells by activation of CPP32-like proteases. A mechanistic clue to the 'response to injury' hypothesis. *Circulation,* 95**,** 1760-3.
Ding, Y., Yi, J., Wang, J. & Sun, Z. 2023. Interleukin-1 receptor antagonist: a promising cytokine against human squamous cell carcinomas. *Heliyon,* 9**,** e14960.
Dinicolantonio, J. J. & O'keefe, J. H. 2018. Importance of maintaining a low omega-6/omega-3 ratio for reducing inflammation. *Open Heart,* 5**,** e000946.
Dole, V. S., Bergmeier, W., Mitchell, H. A., Eichenberger, S. C. & Wagner, D. D. 2005. Activated platelets induce Weibel-Palade-body secretion and leukocyte rolling in vivo: role of P-selectin. *Blood,* 106**,** 2334-9.
Dong, Z. M., Chapman, S. M., Brown, A. A., Frenette, P. S., Hynes, R. O. & Wagner, D. D. 1998. The combined role of P- and E-selectins in atherosclerosis. *J Clin Invest,* 102**,** 145-52.
Dransfield, I., Zagorska, A., Lew, E. D., Michail, K. & Lemke, G. 2015. Mer receptor tyrosine kinase mediates both tethering and phagocytosis of apoptotic cells. *Cell Death Dis,* 6**,** e1646.
Duewell, P., Kono, H., Rayner, K. J., et al. 2010. NLRP3 inflammasomes are required for atherogenesis and activated by cholesterol crystals. *Nature,* 464**,** 1357-61.
Dungan, L. S., Mcguinness, N. C., Boon, L., Lynch, M. A. & Mills, K. H. 2014. Innate IFN-gamma promotes development of experimental autoimmune encephalomyelitis: a role for NK cells and M1 macrophages. *Eur J Immunol,* 44**,** 2903-17.
Durham, A. L., Speer, M. Y., Scatena, M., Giachelli, C. M. & Shanahan, C. M. 2018. Role of smooth muscle cells in vascular calcification: implications in atherosclerosis and arterial stiffness. *Cardiovasc Res,* 114**,** 590-600.
Dyall, S. C. 2017. Interplay Between n-3 and n-6 Long-Chain Polyunsaturated Fatty Acids and the Endocannabinoid System in Brain Protection and Repair. *Lipids,* 52**,** 885-900.

Dyall, S. C., Balas, L., Bazan, N. G., et al. 2022. Polyunsaturated fatty acids and fatty acid-derived lipid mediators: Recent advances in the understanding of their biosynthesis, structures, and functions. *Prog Lipid Res,* 86**,** 101165.
Egawa, M., Mukai, K., Yoshikawa, S., et al. 2013. Inflammatory monocytes recruited to allergic skin acquire an anti-inflammatory M2 phenotype via basophil-derived interleukin-4. *Immunity,* 38**,** 570-80.
El-Behi, M., Ciric, B., Dai, H., et al. 2011. The encephalitogenicity of T(H)17 cells is dependent on IL-1- and IL-23-induced production of the cytokine GM-CSF. *Nat Immunol,* 12**,** 568-75.
Eligini, S., Crisci, M., Bono, E., Songia, P., Tremoli, E., Colombo, G. I. & Colli, S. 2013. Human monocyte-derived macrophages spontaneously differentiated in vitro show distinct phenotypes. *J Cell Physiol,* 228**,** 1464-72.
Elkord, E., Williams, P. E., Kynaston, H. & Rowbottom, A. W. 2005. Human monocyte isolation methods influence cytokine production from in vitro generated dendritic cells. *Immunology,* 114**,** 204-12.
Endemann, G., Stanton, L. W., Madden, K. S., Bryant, C. M., White, R. T. & Protter, A. A. 1993. CD36 is a receptor for oxidized low density lipoprotein. *J Biol Chem,* 268**,** 11811-6.
Epelman, S., Lavine, K. J. & Randolph, G. J. 2014. Origin and functions of tissue macrophages. *Immunity,* 41**,** 21-35.
Fadok, V. A., Bratton, D. L., Konowal, A., Freed, P. W., Westcott, J. Y. & Henson, P. M. 1998. Macrophages that have ingested apoptotic cells in vitro inhibit pro-inflammatory cytokine production through autocrine/paracrine mechanisms involving TGF-b, PGE2 and PAF. *J Clin Invest,* 101**,** 890-898.
Fagerholm, S. C., Guenther, C., Llort Asens, M., Savinko, T. & Uotila, L. M. 2019. Beta2-Integrins and Interacting Proteins in Leukocyte Trafficking, Immune Suppression, and Immunodeficiency Disease. *Front Immunol,* 10**,** 254.
Fazio, S., Dove, D. E. & Linton, M. F. 2005. ACAT inhibition: bad for macrophages, good for smooth muscle cells? *Arterioscler Thromb Vasc Biol,* 25**,** 7-9.
Fazio, S., Major, A. S., Swift, L. L., Gleaves, L. A., Accad, M., Linton, M. F. & Farese, R. V. 2001. Increased atherosclerosis in LDL receptor–null mice lacking ACAT1 in macrophages. *J Clin Invest,* 107**,** 163-171.
Febbraio, M., Podrez, E. A., Smith, J. D., et al. 2000. Targeted disruption of the class B scavenger receptor CD36 protects against atherosclerotic lesion development in mice. *J Clin Invest,* 105**,** 1049-56.
Feig, J. E., Shang, Y., Rotllan, N., et al. 2011. Statins promote the regression of atherosclerosis via activation of the CCR7-dependent emigration pathway in macrophages. *PLoS One,* 6**,** e28534.
Feil, S., Fehrenbacher, B., Lukowski, R., Essmann, F., Schulze-Osthoff, K., Schaller, M. & Feil, R. 2014. Transdifferentiation of vascular smooth muscle cells to macrophage-like cells during atherogenesis. *Circ Res,* 115**,** 662-7.
Feng, Q., Hato, S. V., Langereis, M. A., et al. 2012. MDA5 detects the double-stranded RNA replicative form in picornavirus-infected cells. *Cell Rep,* 2**,** 1187-96.
Fernandez, D. M., Rahman, A. H., Fernandez, N. F., et al. 2019. Single-cell immune landscape of human atherosclerotic plaques. *Nat Med,* 25**,** 1576-1588.

Ferrer-Font, L., Small, S. J., Lewer, B., et al. 2021. Panel Optimization for High-Dimensional Immunophenotyping Assays Using Full-Spectrum Flow Cytometry. *Curr Protoc,* 1**,** e222.
Fisher, E. A. 2016. Regression of Atherosclerosis: The Journey From the Liver to the Plaque and Back. *Arterioscler Thromb Vasc Biol,* 36**,** 226-35.
Flesher, R. P., Herbert, C. & Kumar, R. K. 2014. Resolvin E1 promotes resolution of inflammation in a mouse model of an acute exacerbation of allergic asthma. *Clin Sci (Lond),* 126**,** 805-14.
Flynn, M. C., Pernes, G., Lee, M. K. S., Nagareddy, P. R. & Murphy, A. J. 2019. Monocytes, Macrophages, and Metabolic Disease in Atherosclerosis. *Front Pharmacol,* 10**,** 666.
Fogg, D. K., Sibon, C., Miled, C., et al. 2006. A Clonogenic Bone Marrow Progenitor Specific for Macrophages and Dendritic Cells. *Science,* 311**,** 83-87.
Fong, C. H., Bebien, M., Didierlaurent, A., et al. 2008. An antiinflammatory role for IKKbeta through the inhibition of "classical" macrophage activation. *J Exp Med,* 205**,** 1269-76.
Forstneric, V., Ivicak-Kocjan, K., Ljubetic, A., Jerala, R. & Bencina, M. 2016. Distinctive Recognition of Flagellin by Human and Mouse Toll-Like Receptor 5. *PLoS One,* 11**,** e0158894.
Fotis, L., Agrogiannis, G., Vlachos, I. S., et al. 2012. Intercellular adhesion molecule (ICAM)-1 and vascular cell adhesion molecule (VCAM)-1 at the early stages of atherosclerosis in a rat model. *In Vivo,* 26**,** 243-50.
Franchi, L., Eigenbrod, T., Munoz-Planillo, R., et al. 2014. Cytosolic double-stranded RNA activates the NLRP3 inflammasome via MAVS-induced membrane permeabilization and K+ efflux. *J Immunol,* 193**,** 4214-4222.
Frangos, S. G., Gahtan, V. & Sumpio, B. 1999. Localization of atherosclerosis: role of hemodynamics. *Arch Surg,* 134**,** 1142-9.
Franzoni, G., Bonelli, P., Graham, S. P., et al. 2017. Comparative phenotypic and functional analyses of the effects of autologous plasma and recombinant human macrophage-colony stimulating factor (M-CSF) on porcine monocyte to macrophage differentiation. *Vet Immunol Immunopathol,* 187**,** 80-88.
Fredman, G., Hellmann, J., Proto, J. D., et al. 2016. An imbalance between specialized pro-resolving lipid mediators and pro-inflammatory leukotrienes promotes instability of atherosclerotic plaques. *Nat Commun,* 7**,** 12859.
Freigang, S., Ampenberger, F., Spohn, G., et al. 2011. Nrf2 is essential for cholesterol crystal-induced inflammasome activation and exacerbation of atherosclerosis. *Eur J Immunol,* 41**,** 2040-51.
Fujiwara, K. 2006. Platelet endothelial cell adhesion molecule-1 and mechanotransduction in vascular endothelial cells. *J Intern Med,* 259**,** 373-80.
Furman, D., Campisi, J., Verdin, E., et al. 2019. Chronic inflammation in the etiology of disease across the life span. *Nat Med,* 25**,** 1822-1832.
Furman, M. I., Benoit, S. E., Barnard, M. R., et al. 1998. Increased platelet reactivity and circulating monocyte-platelet aggregates in patients with stable coronary artery disease. *J Am Coll Cardiol,* 31**,** 352-8.
Furth, R. V. & Cohn, Z. A. 1968. The origin and kinetics of mononuclear phagocytes. *J Exp Med,* 128**,** 415-435.
Furth, R. V., Cohn, Z. A., Hirsch, J. G., Humphrey, J. H., Spector, W. G. & Langevoort, H. L. 1972. The mononuclear phagocyte system:a new

clasification of macrophages, monocytes, and their precursor cells. *Bull World Health Organ,* 46**,** 845–852.
Gagnon, L., Filion, L. G., Dubois, C. & Rola-Pleszczynski, M. 1989. Leukotrienes and macrophage activation: augmented cytotoxic activity and enhanced interleukin 1, tumor necrosis factor and hydrogen peroxide production. *Agents Actions,* 26**,** 141-7.
Gause, W. C., Wynn, T. A. & Allen, J. E. 2013. Type 2 immunity and wound healing: evolutionary refinement of adaptive immunity by helminths. *Nat Rev Immunol,* 13**,** 607-14.
Gautier, E. L., Jakubzick, C. & Randolph, G. J. 2009. Regulation of the migration and survival of monocyte subsets by chemokine receptors and its relevance to atherosclerosis. *Arterioscler Thromb Vasc Biol,* 29**,** 1412-8.
Geissmann, F., Jung, S. & Littman, D. R. 2003. Blood monocytes consist of two principal subsets with distinct migratory properties. *Immunity,* 19**,** 71-82.
Geng, S., Chen, K., Yuan, R., et al. 2016. The persistence of low-grade inflammatory monocytes contributes to aggravated atherosclerosis. *Nat Commun,* 7**,** 13436.
Gerl, M. J., Vaz, W. L. C., Domingues, N., et al. 2018. Cholesterol is Inefficiently Converted to Cholesteryl Esters in the Blood of Cardiovascular Disease Patients. *Sci Rep,* 8**,** 14764.
Ghersa, P., Hooft Van Huijsduijnen, R., Whelan, J., Cambet, Y., Pescini, R. & Delamarter, J. F. 1994. Inhibition of E-selectin gene transcription through a cAMP-dependent protein kinase pathway. *Journal of Biological Chemistry,* 269**,** 29129-29137.
Ghosh, S., Zhao, B., Bie, J. & Song, J. 2010. Macrophage cholesteryl ester mobilization and atherosclerosis. *Vascul Pharmacol,* 52**,** 1-10.
Ginhoux, F., Greter, M., Leboeuf, M., et al. 2010. Fate mapping analysis reveals that adult microglia derive from primitive macrophages. *Science,* 330**,** 841-845.
Girardin, S. E., Travassos, L. H., Herve, M., et al. 2003. Peptidoglycan molecular requirements allowing detection by Nod1 and Nod2. *J Biol Chem,* 278**,** 41702-8.
Glazer, E. S., Massey, K. L. & Curley, S. A. 2010. A protocol to effectively create single cell suspensions of adherent cells for multiparameter high-throughput flow cytometry. *In Vitro Cellular & Developmental Biology - Animal,* 46**,** 97-101.
Gleissner, C. A., Shaked, I., Little, K. M. & Ley, K. 2010. CXC chemokine ligand 4 induces a unique transcriptome in monocyte-derived macrophages. *J Immunol,* 184**,** 4810-8.
Goldstein, J. L., Ho, Y. K., Basu, S. K. & Brown, M. S. 1979a. Binding site on macrophages that mediate uptake and degradation of acetylated low density lipoprotein, producing massive cholesterol deposition. *Proc Natl Acad Sci U S A,* 76**,** 333-337.
Goldstein, J. L., Ho, Y. K., Basu, S. K. & Brown, M. S. 1979b. Binding site on macrophages that mediates uptake and degradation of acetylated low density lipoprotein, producing massive cholesterol deposition. *Proceedings of the national academy of sciences,* 76**,** 333-337.
Gomez, I., Foudi, N., Longrois, D. & Norel, X. 2013. The role of prostaglandin E2 in human vascular inflammation. *Prostaglandins Leukot Essent Fatty Acids,* 89**,** 55-63.

Gordon, S. & Martinez, F. O. 2010. Alternative activation of macrophages: mechanism and functions. *Immunity,* 32**,** 593-604.
Gordon, S. & Taylor, P. R. 2005. Monocyte and macrophage heterogeneity. *Nat Rev Immunol,* 5**,** 953-64.
Gouna, G., Klose, C., Bosch-Queralt, M., et al. 2021. TREM2-dependent lipid droplet biogenesis in phagocytes is required for remyelination. *J Exp Med,* 218.
Gown, A. M., Tsukada, T. & Ross, R. 1986. Human atherosclerosis. II. Immunocytochemical analysis of the cellular composition of human atherosclerotic lesions. *Am J Pathol,* 125**,** 191-207.
Grage-Griebenow, E., Flad, H. D., Ernst, M., Bzowska, M., Skrzeczynska, J. & Pryjma, J. 2000. Human MO subsets as defined by expression of CD64 and CD16 differ in phagocytic activity and generation of oxygen intermediates. *Immunobiology,* 202**,** 42-50.
Grage-Griebenow, E., Zawatzky, R., Kahlert, H., Brade, L., Flad, H. & Ernst, M. 2001. Identification of a novel dendritic cell-like subset of CD64(+) / CD16(+) blood monocytes. *Eur J Immunol,* 31**,** 48-56.
Gren, S. T., Rasmussen, T. B., Janciauskiene, S., Hakansson, K., Gerwien, J. G. & Grip, O. 2015. A Single-Cell Gene-Expression Profile Reveals Inter-Cellular Heterogeneity within Human Monocyte Subsets. *PLoS One,* 10**,** e0144351.
Griffin, E. E., Ullery, J. C., Cox, B. E. & Jerome, W. G. 2005. Aggregated LDL and lipid dispersions induce lysosomal cholesteryl ester accumulation in macrophage foam cells. *J Lipid Res,* 46**,** 2052-60.
Grimble, R. F., Howell, W. M., O'reilly, G., et al. 2002. The ability of fish oil to suppress tumor necrosis factor alpha production by peripheral blood mononuclear cells in healthy men is associated with polymorphisms in genes that influence tumor necrosis factor alpha production. *Am J Clin Nutr,* 76**,** 454-9.
Groeneweg, M., Kanters, E., Vergouwe, M. N., Duerink, H., Kraal, G., Hofker, M. H. & De Winther, M. P. 2006. Lipopolysaccharide-induced gene expression in murine macrophages is enhanced by prior exposure to oxLDL. *J Lipid Res,* 47**,** 2259-67.
Gronholm, M., Jahan, F., Bryushkova, E. A., et al. 2016. LFA-1 integrin antibodies inhibit leukocyte alpha4beta1-mediated adhesion by intracellular signaling. *Blood,* 128**,** 1270-81.
Gronloh, M. L. B., Arts, J. J. G., Palacios Martinez, S., et al. 2022. Endothelial transmigration hotspots limit vascular leakage through heterogeneous expression of ICAM-1. *EMBO Rep***,** e55483.
Gruber, E., Heyward, C., Cameron, J. & Leifer, C. 2018. Toll-like receptor signaling in macrophages is regulated by extracellular substrate stiffness and Rho-associated coiled-coil kinase (ROCK1/2). *Int Immunol,* 30**,** 267-278.
Gui, Y., Zheng, H. & Cao, R. Y. 2022. Foam Cells in Atherosclerosis: Novel Insights Into Its Origins, Consequences, and Molecular Mechanisms. *Front Cardiovasc Med,* 9**,** 845942.
Guilliams, M., De Kleer, I., Henri, S., et al. 2013. Alveolar macrophages develop from fetal monocytes that differentiate into long-lived cells in the first week of life via GM-CSF. *J Exp Med,* 210**,** 1977-92.
Guilliams, M., Mildner, A. & Yona, S. 2018. Developmental and Functional Heterogeneity of Monocytes. *Immunity,* 49**,** 595-613.

Han, S., Li, X., Xia, N., et al. 2023. Myeloid Trem2 Dynamically Regulates the Induction and Resolution of Hepatic Ischemia-Reperfusion Injury Inflammation. *Int J Mol Sci,* 24.
Hao, N. B., Lu, M. H., Fan, Y. H., Cao, Y. L., Zhang, Z. R. & Yang, S. M. 2012. Macrophages in tumor microenvironments and the progression of tumors. *Clin Dev Immunol,* 2012**,** 948098.
Harder, J., Franchi, L., Munoz-Planillo, R., Park, J. H., Reimer, T. & Nunez, G. 2009. Activation of the Nlrp3 inflammasome by Streptococcus pyogenes requires streptolysin O and NF-kappa B activation but proceeds independently of TLR signaling and P2X7 receptor. *J Immunol,* 183**,** 5823-9.
Harraz, O. F., Klug, N. R., Senatore, A. J., Hill-Eubanks, D. C. & Nelson, M. T. 2022. Piezo1 Is a Mechanosensor Channel in Central Nervous System Capillaries. *Circ Res,* 130**,** 1531-1546.
Hasturk, H., Abdallah, R., Kantarci, A., Nguyen, D., Giordano, N., Hamilton, J. & Van Dyke, T. E. 2015. Resolvin E1 (RvE1) Attenuates Atherosclerotic Plaque Formation in Diet and Inflammation-Induced Atherogenesis. *Arterioscler Thromb Vasc Biol,* 35**,** 1123-33.
Hayashi, S., Watanabe, N., Nakazawa, K., et al. 2000. Role of P-selectin in inflammation, Neointimal Formation and Vascular Remodelling in Balloon-Injured Rat Carotid Arteries. *Circulation,* 102.
He, K., Song, Y., Daviglus, M. L., Liu, K., Van Horn, L., Dyer, A. R. & Greenland, P. 2004. Accumulated evidence on fish consumption and coronary heart disease mortality: a meta-analysis of cohort studies. *Circulation,* 109**,** 2705-11.
Healy, L. M., Perron, G., Won, S. Y., et al. 2016. MerTK Is a Functional Regulator of Myelin Phagocytosis by Human Myeloid Cells. *J Immunol,* 196**,** 3375-84.
Heger, L., Balk, S., Luhr, J. J., et al. 2018. CLEC10A Is a Specific Marker for Human CD1c(+) Dendritic Cells and Enhances Their Toll-Like Receptor 7/8-Induced Cytokine Secretion. *Front Immunol,* 9**,** 744.
Heine, G. H., Ortiz, A., Massy, Z. A., et al. 2012. Monocyte subpopulations and cardiovascular risk in chronic kidney disease. *Nat Rev Nephrol,* 8**,** 362-9.
Heine, G. H., Ulrich, C., Seibert, E., et al. 2008. CD14(++)CD16+ monocytes but not total monocyte numbers predict cardiovascular events in dialysis patients. *Kidney Int,* 73**,** 622-9.
Herbin, O., Regelmann, A. G., Ramkhelawon, B., Weinstein, E. G., Moore, K. J. & Alexandropoulos, K. 2016. Monocyte Adhesion and Plaque Recruitment During Atherosclerosis Development Is Regulated by the Adapter Protein Chat-H/SHEP1. *Arterioscler Thromb Vasc Biol,* 36**,** 1791-801.
Hernandez, S., Lazcano, R., Serrano, A., et al. 2022. Challenges and Opportunities for Immunoprofiling Using a Spatial High-Plex Technology: The NanoString GeoMx((R)) Digital Spatial Profiler. *Front Oncol,* 12**,** 890410.
Hidalgo, A., Peired, A. J., Wild, M., Vestweber, D. & Frenette, P. S. 2007. Complete identification of E-selectin ligands on neutrophils reveals distinct functions of PSGL-1, ESL-1, and CD44. *Immunity,* 26**,** 477-489.
Higashimori, M., Tatro, J. B., Moore, K. J., Mendelsohn, M. E., Galper, J. B. & Beasley, D. 2011. Role of toll-like receptor 4 in intimal foam cell accumulation in apolipoprotein E-deficient mice. *Arterioscler Thromb Vasc Biol,* 31**,** 50-7.
Hilgendorf, I., Swirski, F. K. & Robbins, C. S. 2015. Monocyte fate in atherosclerosis. *Arterioscler Thromb Vasc Biol,* 35**,** 272-9.

Hinkley, H., Counts, D. A., Voncanon, E. & Lacy, M. 2023. T Cells in Atherosclerosis: Key Players in the Pathogenesis of Vascular Disease. *Cells,* 12.
Hinson, R. M., Williams, J. A. & Shacter, E. 1996. Elevated interleukin 6 is induced by prostaglandin E2 in a murine model of inflammation: possible role of cyclooxygenase-2. *Proc Natl Acad Sci U S A,* 93**,** 4885-90.
Hirayama, D., Iida, T. & Nakase, H. 2017. The Phagocytic Function of Macrophage-Enforcing Innate Immunity and Tissue Homeostasis. *Int J Mol Sci,* 19.
Hodis, H. N. 1995. Reversibility of atherosclerosis--evolving perspectives from two arterial imaging clinical trials: the cholesterol lowering atherosclerosis regression study and the monitored atherosclerosis regression study. *J Cardiovasc Pharmacol,* 25 Suppl 4**,** S25-31.
Hoeffner, N., Paul, A. & Goo, Y. H. 2023. Drug screen identifies verteporfin as a regulator of lipid metabolism in macrophage foam cells. *Sci Rep,* 13**,** 19588.
Hofer, T. P., Van De Loosdrecht, A. A., Stahl-Hennig, C., Cassatella, M. A. & Ziegler-Heitbrock, L. 2019. 6-Sulfo LacNAc (Slan) as a Marker for Non-classical Monocytes. *Front Immunol,* 10**,** 2052.
Holmberg-Thyden, S., Gronbaek, K., Gang, A. O., El Fassi, D. & Hadrup, S. R. 2021. A user's guide to multicolor flow cytometry panels for comprehensive immune profiling. *Anal Biochem,* 627**,** 114210.
Holvoet, P., Perez, G., Zhao, Z., Brouwers, E., Bernar, H. & Collen, D. 1995. Malondialdehyde-modified low density lipoproteins in patients with atherosclerotic disease. *J Clin Invest,* 95**,** 2611-9.
Holvoet, P., Vanhaecke, J., Janssens, S., Van De Werf, F. & Collen, D. 1998. Oxidized LDL and malondialdehyde-modified LDL in patients with acute coronary syndromes and stable coronary artery disease. *Circulation,* 98**,** 1487-94.
Hornschuh, M., Haas, V., Winkel, P. P., et al. 2022. Negative Magnetic Sorting Preserves the Functionality of Ex Vivo Cultivated Non-Adherent Human Monocytes. *Biology (Basel),* 11.
Hou, P., Fang, J., Liu, Z., et al. 2023. Macrophage polarization and metabolism in atherosclerosis. *Cell Death Dis,* 14**,** 691.
Houtkamp, M. A., De Boer, O. J., Van Der Loos, C. M., Van Der Wal, A. C. & Becker, A. E. 2001. Adventitial infiltrates associated with advanced atherosclerotic plaques: structural organization suggests generation of local humoral immune responses. *J Pathol,* 193**,** 263-9.
Howell, K. W., Meng, X., Fullerton, D. A., Jin, C., Reece, T. B. & Cleveland, J. C., Jr. 2011. Toll-like receptor 4 mediates oxidized LDL-induced macrophage differentiation to foam cells. *J Surg Res,* 171**,** e27-31.
Hoyer, F. F., Naxerova, K., Schloss, M. J., et al. 2019. Tissue-Specific Macrophage Responses to Remote Injury Impact the Outcome of Subsequent Local Immune Challenge. *Immunity,* 51**,** 899-914 e7.
Hsu, Y. M. & Yin, M. C. 2016. EPA or DHA enhanced oxidative stress and aging protein expression in brain of d-galactose treated mice. *Biomedicine (Taipei),* 6**,** 17.
Hughes, C. S., Colhoun, L. M., Bains, B. K., et al. 2016. Extracellular cathepsin S and intracellular caspase 1 activation are surrogate biomarkers of particulate-induced lysosomal disruption in macrophages. *Part Fibre Toxicol,* 13**,** 19.

Huh, H. Y., Pearce, S. F., Yesner, L. M., Schindler, J. L. & Silverstein, R. L. 1996. Regulated expression of CD36 during monocyte-to-macrophage differentiation: potential role of CD36 in foam cell formation. *Blood,* 87**,** 2020-8.
Huo, Y., Schober, A., Forlow, S. B., et al. 2003. Circulating activated platelets exacerbate atherosclerosis in mice deficient in apolipoprotein E. *Nat Med,* 9**,** 61-7.
Idzkowska, E., Eljaszewicz, A., Miklasz, P., Musial, W. J., Tycinska, A. M. & Moniuszko, M. 2015. The Role of Different Monocyte Subsets in the Pathogenesis of Atherosclerosis and Acute Coronary Syndromes. *Scand J Immunol,* 82**,** 163-73.
Igarashi, M., Osuga, J., Isshiki, M., et al. 2010. Targeting of neutral cholesterol ester hydrolase to the endoplasmic reticulum via its N-terminal sequence. *J Lipid Res,* 51**,** 274-85.
Iiyama, K., Hajra, L., Iiyama, M., Li, H., Dichiara, M., Medoff, B. D. & Cybulsky, M. I. 1999. Patterns of Vascular Cell Adhesion Molecule-1 and Intercellular Adhesion Molecule-1 Expression in Rabbit and Mouse Atherosclerotic Lesions and at Sites Predisposed to Lesion Formation. *Circulation research***,** 199-207.
Ingersoll, M. A., Spanbroek, R., Lottaz, C., et al. 2010. Comparison of gene expression profiles between human and mouse monocyte subsets. *Blood,* 115**,** e10-9.
Insull, W., Jr. 2009. The pathology of atherosclerosis: plaque development and plaque responses to medical treatment. *Am J Med,* 122**,** S3-S14.
Iqbal, A. J., Fisher, E. A. & Greaves, D. R. 2016. Inflammation-a Critical Appreciation of the Role of Myeloid Cells. *Microbiol Spectr,* 4.
Iring, A., Jin, Y. J., Albarran-Juarez, J., et al. 2019. Shear stress-induced endothelial adrenomedullin signaling regulates vascular tone and blood pressure. *J Clin Invest,* 129**,** 2775-2791.
Isa, S. A., Ruffino, J. S., Ahluwalia, M., Thomas, A. W., Morris, K. & Webb, R. 2011. M2 macrophages exhibit higher sensitivity to oxLDL-induced lipotoxicity than other monocyte/macrophage subtypes. *Lipids Health Dis,* 10**,** 229.
Ishibashi, S., Goldstein, J. L., Brown, M. S., Herz, J. & Burns, D. K. 1994. Massive xanthomatosis and atherosclerosis in cholesterol-fed low density lipoprotein receptor-negative mice. *J Clin Invest,* 93**,** 1885-93.
Ivanov, Ii, Apta, B. H. R., Bonna, A. M. & Harper, M. T. 2019. Platelet P-selectin triggers rapid surface exposure of tissue factor in monocytes. *Sci Rep,* 9**,** 13397.
Jager, N. A., Wallis De Vries, B. M., Hillebrands, J. L., et al. 2016. Distribution of Matrix Metalloproteinases in Human Atherosclerotic Carotid Plaques and Their Production by Smooth Muscle Cells and Macrophage Subsets. *Mol Imaging Biol,* 18**,** 283-91.
Jaitin, D. A., Adlung, L., Thaiss, C. A., et al. 2019. Lipid-Associated Macrophages Control Metabolic Homeostasis in a Trem2-Dependent Manner. *Cell,* 178**,** 686-698 e14.
Jakubzick, C., Gautier, E. L., Gibbings, S. L., et al. 2013. Minimal differentiation of classical monocytes as they survey steady-state tissues and transport antigen to lymph nodes. *Immunity,* 39**,** 599-610.
James, M. J., Gibson, R. A. & Cleland, L. G. 2000. Dietary polyunsaturated fatty acids and inflammatory mediator production. *Am J Clin Nutr,* 71**,** 343S-8S.

Javadifar, A., Rastgoo, S., Banach, M., Jamialahmadi, T., Johnston, T. P. & Sahebkar, A. 2021. Foam Cells as Therapeutic Targets in Atherosclerosis with a Focus on the Regulatory Roles of Non-Coding RNAs. *Int J Mol Sci,* 22.
Jay, A. G., Chen, A. N., Paz, M. A., Hung, J. P. & Hamilton, J. A. 2015. CD36 binds oxidized low density lipoprotein (LDL) in a mechanism dependent upon fatty acid binding. *J Biol Chem,* 290**,** 4590-4603.
Jialal, I., Devaraj, S., Huet, B. A. & Traber, M. 1999. GISSI-Prevenzione trial. *Lancet,* 354**,** 1554; author reply 1556-7.
Jiang, H., Zhou, Y., Nabavi, S. M., et al. 2022. Mechanisms of Oxidized LDL-Mediated Endothelial Dysfunction and Its Consequences for the Development of Atherosclerosis. *Front Cardiovasc Med,* 9**,** 925923.
Jimenez-Uribe, A. P., Valencia-Martinez, H., Carballo-Uicab, G., et al. 2019. CD80 Expression Correlates with IL-6 Production in THP-1-Like Macrophages Costimulated with LPS and Dialyzable Leukocyte Extract (Transferon(R)). *J Immunol Res,* 2019**,** 2198508.
Jin, X. & Kruth, H. S. 2016. Culture of Macrophage Colony-stimulating Factor Differentiated Human Monocyte-derived Macrophages. *J Vis Exp*.
Johansson, I., Monsen, V. T., Pettersen, K., et al. 2015. The marine n-3 PUFA DHA evokes cytoprotection against oxidative stress and protein misfolding by inducing autophagy and NFE2L2 in human retinal pigment epithelial cells. *Autophagy,* 11**,** 1636-51.
Johnson, R. C., Chapman, S. M., Dong, Z. M., et al. 1997. Absence of P-selectin delays fatty streak formation in mice. *J Clin Invest,* 99**,** 1037-43.
Jurk, M., Heil, F., Vollmer, J., Schetter, C., Krieg, A. M., Wagner, H. L., G. & Bauer, S. 2002. Human TLR7 or TLR8 independently confer responsiveness to the antiviral compound R-848. *Nature Immunology,* 3**,** 499.
Justo-Junior, A. S., Villarejos, L. M., Lima, X. T. V., et al. 2019. Monocytes of patients with unstable angina express high levels of chemokine and pattern-recognition receptors. *Cytokine,* 113**,** 61-67.
Kang, J. Y., Nan, X., Jin, M. S., et al. 2009. Recognition of lipopeptide patterns by Toll-like receptor 2-Toll-like receptor 6 heterodimer. *Immunity,* 31**,** 873-84.
Kapellos, T. S., Bonaguro, L., Gemund, I., Reusch, N., Saglam, A., Hinkley, E. R. & Schultze, J. L. 2019. Human Monocyte Subsets and Phenotypes in Major Chronic Inflammatory Diseases. *Front Immunol,* 10**,** 2035.
Kelley, T. W., Graham, M. M., Doseff, A. I., et al. 1999. Macrophage Colony-stimulating Factor Promotes Cell Survival through Akt/Protein Kinase B. *Journal of Biological Chemistry,* 274**,** 26393-26398.
Keyes, K. T., Ye, Y., Lin, Y., Zhang, C., Perez-Polo, J. R., Gjorstrup, P. & Birnbaum, Y. 2010. Resolvin E1 protects the rat heart against reperfusion injury. *Am J Physiol Heart Circ Physiol,* 299**,** H153-64.
Khallou-Laschet, J., Varthaman, A., Fornasa, G., et al. 2010. Macrophage plasticity in experimental atherosclerosis. *PLoS One,* 5**,** e8852.
Khan, S. U., Lone, A. N., Khan, M. S., et al. 2021. Effect of omega-3 fatty acids on cardiovascular outcomes: A systematic review and meta-analysis. *EClinicalMedicine,* 38**,** 100997.
Khantakova, D., Brioschi, S. & Molgora, M. 2022. Exploring the Impact of TREM2 in Tumor-Associated Macrophages. *Vaccines (Basel),* 10.

Kim, K., Shim, D., Lee, J. S., et al. 2018. Transcriptome Analysis Reveals Nonfoamy Rather Than Foamy Plaque Macrophages Are Proinflammatory in Atherosclerotic Murine Models. *Circ Res,* 123**,** 1127-1142.
Kolodgie, F. D., Gold, H. K., Burke, A. P., et al. 2003. Intraplaque hemorrhage and progression of coronary atheroma. *N Engl J Med,* 349**,** 2316-25.
Koltsova, E. K., Hedrick, C. C. & Ley, K. 2013. Myeloid cells in atherosclerosis: a delicate balance of anti-inflammatory and proinflammatory mechanisms. *Curr Opin Lipidol,* 24**,** 371-80.
Kong, X., Qu, X., Li, B., et al. 2017. Modulation of low shear stress-induced eNOS multi-site phosphorylation and nitric oxide production via protein kinase and ERK1/2 signaling. *Mol Med Rep,* 15**,** 908-914.
Kopprasch, S., Pietzsch, J., Westendorf, T., Kruse, H. J. & Grassler, J. 2004. The pivotal role of scavenger receptor CD36 and phagocyte-derived oxidants in oxidized low density lipoprotein-induced adhesion to endothelial cells. *Int J Biochem Cell Biol,* 36**,** 460-71.
Kramer, C. K., Zinman, B., Gross, J. L., Canani, L. H., Rodrigues, T. C., Azevedo, M. J. & Retnakaran, R. 2013. Coronary artery calcium score prediction of all cause mortality and cardiovascular events in people with type 2 diabetes: systematic review and meta-analysis. *BMJ,* 346**,** f1654.
Kratofil, R. M., Kubes, P. & Deniset, J. F. 2017. Monocyte Conversion During Inflammation and Injury. *Arterioscler Thromb Vasc Biol,* 37**,** 35-42.
Krautter, F., Recio, C., Hussain, M. T., Lezama, D. R., Maione, F., Chimen, M. & Iqbal, A. J. 2020. Characterisation of endogenous Galectin-1 and -9 expression in monocyte and macrophage subsets under resting and inflammatory conditions. *Biomed Pharmacother,* 130**,** 110595.
Kromhout, D., Bosschieter, E. B. & De Lezenne Coulander, C. 1985. The inverse relation between fish consumption and 20-year mortality from coronary heart disease. *N Engl J Med,* 312**,** 1205-9.
Kromhout, D., Giltay, E. J., Geleijnse, J. M. & Alpha Omega Trial, G. 2010. n-3 fatty acids and cardiovascular events after myocardial infarction. *N Engl J Med,* 363**,** 2015-26.
Kubles, P., Suzuki, M. & Granger, D. N. 1991. Nitric oxide: an endogenous modulator of leukocyte adhesion. *Physiology/Pharmacology,* 88**,** 4651-4655.
Kubota, Y., Takubo, K., Shimizu, T., et al. 2009. M-CSF inhibition selectively targets pathological angiogenesis and lymphangiogenesis. *J Exp Med,* 206**,** 1089-102.
Kunjathoor, V. V., Febbraio, M., Podrez, E. A., et al. 2002. Scavenger receptors class A-I/II and CD36 are the principal receptors responsible for the uptake of modified low density lipoprotein leading to lipid loading in macrophages. *J Biol Chem,* 277**,** 49982-8.
Lan, Y., Lu, J., Zhang, S., et al. 2024. Piezo1-Mediated Mechanotransduction Contributes to Disturbed Flow-Induced Atherosclerotic Endothelial Inflammation. *J Am Heart Assoc,* 13**,** e035558.
Landsman, L., Bar-On, L., Zernecke, A., et al. 2009. CX3CR1 is required for monocyte homeostasis and atherogenesis by promoting cell survival. *Blood,* 113**,** 963-72.

Larigauderie, G., Furman, C., Jaye, M., et al. 2004. Adipophilin enhances lipid accumulation and prevents lipid efflux from THP-1 macrophages: potential role in atherogenesis. *Arterioscler Thromb Vasc Biol,* 24**,** 504-10.
Larsen, E., Celi, A., Gilbert, G. E., et al. 1989. PADGEM protein: A receptor tht mediates the interaction of activated platelets with neutrophils and monocytes. *Cell press,* 59**,** 305-312.
Lauro, M. L., D'ambrosio, E. A., Bahnson, B. J. & Grimes, C. L. 2017. Molecular Recognition of Muramyl Dipeptide Occurs in the Leucine-rich Repeat Domain of Nod2. *ACS Infect Dis,* 3**,** 264-270.
Lavin, Y., Winter, D., Blecher-Gonen, R., et al. 2014. Tissue-resident macrophage enhancer landscapes are shaped by the local microenvironment. *Cell,* 159**,** 1312-26.
Lavine, K. 2023. Identification of inflammatory lipid-associated macrophages in human carotid atherosclerosis. *Nature cardiovascular research,* 2**,** 604-605.
Lavine, K. J., Epelman, S., Uchida, K., et al. 2014. Distinct macrophage lineages contribute to disparate patterns of cardiac recovery and remodeling in the neonatal and adult heart. *Proc Natl Acad Sci U S A,* 111**,** 16029-34.
Lazarov, T., Juarez-Carreno, S., Cox, N. & Geissmann, F. 2023. Physiology and diseases of tissue-resident macrophages. *Nature,* 618**,** 698-707.
Leng, G. C., Lee, A. J., Fowkes, F. G., Jepson, R. G., Lowe, G. D., Skinner, E. R. & Mowat, B. F. 1998. Randomized controlled trial of gamma-linolenic acid and eicosapentaenoic acid in peripheral arterial disease. *Clin Nutr,* 17**,** 265-71.
Leuschner, F., Rauch, P. J., Ueno, T., et al. 2012. Rapid monocyte kinetics in acute myocardial infarction are sustained by extramedullary monocytopoiesis. *J Exp Med,* 209**,** 123-37.
Levy, B. D., Clish, C. B., Schmidt, B., Gronert, K. & Serhan, C. N. 2001. Lipid mediator class switching during acute inflammation: signals in resolution. *Nat Immunol,* 2**,** 612-9.
Ley, K., Laudanna, C., Cybulsky, M. I. & Nourshargh, S. 2007. Getting to the site of inflammation: the leukocyte adhesion cascade updated. 7**,** 678-689.
Li, C., Wu, X., Liu, S., Shen, D., Zhu, J. & Liu, K. 2020a. Role of Resolvins in the Inflammatory Resolution of Neurological Diseases. *Front Pharmacol,* 11**,** 612.
Li, D. & Wu, M. 2021. Pattern recognition receptors in health and diseases. *Signal Transduct Target Ther,* 6**,** 291.
Li, F., Yang, M., Wang, L., et al. 2012. Autofluorescence contributes to false-positive intracellular Foxp3 staining in macrophages: a lesson learned from flow cytometry. *J Immunol Methods,* 386**,** 101-7.
Li, P., Ma, C., Li, J., et al. 2022. Proteomic characterization of four subtypes of M2 macrophages derived from human THP-1 cells. *J Zhejiang Univ Sci B,* 23**,** 407-422.
Li, T., Li, X., Feng, Y., Dong, G., Wang, Y. & Yang, J. 2020b. The Role of Matrix Metalloproteinase-9 in Atherosclerotic Plaque Instability. *Mediators Inflamm,* 2020**,** 3872367.
Li, X., Ranjith-Kumar, C. T., Brooks, M. T., Dharmaiah, S., Herr, A. B., Kao, C. & Li, P. 2009. The RIG-I-like receptor LGP2 recognizes the termini of double-stranded RNA. *J Biol Chem,* 284**,** 13881-13891.
Libby, P. 2007. Inflammatory Mechanisms: The Molecular Basis of Inflammation and Disease. *Nutrition Reviews,* 65**,** 140-146.

Libby, P., Buring, J. E., Badimon, L., et al. 2019. Atherosclerosis. *Nat Rev Dis Primers,* 5**,** 56.
Lim, H. Y., Lim, S. Y., Tan, C. K., et al. 2018. Hyaluronan Receptor LYVE-1-Expressing Macrophages Maintain Arterial Tone through Hyaluronan-Mediated Regulation of Smooth Muscle Cell Collagen. *Immunity,* 49**,** 1191.
Limbu, R., Cottrell, G. S. & Mcneish, A. J. 2018. Characterisation of the vasodilation effects of DHA and EPA, n-3 PUFAs (fish oils), in rat aorta and mesenteric resistance arteries. *PLoS One,* 13**,** e0192484.
Lin, J. D., Nishi, H., Poles, J., et al. 2019. Single-cell analysis of fate-mapped macrophages reveals heterogeneity, including stem-like properties, during atherosclerosis progression and regression. *JCI Insight,* 4.
Lin, P., Ji, H. H., Li, Y. J. & Guo, S. D. 2021. Macrophage Plasticity and Atherosclerosis Therapy. *Front Mol Biosci,* 8**,** 679797.
Little, M. C., Hurst, R. J. & Else, K. J. 2014. Dynamic changes in macrophage activation and proliferation during the development and resolution of intestinal inflammation. *J Immunol,* 193**,** 4684-95.
Liu, H., Hu, J., Zheng, Q., et al. 2022a. Piezo1 Channels as Force Sensors in Mechanical Force-Related Chronic Inflammation. *Front Immunol,* 13**,** 816149.
Liu, L., Stokes, J. V., Tan, W. & Pruett, S. B. 2022b. An optimized flow cytometry panel for classifying macrophage polarization. *J Immunol Methods,* 511**,** 113378.
Liu, M., He, H. & Chen, L. 2022c. Protective Potential of Maresins in Cardiovascular Diseases. *Front Cardiovasc Med,* 9**,** 923413.
Liu, W., Yin, Y., Zhou, Z., He, M. & Dai, Y. 2014. OxLDL-induced IL-1 beta secretion promoting foam cells formation was mainly via CD36 mediated ROS production leading to NLRP3 inflammasome activation. *Inflamm Res,* 63**,** 33-43.
Liu, Y. J., Li, H., Tian, Y., et al. 2020. PCTR1 ameliorates lipopolysaccharide-induced acute inflammation and multiple organ damage via regulation of linoleic acid metabolism by promoting FADS1/FASDS2/ELOV2 expression and reducing PLA2 expression. *Lab Invest,* 100**,** 904-915.
Liu, Z., Gu, Y., Chakarov, S., et al. 2019. Fate Mapping via Ms4a3-Expression History Traces Monocyte-Derived Cells. *Cell,* 178**,** 1509-1525 e19.
Liu-Bryan, R., Pritzker, K., Firestein, G. S. & Terkeltaub, R. 2005. TLR2 signaling in chondrocytes drives calcium pyrophosphate dihydrate and monosodium urate crystal-induced nitric oxide generation. *J Immunol,* 174**,** 5016-23.
Lougheed, M., Lum, C. M., Ling, W., Suzuki, H., Kodama, T. & Steinbrecher, U. 1997. High affinity saturable uptake of oxidized low density lipoprotein by macrophages from mice lacking the scavenger receptor class A type I/II. *J Biol Chem,* 272**,** 12938-44.
Lougheed, M., Moore, E. D., Scriven, D. R. & Steinbrecher, U. P. 1999. Uptake of oxidized LDL by macrophages differs from that of acetyl LDL and leads to expansion of an acidic endolysosomal compartment. *Arterioscler Thromb Vasc Biol,* 19**,** 1881-90.
Lu, H. Y., Shih, C. M., Huang, C. Y., Wu, A. T. H., Cheng, T. M., Mi, F. L. & Shih, C. C. 2020. Galectin-3 Modulates Macrophage Activation and Contributes Smooth Muscle Cells Apoptosis in Abdominal Aortic Aneurysm Pathogenesis. *Int J Mol Sci,* 21.

Lu, Y. C., Yeh, W. C. & Ohashi, P. S. 2008. LPS/TLR4 signal transduction pathway. *Cytokine,* 42**,** 145-151.
Lund, J. M., Alexopoulou, L., Sato, A., et al. 2004. Recognition of single-stranded RNA viruses by Toll-like receptor 7. *Proc Natl Acad Sci U S A,* 101**,** 5598-603.
Luo, L., Zhu, M. & Zhou, J. 2018. Association between CTSS gene polymorphism and the risk of acute atherosclerotic cerebral infarction in Chinese population: a case-control study. *Biosci Rep,* 38.
Luo, Y., Duan, H., Qian, Y., et al. 2017. Macrophagic CD146 promotes foam cell formation and retention during atherosclerosis. *Cell Res,* 27**,** 352-372.
Luscinskas, F. W., Kansas, G. S., Ding, H., Pizcueta, P., Schleiffenbaum, B. E., Tedder, T. F. & Gimbrone, M. A., Jr. 1994. Monocyte Rolling, Arrest and Spreadingon IL-4-activated Vascular Endothelium under Flow Is Mediated via SequentialAction of L-Selectin, /31-Integrins,and/ 2-Integrins. *J Cell Biol,* 1417-1427.
Lyons, P. A., Koukoulaki, M., Hatton, A., Doggett, K., Woffendin, H. B., Chaudhry, A. N. & Smith, K. G. 2007. Microarray analysis of human leucocyte subsets: the advantages of positive selection and rapid purification. *BMC Genomics,* 8**,** 64.
Maecker, H. T. & Mccoy, P. J. 2010. A model for harmonizing flow cytometry in clinical trials. *Nature Immunology,* 11**,** 975-978.
Maecker, H. T. & Trotter, J. 2006. Flow cytometry controls, instrument setup, and the determination of positivity. *Cytometry A,* 69**,** 1037-42.
Mahdinia, E., Shokri, N., Taheri, A. T., Asgharzadeh, S., Elahimanesh, M. & Najafi, M. 2023. Cellular crosstalk in atherosclerotic plaque microenvironment. *Cell Commun Signal,* 21**,** 125.
Maiellaro, K. & Taylor, W. R. 2007. The role of the adventitia in vascular inflammation. *Cardiovasc Res,* 75**,** 640-8.
Malheiro, V., Elbs-Glatz, Y., Obarzanek-Fojt, M., Maniura-Weber, K. & Bruinink, A. 2017. Harvesting pre-polarized macrophages using thermo-responsive substrates. *Sci Rep,* 7**,** 42495.
Manson, J. E., Bassuk, S. S., Buring, J. E. & Group, V. R. 2020. Principal results of the VITamin D and OmegA-3 TriaL (VITAL) and updated meta-analyses of relevant vitamin D trials. *J Steroid Biochem Mol Biol,* 198**,** 105522.
Manta, C. P., Leibing, T., Friedrich, M., et al. 2022. Targeting of Scavenger Receptors Stabilin-1 and Stabilin-2 Ameliorates Atherosclerosis by a Plasma Proteome Switch Mediating Monocyte/Macrophage Suppression. *Circulation,* 146**,** 1783-1799.
Marcovecchio, P. M., Thomas, G. D., Mikulski, Z., et al. 2017. Scavenger Receptor CD36 Directs Nonclassical Monocyte Patrolling Along the Endothelium During Early Atherogenesis. *Arterioscler Thromb Vasc Biol,* 37**,** 2043-2052.
Martinez, F. O. & Gordon, S. 2014. The M1 and M2 paradigm of macrophage activation: time for reassessment. *F1000Prime Rep,* 6**,** 13.
Maskrey, B. H., Megson, I. L., Whitfield, P. D. & Rossi, A. G. 2011. Mechanisms of resolution of inflammation: a focus on cardiovascular disease. *Arterioscler Thromb Vasc Biol,* 31**,** 1001-6.
Mason, R. P., Dawoud, H., Jacob, R. F., Sherratt, S. C. R. & Malinski, T. 2018. Eicosapentaenoic acid improves endothelial function and nitric oxide bioavailability in a manner that is enhanced in combination with a statin. *Biomed Pharmacother,* 103**,** 1231-1237.

Mason, R. P., Libby, P. & Bhatt, D. L. 2020. Emerging Mechanisms of Cardiovascular Protection for the Omega-3 Fatty Acid Eicosapentaenoic Acid. *Arterioscler Thromb Vasc Biol,* 40**,** 1135-1147.
Mass, E., Nimmerjahn, F., Kierdorf, K. & Schlitzer, A. 2023. Tissue-specific macrophages: how they develop and choreograph tissue biology. *Nat Rev Immunol,* 23**,** 563-579.
Massberg, S., Brand, K., Gruner, S., et al. 2002. A critical role of platelet adhesion in the initiation of atherosclerotic lesion formation. *J Exp Med,* 196**,** 887-96.
Masseau, I. & Bowles, D. K. 2015. Carotid Endothelial VCAM-1 Is an Early Marker of Carotid Atherosclerosis and Predicts Coronary Artery Disease in Swine. *J Biomed Sci Eng,* 8**,** 789-796.
Matsumoto, M., Sata, M., Fukuda, D., Tanaka, K., Soma, M., Hirata, Y. & Nagai, R. 2008. Orally administered eicosapentaenoic acid reduces and stabilizes atherosclerotic lesions in ApoE-deficient mice. *Atherosclerosis,* 197**,** 524-33.
Matsuo, M., Ito, F., Konto, A., Aketa, M., Tomoi, M. & Shimomura, K. 1995. Effect of FR145237, a novel ACAT inhibitor, on atherogenesis in cholesterol-fed and WHHL rabbits. Evidence for a direct effect on the arterial wall. *Biochim Biophys Acta,* 1259**,** 254-60.
May, A. E., Neumann, F.-J., SchöMig, A. & Preissner, K. T. 2000. VLA-4 (α4β1) engagement defines a novel activation pathway for β2 integrin–dependent leukocyte adhesion involving the urokinase receptor. *Blood,* 96**,** 506-513.
Mcever, R. P. & Cummings, R. D. 1997. Role of PSGL-1 binding to selectins in leukocyte recruitment. *J Clin Invest,* 100**,** S97-104.
Medzhitov, R. 2008. Origin and physiological roles of inflammation. *Nature,* 454**,** 428-35.
Medzhitov, R. 2010. Inflammation 2010: new adventures of an old flame. *Cell,* 140**,** 771-6.
Mehta-D'souza, P., Klopocki, A. G., Oganesyan, V., et al. 2017. Glycan Bound to the Selectin Low Affinity State Engages Glu-88 to Stabilize the High Affinity State under Force. *J Biol Chem,* 292**,** 2510-2518.
Meletta, R., Muller Herde, A., Dennler, P., Fischer, E., Schibli, R. & Kramer, S. D. 2016. Preclinical imaging of the co-stimulatory molecules CD80 and CD86 with indium-111-labeled belatacept in atherosclerosis. *EJNMMI Res,* 6**,** 1.
Menegaut, L., Jalil, A., Thomas, C. & Masson, D. 2019. Macrophage fatty acid metabolism and atherosclerosis: The rise of PUFAs. *Atherosclerosis,* 291**,** 52-61.
Merad, M., Sathe, P., Helft, J., Miller, J. & Mortha, A. 2013. The dendritic cell lineage: ontogeny and function of dendritic cells and their subsets in the steady state and the inflamed setting. *Annu Rev Immunol,* 31**,** 563-604.
Merah-Mourah, F., Cohen, S. O., Charron, D., Mooney, N. & Haziot, A. 2020. Identification of Novel Human Monocyte Subsets and Evidence for Phenotypic Groups Defined by Interindividual Variations of Expression of Adhesion Molecules. *Sci Rep,* 10**,** 4397.
Michalak, A., Mosinska, P. & Fichna, J. 2016. Polyunsaturated Fatty Acids and Their Derivatives: Therapeutic Value for Inflammatory, Functional Gastrointestinal Disorders, and Colorectal Cancer. *Front Pharmacol,* 7**,** 459.
Michlewska, S., Dransfield, I., Megson, I. L. & Rossi, A. G. 2009. Macrophage phagocytosis of apoptotic neutrophils is critically regulated by the opposing

actions of pro-inflammatory and anti-inflammatory agents: key role for TNF-alpha. *FASEB J,* 23**,** 844-54.
Mikita, T., Porter, G., Lawn, R. M. & Shiffman, D. 2001. Oxidized low density lipoprotein exposure alters the transcriptional response of macrophages to inflammatory stimulus. *J Biol Chem,* 276**,** 45729-39.
Milutinovic, A., Suput, D. & Zorc-Pleskovic, R. 2020. Pathogenesis of atherosclerosis in the tunica intima, media, and adventitia of coronary arteries: An updated review. *Bosn J Basic Med Sci,* 20**,** 21-30.
Misharin, A. V., Morales-Nebreda, L., Mutlu, G. M., Budinger, G. R. & Perlman, H. 2013. Flow cytometric analysis of macrophages and dendritic cell subsets in the mouse lung. *Am J Respir Cell Mol Biol,* 49**,** 503-10.
Mitchell, J. A., Ali, F., Bailey, L., Moreno, L. & Harrington, L. S. 2008. Role of nitric oxide and prostacyclin as vasoactive hormones released by the endothelium. *Exp Physiol,* 93**,** 141-7.
Mitroulis, I., Alexaki, V. I., Kourtzelis, I., Ziogas, A., Hajishengallis, G. & Chavakis, T. 2015. Leukocyte integrins: role in leukocyte recruitment and as therapeutic targets in inflammatory disease. *Pharmacol Ther,* 147**,** 123-135.
Moazzam, F., Delano, F. A., Zweifach, B. W. & Schmid-Schonbein, G. W. 1997. The leukocyte response to fluid shear stress. *Proc Natl Acad Sci U S A,* 94**,** 5338-5343.
Mogensen, T. H. 2009. Pathogen recognition and inflammatory signaling in innate immune defenses. *Clin Microbiol Rev,* 22**,** 240-73, Table of Contents.
Mohd Idrus, F. N., Ahmad, N. S., Hoe, C. H., et al. 2021. Differential polarization and the expression of efferocytosis receptor MerTK on M1 and M2 macrophages isolated from coronary artery disease patients. *BMC Immunol,* 22**,** 21.
Moore, K. J. & Freeman, M. W. 2006. Scavenger receptors in atherosclerosis: beyond lipid uptake. *Arterioscler Thromb Vasc Biol,* 26**,** 1702-11.
Moore, K. J., Kunjathoor, V. V., Koehn, S. L., et al. 2005. Loss of receptor-mediated lipid uptake via scavenger receptor A or CD36 pathways does not ameliorate atherosclerosis in hyperlipidemic mice. *J Clin Invest,* 115**,** 2192-201.
Moore, K. J., Sheedy, F. J. & Fisher, E. A. 2013. Macrophages in atherosclerosis: a dynamic balance. *Nat Rev Immunol,* 13**,** 709-21.
Moore, K. J. & Tabas, I. 2011. Macrophages in the pathogenesis of atherosclerosis. *Cell,* 145**,** 341-55.
Moradi Sarabi, M., Doosti, M., Einollahi, N., Hesami, S. S. & Dashti, N. 2014. Effect of eicosapentaenoic acid on the expression of ABCG1 gene in the human monocyte THP-1 cells. *Acta Med Iran,* 52**,** 176-81.
Moss, J. W., Davies, T. S., Garaiova, I., Plummer, S. F., Michael, D. R. & Ramji, D. P. 2016. A Unique Combination of Nutritionally Active Ingredients Can Prevent Several Key Processes Associated with Atherosclerosis In Vitro. *PLoS One,* 11**,** e0151057.
Mosser, D. M. & Edwards, J. P. 2008. Exploring the full spectrum of macrophage activation. *Nat Rev Immunol,* 8**,** 958-69.
Mu, W., Chen, M., Gong, Z., Zheng, F. & Xing, Q. 2015. Expression of vascular cell adhesion molecule-1 in the aortic tissues of atherosclerotic patients and the associated clinical implications. *Exp Ther Med,* 10**,** 423-428.

Mukherjee, R., Kanti Barman, P., Kumar Thatoi, P., Tripathy, R., Kumar Das, B. & Ravindran, B. 2015. Non-Classical monocytes display inflammatory features: Validation in Sepsis and Systemic Lupus Erythematous. *Sci Rep,* 5**,** 13886.
Munch, G., Bultmann, A., Li, Z., Holthoff, H. P., Ullrich, J., Wagner, S. & Ungerer, M. 2012. Overexpression of ABCG1 protein attenuates arteriosclerosis and endothelial dysfunction in atherosclerotic rabbits. *Heart Int,* 7**,** e12.
Munoz-Rojas, A. R., Kelsey, I., Pappalardo, J. L., Chen, M. & Miller-Jensen, K. 2021. Co-stimulation with opposing macrophage polarization cues leads to orthogonal secretion programs in individual cells. *Nat Commun,* 12**,** 301.
Murphy, A. J. & Tall, A. R. 2014. Proliferating macrophages populate established atherosclerotic lesions. *Circ Res,* 114**,** 236-8.
Murray, P. J. & Wynn, T. A. 2011. Protective and pathogenic functions of macrophage subsets. *Nat Rev Immunol,* 11**,** 723-37.
Musson, R. A. 1983. Human serum induces maturation of human monocytes in vitro. Changes in cytolytic activity, intracellular lysosomal enzymes, and nonspecific esterase activity. *Am J Pathol,* 111**,** 331-340.
Nagatake, T., Shibata, Y., Morimoto, S., et al. 2021. 12-Hydroxyeicosapentaenoic acid inhibits foam cell formation and ameliorates high-fat diet-induced pathology of atherosclerosis in mice. *Sci Rep,* 11**,** 10426.
Nagy, L., Tontonoz, P., Alvarez, J. G., Chen, H. & Evans, R. M. 1998. Oxidized LDL regulates macrophage gene expression through ligand activation of PPARgamma. *Cell,* 93**,** 229-40.
Nahon, J. E., Hoekstra, M., Van Hulst, S., et al. 2019. Hematopoietic Stabilin-1 deficiency does not influence atherosclerosis susceptibility in LDL receptor knockout mice. *Atherosclerosis,* 281**,** 47-55.
Nahrendorf, M., Swirski, F. K., Aikawa, E., et al. 2007. The healing myocardium sequentially mobilizes two monocyte subsets with divergent and complementary functions. *J Exp Med,* 204**,** 3037-47.
Naito, M., Takahashi, K. & Nishikawa, S. 1990. Development, differentiation, and maturation of macrophages in the fetal mouse liver. *J Leukoc Biol,* 48**,** 27-37.
Nakashima, Y., Raines, E. W., Plump, A. S., Breslow, J. L. & Ross, R. 1998. Upregulation of VCAM-1 and ICAM-1 at atherosclerosis-prone sites on the endothelium in the ApoE-deficient mouse. *Arterioscler Thromb Vasc Biol,* 18**,** 842-51.
Nathan, C. & Ding, A. 2010. Nonresolving inflammation. *Cell,* 140**,** 871-82.
Nguyen, R., Perfetto, S., Mahnke, Y. D., Chattopadhyay, P. & Roederer, M. 2013. Quantifying spillover spreading for comparing instrument performance and aiding in multicolor panel design. *Cytometry A,* 83**,** 306-15.
Nicholson, A. C., Frieda, S., Pearce, A. & Silverstein, R. 1995. Oxidised LDL binds to CD36 on human monocyte-derived macrophages and transfcted cell lines. *Ateriosclerosis Thromb Biol,* 15**,** 269-275.
Nickel, T., Schmauss, D., Hanssen, H., et al. 2009. oxLDL uptake by dendritic cells induces upregulation of scavenger-receptors, maturation and differentiation. *Atherosclerosis,* 205**,** 442-50.
Nicolosi, R. J., Wilson, T. A. & Krause, B. R. 1998. The ACAT inhibitor, CI-1011 is effective in the prevention and regression of aortic fatty streak area in hamsters. *Atherosclerosis,* 137**,** 77-85.

Nielsen, M. C., Andersen, M. N. & Moller, H. J. 2020. Monocyte isolation techniques significantly impact the phenotype of both isolated monocytes and derived macrophages in vitro. *Immunology,* 159**,** 63-74.
Njoroge, J. M., Mitchell, L. B., Centola, M., Kastner, D., Raffeld, M. & Miller, J. L. 2001. Characterization of viable autofluorescent macrophages among cultured peripheral blood mononuclear cells. *Cytometry,* 44**,** 38-44.
Noble, K. E., Panayiotidis, P., Collins, P. W., Hoffbrand, A. V. & Yong, K. L. 1996. Monocytes induce E-selectin gene expression in endothelial cells: role of CD11/CD18 and extracellular matrix proteins. *Eur J Immunol,* 26**,** 2944-51.
Nogiec, A., Bzowska, M., Demczuk, A., Varol, C. & Guzik, K. 2020. Phenotype and Response to PAMPs of Human Monocyte-Derived Foam Cells Obtained by Long-Term Culture in the Presence of oxLDLs. *Front Immunol,* 11**,** 1592.
Nogieć, A., Bzowska, M., Demczuk, A., Varol, C. & Guzik, K. 2020. Phenotype and Response to PAMPs of Human Monocyte-Derived Foam Cells Obtained by Long-Term Culture in the Presence of oxLDLs. *Front Immunol,* 11**,** 1592.
Nourshargh, S. & Alon, R. 2014. Leukocyte migration into inflamed tissues. *Immunity,* 41**,** 694-707.
Ohlsson, B. G., Englund, M. C., Karlsson, A. L., et al. 1996. Oxidized low density lipoprotein inhibits lipopolysaccharide-induced binding of nuclear factor-kappaB to DNA and the subsequent expression of tumor necrosis factor-alpha and interleukin-1beta in macrophages. *J Clin Invest,* 98**,** 78-89.
Okabe, Y. & Medzhitov, R. 2014. Tissue-specific signals control reversible program of localization and functional polarization of macrophages. *Cell,* 157**,** 832-44.
Omura, M., Kobayashi, S., Mizukami, Y., Mogami, K., Todoroki-Ikeda, N., Miyake, T. & Matsuzaki, M. 2001. Eicosapentaenoic acid (EPA) induces Ca(2+)-independent activation and translocation of endothelial nitric oxide synthase and endothelium-dependent vasorelaxation. *FEBS Lett,* 487**,** 361-6.
Orekhov, A. N., Sukhorukov, V. N., Nikiforov, N. G., et al. 2020. Signaling Pathways Potentially Responsible for Foam Cell Formation: Cholesterol Accumulation or Inflammatory Response-What is First? *Int J Mol Sci,* 21.
Ostermann, G., Weber, K. S., Zernecke, A., Schroder, A. & Weber, C. 2002. JAM-1 is a ligand of the beta(2) integrin LFA-1 involved in transendothelial migration of leukocytes. *Nat Immunol,* 3**,** 151-8.
Østerud, B. & Bjørklid, E. 2003. Role of Monocytes in Atherogenesis. *Physiol. Rev.,* 83**,** 1069-1112.
Ott, L. W., Resing, K. A., Sizemore, A. W., et al. 2007. Tumor Necrosis Factor-alpha- and interleukin-1-induced cellular responses: coupling proteomic and genomic information. *J Proteome Res,* 6**,** 2176-85.
Ouimet, M., Barrett, T. J. & Fisher, E. A. 2019. HDL and Reverse Cholesterol Transport. *Circ Res,* 124**,** 1505-1518.
Ouimet, M., Franklin, V., Mak, E., Liao, X., Tabas, I. & Marcel, Y. L. 2011. Autophagy regulates cholesterol efflux from macrophage foam cells via lysosomal acid lipase. *Cell Metab,* 13**,** 655-67.
Owsiany, K. M., Alencar, G. F. & Owens, G. K. 2019. Revealing the Origins of Foam Cells in Atherosclerotic Lesions. *Arterioscler Thromb Vasc Biol,* 39**,** 836-838.
Pang, L. & Knox, A. J. 1997. Effect of interleukin-1 beta, tumour necrosis factor-alpha and interferon-gamma on the induction of cyclo-oxygenase-2 in cultured human airway smooth muscle cells. *Br J Pharmacol,* 121**,** 579-87.

Papaspyridonos, M., Mcneill, E., De Bono, J. P., Smith, A., Burnand, K. G., Channon, K. M. & Greaves, D. R. 2008. Galectin-3 is an amplifier of inflammation in atherosclerotic plaque progression through macrophage activation and monocyte chemoattraction. *Arterioscler Thromb Vasc Biol,* 28**,** 433-40.
Park, B. S., Song, D. H., Kim, H. M., Choi, B. S., Lee, H. & Lee, J. O. 2009. The structural basis of lipopolysaccharide recognition by the TLR4-MD-2 complex. *Nature,* 458**,** 1191-5.
Park, J. Y., Pillinger, M. H. & Abramson, S. B. 2006. Prostaglandin E2 synthesis and secretion: the role of PGE2 synthases. *Clin Immunol,* 119**,** 229-40.
Park, M. D., Silvin, A., Ginhoux, F. & Merad, M. 2022. Macrophages in health and disease. *Cell,* 185**,** 4259-4279.
Passlick, B., Flieger, D. & Ziegler-Heitbrock, H. W. 1989. Identification and characterization of a novel monocyte subpopulation in human peripheral blood. *Blood,* 74**,** 2527-2534.
Pastore, M., Grimaudo, S., Pipitone, R. M., Lori, G., Raggi, C., Petta, S. & Marra, F. 2019. Role of Myeloid-Epithelial-Reproductive Tyrosine Kinase and Macrophage Polarization in the Progression of Atherosclerotic Lesions Associated With Nonalcoholic Fatty Liver Disease. *Front Pharmacol,* 10**,** 604.
Patel, A. A., Zhang, Y., Fullerton, J. N., et al. 2017. The fate and lifespan of human monocyte subsets in steady state and systemic inflammation. *J Exp Med,* 214**,** 1913-1923.
Patterson, M. T., Firulyova, M. M., Xu, Y., et al. 2023. Trem2 promotes foamy macrophage lipid uptake and survival in atherosclerosis. *Nat Cardiovasc Res,* 2**,** 1015-1031.
Pennathur, S., Pasichnyk, K., Bahrami, N. M., Zeng, L., Febbraio, M., Yamaguchi, I. & Okamura, D. M. 2015. The macrophage phagocytic receptor CD36 promotes fibrogenic pathways on removal of apoptotic cells during chronic kidney injury. *Am J Pathol,* 185**,** 2232-45.
Perrot, C. Y., Herrera, J. L., Fournier-Goss, A. E. & Komatsu, M. 2020. Prostaglandin E2 breaks down pericyte-endothelial cell interaction via EP1 and EP4-dependent downregulation of pericyte N-cadherin, connexin-43, and R-Ras. *Sci Rep,* 10**,** 11186.
Piechota, M., Banaszewska, A., Dudziak, J., Slomczynski, M. & Plewa, R. 2012. Highly upregulated expression of CD36 and MSR1 in circulating monocytes of patients with acute coronary syndromes. *Protein J,* 31**,** 511-8.
Pilkington, S. M., Rhodes, L. E., Al-Aasswad, N. M., Massey, K. A. & Nicolaou, A. 2014. Impact of EPA ingestion on COX- and LOX-mediated eicosanoid synthesis in skin with and without a pro-inflammatory UVR challenge--report of a randomised controlled study in humans. *Mol Nutr Food Res,* 58**,** 580-90.
Pillois, X., Gautier, T., Bouillet, B., et al. 2012. Constitutive inhibition of plasma CETP by apolipoprotein C1 is blunted in dyslipidemic patients with coronary artery disease. *J Lipid Res,* 53**,** 1200-9.
Pirro, M., Schoof, E., Van Vliet, S. J., et al. 2019. Glycoproteomic Analysis of MGL-Binding Proteins on Acute T-Cell Leukemia Cells. *J Proteome Res,* 18**,** 1125-1132.
Plump, A. S., Smith, J. D., Hayek, T., et al. 1992. Severe hypercholesterolemia and atherosclerosis in apolipoprotein E-deficient mice created by homologous recombination in ES cells. *Cell,* 71**,** 343-53.

Pober, J. S. & Sessa, W. C. 2007. Evolving functions of endothelial cells in inflammation. *Nat Rev Immunol,* 7**,** 803-15.
Podrez, E. A., Febbraio, M., Sheibani, N., et al. 2000. Macrophage scavenger receptor CD36 is the major receptor for LDL modified by monocyte-generated reactive nitrogen species. *J Clin Invest,* 105**,** 1095-108.
Porcheray, F., Viaud, S., Rimaniol, A. C., et al. 2005. Macrophage activation switching: an asset for the resolution of inflammation. *Clin Exp Immunol,* 142**,** 481-9.
Raggatt, L. J., Wullschleger, M. E., Alexander, K. A., et al. 2014. Fracture healing via periosteal callus formation requires macrophages for both initiation and progression of early endochondral ossification. *Am J Pathol,* 184**,** 3192-204.
Raggi, F., Pelassa, S., Pierobon, D., et al. 2017. Regulation of Human Macrophage M1-M2 Polarization Balance by Hypoxia and the Triggering Receptor Expressed on Myeloid Cells-1. *Front Immunol,* 8**,** 1097.
Rahman, K. & Fisher, E. A. 2018. Insights From Pre-Clinical and Clinical Studies on the Role of Innate Inflammation in Atherosclerosis Regression. *Front Cardiovasc Med,* 5**,** 32.
Rahman, Z. S., Shao, W. H., Khan, T. N., Zhen, Y. & Cohen, P. L. 2010. Impaired apoptotic cell clearance in the germinal center by Mer-deficient tingible body macrophages leads to enhanced antibody-forming cell and germinal center responses. *J Immunol,* 185**,** 5859-68.
Rainger, G. E., Fisher, A. C. & G.B. Nash 1997. Endothelial-borne platelet-activating factor and interleukin-8 rapidly immobilize rolling neutrophils. *Am J Physiol,* 272**,** 114-122.
Ramon, S., Dalli, J., Sanger, J. M., et al. 2016. The Protectin PCTR1 Is Produced by Human M2 Macrophages and Enhances Resolution of Infectious Inflammation. *Am J Pathol,* 186**,** 962-73.
Rantakari, P., Patten, D. A., Valtonen, J., et al. 2016. Stabilin-1 expression defines a subset of macrophages that mediate tissue homeostasis and prevent fibrosis in chronic liver injury. *Proc Natl Acad Sci U S A,* 113**,** 9298-303.
Reschen, M. E., Gaulton, K. J., Lin, D., Soilleux, E. J., Morris, A. J., Smyth, S. S. & O'callaghan, C. A. 2015. Lipid-induced epigenomic changes in human macrophages identify a coronary artery disease-associated variant that regulates PPAP2B Expression through Altered C/EBP-beta binding. *PLoS Genet,* 11**,** e1005061.
Richards, D. M., Hettinger, J. & Feuerer, M. 2013. Monocytes and macrophages in cancer: development and functions. *Cancer Microenviron,* 6**,** 179-91.
Rinder, H. M., Bonan, J. L., Rinder, C. S., Ault, K. A. & Smith, B. R. 1991. Dynamics of leukocyte-platelet adhesion in whole blood. *Blood,* 78**,** 1730-7.
Rittchen, S. & Heinemann, A. 2019. Therapeutic Potential of Hematopoietic Prostaglandin D(2) Synthase in Allergic Inflammation. *Cells,* 8.
Rittchen, S., Rohrer, K., Platzer, W., et al. 2020. Prostaglandin D(2) strengthens human endothelial barrier by activation of E-type receptor 4. *Biochem Pharmacol,* 182**,** 114277.
Robbins, C. S., Chudnovskiy, A., Rauch, P. J., et al. 2012. Extramedullary hematopoiesis generates Ly-6C(high) monocytes that infiltrate atherosclerotic lesions. *Circulation,* 125**,** 364-74.

Robbins, C. S., Hilgendorf, I., Weber, G. F., et al. 2013. Local proliferation dominates lesional macrophage accumulation in atherosclerosis. *Nat Med,* 19**,** 1166-72.
Robbins, C. S. & Swirski, F. K. 2010. The multiple roles of monocyte subsets in steady state and inflammation. *Cell Mol Life Sci,* 67**,** 2685-93.
Robichaud, S., Fairman, G., Vijithakumar, V., et al. 2021. Identification of novel lipid droplet factors that regulate lipophagy and cholesterol efflux in macrophage foam cells. *Autophagy,* 17**,** 3671-3689.
Robichaud, S., Rasheed, A., Pietrangelo, A., et al. 2022. Autophagy Is Differentially Regulated in Leukocyte and Nonleukocyte Foam Cells During Atherosclerosis. *Circ Res,* 130**,** 831-847.
Rogacev, K. S., Cremers, B., Zawada, A. M., et al. 2012. CD14++CD16+ monocytes independently predict cardiovascular events: a cohort study of 951 patients referred for elective coronary angiography. *J Am Coll Cardiol,* 60**,** 1512-20.
Rogers, M. A., Liu, J., Song, B. L., Li, B. L., Chang, C. C. & Chang, T. Y. 2015. Acyl-CoA:cholesterol acyltransferases (ACATs/SOATs): Enzymes with multiple sterols as substrates and as activators. *J Steroid Biochem Mol Biol,* 151**,** 102-7.
Ross, R. 1995. Cell biology of atherosclerosis. *Annu Rev Physiol,* 57**,** 791-804.
Rostam, H. M., Reynolds, P. M., Alexander, M. R., Gadegaard, N. & Ghaemmaghami, A. M. 2017. Image based Machine Learning for identification of macrophage subsets. *Sci Rep,* 7**,** 3521.
Roussel, M., Ferrell, P. B., Jr., Greenplate, A. R., et al. 2017. Mass cytometry deep phenotyping of human mononuclear phagocytes and myeloid-derived suppressor cells from human blood and bone marrow. *J Leukoc Biol,* 102**,** 437-447.
Rugtveit, J., Scott, H., Halstensen, T. S., Norstein, J. & Brandtzaeg, P. 1996. Expression of the L1 antigen (calprotectin) by tissue macrophages reflects recent recruitment from peripheral blood rather than upregulation of local synthesis: implications for rejection diagnosis in formalin-fixed kidney specimens. *J Pathol,* 180**,** 194-9.
Sadhu, C., Ting, H. J., Lipsky, B., Hensley, K., Garcia-Martinez, L. F., Simon, S. I. & Staunton, D. E. 2007. CD11c/CD18: novel ligands and a role in delayed-type hypersensitivity. *J Leukoc Biol,* 81**,** 1395-403.
Safi, W., Kuehnl, A., Nussler, A., Eckstein, H. H. & Pelisek, J. 2016. Differentiation of human CD14+ monocytes: an experimental investigation of the optimal culture medium and evidence of a lack of differentiation along the endothelial line. *Exp Mol Med,* 48**,** e227.
Sahbandar, I. N., Ndhlovu, L. C., Saiki, K., et al. 2020. Relationship between Circulating Inflammatory Monocytes and Cardiovascular Disease Measures of Carotid Intimal Thickness. *J Atheroscler Thromb,* 27**,** 441-448.
Saito, T. & Gale, M., Jr. 2008. Differential recognition of double-stranded RNA by RIG-I-like receptors in antiviral immunity. *J Exp Med,* 205**,** 1523-7.
Salehipour, M., Javadi, E., Reza, J. Z., et al. 2010. Polyunsaturated fatty acids and modulation of cholesterol homeostasis in THP-1 macrophage-derived foam cells. *Int J Mol Sci,* 11**,** 4660-72.
Saliba-Gustafsson, P., Pedrelli, M., Gertow, K., et al. 2019. Subclinical atherosclerosis and its progression are modulated by PLIN2 through a feed-forward loop between LXR and autophagy. *J Intern Med,* 286**,** 660-675.

Salina, A. C. G., Brandt, S. L., Klopfenstein, N., et al. 2020. Leukotriene B(4) licenses inflammasome activation to enhance skin host defense. *Proc Natl Acad Sci U S A,* 117**,** 30619-30627.
Santana Nunez, D., Malik, A. B., Lee, Q., et al. 2023. Piezo1 induces endothelial responses to shear stress via soluble adenylyl Cyclase-IP(3)R2 circuit. *iScience,* 26**,** 106661.
Schober, A., Zernecke, A., Liehn, E. A., Von Hundelshausen, P., Knarren, S., Kuziel, W. A. & Weber, C. 2004. Crucial role of the CCL2/CCR2 axis in neointimal hyperplasia after arterial injury in hyperlipidemic mice involves early monocyte recruitment and CCL2 presentation on platelets. *Circ Res,* 95**,** 1125-33.
Schrijvers, D. M., De Meyer, G. R., Herman, A. G. & Martinet, W. 2007. Phagocytosis in atherosclerosis: Molecular mechanisms and implications for plaque progression and stability. *Cardiovasc Res,* 73**,** 470-80.
Schuh, J., Fairclough, G. F., Jr. & Haschemeyer, R. H. 1978. Oxygen-mediated heterogeneity of apo-low-density lipoprotein. *Proc Natl Acad Sci U S A,* 75**,** 3173-7.
Schwab, J. M., Chiang, N., Arita, M. & Serhan, C. N. 2007. Resolvin E1 and protectin D1 activate inflammation-resolution programmes. *Nature,* 447**,** 869-74.
Scott, S. R., Mcmahon, E. J., Pop, S. M., et al. 2001. Phagocytosis and clearance of apoptotic cells is mediated by MER. *nature,* 411**,** 207-211.
Scott, T. E., Lewis, C. V., Zhu, M., Wang, C., Samuel, C. S., Drummond, G. R. & Kemp-Harper, B. K. 2023. IL-4 and IL-13 induce equivalent expression of traditional M2 markers and modulation of reactive oxygen species in human macrophages. *Sci Rep,* 13**,** 19589.
Seimon, T. A., Nadolski, M. J., Liao, X., et al. 2010. Atherogenic lipids and lipoproteins trigger CD36-TLR2-dependent apoptosis in macrophages undergoing endoplasmic reticulum stress. *Cell Metab,* 12**,** 467-82.
Sekimoto, T., Koba, S., Mori, H., et al. 2023. Association between Eicosapentaenoic Acid to Arachidonic Acid Ratio and Characteristics of Plaque Rupture. *J Atheroscler Thromb,* 30**,** 1687-1702.
Sekiya, M., Osuga, J., Nagashima, S., et al. 2009. Ablation of neutral cholesterol ester hydrolase 1 accelerates atherosclerosis. *Cell Metab,* 10**,** 219-28.
Sekiya, M., Yamamuro, D., Ohshiro, T., et al. 2014. Absence of Nceh1 augments 25-hydroxycholesterol-induced ER stress and apoptosis in macrophages. *J Lipid Res,* 55**,** 2082-92.
Senbanerjee, S., Lin, Z., Atkins, G. B., et al. 2004. KLF2 Is a novel transcriptional regulator of endothelial proinflammatory activation. *J Exp Med,* 199**,** 1305-15.
Seo, J. W., Yang, E. J., Yoo, K. H. & Choi, I. H. 2015. Macrophage Differentiation from Monocytes Is Influenced by the Lipid Oxidation Degree of Low Density Lipoprotein. *Mediators Inflamm,* 2015**,** 235797.
Serbina, N. V., Jia, T., Hohl, T. M. & Pamer, E. G. 2008. Monocyte-mediated defense against microbial pathogens. *Annu Rev Immunol,* 26**,** 421-52.
Serbina, N. V. & Pamer, E. G. 2006. Monocyte emigration from bone marrow during bacterial infection requires signals mediated by chemokine receptor CCR2. *Nat Immunol,* 7**,** 311-7.
Serhan, C. N. 2005. Lipoxins and aspirin-triggered 15-epi-lipoxins are the first lipid mediators of endogenous anti-inflammation and resolution. *Prostaglandins Leukot Essent Fatty Acids,* 73**,** 141-62.

Serhan, C. N., Chiang, N. & Van Dyke, T. E. 2008. Resolving inflammation: dual anti-inflammatory and pro-resolution lipid mediators. *Nat Rev Immunol,* 8**,** 349-61.
Serhan, C. N., Clish, C. B., Brannon, J., Colgan, S. P., Chiang, N. & Gronert, K. 2000. Novel functional sets of lipid-derived mediators with antiinflammatory actions generated from omega-3 fatty acids via cyclooxygenase 2-nonsteroidal antiinflammatory drugs and transcellular processing. *J Exp Med,* 192**,** 1197-204.
Sethi, S., Ziouzenkova, O., Ni, H., Wagner, D. D., Plutzky, J. & Mayadas, T. N. 2002. Oxidized omega-3 fatty acids in fish oil inhibit leukocyte-endothelial interactions through activation of PPAR alpha. *Blood,* 100**,** 1340-6.
Sheikh, S., Rainger, G. E., Gale, Z., Rahman, M. & Nash, G. B. 2003. Exposure to fluid shear stress modulates the ability of endothelial cells to recruit neutrophils in response to tumor necrosis factor-alpha: a basis for local variations in vascular sensitivity to inflammation. *Blood,* 102**,** 2828-34.
Shen, W. J., Azhar, S. & Kraemer, F. B. 2018. SR-B1: A Unique Multifunctional Receptor for Cholesterol Influx and Efflux. *Annu Rev Physiol,* 80**,** 95-116.
Sheppe, A. E. F. & Edelmann, M. J. 2021. Roles of Eicosanoids in Regulating Inflammation and Neutrophil Migration as an Innate Host Response to Bacterial Infections. *Infect Immun,* 89**,** e0009521.
Shi, C. & Pamer, E. G. 2011. Monocyte recruitment during infection and inflammation. *Nat Rev Immunol,* 11**,** 762-74.
Shirakura, K., Baluk, P., Nottebaum, A. F., Ipe, U., Peters, K. G., Mcdonald, D. M. & Vestweber, D. 2023. Shear stress control of vascular leaks and atheromas through Tie2 activation by VE-PTP sequestration. *EMBO Mol Med,* 15**,** e16128.
Singaraja, R. R., Fievet, C., Castro, G., et al. 2002. Increased ABCA1 activity protects against atherosclerosis. *J Clin Invest,* 110**,** 35-42.
Siriwardhana, N., Kalupahana, N. S., Fletcher, S., et al. 2012. n-3 and n-6 polyunsaturated fatty acids differentially regulate adipose angiotensinogen and other inflammatory adipokines in part via NF-kappaB-dependent mechanisms. *J Nutr Biochem,* 23**,** 1661-7.
Smiljanovic, B., Radzikowska, A., Kuca-Warnawin, E., et al. 2018. Monocyte alterations in rheumatoid arthritis are dominated by preterm release from bone marrow and prominent triggering in the joint. *Ann Rheum Dis,* 77**,** 300-308.
Soehnlein, O., Drechsler, M., Doring, Y., et al. 2013. Distinct functions of chemokine receptor axes in the atherogenic mobilization and recruitment of classical monocytes. *EMBO Mol Med,* 5**,** 471-81.
Soehnlein, O. & Libby, P. 2021. Targeting inflammation in atherosclerosis - from experimental insights to the clinic. *Nat Rev Drug Discov,* 20**,** 589-610.
Song, Z., Lv, S., Wu, H., Qin, L., Cao, H., Zhang, B. & Ren, S. 2020. Identification of foam cell biomarkers by microarray analysis. *BMC Cardiovasc Disord,* 20**,** 211.
Spann, N. J., Garmire, L. X., Mcdonald, J. G., et al. 2012. Regulated accumulation of desmosterol integrates macrophage lipid metabolism and inflammatory responses. *Cell,* 151**,** 138-52.
Sparrow, C. P., Parthasarathy, S. & Steinberg, D. 1989. A macrophage receptor that recognizes oxidized low density lipoprotein but not acetylated low density lipoprotein. *J Biol Chem,* 264**,** 2599-604.

Spite, M., Claria, J. & Serhan, C. N. 2014. Resolvins, specialized proresolving lipid mediators, and their potential roles in metabolic diseases. *Cell Metab,* 19**,** 21-36.
Staprans, I., Pan, X. M., Rapp, J. H., Grunfeld, C. & Feingold, K. R. 2000. Oxidized cholesterol in the diet accelerates the development of atherosclerosis in LDL receptor- and apolipoprotein E-deficient mice. *Arterioscler Thromb Vasc Biol,* 20**,** 708-14.
Stary, H. C. 1989. Evolution and progression of atherosclerotic lesions in coronary arteries of children and young adults. *Arteriosclerosis,* 9**,** I19-32.
Stary, H. C. 2000. Natural history and histological classification of atherosclerotic lesions: an update. *Arterioscler Thromb Vasc Biol,* 20**,** 1177-8.
Stein, M., Keshav, S., Harris, N. & Gordon, S. 1992. Interleukin 4 potently enhances murine macrophages mannose receptor activity: a marker of alternative immunologic macrophage activation. *J Exp Med,* 176**,** 287-292.
Steinl, D. C. & Kaufmann, B. A. 2015. Ultrasound imaging for risk assessment in atherosclerosis. *Int J Mol Sci,* 16**,** 9749-69.
Stemme, S., Faber, B., Holm, J., Wiklund, O., Witztum, J. L. & Hansson, G. K. 1995. T lymphocytes from human atherosclerotic plaques recognize oxidized low density lipoprotein. *Proc Natl Acad Sci U S A,* 92**,** 3893-7.
Stewart, C. R., Stuart, L. M., Wilkinson, K., et al. 2010. CD36 ligands promote sterile inflammation through assembly of a Toll-like receptor 4 and 6 heterodimer. *Nat Immunol,* 11**,** 155-61.
Stoger, J. L., Gijbels, M. J., Van Der Velden, S., et al. 2012. Distribution of macrophage polarization markers in human atherosclerosis. *Atherosclerosis,* 225**,** 461-8.
Stout, R. D., Jiang, C., Matta, B., Tietzel, I., Watkins, S. K. & Suttles, J. 2005. Macrophages sequentially change their functional phenotype in response to changes in microenvironmental influences. *J Immunol,* 175**,** 342-9.
Sumagin, R., Prizant, H., Lomakina, E., Waugh, R. E. & Sarelius, I. H. 2010. LFA-1 and Mac-1 define characteristically different intralumenal crawling and emigration patterns for monocytes and neutrophils in situ. *J Immunol,* 185**,** 7057-66.
Suzuki, K., Kumanogoh, A. & Kikutani, H. 2008. Semaphorins and their receptors in immune cell interactions. *Nat Immunol,* 9**,** 17-23.
Swanson, L., Katkar, G. D., Tam, J., et al. 2020. TLR4 signaling and macrophage inflammatory responses are dampened by GIV/Girdin. *Proc Natl Acad Sci U S A,* 117**,** 26895-26906.
Sweet, D. R., Padmanabhan, R., Liao, X., et al. 2023. Kruppel-Like Factors Orchestrate Endothelial Gene Expression Through Redundant and Non-Redundant Enhancer Networks. *J Am Heart Assoc,* 12**,** e024303.
Swirski, F. K., Libby, P., Aikawa, E., Alcaide, P., Luscinskas, F. W., Weissleder, R. & Pittet, M. J. 2007. Ly-6Chi monocytes dominate hypercholesterolemia-associated monocytosis and give rise to macrophages in atheromata. *J Clin Invest,* 117**,** 195-205.
Taban, Q., Mumtaz, P. T., Masoodi, K. Z., Haq, E. & Ahmad, S. M. 2022. Scavenger receptors in host defense: from functional aspects to mode of action. *Cell Commun Signal,* 20**,** 2.

Tabas, I. & Bornfeldt, K. E. 2016. Macrophage Phenotype and Function in Different Stages of Atherosclerosis. *Circ Res,* 118**,** 653-67.
Tacke, F., Alvarez, D., Kaplan, T. J., et al. 2007. Monocyte subsets differentially employ CCR2, CCR5, and CX3CR1 to accumulate within atherosclerotic plaques. *J Clin Invest,* 117**,** 185-94.
Takei, A., Huang, Y. & Lopes-Virella, M. F. 2001. Expression of adhesion molecules by human endothelial cells exposed to oxidized low density lipoprotein. Influences of degree of oxidation and location of oxidized LDL. *Atherosclerosis,* 154**,** 79-86.
Takeshita, F., Leifer, C. A., Gursel, I., Ishii, K. J., Takeshita, S., Gursel, M. & Klinman, D. M. 2001. Cutting edge: Role of Toll-like receptor 9 in CpG DNA-induced activation of human cells. *J Immunol,* 167**,** 3555-8.
Takeuchi, O., Kawai, T., Muhiradt, P. F., et al. 2001. Discrimination of bacterial lipoproteins by Toll-likr receptor 6. *International Immunology,* 13**,** 993-940.
Takeuchi, O., Sato, S., Horiuchi, T., et al. 2002. Cutting edge: role of Toll-like receptor 1 in mediating immune response to microbial lipoproteins. *J Immunol,* 169**,** 10-4.
Tallone, T., Turconi, G., Soldati, G., Pedrazzini, G., Moccetti, T. & Vassalli, G. 2011. Heterogeneity of human monocytes: an optimized four-color flow cytometry protocol for analysis of monocyte subsets. *J Cardiovasc Transl Res,* 4**,** 211-9.
Tauber, A. I. 2003. Metchnikoff and the phagocytosis theory. *Nat Rev Mol Cell Biol,* 4**,** 897-901.
Teh, Y. C., Ding, J. L., Ng, L. G. & Chong, S. Z. 2019. Capturing the Fantastic Voyage of Monocytes Through Time and Space. *Front Immunol,* 10**,** 834.
Theofilis, P., Sagris, M., Oikonomou, E., Antonopoulos, A. S., Siasos, G., Tsioufis, C. & Tousoulis, D. 2021. Inflammatory Mechanisms Contributing to Endothelial Dysfunction. *Biomedicines,* 9.
Thiel, M., Wolfs, M. J., Bauer, S., et al. 2009. Efficiency of T-cell costimulation by CD80 and CD86 cross-linking correlates with calcium entry. *Immunology,* 129**,** 28-40.
Thies, F., Garry, J. M. C., Yaqoob, P., et al. 2003. Association of n-3 polyunsaturated fatty acids with stability of atherosclerotic plaques: a randomised controlled trial. *The Lancet,* 361**,** 477-485.
Thomas, A. C., Eijgelaar, W. J., Daemen, M. J. & Newby, A. C. 2015a. The pro-fibrotic and anti-inflammatory foam cell macrophage paradox. *Genom Data,* 6**,** 136-8.
Thomas, G., Tacke, R., Hedrick, C. C. & Hanna, R. N. 2015b. Nonclassical patrolling monocyte function in the vasculature. *Arterioscler Thromb Vasc Biol,* 35**,** 1306-16.
Thomas, G. D., Hamers, A. a. J., Nakao, C., et al. 2017. Human Blood Monocyte Subsets: A New Gating Strategy Defined Using Cell Surface Markers Identified by Mass Cytometry. *Arterioscler Thromb Vasc Biol,* 37**,** 1548-1558.
Tian, J., Gu, X., Sun, Y., Ban, X., Xiao, Y., Hu, S. & Yu, B. 2012. Effect of statin therapy on the progression of coronary atherosclerosis. *BMC Cardiovasc Disord,* 12**,** 70.
Titos, E., Rius, B., Gonzalez-Periz, A., et al. 2011. Resolvin D1 and its precursor docosahexaenoic acid promote resolution of adipose tissue inflammation by

eliciting macrophage polarization toward an M2-like phenotype. *J Immunol,* 187**,** 5408-18.
Tjonahen, E., Oh, S. F., Siegelman, J., et al. 2006. Resolvin E2: identification and anti-inflammatory actions: pivotal role of human 5-lipoxygenase in resolvin E series biosynthesis. *Chem Biol,* 13**,** 1193-202.
Touil, H., Li, R., Zuroff, L., et al. 2023. Cross-talk between B cells, microglia and macrophages, and implications to central nervous system compartmentalized inflammation and progressive multiple sclerosis. *EBioMedicine,* 96**,** 104789.
Traub, O. & Berk, B. C. 1998. Laminar shear stress. Mechanisms by which endothelial cells transduce an atheroprotective force. *Arterioscler Thromb Vasc Biol,* 18**,** 677-685.
Trogan, E., Feig, J. E., Dogan, S., et al. 2006. Gene expression changes in foam cells and the role of chemokine receptor CCR7 during atherosclerosis regression in ApoE-deficient mice. *Proc Natl Acad Sci U S A,* 103**,** 3781-6.
Tsou, C. L., Peters, W., Si, Y., et al. 2007. Critical roles for CCR2 and MCP-3 in monocyte mobilization from bone marrow and recruitment to inflammatory sites. *J Clin Invest,* 117**,** 902-9.
Tsukamoto, K., Kinoshita, M., Kojima, K., et al. 2002. Synergically increased expression of CD36, CLA-1 and CD68, but not of SR-A and LOX-1, with the progression to foam cells from macrophages. *J Atheroscler Thromb,* 9**,** 57-64.
Tull, S. P., Yates, C. M., Maskrey, B. H., et al. 2009. Omega-3 Fatty acids and inflammation: novel interactions reveal a new step in neutrophil recruitment. *PLoS Biol,* 7**,** e1000177.
Tushinski, R. J., Oliver, I. T., Guilbert, L. J., Tynan, P. W., Warner, J. R. & Stanley, E. R. 1982. Survival of Mononuclear Phagocytes Depends

on a Lineage-Specific Growth Factor That the

Differentiated Cells Selectively Destroy. *Cell,* 28**,** 71-81.
Tzircotis, G., Braga, V. M. & Caron, E. 2011. RhoG is required for both FcgammaR- and CR3-mediated phagocytosis. *J Cell Sci,* 124**,** 2897-902.
Unuvar Purcu, D., Korkmaz, A., Gunalp, S., et al. 2022. Effect of stimulation time on the expression of human macrophage polarization markers. *PLoS One,* 17**,** e0265196.
Uotila, L. M., Jahan, F., Soto Hinojosa, L., Melandri, E., Gronholm, M. & Gahmberg, C. G. 2014. Specific phosphorylations transmit signals from leukocyte beta2 to beta1 integrins and regulate adhesion. *J Biol Chem,* 289**,** 32230-32242.
Valente, A. J., Irimpen, A. M., Siebenlist, U. & Chandrasekar, B. 2014. OxLDL induces endothelial dysfunction and death via TRAF3IP2: inhibition by HDL3 and AMPK activators. *Free Radic Biol Med,* 70**,** 117-28.
Vallania, F., Zisman, L., Macaubas, C., et al. 2021. Multicohort Analysis Identifies Monocyte Gene Signatures to Accurately Monitor Subset-Specific Changes in Human Diseases. *Front Immunol,* 12**,** 659255.
Van Der Kooij, M. A., Von Der Mark, E. M., Kruijt, J. K., Van Velzen, A., Van Berkel, T. J. & Morand, O. H. 1997. Human monocyte-derived macrophages express an approximately 120-kD Ox-LDL binding protein with strong identity to CD68. *Arterioscler Thromb Vasc Biol,* 17**,** 3107-16.

Van Gils, J. M., Derby, M. C., Fernandes, L. R., et al. 2012. The neuroimmune guidance cue netrin-1 promotes atherosclerosis by inhibiting the emigration of macrophages from plaques. *Nat Immunol,* 13**,** 136-43.
Van Popele, N. M., Mattace-Raso, F. U., Vliegenthart, R., et al. 2006. Aortic stiffness is associated with atherosclerosis of the coronary arteries in older adults: the Rotterdam Study. *J Hypertens,* 24**,** 2371-6.
Van Tits, L. J., Stienstra, R., Van Lent, P. L., Netea, M. G., Joosten, L. A. & Stalenhoef, A. F. 2011. Oxidized LDL enhances pro-inflammatory responses of alternatively activated M2 macrophages: a crucial role for Kruppel-like factor 2. *Atherosclerosis,* 214**,** 345-9.
Vanderbeke, L., Van Mol, P., Van Herck, Y., et al. 2021. Monocyte-driven atypical cytokine storm and aberrant neutrophil activation as key mediators of COVID-19 disease severity. *Nat Commun,* 12**,** 4117.
Varasteh, Z., De Rose, F., Mohanta, S., et al. 2021. Imaging atherosclerotic plaques by targeting Galectin-3 and activated macrophages using ((89)Zr)-DFO-Galectin3-F(ab')(2) mAb. *Theranostics,* 11**,** 1864-1876.
Varol, C., Mildner, A. & Jung, S. 2015. Macrophages: development and tissue specialization. *Annu Rev Immunol,* 33**,** 643-75.
Virmani, R., Kolodgie, F. D., Burke, A. P., Farb, A. & Schwartz, S. M. 2000. Lessons from sudden coronary death: a comprehensive morphological classification scheme for atherosclerotic lesions. *Arterioscler Thromb Vasc Biol,* 20**,** 1262-75.
Volkov, A. M., Murashov, I. S., Polonskaya, Y. V., et al. 2018. [Changes of Content of Matrix Metalloproteinases and Their Tissue Expression in Various Types of Atherosclerotic Plaques]. *Kardiologiia***,** 12-18.
W.D., J. 1977. The separation, long term cultivation and maturation fo the human monocyte. *The Journal of Experimental Medicine,* 146**,** 1613-1626.
Wang, D., Yang, Y., Lei, Y., et al. 2019a. Targeting Foam Cell Formation in Atherosclerosis: Therapeutic Potential of Natural Products. *Pharmacol Rev,* 71**,** 596-670.
Wang, J., Li, R., Peng, Z., Hu, B., Rao, X. & Li, J. 2020. HMGB1 participates in LPS-induced acute lung injury by activating the AIM2 inflammasome in macrophages and inducing polarization of M1 macrophages via TLR2, TLR4, and RAGE/NF-kappaB signaling pathways. *Int J Mol Med,* 45**,** 61-80.
Wang, L. X., Zhang, S. X., Wu, H. J., Rong, X. L. & Guo, J. 2019b. M2b macrophage polarization and its roles in diseases. *J Leukoc Biol,* 106**,** 345-358.
Wang, M., Subramanian, M., Abramowicz, S., et al. 2014. Interleukin-3/granulocyte macrophage colony-stimulating factor receptor promotes stem cell expansion, monocytosis, and atheroma macrophage burden in mice with hematopoietic ApoE deficiency. *Arterioscler Thromb Vasc Biol,* 34**,** 976-84.
Wang, M. D., Kiss, R. S., Franklin, V., Mcbride, H. M., Whitman, S. C. & Marcel, Y. L. 2007. Different cellular traffic of LDL-cholesterol and acetylated LDL-cholesterol leads to distinct reverse cholesterol transport pathways. *J Lipid Res,* 48**,** 633-45.
Wang, S., Chennupati, R., Kaur, H., Iring, A., Wettschureck, N. & Offermanns, S. 2016. Endothelial cation channel PIEZO1 controls blood pressure by mediating flow-induced ATP release. *J Clin Invest,* 126**,** 4527-4536.

Wang, S., Wu, D., Matthan, N. R., Lamon-Fava, S., Lecker, J. L. & Lichtenstein, A. H. 2009. Reduction in dietary omega-6 polyunsaturated fatty acids: eicosapentaenoic acid plus docosahexaenoic acid ratio minimizes atherosclerotic lesion formation and inflammatory response in the LDL receptor null mouse. *Atherosclerosis,* 204**,** 147-55.
Wang, Y., Zhang, Y., Wang, Z., et al. 2019c. Optical/MRI dual-modality imaging of M1 macrophage polarization in atherosclerotic plaque with MARCO-targeted upconversion luminescence probe. *Biomaterials,* 219**,** 119378.
Wanke, F., Gutbier, S., Rummelin, A., et al. 2021. Ligand-dependent kinase activity of MERTK drives efferocytosis in human iPSC-derived macrophages. *Cell Death Dis,* 12**,** 538.
Watanabe, N., Gao, S., Wu, Z., et al. 2021. Analysis of deficiency of adenosine deaminase 2 pathogenesis based on single-cell RNA sequencing of monocytes. *J Leukoc Biol,* 110**,** 409-424.
Watanabe, S., Alexander, M., Misharin, A. V. & Budinger, G. R. S. 2019. The role of macrophages in the resolution of inflammation. *J Clin Invest,* 129**,** 2619-2628.
Weber, C. & Noels, H. 2011. Atherosclerosis: current pathogenesis and therapeutic options. *Nat Med,* 17**,** 1410-22.
Wesa, A. K. & Galy, A. 2001. IL-1 beta induces dendritic cells to produce IL-12. *Int Immunol,* 13**,** 1053-61.
Westerterp, M. & Tall, A. R. 2020. A new pathway of macrophage cholesterol efflux. *Proc Natl Acad Sci U S A,* 117**,** 11853-11855.
Westerterp, M., Van Eck, M., De Haan, W., Offerman, E. H., Van Berkel, T. J., Havekes, L. M. & Rensen, P. C. 2007. Apolipoprotein CI aggravates atherosclerosis development in ApoE-knockout mice despite mediating cholesterol efflux from macrophages. *Atherosclerosis,* 195**,** e9-16.
Westhorpe, C. L., Dufour, E. M., Maisa, A., Jaworowski, A., Crowe, S. M. & Muller, W. A. 2012. Endothelial cell activation promotes foam cell formation by monocytes following transendothelial migration in an in vitro model. *Exp Mol Pathol,* 93**,** 220-6.
White, G. E., Mcneill, E., Channon, K. M. & Greaves, D. R. 2014. Fractalkine promotes human monocyte survival via a reduction in oxidative stress. *Arterioscler Thromb Vasc Biol,* 34**,** 2554-62.
Williams, J. A. & Shacter, E. 1997. Regulation of macrophage cytokine production by prostaglandin E2. Distinct roles of cyclooxygenase-1 and -2. *J Biol Chem,* 272**,** 25693-9.
Williams, K. J. & Tabas, I. 1995. The response-to-retention hypothesis of early atherogenesis. *Arteriosclerosis, Thrombosis, and Vascular Biology,* 15**,** 551-561.
Winkels, H., Ehinger, E., Vassallo, M., et al. 2018. Atlas of the Immune Cell Repertoire in Mouse Atherosclerosis Defined by Single-Cell RNA-Sequencing and Mass Cytometry. *Circ Res,* 122**,** 1675-1688.
Winkels, H. & Wolf, D. 2021. Heterogeneity of T Cells in Atherosclerosis Defined by Single-Cell RNA-Sequencing and Cytometry by Time of Flight. *Arterioscler Thromb Vasc Biol,* 41**,** 549-563.
Wolf, D., Anto-Michel, N., Blankenbach, H., et al. 2018. A ligand-specific blockade of the integrin Mac-1 selectively targets pathologic inflammation while maintaining protective host-defense. *Nat Commun,* 9**,** 525.

Wolf, D. & Ley, K. 2019. Immunity and Inflammation in Atherosclerosis. *Circ Res,* 124**,** 315-327.
Wong, K. L., Tai, J. J., Wong, W. C., et al. 2011. Gene expression profiling reveals the defining features of the classical, intermediate, and nonclassical human monocyte subsets. *Blood,* 118**,** e16-31.
Woollard, K. J. & Geissmann, F. 2010. Monocytes in atherosclerosis: subsets and functions. *Nat Rev Cardiol,* 7**,** 77-86.
Wragg, J. W., Durant, S., Mcgettrick, H. M., Sample, K. M., Egginton, S. & Bicknell, R. 2014. Shear stress regulated gene expression and angiogenesis in vascular endothelium. *Microcirculation,* 21**,** 290-300.
Wright, R. D. & Cooper, D. 2014. Glycobiology of leukocyte trafficking in inflammation. *Glycobiology,* 24**,** 1242-51.
Wu, H., Gower, R. M., Wang, H., et al. 2009. Functional role of CD11c+ monocytes in atherogenesis associated with hypercholesterolemia. *Circulation,* 119**,** 2708-17.
Wu, J., He, S., Song, Z., et al. 2023. Macrophage polarization states in atherosclerosis. *Front Immunol,* 14**,** 1185587.
Wynn, T. A., Chawla, A. & Pollard, J. W. 2013. Macrophage biology in development, homeostasis and disease. *Nature,* 496**,** 445-55.
Xu, C., Liu, W., You, X., et al. 2015. PGF2alpha modulates the output of chemokines and pro-inflammatory cytokines in myometrial cells from term pregnant women through divergent signaling pathways. *Mol Hum Reprod,* 21**,** 603-14.
Xu, J. & Yang, Y. 2023. Identification of candidate biomarkers and mechanisms in foam cell formation from heterogeneous cellular origins via integrated transcriptome analysis. *Ann Transl Med,* 11**,** 189.
Xu, S., Huang, Y., Xie, Y., et al. 2010a. Evaluation of foam cell formation in cultured macrophages: an improved method with Oil Red O staining and DiI-oxLDL uptake. *Cytotechnology,* 62**,** 473-81.
Xu, Z. Z., Zhang, L., Liu, T., et al. 2010b. Resolvins RvE1 and RvD1 attenuate inflammatory pain via central and peripheral actions. *Nat Med,* 16**,** 592-7, 1p following 597.
Xue, J., Schmidt, S. V., Sander, J., et al. 2014. Transcriptome-based network analysis reveals a spectrum model of human macrophage activation. *Immunity,* 40**,** 274-88.
Yagi, S., Fukuda, D., Aihara, K. I., Akaike, M., Shimabukuro, M. & Sata, M. 2017. n-3 Polyunsaturated Fatty Acids: Promising Nutrients for Preventing Cardiovascular Disease. *J Atheroscler Thromb,* 24**,** 999-1010.
Yamaguchi, A., Botta, E. & Holinstat, M. 2022. Eicosanoids in inflammation in the blood and the vessel. *Front Pharmacol,* 13**,** 997403.
Yang, J., Zhang, L., Yu, C., Yang, X. & Wang, H. 2014. Monocyte and macrophage differentiation: circulation inflammatory monocyte as biomarker for inflammatory diseases. *Biomarker research,* 2**,** 1-9.
Yang, Y., Luo, N. S., Ying, R., et al. 2017. Macrophage-derived foam cells impair endothelial barrier function by inducing endothelial-mesenchymal transition via CCL-4. *Int J Mol Med,* 40**,** 558-568.
Yilmaz, A., Lochno, M., Traeg, F., et al. 2004. Emergence of dendritic cells in rupture-prone regions of vulnerable carotid plaques. *Atherosclerosis,* 176**,** 101-10.

Yokoyama, M., Origasa, H., Matsuzaki, M., et al. 2007a. Effects of eicosapentaenoic acid on major coronary events in hypercholesterolaemic patients (JELIS): a randomised open-label, blinded endpoint analysis. *The Lancet,* 369**,** 1090-1098.
Yokoyama, M., Origasa, H., Matsuzaki, M., et al. 2007b. Effects of eicosapentaenoic acid on major coronary events in hypercholesterolaemic patients (JELIS): a randomised open-label, blinded endpoint analysis. *Lancet,* 369**,** 1090-8.
Yona, S. & Gordon, S. 2015. From the Reticuloendothelial to Mononuclear Phagocyte System - The Unaccounted Years. *Front Immunol,* 6**,** 328.
Yona, S., Kim, K. W., Wolf, Y., et al. 2013. Fate mapping reveals origins and dynamics of monocytes and tissue macrophages under homeostasis. *Immunity,* 38**,** 79-91.
Yrlid, U., Jenkins, C. D. & Macpherson, G. G. 2006. Relationships between distinct blood monocyte subsets and migrating intestinal lymph dendritic cells in vivo under steady-state conditions. *J Immunol,* 176**,** 4155-62.
Yu, X. H., Fu, Y. C., Zhang, D. W., Yin, K. & Tang, C. K. 2013. Foam cells in atherosclerosis. *Clin Chim Acta,* 424**,** 245-52.
Yu, Y., Lucitt, M. B., Stubbe, J., et al. 2009. Prostaglandin F2alpha elevates blood pressure and promotes atherosclerosis. *Proc Natl Acad Sci U S A,* 106**,** 7985-90.
Yvan-Charvet, L., Ranalletta, M., Wang, N., et al. 2007. Combined deficiency of ABCA1 and ABCG1 promotes foam cell accumulation and accelerates atherosclerosis in mice. *J Clin Invest,* 117**,** 3900-8.
Zakkar, M., Van Der Heiden, K., Luong Le, A., et al. 2009. Activation of Nrf2 in endothelial cells protects arteries from exhibiting a proinflammatory state. *Arterioscler Thromb Vasc Biol,* 29**,** 1851-7.
Zamai, L., Bareggi, R., Santavanere, E. & Vitale, M. 1993. Substraction of autofluorescent dead cellsfrom the lymphocyte flow cytometric binding assay. *Cytometry,* 14**,** 951-954.
Zambrano-Zaragoza, J. F., Romo-Martinez, E. J., Duran-Avelar Mde, J., Garcia-Magallanes, N. & Vibanco-Perez, N. 2014. Th17 cells in autoimmune and infectious diseases. *Int J Inflam,* 2014**,** 651503.
Zarbock, A., Ley, K., Mcever, R. P. & Hidalgo, A. 2011. Leukocyte ligands for endothelial selectins: specialized glycoconjugates that mediate rolling and signaling under flow. *Blood,* 118**,** 6743-51.
Zaric, B. L., Radovanovic, J. N., Gluvic, Z., et al. 2020. Atherosclerosis Linked to Aberrant Amino Acid Metabolism and Immunosuppressive Amino Acid Catabolizing Enzymes. *Front Immunol,* 11**,** 551758.
Zawada, A. M., Rogacev, K. S., Rotter, B., Winter, P., Marell, R. R., Fliser, D. & Heine, G. H. 2011. SuperSAGE evidence for CD14++CD16+ monocytes as a third monocyte subset. *Blood,* 118**,** e50-61.
Zeiher, A. M., Fosslthaler, B. S.-U., B & Buss, R. 1995. Nitric oxide modulates the expression of monocyte chemoattractant protein-1 in cultured human endothelial cells. *Circ Res,* 76**,** 980-986.
Zernecke, A. 2015. Dendritic cells in atherosclerosis: evidence in mice and humans. *Arterioscler Thromb Vasc Biol,* 35**,** 763-70.

Zha, Q. B., Wei, H. X., Li, C. G., et al. 2016. ATP-Induced Inflammasome Activation and Pyroptosis Is Regulated by AMP-Activated Protein Kinase in Macrophages. *Front Immunol,* 7**,** 597.
Zhang, C., Yang, M. & Ericsson, A. C. 2021. Function of Macrophages in Disease: Current Understanding on Molecular Mechanisms. *Front Immunol,* 12**,** 620510.
Zhang, H., Yang, K., Chen, F., et al. 2022a. Role of the CCL2-CCR2 axis in cardiovascular disease: Pathogenesis and clinical implications. *Front Immunol,* 13**,** 975367.
Zhang, S. H., Reddick, R. L., Piedrahita, J. A. & Maeda, N. 1992. Spontaneous hypercholesterolemia and arterial lesions in mice lacking apolipoprotein E. *Science,* 258**,** 468-71.
Zhang, X., Xie, Y., Zhou, H., Xu, Y., Liu, J., Xie, H. & Yan, J. 2014. Involvement of TLR4 in oxidized LDL/β2GPI/anti-β2GPI-induced transformation of macrophages to foam cells. *J Atheroscler Thromb,* 21**,** 1140-51.
Zhang, X., Zheng, B., Zhao, L., et al. 2022b. KLF4-PFKFB3-driven glycolysis is essential for phenotypic switching of vascular smooth muscle cells. *Commun Biol,* 5**,** 1332.
Zhong, C., Yang, X., Feng, Y. & Yu, J. 2020. Trained Immunity: An Underlying Driver of Inflammatory Atherosclerosis. *Front Immunol,* 11**,** 284.
Zhou, L., Somasundaram, R., Nederhof, R. F., Dijkstra, G., Faber, K. N., Peppelenbosch, M. P. & Fuhler, G. M. 2012. Impact of human granulocyte and monocyte isolation procedures on functional studies. *Clin Vaccine Immunol,* 19**,** 1065-74.
Zhuang, J., Han, Y., Xu, D., et al. 2017. Comparison of circulating dendritic cell and monocyte subsets at different stages of atherosclerosis: insights from optical coherence tomography. *BMC Cardiovasc Disord,* 17**,** 270.
Ziegler-Heitbrock, H. W., Fingerle, G., Strobel, M., et al. 1993. The novel subset of CD14+/CD16+ blood monocytes exhibits features of tissue macrophages. *Eur J Immunol,* 23**,** 2053-8.
Ziegler-Heitbrock, L. 2014. Monocyte subsets in man and other species. *Cell Immunol,* 289**,** 135-9.
Ziegler-Heitbrock, L., Ancuta, P., Crowe, S., et al. 2010. Nomenclature of monocytes and dendritic cells in blood. *Blood,* 116**,** e74-80.
Zizzo, G., Hilliard, B. A., Monestier, M. & Cohen, P. L. 2012. Efficient clearance of early apoptotic cells by human macrophages requires M2c polarization and MerTK induction. *J Immunol,* 189**,** 3508-20.

Appendix

Appendix Table 1: Median fluorescence intensity (MFI) of flow cytometry panel markers on foam cells treated with modified forms of LDL derived from M1, M2 and M0 polarised macrophages

Macrophage markers		M0 (MFI)		M1 (MFI)		M2 (MFI)	
		24hr LDL	24hr LDL + repolarisation	24hr LDL	24hr LDL + repolarisation	24hr LDL	24hr LDL + repolarisation
CD68	Untreated	3656.333 ± 893.780	3596.000 ± 411.461	3282.667 ± 443.880	3569.667 ± 404.317	3195.333 ± 391.769	3703.667 ± 434.076
	oxLDL	3661.000 ± 722.249	3282.333 ± 333.869	3407.000 ± 456.00	3341.000 ± 493.061	3647.000 ± 253.054	3952.000 ± 345.023
	AcLDL	2820.667 ± 484.831	3452.667 ± 172.009	3649.000 ± 254.308	3289.333 ± 458.051	3498.667 ± 380.076	3618.333 ± 455.690
	MALDL	3680.333 ± 725.281	3775.333 ± 113.895	3712.000 ± 140.461	3364.000 ± 468.583	3498.333 ± 418.512	3868.333 ± 595.249
CD11c	Untreated	1186.667 ± 76.838	1209.667 ± 158.348	1002.667 ± 9.684	995.667 ± 32.220	1377.667 ± 40.810	1301.667 ± 109.837
	oxLDL	1281.667 ± 101.627	1275.667 ± 99.633	1015.667 ± 22.747	1029.000 ± 13.577	1394.333 ± 88.959	1455.000 ± 156.815
	AcLDL	1389.333 ± 113.055	1395.333 ± 103.949	1088.333 ± 22.519	1086.667 ± 16.149	1566.667 ± 50.959	1465.667 ± 103.170
	MALDL	1154.667 ± 78.191	1229.667 ± 105.742	999.333 ± 5.812	1010.000 ± 11.547	1371.667 ± 54.229	1306.667 ± 128.963
MerTk	Untreated	5503.667 ± 1135.851	5388.667 v 2007.953	1527.667 ± 253.798	907.000 ± 59.811	3472.333 ± 552.148	3013.667 ± 585.057
	oxLDL	5967.333 ± 776.999	5726.333 ± 765.442	1644.000 ± 245.175	968.000 ± 95.438	3793.333 ± 469.307	3351.333 ± 750.916

MerTk	**AcLDL**	6975.667 ± 1067.190	6929.000 ± 919.389	1872.000 ± 306.128	1045.333 ± 105.723	4142.333 ± 695.286	3650.333 ± 938.446
	MALDL	5614.000 ± 792.632	6412.333 ± 890.689	1733.333 ± 337.558	954.667 ± 89.713	4157.333 ± 354.552	3440.333 ± 845.616
M1-like markers		**M0 (MFI)**		**M1 (MFI)**		**M2 (MFI)**	
		24hr LDL	**24hr LDL + repolarisation**	**24hr LDL**	**24hr LDL + repolarisation**	**24hr LDL**	**24hr LDL + repolarisation**
CD80	**Untreated**	3987.333 ± 459.164	3931.667 ± 315.331	12418.333 ± 2352.560	17650.000 ± 1406.809	7738.000 ± 1107.626	8332.333 ± 1061.039
	oxLDL	4332.000 ± 393.892	3832.667 ± 308.671	11408.667 ± 1356.458	17757.333 ± 1365.892	7853.667 ± 707.387	8900.000 ± 962.429
	AcLDL	4037 ± 667 ± 433.667	4009.333 ± 436.596	12151.667 ± 2154.907	17075.667 ± 1804.619	8613.667 ± 1526.980	8765.000 ± 1288.013
	MALDL	3738.000 ± 406.543	4009.667 ± 403.125	12539.000 ± 1865.479	178846.000 ± 1661.056	8252.677 ± 1010.169	8430.667 ± 683.312
CD86	**Untreated**	1114.667 ± 233.340	1036.333 ± 66.218	3154.000 ± 1534.982	4824.667 ± 1502.543	1371.667 ± 265.581	1916.667 ± 567.150
	oxLDL	1097.000 ± 223.984	1145.667 ± 158.746	2631.000 ± 1050.429	4598.333 ± 1231.300	1694.667 ± 431.263	2215.667 ± 709.202
	AcLDL	1017.667 ± 166.374	958.333 ± 133.362	2879.000 ± 1322.524	4288.667 ± 737.500	2255.000 ± 633.585	3159.000 ± 1362.852
	MALDL	832.333 ± 241.333	889.333 ± 174.839	2935.667 ± 1312.635	4496.000 ± 993.975	1743.333 ± 417.108	2814.667 ± 1029.915
HLA-DR	**Untreated**	1722.667 ± 292.322	1699.667 ± 80.590	1599.667 ± 530.875	2110.667 ± 469.343	2129.000 ± 399.782	2001.667 ± 272.898
	oxLDL	1866.000 ± 302.550	1791.000 ± 169.555	1514.667 ± 403.090	2056.667 ± 424.213	2286.000 ± 397.747	2349.000 ± 169.555
	AcLDL	1556.333 ± 186.241	1601.333 v 104.745	1633.000 ± 576.003	2024.667 ± 302.085	22424.667 ± 580.163	2431.667 ± 434.314

	MALDL	1481.667 ± 243.513	1763.667 ± 173.051	1680.333 ± 501.159	2047.667 ± 451.224	2374.000 ± 461.670	2197.333 ± 310.467
M2-like marker		**M0 (MFI)**		**M1 (MFI)**		**M2 (MFI)**	
		24hr LDL	**24hr LDL + repolarisation**	**24hr LDL**	**24hr LDL + repolarisation**	**24hr LDL**	**24hr LDL + repolarisation**
CD206	**Untreated**	4254.333 ± 147.097	4700.667 ± 430.009	3714.667 ± 66.419	3666.667 ± 44.126	6979.000 ± 1404.110	5733.333 ± 526.582
	oxLDL	4473.667 ± 211.472	4665.667 ± 202.814	3759.667 ± 41.156	3691.000 ± 25.000	6686.667 ± 1829.457	5975.000 ± 688.382
	AcLDL	4688.667 ± 127.004	4525.667 ± 204.146	3742.667 ± 118.075	3687.000 ± 61.025	6046.667 ± 1016.025	5367.667 ± 340.256
	MALDL	4387.000 ± 199.923	4568.000 ± 243.575	3687.333 ± 76.890	3804.333 ± 18.270	6565.133 ± 1114.948	5293.667 ± 363.308

Scavenger receptors		M0 (MFI)		M1 (MFI)		M2 (MFI)	
		24hr LDL	**24hr LDL + repolarisation**	**24hr LDL**	**24hr LDL + repolarisation**	**24hr LDL**	**24hr LDL + repolarisation**
CD36	**Untreated**	716.667 ± 57.696	704.000 ± 15.395	510.000 ± 48.775	457.000 ± 29.366	1179.000 ± 327.970	1103.333 ± 148.424
	oxLDL	761.67 ± 42.262	767.000 ± 7.506	503.000 ± 36.056	456.667 ± 20.626	1152.667 ± 346.859	1231.000 ± 190.337
	AcLDL	814.333 ± 40.193	866.333 ± 33.208	499.000 ± 46.487	454.000 ± 27.301	1386.667 ± 402.973	1330.333 ± 236.191
	MALDL	802.333 ± 24.320	947.333 ± 53.436	508.000 ± 46.576	440.667 ± 20.827	1345.333 ± 354.778	1253.333 ± 229.537
CD204	**Untreated**	703.667 ± 63.572	795.000 ± 118.543	655.333 ± 42.191	662.333 ± 26.422	716.333 ± 37.494	688.000 ± 6.658
	oxLDL	697.333 ± 62.408	742.000 ± 33.262	665.333 ± 40.342	697.000 ± 14.012	713.667 ± 61.756	735.000 ± 31.086
	AcLDL	719.333 ± 40.309	738.667 ± 26.566	688.333 ± 34.362	753.000 ± 25.239	726.333 ± 46.927	733.333 ± 39.270
	MALDL	801.000 ± 7.767	805.667 ± 10.990	740.000 ± 18.339	786.000 ± 26.274	901.000 ± 103.330	818.000 ± 62.426
Stabilin-1	**Untreated**	1821.67 ± 413.907	1351.000 ± 267.627	1056.000 ± 145.823	950.667 ± 126.451	1626.000 ± 461.556	1362.333 ± 284.941
	oxLDL	1893.33 ± 510.648	1442.667 ± 224.882	1051.667 ± 135.169	1009.667 ± 107.880	1614.667 ± 448.692	1395.000 ± 381.083
	AcLDL	1649.667 ± 462.036	1394.667 ± 247.349	991.333 ± 88.171	1059.333 ± 119.861	1581.333 ± 448.340	1352.667 ± 232.798
	MALDL	1603.667 ± 316.277	1277.333 ± 124.025	1026.333 ± 67.088	996.000 ± 89.366	1569.000 ± 351.099	1196.667 ± 236.678